Unravelling the Cell Adhesion Defect in Meckel-Gruber Syndrome

Submitted by

Benjamin Roland Alexander Meadows

as a thesis for the degree of

Doctor of Philosophy in Biological Sciences

in September 2016

I certify that all material in this thesis which is not my own work has been identified and that no material has previously been submitted and approved for the award of a degree by this or any other University.

……

Acknowledgements

The first people who must be thanked are my fellow Dawe group members Kate McIntosh, Kat Curry, and half of Holly Hardy, as well as all past group members and Helen herself, who has always been a supportive and patient supervisor with a worryingly encyclopaedic knowledge of the human proteome.

Some (in the end, distressingly small) parts of this project would not have been possible without my western blot consultancy team, including senior western blot consultant Joe Costello and junior consultants Afsoon Sadeghi-Azadi, Jack Chen, Luis Godinho, Tina Schrader, Stacey Scott, Lucy Green, and Lizzy Anderson.

James Wakefield is thanked for improvising a protocol for actin co-sedimentation out of almost thin air. Most surprisingly, it worked.

Special thanks are due to the many undergraduates who have contributed to this project, without whose hard work many an *n* would be low: Beth Hickton, Grace Howells, Annie Toynbee, Alex Oldfield, Leonie Hawksley, and Georgie McDonald.

Peter Splatt and Christian Hacker are thanked for their help with electron microscopy. Karen Moore, Audrey Farbos, and Konrad Paszkiewicz from the Sequencing Service are acknowledged for their work which enabled the differential expression analysis which informed much of this project, and Kate Heesom (of the University of Bristol Proteomics Facility) is thanked for performing the TMT-MS. Jeremy Metz is acknowledged for his efforts to automate image analysis – I'm sorry Jeremy, but undergraduates work better than computers.

From the Biomedical Physics group, C. Peter Winlove, Peter Petrov, Barbara Sarri, and Ellen Green are thanked for their help with micropipetting experiments and cell spreading analysis, and for their endless patience and generosity.

I would especially like to acknowledge the members of Gero Steinberg's group, including Yujiro Higuchi, Sreedhar Kilaru, Anna Shiel, Ewa Bielska, Natalie Clark, Martin Schuster, Yvonne Roger, Gero himself, and all others who taught me a huge amount when I was just starting in the lab.

I would like to thank my family, small as it is, for their support and/or forbearance, especially during the dangerous writing up time.

Finally I would like to thank all current and past members of lab 211, which despite the occasional fire, broken floor, flood, asbestos warning, insect infestation, threat of excess cardboard, and outbreak of pregnancy, has been the best-run lab I have ever known. In particular Sam Mitchell, Andrena Ellis, Charli Mardon, and Andy Early are thanked for keeping the lab in check, in their own special ways.

Abstract

Meckel-Gruber syndrome (MKS) is a universally lethal heritable human disease characterised by CNS malformations, cystic kidney, polydactyly, and liver fibrosis. MKS is classed as one of the ciliopathies due to its association with dysfunctional primary cilia, signalling organelles found on most cells in the human body. Some of the symptoms of MKS can be explained as a consequence of disrupted developmental signalling through the primary cilium, other defects are harder to explain, and evidence now exists for non-ciliary influences on ciliopathies. The nature of these influences, and the implications they may have for our understanding of ciliary function and the aetiology of MKS, remain unclear. In this thesis, defects in cell-extracellular matrix (ECM) interaction in MKS are investigated to determine whether MKS proteins have a role in this process, and if so, whether this role may be involved in MKS pathology. A combination of transcriptomic, proteomic, and cell imaging approaches are used to demonstrate that MKS patient cells produce a defective extracellular matrix, and that the MKS protein TMEM67 is present at the cell surface at sites of cell-ECM interaction. It is shown that the full-length TMEM67 protein is required for correct ECM morphology, and it is further shown that the abnormal extracellular matrix morphology in MKS cells underlies other defects, including failure to build cilia and alterations to the actin cytoskeleton. This represents the first set of causal relationships identified between the cellular defects in this complex disease. It is further shown that treatment with developmental signalling pathway antagonists can rescue these defects, potentially revealing a new avenue of therapeutic intervention for MKS. Finally, possible upstream defects are investigated that might underlie the ECM defect,

including alterations to cell spreading behaviour and cell deformation resistance.

Table of contents

List of tables

List of figures

Chapter 1

Chapter 3

Chapter 4

Chapter 5

Chapter 6

List of abbreviations

AbDil – Antibody dilution (buffer)
ALMS – Alström syndrome
ARHGEF1 – Rho guanine nucleotide exchange factor 1
AT1 – Angiotensin receptor 1
ATP – Adenosine triphosphate
BB – Basal body
BBS – Bardet-Biedl syndrome
BM – Basement membrane
BSA – Bovine serum albumin
CC2D2 – Coiled-coil 2 domain containing 2 (protein)
CCD – Charge-coupled device
CDM – Cell-derived matrix
CEP290 – Centrosomal protein of 290 KDa
CNS – Central nervous system
COACH – Cerebellar vermis hypoplasia, oligophenia, ataxia, coloboma, and hepatic fibrosis (syndrome)
CP110 – Centriolar coiled-coil protein of 110 KDa
CRYAB – Alpha-B crystallin
DAPI – 4',6-diamidino-2-phenylindole
DAVID – Database for annotation, visualisation and integrated discovery
DIC – Differential interference contrast
DMEM – Dulbecco's modified Eagle's medium
Dvl – Dishevelled
ECL – Electrochemiluminescence
ECM – Extracellular matrix
EGTA - ethylene glycol-bis(β-aminoethyl ether)-N,N,N',N'-tetraacetic acid
ER – Endoplasmic reticulum
FA – Focal adhesion
GTPase – Guanosine triphosphatase

HEPES – 4-(2-hydroxyethyl)-1-piperazineethanesulfonic acid
FA – Formaldehyde
FIJI – FIJI is just ImageJ
FLNA – Filamin A
FN – Fibronectin
GFOGER – The GFOGER peptide sequence
Farp1 – FERM, RhoGEF and pleckstrin domain-containing protein 1
Hh – Hedgehog (pathway)
HSC – Hepatic stellate cell
IFT – Intraflagellar transport
JATD – Jeune syndrome
JBTS – Joubert syndrome
LAMA – Laminin alpha
LINC – Linker of nucleoskeleton and cytoskeleton
MAdCAM – Mucosal addressin cell adhesion molecule
MEF – Mouse embryonic fibroblast
MeOH – Methanol
MIM – Mendelian Inheritance in Man (online database)
MKS – Meckel Gruber syndrome
MMP – Matrix metallopeptidase
mRNA – Messenger RNA
MT – Microtubule
NPHP – Nephronophthisis
OFD – Orofaciodigital syndrome
Pa – Pascal (unit of pressure)
PBS – Phosphate-buffered saline
PBST – PBS plus Tween
PCP – Planar cell polarity
PDGF – Platelet-derived growth factor
PKD – Polycystic kidney disease
PPAR – Peroxisome proliferator activated receptor
Ptch1 – Patched 1
ROCK – Rho-associated protein kinase
ROR2 – Receptor tyrosine kinase like orphan receptor 2
RIPA – Radioimmunoprecipitation assay (buffer)
RPGRIP1 – Retinitis pigmentosa GTPase regulator interacting protein 1
RPGRIP1L – RPGRIP1-like
RGD – The Arg-Gly-Asp peptide sequence
RNA – Ribonucleic acid
RPE – Retinal pigment epithelium
SEM – Scanning electron microscopy
Shh – Sonic hedgehog (pathway)
siRNA – Short interfering RNA
SLS – Standard linear solid (viscoelastic model)
Src – Sarcoma
TCTN – Tectonic
TGF – Transforming growth factor
TGFβR1 – TGF-β receptor 1
TRIKinII – TGF-β receptor 1 kinase inhibitor II
TMEM – Transmembrane (protein)
TTBK2 – Tau tubulin kinase 2
TZ – Transition zone
VDAC1 – Voltage-dependent anion-selective channel protein 1
Wnt – Wingless (signalling pathway)
Wpk – Wistar polycystic kidney

Chapter 1

Introduction

Chapter 1: Introduction

1.1 Cilia and ciliopathies

1.1.1 Introduction to cilia

Cilia are organelles found in almost all cells of the vertebrates. Their basic structure (Figure 1.1) is a protrusion of the plasma membrane into the extracellular space, reinforced by an internal structure of specialised doublet microtubules – the axoneme (Figure 1.1, green). At the base of the cilium, a centriole (termed the “basal body” in this context) (Figure 1.1, orange) is responsible for organising these microtubules. The cilium is a highly specialised compartment with a large, distinct proteome, maintained by selective barriers to both cytoplasmic and membrane diffusion (Satir & Christensen, 2008).

There are two major types of cilium: motile cilia and the non-motile primary cilia. In animals, motile cilia are found in specific tissues such as the tracheal epithelium, where they are frequently present in large numbers on a single cell and are responsible for driving fluid flow by directional beating. The eukaryotic flagellum, a structure responsible for the motility of many unicellular eukaryotes and the spermatocytes of diverse multicellular species, is an elongated motile cilium. Primary cilia are more widespread throughout the human body than motile cilia, with a single primary cilium found on most cells (Singla & Reiter, 2006; Eggenschwiler & Anderson, 2007). The few non-ciliated human tissues include hepatocytes, differentiated cells of myeloid or lymphoid origin, and umbilical vein endothelia (reviewed by Wheatley, 1995). Cell types which usually live in suspension do not make primary cilia, suggesting that contact with a substratum is important for primary cilium formation (Albrecht-Buehler,

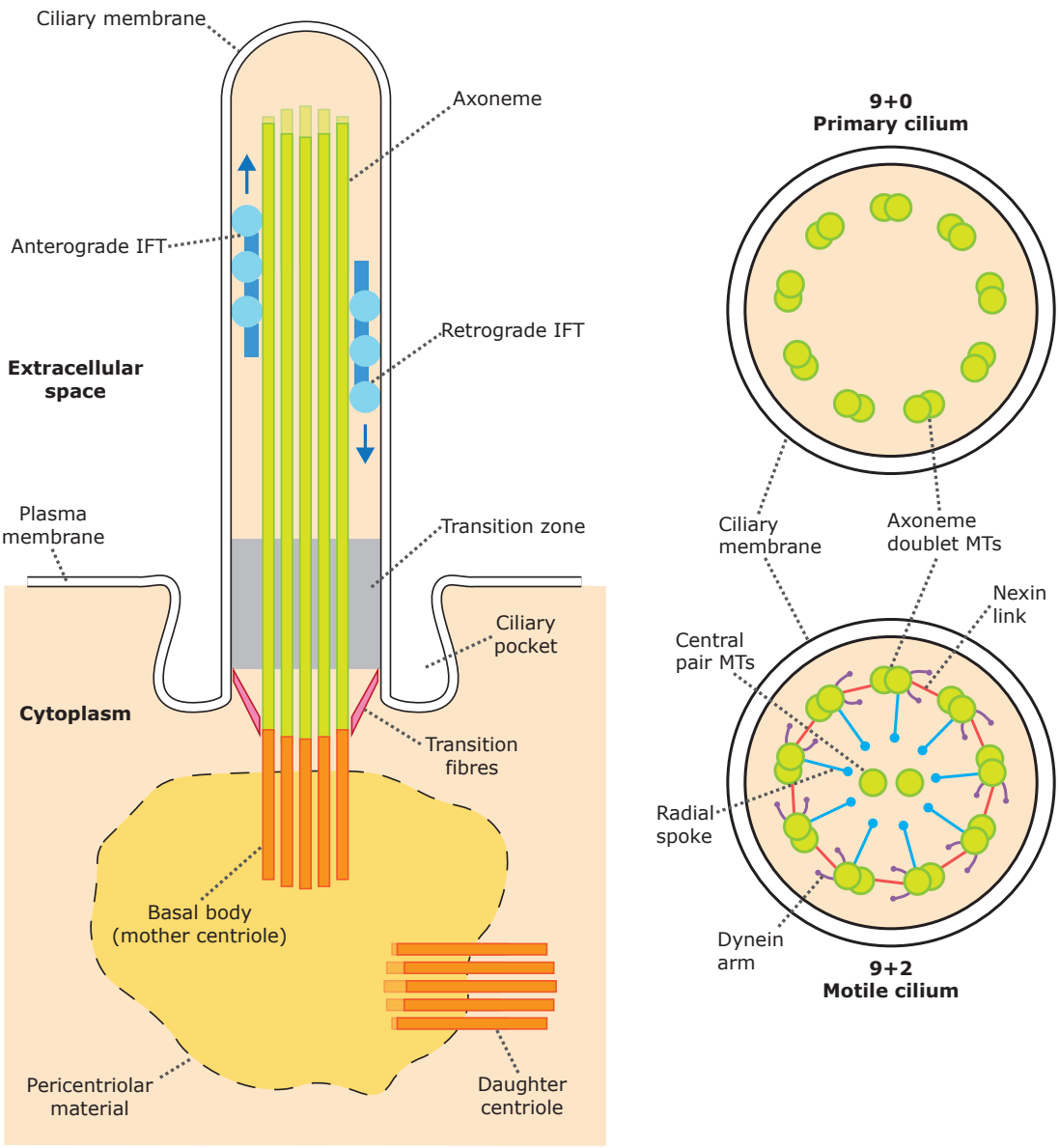

Figure 1.1: Structure of the cilium.

Left: Diagram of a longitudinal section through a cilium and basal body.

Right: Diagrams of transverse sections through a primary cilium and a motile cilium. The primary cilium has a 9-fold symmetrical arrangement of axoneme microtubule doublets (a 9+0 structure). A motile cilium contains the same 9-fold symmetrical MT doublets, but also various additional structures including a central pair of MTs (a 9+2 structure).

1977; Wheatley, 1995). Primary cilia have a mainly sensory role, detecting and transducing signals from diverse inputs such as developmental signalling molecules, mechanical forces, light (in the modified cilia of rod and cone cells in the eye), and odorants in the olfactory sensory system (Singla & Reiter, 2006). Motile cilia have been recognised more recently to also function as sensors (Bloodgood, 2010; Satir & Christensen, 2008).

Cilia are an ancient evolutionary adaptation, present in the last common ancestor of all extant eukaryotes (Cavalier-Smith, 2002; Mitchell, 2004; Satir *et al*, 2008). A small core set of ciliary proteins are widely conserved across ciliated eukaryotes (Broadhead *et al*, 2006; Satir & Christensen, 2007), though the full ciliary proteome, which in many species has been estimated to contain a number of proteins at least in the low hundreds (Ishikawa *et al*, 2012; Yuan & Sun, 2013; Arnaiz *et al*, 2009), is much more variable (Broadhead *et al*, 2006). This may indicate that while the basic architecture of the cilium is conserved, ciliary function has been subject to considerable evolutionary divergence. Some eukaryotes, including groups within the gymnosperms and the entire angiosperm lineage, have lost cilia (Finet *et al*, 2012; Bremer *et al*, 1987; Renzaglia & Garbary, 2001). However, some ciliary proteins remain conserved in these non-ciliated species, implying these proteins have (either ancestral or acquired) non-ciliary roles (Hodges *et al*, 2011).

Ciliary signalling is important in a wide range of signal transduction pathways, including those of profound developmental importance such as Wnt and Hedgehog signalling (Goetz & Anderson, 2010; Singla & Reiter, 2006) (see section 1.1.5 for more details). The widespread importance of cilia has not always been recognised; for example, their role in the central nervous system was long ignored despite the ubiquity of neuronal primary cilia (Fuchs &

Schwark, 2004). This was partly because of the difficulty of detecting primary cilia in ultrastructural studies (where they appear in only a small percentage of transmission electron micrographic sections), and partly due to a persistent false impression among researchers that non-motile cilia were vestigial structures without any function and thus not worthy of note (reviewed by Fuchs & Schwark, 2004).

1.1.2 Ciliary structure

Cilia are projections of the cell surface into the extracellular space, supported by an internal scaffold of doublet microtubules (MTs) – the "axoneme" (Figure 1.1, green) These MTs are templated from the basal body (Figure 1.1, orange) at the ciliary base. The basal body is a modified centriole; centrioles function as foci for the MT cytoskeleton in mitosis and are part of the centrosome, which serves as a MT organising centre (Lüders & Stearns, 2007). See Figure 1.1 for an overview of ciliary structure.

Motile cilia contain additional structures not present in primary cilia such as a central microtubule pair, dynein and nexin arms, and radial spokes, which contribute to their motility (Porter & Sale, 2000).

1.1.3 Ciliogenesis

Ciliogenesis, the process by which cilia are assembled, begins when the centrosome migrates to and "docks" with the cortical cytoskeleton at the apical cell surface, where the mother centriole acts as the basal body, which is required for ciliary assembly (Barker *et al*, 2015).

Prior to ciliogenesis, the centrosome is typically found near the centre of the cell physically attached to the nucleus (Figure 1.2, panel 1). The suspected linker between the centrosome and nucleus is the LINC complex, composed of KASH

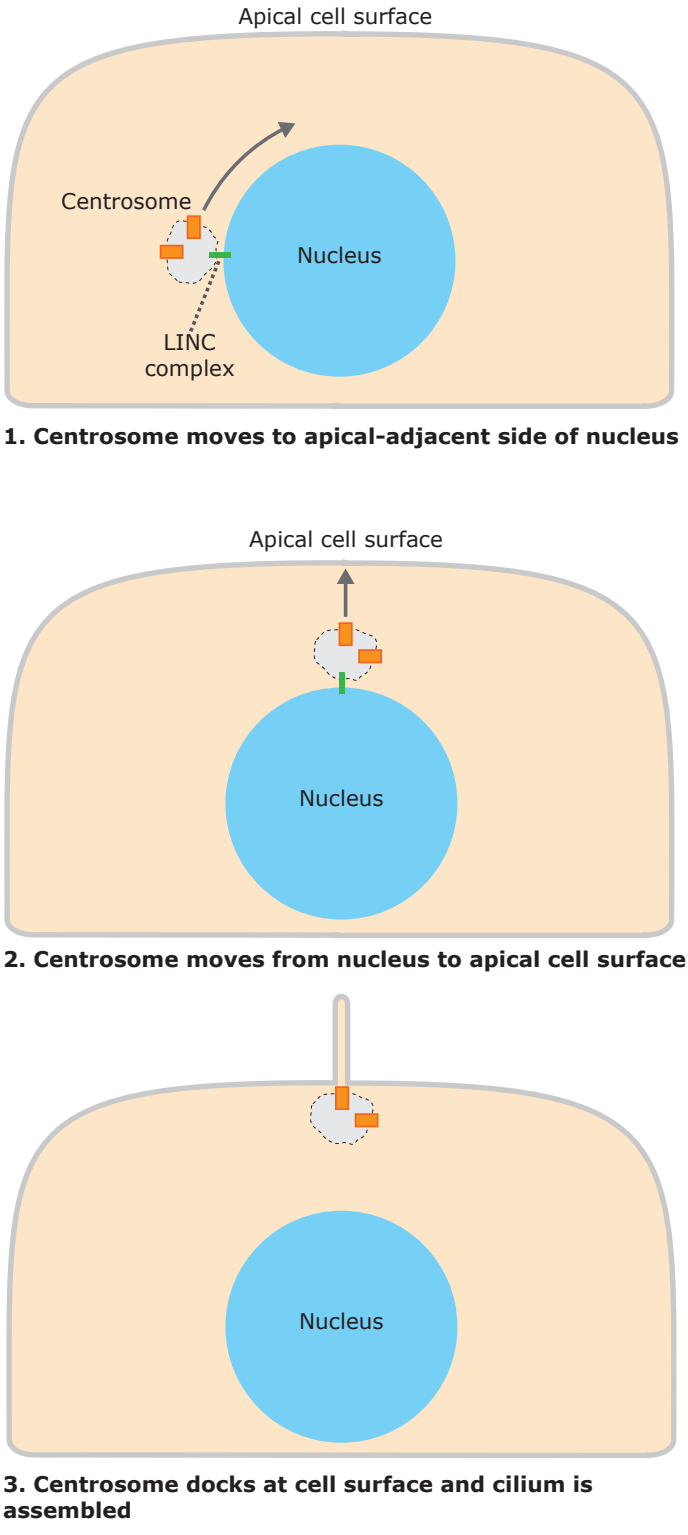

Figure 1.2: Centrosome migration prior to ciliogenesis.

Centrosome migration is a two-step process. Initially (1), the centrosome is attached to the nucleus (by the LINC complex), away from the apical cell surface. Without detaching, the centrosome moves around the nucleus (or the nucleus itself rotates) to bring the centrosome close to the apical cell surface (2). In the second step, the centrosome detaches from the nucleus and moves to the apical cell surface, where it docks and ciliogenesis takes place (3).

domain proteins on the outer nuclear membrane which are linked to SUN proteins on the inner nuclear membrane, and to the actin, MT, and intermediate filament cytoskeletons; LINC complexes are responsive to mechanical forces transduced through the cytoskeleton and are able to orchestrate global cytoskeletal organisation (reviewed by Starr & Fridolfsson, 2010). Centrosome migration for ciliogenesis is a two-step process where first, the centrosome moves around the nucleus until it is at the nearest point to its cell surface target site (Figure 1.2, panel 2), then disengages from the nucleus and migrates to the plasma membrane by a separate mechanism (Barker *et al*, 2015; Tsun *et al*, 2011; Yi *et al*, 2013) (Figure 1.2, panel 3). It is not clear whether the nucleus itself rotates, or the centrosome moves around the nuclear envelope without nuclear rotation.

While the process of migration and docking has been well-studied ultrastructurally, it was not well understood at a molecular level until recently. Even so, many studies report data only for motile cilia in multiciliated cells rather than primary cilia, for which ciliogenesis may differ in important mechanistic details (Dawe *et al*, 2007a; Barker *et al*, 2015). A large number of proteins are required for ciliogenesis including multiple actin-binding proteins (Kim *et al*, 2010; Wheway *et al*, 2015), and the actin cytoskeleton, as well as myosin, are essential for migration and docking (Boisvieux-Ulrich *et al*, 1990; Boisvieux Ulrich *et al*, 1987; Kim *et al*, 2015, 2010; Klotz *et al*, 1986; Lemullois *et al*, 1988, 1987; Pan *et al*, 2007; Park *et al*, 2008; Pitaval *et al*, 2010; Yan & Zhu, 2013). Microtubules (MTs) are not required (Bolvar *et al*, 2001; Boisvieux Ulrich *et al*, 1987), even though MTs are responsible for centrosome positioning in other contexts (Plotnikova *et al*, 2008; Pugacheva *et al*, 2007; Burakov *et al*, 2003), implying that during ciliogenesis a different mechanism takes over control of

centrosome positioning. Wnt/PCP and RhoA signalling have been implicated in actin remodelling required for docking (Gray *et al*, 2009; Pan *et al*, 2007; Park *et al*, 2006, 2008; Carvajal-Gonzalez *et al*, 2016; Song *et al*, 2010; Gray *et al*, 2011; Borovina *et al*, 2010; Epting *et al*, 2015). Kim *et al.* identified regulators of ciliogenesis and ciliary length, and found that actin regulators were commonly implicated; they also found that inhibition of actin polymerisation facilitated ciliary extension (Kim *et al*, 2010). This may indicate that ciliogenesis and ciliary extension is dependent on low levels of polymerised actin in the cilium's immediate area. In human retinal pigment epithelial (RPE1) cells, lack of spatial confinement of the cell leads to an altered actin cytoskeleton, altered nucleus-centrosome axis, and prevention of ciliogenesis that was rescued by actin depolymerisation (Pitaval *et al*, 2010). Assembly of denser actin bundles, and thus increased tension in the cytoskeleton, may therefore be expected to lead to ciliogenesis defects.

Ciliogenesis is also linked to cytoskeletal tension through YAP/TAZ signalling. YAP and TAZ are transcriptional regulators that can act downstream of the Hippo kinase cascade, or independently of Hippo, though it is common in the literature to refer to all YAP/TAZ activity as Hippo signalling (Piccolo *et al*, 2014). YAP/TAZ signalling is a conserved pathway that controls organ size and tissue homeostasis (Pan, 2010). YAP/TAZ activity is regulated by mechanical stimuli from the extracellular matrix (Halder *et al*, 2012), by actin stress fibres through the Hippo cascade (Wada *et al*, 2011; Zhao *et al*, 2012), or through tension in the actin cytoskeleton independently of Hippo (Dupont *et al*, 2011). Cells grown on pliant substrates have inhibited YAP/TAZ activity with localisation in the cytoplasm, whereas cells on rigid substrates have high YAP/TAZ activity, predominantly localised in the nucleus (Dupont *et al*, 2011).

Epithelial tissue architecture (characterised by basolaterally polarised cells and cell-cell adhesion) has a suppressive effect on YAP/TAZ signalling (Martin-Belmonte & Perez-Moreno, 2012). YAP/TAZ knockdown induces ciliogenesis, and hyperactivation suppresses ciliogenesis (Kim *et al*, 2015). These finding imply that ciliogenesis is dependent on the mechanical microenvironment of the cell, and might be blocked by stimuli that increase cytoskeletal or extracellular substrate tension and thus activate YAP/TAZ signalling.

The mother centriole must be modified with various accessory structures including distal and subdistal appendages before it is competent to template the axoneme; acquiring the full set of modifications takes one and a half cell cycles (Vorobjev & Chentsov, 1982). In the absence of distal appendages, centrioles successfully migrate to the cell surface but cannot orient correctly to the membrane and fail to dock (Tanos *et al*, 2013). Association of the mother centriole with a ciliary vesicle, which forms a double-membrane “sheath” around the distal end of the centriole, is dependent upon the presence of distal appendages (Schmidt *et al*, 2012; Joo *et al*, 2013) and may be involved in docking (Sorokin, 1962). While the role of the ciliary vesicle is not completely clear, it is thought that in at least some contexts the centriole/basal body elongates an axoneme within the sheath while the ciliary vesicle grows by fusion with secondary vesicles, then the ciliary vesicle fuses with the plasma membrane to form the ciliary pocket (an invagination of the plasma membrane around the base of the cilium), and the inner membrane of the sheath around the axoneme becomes the ciliary membrane (Ghossoub *et al*, 2011). In this model, vesicular trafficking to the site of ciliation is essential for docking, not just for elongation. The ciliary vesicle is thought to be derived from the Golgi (Sorokin, 1962), and ciliogenesis is dependent on a Rab8a-Rab11 cascade that

initiates trafficking of post-Golgi vesicles to the centrosome (Yoshimura *et al*, 2007; Westlake *et al*, 2011). Rabin8 (an activator of Rab8) rapidly relocalises to the centrosome upon serum-starvation (Westlake *et al*, 2011) (serum-starvation initiates ciliogenesis), suggesting that this pathway is rapidly responsive to ciliogenesis initiation signalling.

The protein CP110 caps the distal end of mature centrioles, and has been found to block ciliogenesis until it is removed (Tsang *et al*, 2008; Goetz *et al*, 2012), but only in cultured cells; a study *in vivo* found that CP110 promotes cilium formation and is required for centriole docking (Yadav *et al*, 2016), suggesting context-dependent ciliogenesis suppression and promotion functions. TTBK2 promotes the removal of CP110 from the centriole as well as promoting recruitment of ciliary assembly factors (Goetz *et al*, 2012), but its upstream effectors are unclear; CEP110 removal may be triggered by docking of the centriole to the cell surface (Tanos *et al*, 2013). This is inconsistent with the ciliary vesicle model since axoneme extension should be blocked while CEP110 is present; in this case, it may be necessary that CEP110 is removed upon association of the centriole with the ciliary vesicle, prior to docking with the cell surface. The exact timing of these events is still to be determined.

Once the centriole has docked and become the basal body, axoneme extension takes place to extend the cilium. The axonemal microtubules are elongated only at the distal ends (Johnson & Rosenbaum, 1992), at the tip of the growing cilium, the farthest point from the basal body and the cell. There is therefore a requirement for material to be transported along the entire length of the cilium (Hao *et al*, 2011). Nevertheless, this stage of ciliogenesis is fast: fully-formed cilia can be assembled within ten minutes after centriole docking (Dingle & Fulton, 1966). This implies rapid import and transport of ciliary building

materials. Transport along the cilium is achieved by a process called Intraflagellar Transport (IFT) , a kinesin-2- and dynein-dependent bidirectional transport mechanism running in “IFT trains” along the axonemal microtubules (Figure 1.1, blue arrows) (Rosenbaum & Witman, 2002; Kozminski *et al*, 1993). Defective cilium assembly can result from mutations in IFT proteins (Adams *et al*, 1982; Cole *et al*, 1998), indicating that IFT is required to build a cilium. IFT is also essential for maintenance of a cilium once assembled (Krock & Perkins, 2008; Pazour *et al*, 2002), for ciliary disassembly (Ishikawa & Marshall, 2011; Pan & Snell, 2005), and for cilium-dependent signalling (May *et al*, 2005; Huangfu *et al*, 2003). The cilium therefore is a structure that relies on continuous, active turnover and maintenance, and is highly sensitive to disruption of these processes.

1.1.4 Ciliary compartmentalisation

Essential to the cilium’s role in signalling is its status as a specialised compartment. Most organelles are bounded by a membrane which prevents free diffusion of molecules between the organelle lumen and the cytoplasm. The cilium, by contrast, has no membrane barrier at the base, its membrane being continuous with the plasma membrane. However, there is thought to be a “ciliary gate” that serves as a barrier to diffusion near the base of the cilium, in a region termed the transition zone (TZ) (Figure 1.1, grey area). This barrier is size-dependent, allowing small molecules to diffuse freely but preventing passage of larger objects (Kee *et al*, 2012). Even among objects that can pass the barrier, larger objects are delayed in comparison to smaller objects (Breslow *et al*, 2013; Lin *et al*, 2013). The selectivity appears to be purely based on object size rather than mass, as fusion of the spatially compact but heavy GFP moiety to proteins did not limit their ability to enter the cilium (Kee & Verhey,

2013; Harris *et al*, 2016; Craft *et al*, 2015). IFT is believed to be necessary for import and export of large ciliary component proteins, as it is capable of transporting cargo past this barrier (Rosenbaum & Witman, 2002). In ultrastructural studies Y-shaped structures are seen in sections through the TZ (Figure 1.3); the protein composition of these "Y-links" is not yet clear, but evidence is summarised in section 1.3.2 below. Between the basal body (BB) and the TZ are structures termed the "transition fibres" (Figure 1.1, pink), arranged in a radial "pinwheel" around the BB. These appear to be derived from the distal appendages of the BB, and link the BB to the periciliary membrane at the base of the TZ. The close spacing of the transition fibres provides a further size-dependent barrier to diffusion, entirely excluding vesicles from the cilium (Doolin & Birge, 1966; Geimer & Melkonian, 2004; Hagiwara *et al*, 2008; Ringo, 1967; Boquist, 1970; Reese, 1965). The transition fibres also serve as a docking site for IFT (Deane *et al*, 2001). The transition fibres are sometimes considered part of the TZ (Andersen *et al*, 1991), but are more often described as part of the BB (Reiter *et al*, 2012), though they are in close association with both.

In addition to the diffusion barrier between the ciliary lumen and the cytoplasm, there is also a suspected barrier to free diffusion of membrane proteins between the ciliary membrane and the wider plasma membrane, even though the two are continuous. This barrier is suspected to involve the "ciliary necklace" in the TZ; a distinct membrane region visible in electron micrographs as a regular pattern of protrusions (Gilula & Satir, 1972), which are likely to be the outer ends of the Y-links, either protruding through or deforming the ciliary membrane.

As a result of the gated entry to the cilium, both the ciliary membrane and cytoplasm are able to maintain a specialised composition; for example,

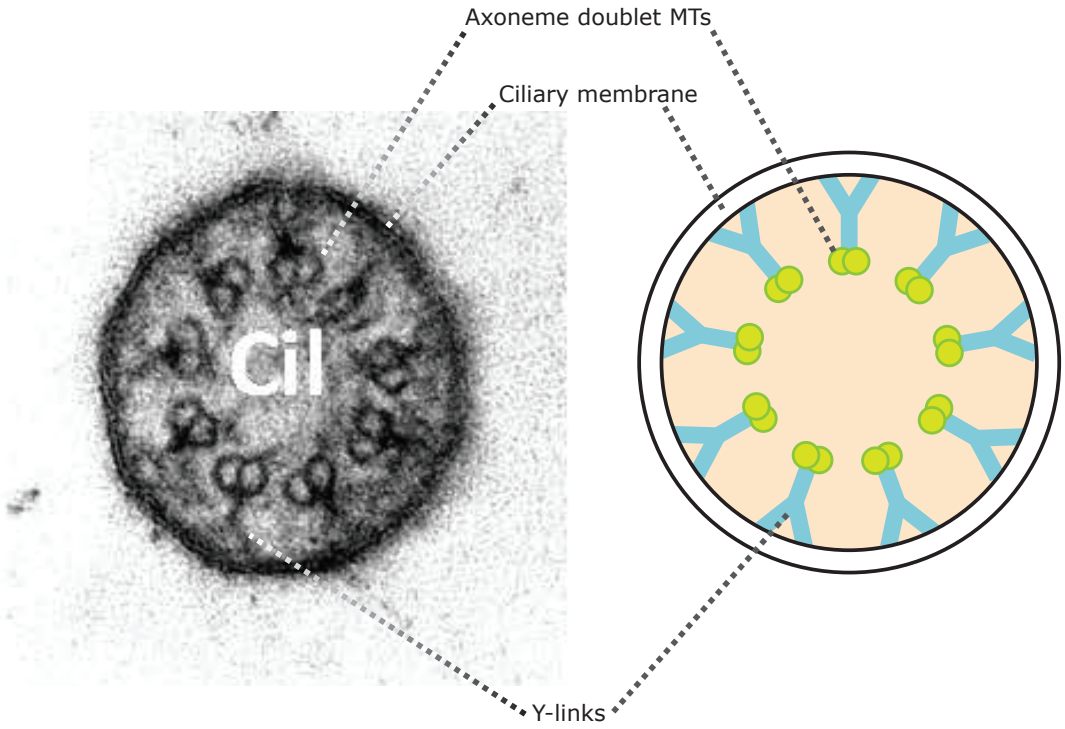

Figure 1.3: Y-links connect the axoneme to the ciliary membrane within the ciliary transition zone (TZ).

Left: Transmission electron micrograph showing a transverse section through a ciliary TZ.

Right: Schematic representation of the structure of the TZ.

enrichment in signalling components (Rohatgi & Snell, 2010; Garcia-Gonzalo & Reiter, 2012). Activation or inhibition of signalling pathways may thus rely on selective import or export of signalling components to or from the cilium; for example, Ptch1 must be exported from the cilium as part of the activation of the Hh pathway (Rohatgi *et al*, 2007). When ciliary compartmentalisation is compromised, these signalling pathways can become aberrant.

The precise nature of the diffusion barrier in the TZ is controversial. In addition to the TZ itself, evidence suggests that septins may form a barrier (Hu *et al*, 2010), while some authors propose a "ciliary pore complex" with similarities to the nuclear pore complex (Kee *et al*, 2012), supported by the finding that ciliary entry of at least some cargo is controlled by importins (Dishinger *et al*, 2010; Hurd *et al*, 2011; Torrado *et al*, 2016) which are more familiar as nuclear import factors. At the other extreme, Francis *et al* (2011) proposed that there is no need for a selective barrier to explain ciliary enrichment or exclusion, suggesting this can be explained by cytoskeletal retention of specific components preventing free diffusion instead.

1.1.5 Cilium-dependent signalling

Primary cilia act as the cell's "antennae", receiving a wide variety of extracellular signals, including developmental signals, chemical signals, and mechanical signals (Figure 1.4).

Developmental patterning in vertebrates is largely controlled by morphogens which activate developmental signalling pathways when they bind to receptors on the cell surface. Three of the most important developmental signalling pathways are Wnt, Hedgehog (Hh), and Notch. Cilia are known to be essential for Hh signalling (Eggenschwiler, 2012; Huangfu *et al*, 2003), important for

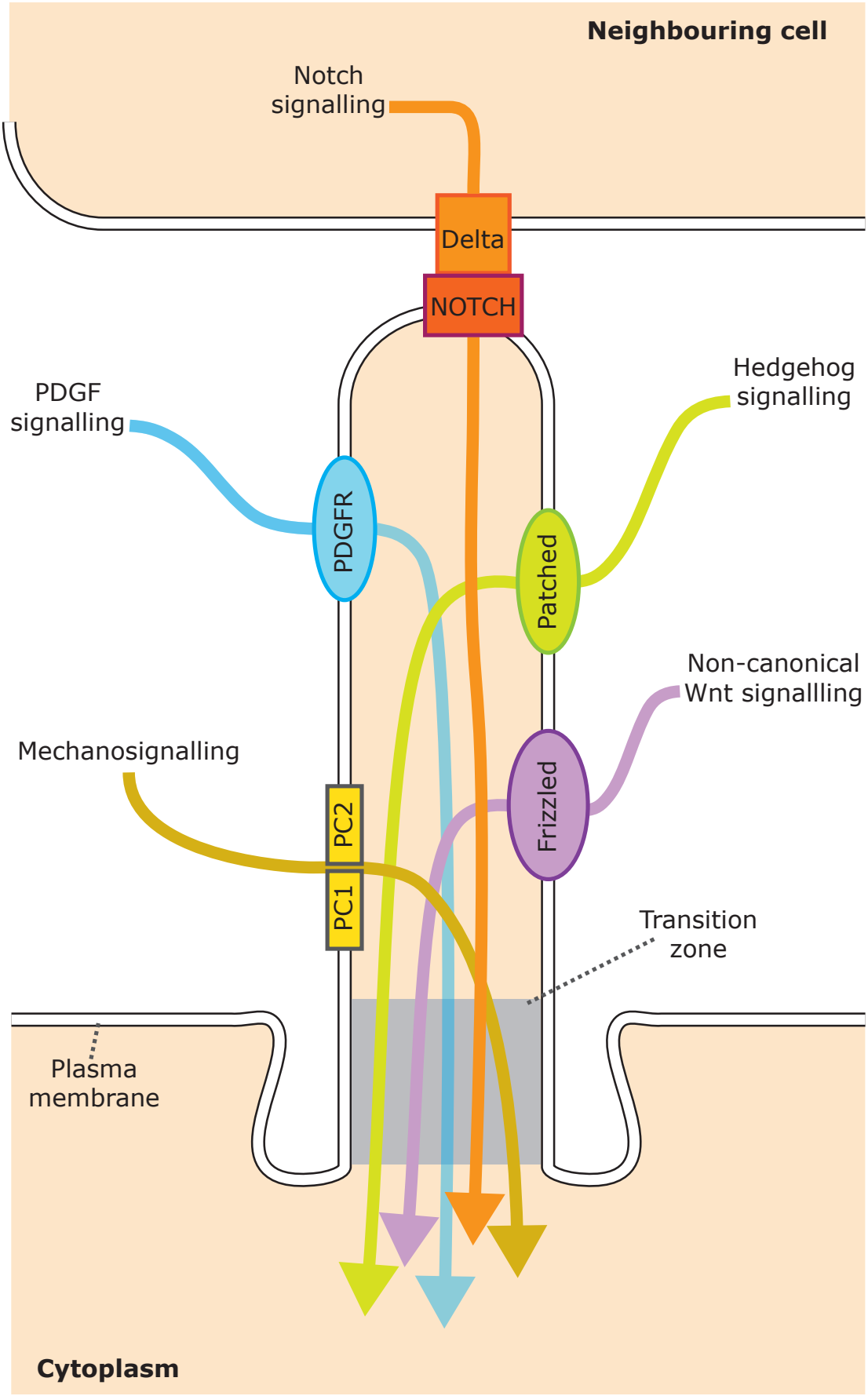

Figure 1.4: Signalling pathways proposed to be transduced through the cilium. The ciliary membrane is decorated with receptors for various pathways, all of which must be transduced via the TZ.

some Notch signalling (Ezratty *et al*, 2011), and have a controversial relationship with Wnt signalling (Wallingford & Mitchell, 2011).

Hedgehog signalling

Mammals have three instances of the hedgehog (Hh) pathway initiated by three different ligands: Indian, Desert, and Sonic (Shh). Shh in particular establishes ventral polarity in the neural tube (Echelard *et al*, 1993; Ericson *et al*, 1997), and posterior polarity (Ehlen *et al*, 2006) in the limb bud (Ingham & McMahon, 2001; Laufer *et al*, 1994), making it responsible for the patterning of digits in a concentration-dependent manner: high levels of Shh produce additional digits (polydactyly), and deletion results in a single digit representing the most ventral digit (the thumb in humans), which is the only digit to not depend on Shh (Ehlen *et al*, 2006). During the development of the central nervous system (CNS), Shh is produced in the notochord to specify the ventral neural tube and neural stem cell fate (Han *et al*, 2008).

On a molecular level, the Hh ligand binds to Patched1 (Ptch1), a transmembrane receptor protein found on the primary cilium membrane, resulting in the translocation of Ptch1 out of the cilium and the entry of Smoothened (Smo) (Rohatgi *et al*, 2007). Activated Smo prevents processing of the Glioma (Gli) transcription factor; in the absence of Hh, Gli is processed to a repressor form which prevents transcription of Hh target genes. When the Hh pathway is activated, Gli is instead converted to an active form (GliA) and target gene transcription is promoted (Ruiz i Altaba, 1999). Processing of Gli into either active or repressor forms is dependent on IFT downstream of Ptch1/Smo (May *et al*, 2005; Huangfu & Anderson, 2005; Liu *et al*, 2005), so ciliary dysfunction can result in complex phenotypes where some alterations are due to hyperactivated Hh, and some due to hypoactivation.

Hh signalling depends on the cell being able to control the compartmentalisation of Hh pathway components to the cilium, and on the trafficking activity that translocates them in response to signalling (Rohatgi *et al*, 2007; Wong & Reiter, 2008; Eggenschwiler, 2012). If this control became compromised, Hh defects such as altered digit number and altered CNS development would be expected. Equally, the presence of such symptoms implicates Hh signalling and ciliary function. Defects in ciliogenesis lead to multiple CNS malformations (Louvi & Grove, 2011).

Wnt signalling

Wnt signalling has wide responsibilities in cell fate determination and body axis patterning during embryonic development. Wnt is typically divided into three major pathways: one canonical (or β-catenin dependent) pathway, and the two non-canonical (β-catenin independent) pathways: the planar cell polarity (PCP) pathway, and the Wnt/calcium pathway. This is a simplification as there are a number of other Wnt pathways, and all Wnt pathways overlap via crosstalk to some degree (De, 2011).

Canonical Wnt signalling is fairly well-characterised. In the absence of canonical Wnt, β-catenin is complexed with axin, APC, and GSK3-β (termed the "destruction complex"). This results in phosphorylation of β-catenin, which is targeted for degradation. Canonical Wnt signalling is activated when a Wnt ligand binds to a Frizzled cell surface receptor, which leads to uncoupling of the destruction complex and stabilisation of β-catenin, which is then able to enter the nucleus and activate transcription of Wnt target genes (Reya & Clevers, 2005; van Amerongen & Nusse, 2009). Canonical Wnt is involved in cell proliferation, and hyperactivated Wnt is often seen in cancer (Anastas & Moon,

2013), with APC mutations frequently implicated (Reya & Clevers, 2005; Sparks *et al*, 1998).

The non-canonical PCP pathway is mediated by Rho family GTPases (including Rho, Rac, and Cdc42) (Schlessinger *et al*, 2009). PCP signalling controls cell polarity and the arrangement of the cytoskeleton (Winter *et al*, 2001), and thus controls overall cell morphology, but does not directly alter gene expression (Wallingford & Mitchell, 2011). Loss of core components of the PCP pathway leads to the development of kidney cysts (Cao *et al*, 2010).

When the non-canonical Wnt/calcium pathway is activated, intracellular calcium ion levels are increased, which in turn activates calcium-sensitive enzymes, leading to downstream alterations in gene expression (Kestler & Kühl, 2008; De, 2011). This pathway is not as well-studied as the canonical or PCP pathways, but has been implicated in kidney development (Burn *et al*, 2011), convergent extension movement (Freisinger *et al*, 2010) (a process essential for neural tube closure and correct CNS development), and dorsoventral polarity (Kühl *et al*, 2000; De, 2011).

The connections between Wnt and cilia are not yet clear. According to a number of studies, the canonical Wnt pathway is hyperactivated when cilia or ciliary proteins are disrupted (Gerdes *et al*, 2007; Corbit *et al*, 2008; McDermott *et al*, 2010; Voronina *et al*, 2009), implying that the cilium has a moderating role on canonical Wnt. However, other studies have found no alteration in canonical Wnt in the absence of cilia (Huang & Schier, 2009; Ocbina *et al*, 2009). This may suggest that ciliary involvement in canonical Wnt is specific to cell type; in any case, this relationship is still not well-understood (Wallingford & Mitchell, 2011). A number of studies also implicate cilia in non-canonical PCP signalling;

in contrast to canonical Wnt, PCP is not hyperactivated but disrupted when cilia are disrupted (Simons *et al*, 2005; Ross *et al*, 2005; Ferrante *et al*, 2009; Wallingford & Mitchell, 2011), suggesting that the relationship between this pathway and cilia is quite different. This has led to the hypothesis that cilia contain a "switch" between canonical and non-canonical Wnt, mediated by increased expression of the ciliary Wnt component interactor Inversin in response to extracellular signals; correct activation of this switch may be essential for development of organs such as the kidney (Simons *et al*, 2005; Goetz & Anderson, 2010; Singla & Reiter, 2006).

Though cilia are implicated in non-canonical Wnt signalling, non-canonical Wnt is conversely a prerequisite for correct organisation and function of motile cilia in some cell types, such as multiciliated epithelial cells (Del Bigio, 2010; Kishimoto & Sawamoto, 2012). This signalling dependency is most likely needed for correct ciliary polarisation; however, since motile cilia are also able to function in many of the signalling roles of primary cilia (Bloodgood, 2010), this could lead to further increases in signalling activity downstream, further complicating Wnt signalling response in these cells.

Notch signalling

The Notch pathway is mediated by Notch receptors on the cell surface which bind a number of ligands, prominently Delta and Jagged. These, and most other Notch ligands, are transmembrane proteins on the surface of neighbouring cells rather than secreted extracellular ligands (Bray, 2006). This means Notch signalling is generally only between cells in close physical contact rather than at a distance, as is common for other signalling pathways. Notch signalling is important in a number of developmental contexts, such as establishment of tissue boundaries and lineage determination; it is particularly involved in neural

cell fate specification (Lowell *et al*, 2006; Louvi & Artavanis-Tsakonas, 2006; Bray, 2006). Aberrant Notch can alter the development of the vasculature (Roca & Adams, 2007) or induce kidney cyst formation (Surendran *et al*, 2010). This indicates that Notch is important for correct overall organ development, even though most of its activity is local.

Components of the Notch pathway, including Notch receptors, localise to cilia (among other localisations), and elimination of cilia produces defects in Notch response (Ezratty *et al*, 2011). As with non-canonical Wnt, Notch signalling can also regulate cilia; for example, controlling ciliary length at Kupffer's vesicle (KV) in zebrafish (Lopes *et al*, 2010). KV is a structure homologous to the embryonic node in animals that establishes left/right asymmetry in a cilium-dependent process (Essner *et al*, 2002). Controlling the cilia in this structure confers Notch with broad developmental influence.

Other ciliary signalling roles

The platelet-derived growth factor (PDGF) pathway influences various proliferative and migration behaviours in many cell types. Components of this pathway localise to cilia, and cells with shortened cilia show abnormal PDGF response (Schneider *et al*, 2005; Eggenschwiler & Anderson, 2007), consistent with at least partial dependence on cilia.

The role of cilia as sensors extends beyond developmental signalling. Cilia in olfactory cells are responsible for odour detection (Kleene, 2008; Castillo *et al*, 2010), enabling the sense of smell; modified cilia in the rod and cone cells of the eye detect light (Lamb *et al*, 2007), enabling vision. Cilia in many tissues function as mechanosensors (Nguyen & Jacobs, 2013; Nauli *et al*, 2013). The major ciliary mechanotransduction pathway was thought to be calcium ion

dependent, in a pathway downstream of Ca^{2+} influx into the cilium in response to compression (Wann *et al*, 2012), but this model has recently been called into question by a study that found no evidence of the expected cilium-specific Ca^{2+} influx in observations of multiple tissues where cilium-dependent calcium signalling had been thought to be important, including kidney epithelia and embryonic nodal cells (Delling *et al*, 2016), so it may be that the reported changes in calcium signalling are actually reflective of cell body calcium flux downstream of another mechanosensory mechanism in cilia. An example of a possible alternative mechanism is the cilium-dependent mechanotransduction in osteocytes that has been reported to be calcium-independent (Malone *et al*, 2007) in a pathway involving cAMP, downstream of ion channels in the cilium (Kwon *et al*, 2010), though there have also been observations of ciliary Ca^{2+} influx in the cilia of these cells (Lee *et al*, 2015), so it may be that calcium signalling in this case was not recognised because it was solely ciliary Ca^{2+} influx, and not associated with changes to calcium ion signalling in the cell body. The specific signalling pathways involved in ciliary mechanotransduction thus remain somewhat unclear, and some authors have proposed that mechanotransduction may not originate in the cilium at all, at least in certain contexts (Delling *et al*, 2016). Cilia are not absolutely essential to mechanotransduction as, for example, non-ciliated endothelial cells are still responsive to flow (though ciliated cells have increased flow sensitivity) (Hierck *et al*, 2008). Nevertheless, ciliary mechanotransduction has been regarded as essential to many processes including kidney development (Singla & Reiter, 2006) and control of extracellular matrix secretion (Wann *et al*, 2012). Cilia are mechanically coupled to the extracellular matrix in cartilage (McGlashan *et al*, 2006), which likely allows them to detect mechanical signals transmitted

through the ECM. This may also be true in other tissues, raising difficulties in the interpretation of studies conducted under non-physiological cell culture conditions where an organised ECM was not present.

The cilium is thus a highly multifunctional sensory and signalling platform, able to integrate and transduce signals from a wide range of biological and non-biological sources (Figure 1.3) to control gene expression, cell polarity and cytoskeletal dynamics (in the case of PCP signalling), and developmental patterning on the level of individual tissues, whole organs, or entire body axes. Transduction of these signals depends on control of ciliary entry and exit through the TZ (Figure 1.3), and therefore, disruption to the TZ is a plausible explanation for developmental disease associated with these pathways.

1.1.6 Cilia in development

As a consequence of their sensory and signalling roles, functional cilia are essential for correct development of multiple organ systems, including the central nervous system, heart and vasculature, kidney, liver, and skeleton (Tasouri & Tucker, 2011; Goetz & Anderson, 2010).

1.1.7 Ciliopathies

The importance of ciliary signalling in development is such that defects in ciliogenesis or ciliary function have profound developmental consequences. The **ciliopathies** are the category of diseases caused by disrupted ciliary function (Schwartz *et al*, 2011; Badano *et al*, 2006). In general, ciliopathies are hereditary diseases caused by mutations in genes encoding ciliary or basal body proteins (Logan *et al*, 2011).

Currently identified ciliopathies include Bardet-Biedl syndrome (BBS) (Ansley *et al*, 2003), Alström syndrome (ALMS) (Karska-Basta *et al*, 2007; Collin *et al*,

2002), nephronophthisis (NPHP) (Hildebrandt *et al*, 2009), Joubert syndrome (JBTS) (Parisi, 2009), Jeune syndrome (JATD) (Beales *et al*, 2007), orofaciodigital syndrome (OFD) (Macca & Franco, 2009), and Meckel-Gruber syndrome (MKS) (Tobin & Beales, 2009).

The ciliopathies exhibit overlapping phenotypes (Table 1.1), and in many cases a single gene is allelic for several of these diseases, with syndromic presentation dependent on the mutation (Valente *et al*, 2010; Leitch *et al*, 2008; Norris & Grimes, 2012), or affected by the presence of modifying alleles (Khanna *et al*, 2009). For example, mutations in the MKS gene *TMEM67* can also cause JBTS (Baala *et al*, 2007b), NPHP (Otto *et al*, 2009), and COACH syndrome (Brancati *et al*, 2009) as well as modifying BBS (Leitch *et al*, 2008).

The ciliopathies thus represent a collection of pathologies with similar presentation, linked by a common aetiology in ciliary dysfunction, suggesting that the phenotypes observed may all have a common root in disruption of cilium-dependent processes.

Meckel-Gruber syndrome is the focus of this thesis, and will be discussed in more detail below (section 1.3).

	Alström	BBS	JBTS	Jeune	MKS	NPHP	OFD
Cleft palate							
Cognitive defects					?		
Deafness					?		
Encephalocele							
Liver disease							
Obesity					?		
Polydactyly							
Cystic kidney							
Retinopathy					?		
Situs inversus							
Skeletal defects							

Table 1.1: Presentation of clinical symptoms in ciliopathy syndromes. Shaded boxes indicate the symptom is commonly reported. For MKS, question marks denote symptoms that are not reported, but may be masked by lethality. Data from Norris & Grimes (2012).

Increasingly, components of the cilium have been found to play other roles in the cell outside the cilium and its environs (summarised in Figure 1.5). Even IFT proteins, once thought to constitute a highly specialised transport mechanism

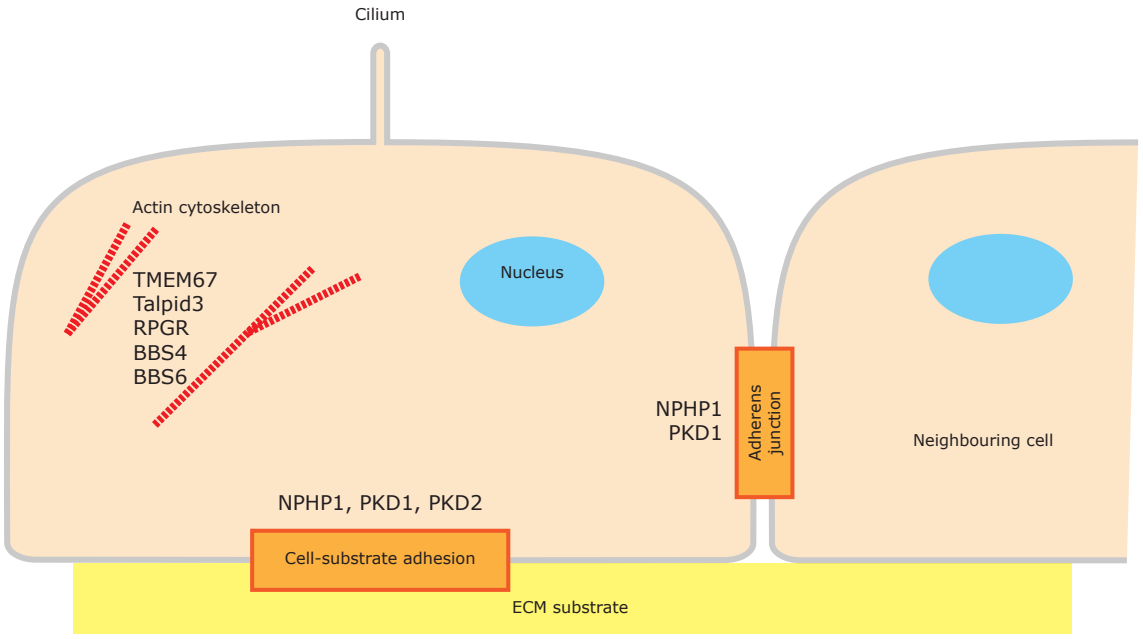

Figure 1.5: Non-ciliary roles for ciliopathy proteins. Summary cartoon showing ciliopathy proteins that have been implicated in cellular processes outside the cilium (Benzing et al, 2001; Huan & van Adelsberg, 1999; Mangos et al, 2010; Adams et al, 2010; Gakovic et al, 2011; Hernandez-Hernandez et al, 2013; Stephen et al, 2015).

present only on ciliary axonemes, have been found to be involved in trafficking and exocytosis in non-ciliated cells (Finetti *et al*, 2009), in cell division and cytokinesis at sites outside the cilium/flagellum (Qin *et al*, 2007; Wood *et al*, 2012), and to have a cilium-independent role in cell migration (Boehlke *et al*, 2015); all indicating that IFT proteins have a wider role in various cellular processes than was previously thought.

The actin cytoskeleton is a multifunctional scaffold that pervades the cell, responsible for control of cell shape, mechanical force generation, and cell motility (Le Clainche & Carlier, 2008; Pollard & Cooper, 2009). Many ciliary proteins, including TMEM67 (Dawe *et al*, 2009; Adams *et al*, 2012), BBS proteins (Hernandez & Beales, 2010; Hernandez-Hernandez *et al*, 2013), *Talpid3* (Yin *et al*, 2009), and RPGR (mutations in which cause the ciliopathy retinitis pigmentosa) (Gakovic *et al*, 2011) interact with the actin cytoskeleton; BBS4, BBS6, and BBS8 regulate actin via the actin remodelling protein RhoA (Hernandez-Hernandez *et al*, 2013).

One of the major types of structure that interact with actin are adhesions. These include focal adhesions, which physically connect cells to extracellular matrix substrates, and adherens junctions, which physically link neighbouring cells (see section 1.2 for details). Ciliary proteins are often found to interact with these adhesion sites: for example, TMEM67 interacts with filamin A, an actin-binding and cell-substrate adhesion associated protein (Adams *et al*, 2012); and BBS proteins may regulate the actin cytoskeleton by stabilising focal adhesions (Hernandez-Hernandez *et al*, 2013). The NPHP proteins nephrocystin-1, polycystin-1, and polycystin-2 have all been associated with adhesions: nephrocystin-1 and polycystin-1 both localise to adherens junctions and focal adhesions (Donaldson *et al*, 2000, 2002; Wilson *et al*, 1999; Markoff *et al*,

2007), and polycystin-2 interacts with adhesion proteins (Li *et al*, 2005). Ciliopathy proteins may be required for formation of these adhesions (Voronina *et al*, 2009), suggesting a significant role for these proteins independent of cilia.

While the ciliopathy proteins are mostly united by their relationship to cilia, recent work suggests their roles within the cell are more diverse. Important interactions with the cytoskeleton and with adhesion complexes suggest a wider role in regulation throughout the cell. The causal relationships between the ciliary and non-ciliary cellular phenotypes , however, remain unclear, as do their influence on disease pathology.

1.2 Cell adhesion and the extracellular matrix

1.2.1 Cell adhesion

Cells form surface adhesion complexes to physically attach to other cells and to the extracellular matrix. This is a capability fundamental to multicellularity and of critical importance for development, which is likely to be altered in MKS and ciliopathies in general.

The major structure for cell-substrate adhesion is the focal adhesion complex (Figure 1.6). This is composed of transmembrane integrin dimers which bind directly to extracellular ligands. Integrins are substrate-specific, only binding to a subset of the possible extracellular matrix (ECM) components in a cell's environment (Barczyk *et al*, 2010). On the intracellular side of the adhesion, an immensely variable adhesion complex is assembled depending on many contextual cues including the substrate, the cell type, and various regulatory signals. Proteins often found in this complex include talin, vinculin, paxillin, and zyxin. The complex recruits and cross-links actin stress fibres. A mature focal adhesion forms a strong physical connection between the actin cytoskeleton

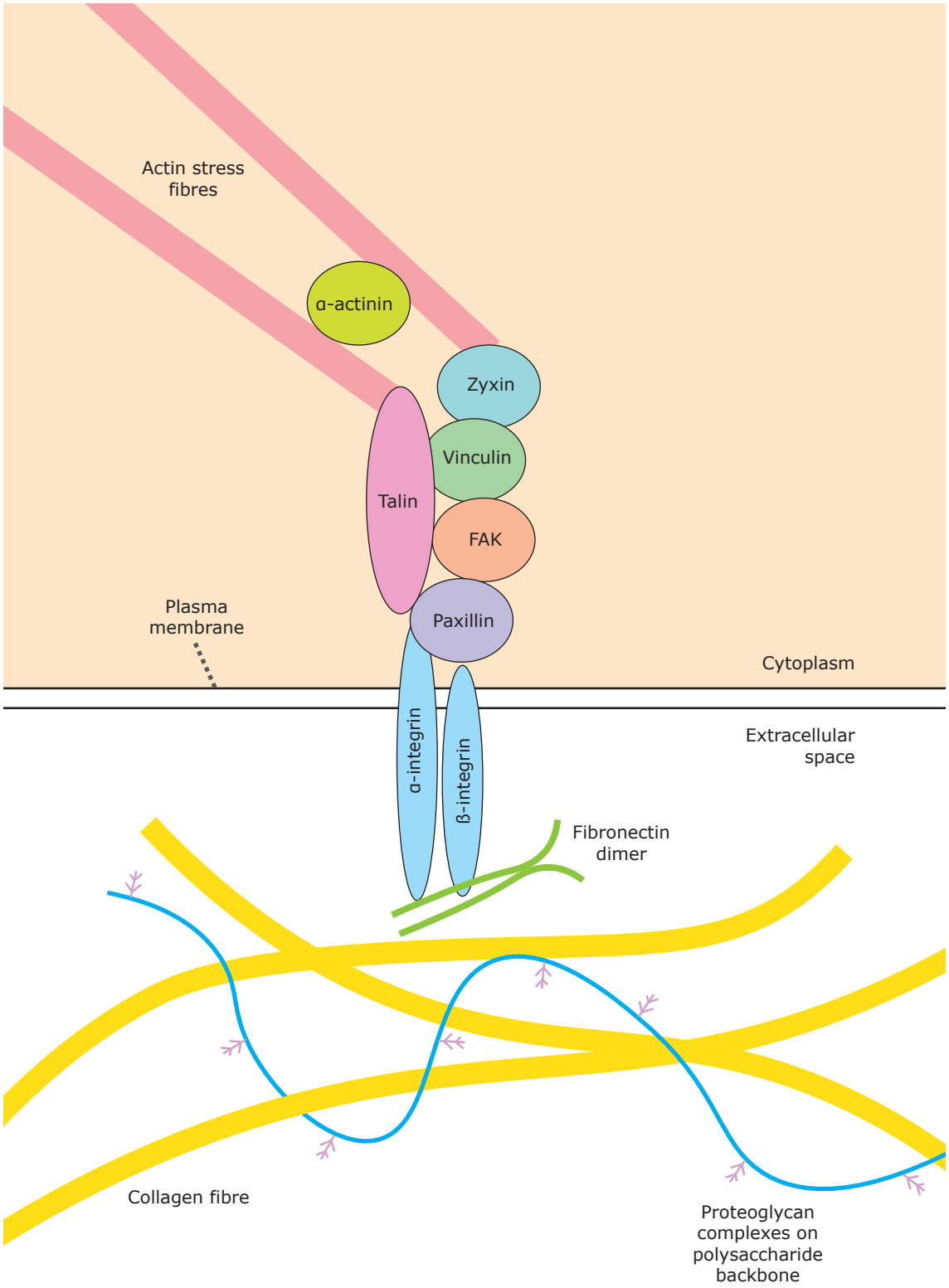

Figure 1.6: Structure of the focal adhesion complex and the ECM. Only the core components of the FA and the most prominent components of the ECM are shown.

and the extracellular ligand, as well as serving as a mechanosensor, typically by increasing adhesion protein recruitment in response to increased tension, and disassembly in response to decreased tension (Xu *et al*, 2012; Wehrle-Haller, 2012).

Other adhesion structures exist, such as adherens junctions, desmosomes, and hemidesmosomes. While all the adhesion structures are functionally distinct, they have structural similarities and some shared protein components (Yeatman, 2004), suggesting some shared regulation.

Adhesions are essential for the migration of cells on a 2D surface, as they represent the points of attachment through which cells exert tractional forces on the substrate. While this is well-established for cells migrating on a 2D surface, the importance of adhesions for cells undergoing amoeboid migration in 3D gels – generally a more physiologically relevant model – is more controversial. Amoeboid migration has been described as adhesion-independent (Harunaga & Yamada, 2011). However, Nagano *et al* (2010) proposed, based on the importance of adhesion proteins for amoeboid migration, that adhesions were present but too small and/or transient to be easily visualised. Subsequently, Kubow & Horwitz (2011), by further refining imaging conditions, were able to visualise paxillin-containing adhesions forming at cell-substrate interfaces in cells migrating in 3D gels, providing evidence that the focal adhesion complex is not an artefact of 2D migration, but is indeed employed by cells under physiological conditions.

1.2.2 Focal adhesion morphology

Focal adhesions (FAs) are protein complexes that assemble at the plasma membrane, where they form physical links between the extracellular matrix

(ECM) and the cytoskeleton. The major component of FAs which mediate attachment to the ECM are the integrins.

Integrins

The integrins are a family of transmembrane proteins that mediate adhesion and signalling between a cell and the extracellular matrix (Barczyk *et al*, 2010), as well as directly between cells in some situations, especially in the immunological synapse where a T cell makes adhesive contact with an antigen-presenting cell as part of the immune response (Hynes, 1992; Dustin, 2002). Integrins are expressed on many cell types, and any one cell will generally express multiple integrins (Hynes, 1992).

Together with other core components of the adhesion complex, integrins originated prior to the divergence of the opisthokonts and therefore ancestrally to the metazoans (and to the fungi and choanoflagellates, although they have been lost from those lineages) (Sebé-Pedrós *et al*, 2010). Integrins are found in all multicellular animals, and through gene duplication, appear to have evolved alongside complex body plans to fulfil the increasing need for control of cell positioning by adherence and migration both during development and regeneration (Johnson *et al*, 2009).

Integrins form heterodimers involving one α- and one β-integrin. Both subunits are transmembrane proteins with a large region extending into the extracellular space. Most vertebrates, including humans, have a consistent number of conserved integrin genes (18 α- and 8 β-integrins), which associate (through non-covalent interactions) into 24 integrin dimers (Barczyk *et al*, 2010; Hynes, 2002). The limited number of known integrin dimers implies highly specific dimerisation: if α- and β-integrins could bind one another indiscriminately, there

would be 144 such dimers. In contrast, many integrins bind exclusively to one partner; β1-integrin is the most prolific, binding to 11 of the 18 α-integrins.

Some integrins have tightly limited distribution and a restricted set of binding partners, and thus are probably specialised for few or single functions. For example, the expression of αEβ7 integrin is near exclusive to T lymphocytes in mucosal tissue (Kilshaw, 1999), and it has only two known ligands: E-cadherin, an adhesion receptor present on epithelial cells, and mucosal addressin cell adhesion molecule 1 (MAdCAM-1), which is expressed predominantly in mucosal tissue at endothelial sites of leukocyte extravasation (Humphries *et al*, 2006; Shyjan *et al*, 1996). This integrin, therefore, appears to be highly specialised for a role in leukocyte extravasation, the process that allows leukocytes circulating in the vasculature to exit into neighbouring tissues at sites requiring an immune response. Most integrins, however, have more widespread functionality.

The major ligands of integrins are extracellular matrix (ECM) components. A number of integrins recognise and bind to the common RGD amino acid sequence found in ECM components including fibronectin and vitronectin (Pierschbacher & Ruoslahti, 1984; Ruoslahti & Pierschbacher, 1986; Pytela *et al*, 1987; Cherny *et al*, 1993), which are widely distributed in the body. Others recognise laminins, collagens (often via the GFOGER motif (Knight *et al*, 1998, 2000; Xu *et al*, 2000)), minor basement membrane components, or are involved in the immune response and so recognise cell-surface ligands instead of ECM components (LeBleu *et al*, 2007; Timpl *et al*, 1979).

Focal adhesions

Focal adhesions (FAs) were first described by Abercrombie *et al* (1971), who observed them as close associations between the cell edge and the substratum in electron micrographs of migrating fibroblasts.

A single focal adhesion is a large linked complex involving many integrins and other components. Focal adhesion formation can be initiated when cell-surface integrins interact with extracellular ligands or are activated by signalling molecules. The integrins form clusters in the plasma membrane and recruit other adhesion components. Among the integrins, those dimers containing β1 and β3 in particular are predominant in focal adhesions, whereas others, such as the leukocyte-specific integrins, or otherwise specialised integrins such as β4 and β5, are not usually found in FAs (Petit & Thiery, 2000). Early, small cell-matrix adhesions are termed focal complexes, whereas more mature adhesions may be called focal contacts, adhesion plaques, or if elongated, fibrillar adhesions (Riveline *et al*, 2001; Geiger & Bershadsky, 2001).

Active disassembly is required for FA turnover, especially in situations such as the rear of migrating cells. In such cells, many (~80%) of the integrins are physically broken free of the cell and the cytoskeleton, and left behind attached to the substratum as the cell moves forward. The remainder are taken up into vesicles and recycled (Palecek *et al*, 1996; Petit & Thiery, 2000).

1.2.3 The extracellular matrix

The extracellular matrix (ECM), present in all animals, is a complex, multifunctional structure that surrounds, protects, and supports cells. The ECM was once viewed as an inert scaffold with purely structural functions. In fact, the ECM is a dynamic structure that has many roles in development and tissue

maintenance. As well as providing a substrate for adhesion, components of the ECM are ligands for signalling interactions, and the ECM serves as a reservoir for growth factors, holding them in position and making them available for detection by cells (Singh *et al*, 2010).

The ECM is a diverse structure composed of multiple protein networks as well as proteoglycans and other molecules (Schaefer & Schaefer, 2010; Hynes, 2009) (Figure 1.6). A brief review of the major ECM proteins follows.

Collagen

Collagen is the major component of the ECM in most tissues. It is the most abundant of all proteins in the metazoa, and the most abundant protein on Earth (Buehler, 2006). (The plant biopolymers cellulose and lignin are more abundant, but are not classed as proteins). In the human body, collagen makes up one third of the protein content by mass (Shoulders & Raines, 2009). Twenty-eight collagens encoded by different genes have been identified so far; most recently collagen XXVIII was described by Veit *et al* (2006). Splice variants further expand the diversity of the collagen ECM: for example, Collagen IV has 6 identified isoforms (LeBleu *et al*, 2007).

The procollagen precursor has a characteristic repeating amino acid motif gly-pro-x, where x can be any amino acid. This gives rise to a triple helical structure. Different types of collagen are mainly defined by interruptions to this triple helix (Pauling & Corey, 1951; Shoulders & Raines, 2009).

Among the collagen types, the major distinction is between fibrillar and non-fibrillar collagens. Collagens I, II and III, which make up 80-90% of all collagen in the body, are the major fibrillar collagens (Buehler, 2006). Fibrillar collagens are assembled from their triple-helical base units into fibrils, and then into fibres.

The non-fibrillar collagens have a number of different forms, including sheets; some serve to cross-link fibrillar collagens (Shoulders & Raines, 2009). Procollagens are assembled into macromolecules (probably in the ER prior to secretion), then fibrils and fibres are formed in the extracellular space (Canty & Kadler, 2002).

Fibrillar collagens form a network throughout the ECM that provides its main source of mechanical strength, especially against stretching forces. For example, tendons, connective tissue structures specialised for withstanding tension, contain a highly organised array of collagen fibres (Canty & Kadler, 2002). Defects in collagen formation lead to serious disease even after completion of development: for example, the major symptoms of scurvy are due to reduced ability to properly assemble collagen (Peterkofsky, 1991).

Fibronectin

Fibronectin (FN) is a ubiquitous fibrillar ECM glycoprotein, present in all tissues at all stages of life. It is encoded by a single gene, yielding an ~8 Kb mRNA transcript. Isoforms are generated by alternative splicing – in humans, 20 FN isoforms have been identified (Singh *et al*, 2010).

FN molecules associate at their C-termini to form a dimer shaped like a wishbone, or a pair of tongs. The molecule contains many binding domains, including domains for binding other FN molecules , other ECM components such as collagen, and an RGD domain that binds to the cell surface via certain RGD-binding integrins; most prominently α5β1 integrin, but also αvβ3 and αvβ6 integrins (Busk *et al*, 1992; Danen *et al*, 2002; Singh *et al*, 2010; Hynes, 1992). These binding activities are essential for the assembly of the FN network and its connection to the rest of the ECM.

FN assembly is a cell-mediated process (McDonald, 1988). Initially, a FN dimer is secreted into the extracellular space and then binds to a cell-surface integrin. This initiates interaction with other extracellular FN dimers via the N-terminal assembly domain. Subsequent changes in conformation expose yet more FN binding sites. Eventually, FN assembles into fibrils that form both linear and branched networks in the intercellular space, allowing FN to serve as a structural network in its own right (Singh *et al*, 2010), and as an intermediate that promotes the assembly of collagen networks and links those networks to cells (Velling *et al*, 2002). The FN matrix is physically flexible in comparison to other ECM networks (Zamir *et al*, 2000).

Early fibroblast cultures show thin FN fibrils; later cultures with a more mature ECM have clustered bundles of FN fibrils. FN is ubiquitous, but levels can vary to some extent: for example, an increased level of FN is found around the neural tube during development (Martins-Green & Tokuyasu, 1988; George *et al*, 1993). Mice without fibronectin exhibit neural tube deformation and fail to complete embryogenesis (George *et al*, 1993).

FN is also found in a soluble form, as a component of blood that is important in the clotting response. Soluble FN does not form fibrils, even at high concentrations, until activated by interaction with integrins (Singh *et al*, 2010; Wierzbicka-Patynowski & Schwarzbauer, 2003; Schwarzbauer & Sechler, 1999).

Laminin

Laminin was first isolated by Timpl *et al* (1979). While basal metazoans such as *Hydra* have only one laminin, most species have many laminin isoforms with typically high similarity in all but a few protein domains (Domogatskaya *et al*,

2012). Laminins assemble into a cruciform heterotrimer, which then makes further connections to assemble an ECM network. It has no RGD binding sites, but possesses a non-RGD integrin-binding domain which is recognised by laminin-specific integrins (Tryggvason, 1993).

Organisation of the ECM

There are two major types of ECM: **interstitial matrix** and **basement membrane**.

The interstitial matrix, or stroma, is the major form of ECM which surrounds cells in many tissues, and predominates in connective tissues. It is diverse, but typically contains high levels of collagens I, II, and III, as well as the ubiquitous fibronectin, alongside many other components (Hynes, 2009; McDonald, 1988).

The basement membrane (BM), or basal lamina, is a specialised sheet of ECM that underlies and supports epithelia (Singh *et al*, 2010). Its major components are laminin, nidogen/entactin, perlecan, and collagens IV(LeBleu *et al*, 2007), XV, and XVIII (Hynes, 2009). This core set, or "toolkit", of BM components is present in all sequenced metazoans, and were likely essential to the evolution of multi-layered body plans in the animals (Hynes, 2009; Whittaker *et al*, 2006). Collagen IV is the major collagen in BMs, and is not normally found elsewhere at significant concentrations (Whittaker *et al*, 2006), though it can accumulate in the interstitial matrix of fibrotic tissue (Vleming *et al*, 1995; Sharma *et al*, 1993). Every BM contains at least one laminin type, with the type(s) present being a major determining factor in the properties of the BM (Aumailley, 2013).

The BM is formed by a self-assembling scaffold comprised of a collagen IV suprastructure and a network of polymerised laminin. Nidogen/entactin and

perlecans form stabilising bridges between these two structures (LeBleu *et al*, 2007).

One of the major functions of epithelia is to block free diffusion of molecules. The BM is not responsible for this function; the BM itself is highly permeable (Loewenstein & Kanno, 1964). Instead, the epithelial cell layer forms “tight” (or “occluding”) junctions to establish the barrier to diffusion (Madara & Dharmsathaphorn, 1985).

The ECM in development

Most cells are in continuous close contact with the ECM facilitated by adhesions. The ECM’s composition varies dramatically between different tissues; these serve as cues for cells to determine their position with the body, and thus how they should develop. The signals conveyed by the ECM are able to control cell survival, proliferation, differentiation, polarity, and migration (Nelson & Bissell, 2006; Roskelley *et al*, 1995; Lukashev & Werb, 1998).

ECM components are secreted and assembled from a very early stage in embryogenesis (Rozario & DeSimone, 2010). This initial assembly of the ECM is still not a completely understood process, but incorrect or delayed ECM assembly is involved in diseases including fibrosis (overproduction of ECM), tumorigenesis, skeletal malformations and a range of birth defects (Singh *et al*, 2010).

The ECM is a major orchestrator of CNS development (Sobeih & Corfas, 2002), and ECM remodelling in the brain may be involved in memory consolidation (Wright *et al*, 2002).

Mechanical forces transmitted through the ECM activate cellular mechanotransduction pathways, influencing cytoskeletal architecture and gene

expression (Jahed *et al*, 2014). This influences cellular dynamics but also feeds back into the maintenance of ECM homeostasis through integrin signalling (Humphrey *et al*, 2014).

1.3 Meckel-Gruber syndrome

1.3.1 MKS clinical presentation and genetics

The focus of this thesis is the ciliopathy termed Meckel-Gruber syndrome, or Meckel syndrome (MKS; MIM 249000). MKS is an autosomally recessive heritable human disease universally lethal to patients, in whom death typically occurs before or shortly after birth (Alexiev *et al*, 2006). Incidence varies; MKS is relatively rare in Great Britain (1 in 140 000 births) (Seller, 1978) and uncommon in the general European population (1 in 39 000) (Barisic *et al*, 2015) but more common in North African (1 in 3500), Belgian (1 in 3000), and Finnish (1 in 9000) populations (Salonen *et al*, 1984b; Roume *et al*, 1997; Salonen *et al*, 1984a; Chen, 2006; Myageri *et al*, 2013), though these figures may be distorted by differential diagnosis across different healthcare systems. As is generally the case for recessively inheritable diseases, a family history of consanguinity is often linked to incidence of MKS (Szymanska *et al*, 2012; Modell & Darr, 2002).

MKS has variable presentation in patients, but is often characterised by a triad of symptoms as originally described by Meckel: kidney cystic dysplasia (100% of patients), occipital encephalocele (90%), and polydactyly (80%) (Salonen *et al*, 1984b; Salonen & Paavola, 1998). Symptoms such as liver fibrosis, fibrotic alterations to other organs, cleft palate and other midline defects, heart defects, defects of the eye, and various malformations of the central nervous system (CNS) are also often present and may contribute to a diagnosis of MKS

(Salonen *et al*, 1984b; Salonen & Paavola, 1998). Salonen *et al* (1984a) replaced polydactyly in the diagnostic triad with liver fibrosis, but this has not been universally followed by other authors.

MKS exhibits a combination of most of the symptoms found in other ciliopathies, making it one of the most severe (Table 1.1). Symptoms such as obesity and deafness are common in other ciliopathies but are not reported for MKS. However, early lethality is universal in MKS; typically the proximal cause of death is pulmonary hypoplasia (Ramachandran *et al*, 2006; Eckmann-Scholz *et al*, 2012; Alexiev *et al*, 2006; Ickowicz *et al*, 2006). This early lethality would mask the presentation of late-onset symptoms, so the phenotypic overlap represented in Table 1.1 may underrepresent the true underlying similarity between these syndromes.

To date, 14 genes have been identified (Table 1.2) in which mutations are causative for MKS. Three more (C5orf42, EVC2, and SEC8/EXOC4) are proposed as likely candidates on the basis of mutation analysis and exome sequencing (Shaheen *et al*, 2013b), but have not yet been confirmed outside the original study. *TMEM67* (*MKS3*) and *TMEM216* (*MKS2*) are the focus of this thesis and will be discussed in more depth below (see sections 1.3.4 and 1.3.5).

MKS locus	Gene name(s)	Protein name(s)	Expression pattern (if reported)	Reference for identification as an MKS gene
MKS1	*MKS1, BBS13*	**MKS1**		(Kyttälä *et al*, 2006)
MKS2	*TMEM216, JBTS2, CORS2*	**TMEM216 / MKS2**	CNS, limb bud, kidney, cartilage(Valente *et al*, 2010)	(Edvardson *et al*, 2010; Valente *et al*, 2010)
MKS3	*TMEM67, JBTS6, NPHP11*	**TMEM67 / MKS3 / Meckelin**	CNS, limb bud, cartilage, intestine, stomach, kidney(Dawe *et al*, 2007b)	(Smith *et al*, 2006)
MKS4	*CEP290, KIAA0373, 3H11AG, JBTS5, SLSN6, LCA10, BBS14, NPHP6*	**CEP290**		(Baala *et al*, 2007a)
MKS5	*RPGRIP1L, KIAA1005, JBTS7, NPHP8*	**RPGRIP1L / Fantom**		(Delous *et al*, 2007)
MKS6	*CC2D2A, KIAA1345*	**CC2D2A**	Expressed strongly in prostate, pancreas, kidney, lung, liver, retina, fetal brain, fetal kidney(Gorden *et al*, 2008)	(Tallila *et al*, 2008; Noor *et al*, 2008)
MKS7	*NPHP3, NPH3, RHPD, KIAA2000*	**Nephrocystin-3**	Very low expression in brain and lung(Wright *et al*, 2011)	(Bergmann *et al*, 2008)
MKS8	*TCTN2, TECT2*	**Tectonic 2**		(Shaheen *et al*, 2011)
MKS9	*B9D1, MKSR1*	**B9 domain-containing protein 1 (B9D1).**		(Hopp *et al*, 2011)
MKS10	*B9D2, MKSR2*	**B9 domain-containing protein 2 (B9D2).**		(Dowdle *et al*, 2011)
MKS11	*JBTS20*	**TMEM231**		(Shaheen *et al*, 2013a)
MKS12	*KIF14*	**KIF14**		(Filges *et al*, 2014)
MKS13	*TMEM107*	**TMEM107**		(Shaheen *et al*, 2015)
	CSPP1	**Centrosome spindle pole-associated protein 1**		(Shaheen *et al*, 2014)

Table 1.2: MKS genes identified so far (UniProt Consortium, 2013; Hamosh *et al*, 2005)

1.3.2 Cell biology of MKS

Ciliogenesis in ciliopathies

The first stage of ciliogenesis is the migration of the centrosome to the apical cell surface in order to become the basal body; in the absence of a docked basal body the cilium cannot form. While this process is not well-understood, there is ample evidence that MKS proteins and other ciliopathy proteins are required. In mice, basal body docking and ciliogenesis are prevented by knockdown of *Mks1* (Dawe *et al*, 2007b), *Mks2* (Valente *et al*, 2010), or *Mks3* (Dawe *et al*, 2007b). Similar phenotypes are seen in human cells: functional MKS1 and TMEM67 (MKS3) are required for docking and ciliogenesis (Dawe *et al*, 2007b), and *TMEM216* (*MKS2*) mutations cause failure of ciliogenesis (Lee *et al*, 2012) However, a study in *Mks1*^{krc} mice, which are reported to abolish *Mks1* at the transcript level, did not reproduce the failed ciliogenesis phenotype (Weatherbee *et al*, 2009). Similary, *wpk* (*TMEM67* orthologue) rats did not show a ciliogenesis defect, though they did have altered cilium and flagellum lengths (Tammachote *et al*, 2009). These may be results peculiar to the models, or may indicate an alternate pathway to ciliogenesis that is activated under certain conditions. (See Table 1.3 for a list of published MKS models and their phenotypic presentation.)

In the case of *TMEM216*, defective ciliogenesis is accompanied by, and likely a consequence of, blocked centrosome docking (Valente *et al*, 2010) and hyperactivation of RhoA, an actin regulator; inhibition of Rho rescued the centrosome docking defect (Valente *et al*, 2010), suggesting that Rho hyperactivation is upstream of ciliary dysfunction in TMEM216-deficient cells.

These defects have many commonalities with non-MKS ciliopathies. An example of a non-MKS gene which abolishes ciliation when mutated or knocked

down is *TALPID3. TALPID3* orthologues in mouse (Yin *et al*, 2009), chick (Davey *et al*, 2006), and zebrafish (Ben *et al*, 2011) models are implicated in pathologies including limb patterning and neural tube defects (Davey *et al*, 2006; Bangs *et al*, 2011), and indeed *TALPID3* mutations cause severe disease in humans with symptoms including short-rib polydactyly and abnormal neural tube dorsoventral patterning (Alby *et al*, 2015; Stephen *et al*, 2015; Malicdan *et al*, 2015), often leading to a JBTS diagnosis, but not to MKS: retinal, renal, and liver defects are not reported (Bachmann- Gagescu *et al*, 2015; Hamosh *et al*, 2005). TALPID3 orthologues localise to the centrosome and are essential for ciliogenesis in all these organisms (Yin *et al*, 2009; Bangs *et al*, 2011; Ben *et al*, 2011). In mice Talpid3 has been shown to be essential for basal body docking (Bangs *et al*, 2011; Yin *et al*, 2009), suggesting failure of docking may be at the root of *TALPID3* ciliogenesis phenotypes, as is suspected for MKS. This raises the question: why does *TALPID3* mutation not cause all the symptoms seen in MKS, if it has the same effect on ciliation? Non-ciliary roles for MKS proteins would provide a possible explanation.

Docking failure is not always implicated in ciliogenesis defects, however. TCTN1, a JBTS protein, is not required for docking but is required for ciliogenesis in some tissues (Garcia-Gonzalo *et al*, 2011). This suggests that ciliogenesis is regulated in a tissue-specific manner; since most studies investigate only one or a few tissues, the true complexity of this regulation may not yet be clear. Another example is *Ofd1* (a protein associated with the ciliopathy orofaciodigital syndrome, OFD), a component of the centriole responsible for control of centriole length; in its absence, centrioles are abnormally elongated and defective in IFT protein recruitment, and ciliogenesis is impaired (Singla *et al*, 2010). After centrosome docking, correct ciliary protein

import via IFT is the next function required to correctly assemble a cilium, so in general, ciliogenesis defects not accompanied by docking failure are probably due to defective import, either due to defective IFT or defective recruitment of IFT and cargo to the ciliary base.

Cilium length control

The length of a cilium results from balanced assembly and disassembly depending on balanced anterograde and retrograde IFT. Disruption of ciliary import or IFT would be expected to result in shortened cilia as this balance is perturbed. This shortening has been reported for TMEM67: *TMEM67/MKS3* knockdown causes shortening and loss of cilia in mouse and human cells (Dawe *et al*, 2007b) and *Paramecium* (Picariello *et al*, 2014). However, some results do not agree with these findings. *Wpk* is the rat orthologue of *TMEM67*. *Wpk* rat spermatids have shortened flagella, but in renal collecting duct cysts, cilia are elongated (Tammachote *et al*, 2009). In the same study, *TMEM67* patient cells were found to have longer cilia. This appears to contradict the result obtained by Dawe *et al* (2007b), but the results were obtained under different conditions so are not directly comparable. *C. elegans* mks-3 mutants also show lengthened cilia (Williams *et al*, 2010). It can be concluded that TMEM67 has a role in cilium length control, but one that is complex and not fully understood. Given that the ciliary TZ is implicated in cilium length control (Roberson *et al*, 2015), this may be tied to TMEM67's role in the TZ complex.

Beyond MKS, other ciliopathy proteins influence cilium length; for example, BBS proteins have been reported to do so via alteration of RhoA levels, which leads to disruption of the actin cytoskeleton, including disruption of stress fibres (contractile actin bundles that provide intracellular tension and are important in

migration and adhesion) (Hernandez-Hernandez *et al*, 2013). However, these ciliopathy proteins are also associated with the TZ.

Transition zone

As described above (section 1.1.4), ciliary compartmentalisation is critical for ciliary signalling, and the barrier responsible for maintaining ciliary compartmentalisation is in the region of the cilium near the base, termed the ciliary transition zone (TZ). Proper cilium function depends on the TZ (Czarnecki & Shah, 2012; Reiter *et al*, 2012). A large number of ciliopathy proteins, including TMEM67 and TMEM216, have been found to localise to the TZ (Dawe *et al*, 2007b; Lee *et al*, 2012; Klinger *et al*, 2013; Gorden *et al*, 2008; Sang *et al*, 2011; Wright *et al*, 2011; Bialas *et al*, 2009; Chih *et al*, 2012; Fliegauf *et al*, 2006), many of them in a network of physically interacting proteins (Figure 1.7) (Garcia-Gonzalo *et al*, 2011). This network is composed of two functional modules; one “NPHP module” containing proteins mainly implicated in NPHP (Figure 1.7, orange), the other an “MKS module” containing MKS and JBTS proteins (Figure 1.7, green) (Chih *et al*, 2012; Garcia-Gonzalo & Reiter, 2012; Garcia-Gonzalo *et al*, 2011).

As mentioned before, the TZ contains structures called “Y-links”, based on their Y-shaped appearance under electron microscopy (Figure 1.3), which link the axonemal microtubules to the surrounding membrane, and have been proposed to be involved in the barrier function of the TZ (Williams *et al*, 2011). This is supported by studies in *Chlamydomonas CEP290* (*MKS4*) mutants and *C. elegans* mutants which lack Y-links: proteins fail to accumulate in the ciliary membrane (Craige *et al*, 2010; Garcia-Gonzalo *et al*, 2011), suggesting that these structures are at least partly responsible for the diffusion barrier. The composition of the Y-links is unknown, but it is suspected to involve the TZ

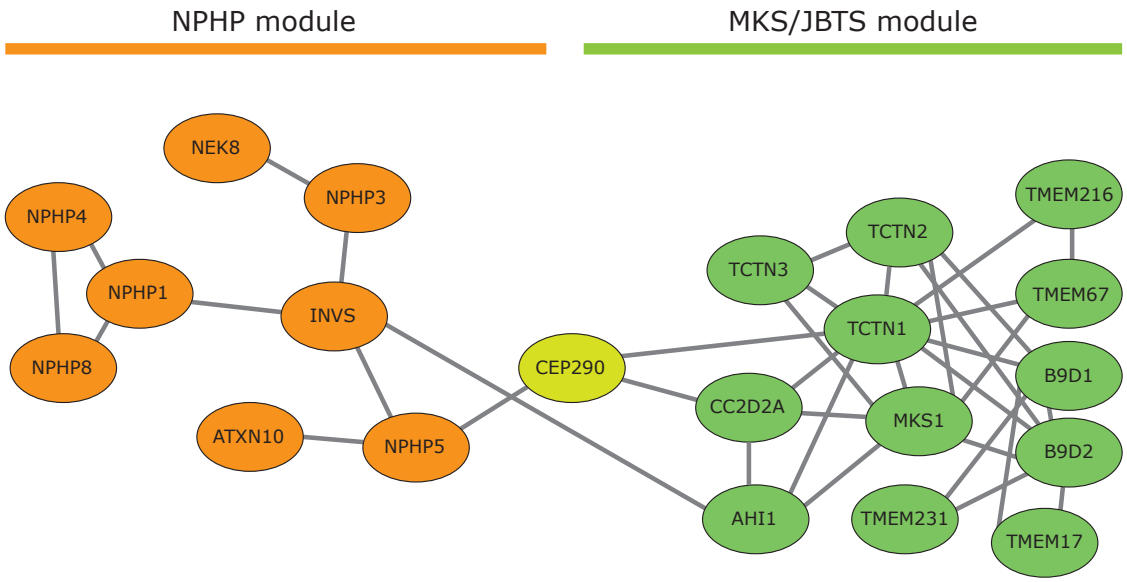

Figure 1.7: The transition zone protein network. The network comprises two modules, one made up predominantly of NPHP proteins (orange), the other of MKS and JBTS proteins (green), including TMEM67 and TMEM216. The two networks are linked through the MKS/JBTS protein CEP290 (light green), as well as through an Inversin/AHI1 interaction. Grey lines indicate evidence for direct interaction. Data from Garcia-Gonzalo & Reiter (2012).

complex of ciliopathy proteins. In this model, the transmembrane proteins such as TMEM67 and TMEM216 would be at the ends of the Y-links where they interact with the membrane, consistent with the predicted structure of the complex Figure 1.7).

Evidence for the spatial relationships between ciliopathy proteins within the TZ has been mainly obtained by super-resolution imaging (Yang *et al*, 2015; Pratt *et al*, 2016). Yang *et al* showed that the human ciliary TZ contains at least two regions with different protein compositions: RPGRIP1L and MKS1 are found in a distal band and CEP290 in a more proximal band (closer to the basal body) within the TZ (Yang *et al*, 2015). Based on this, Yang *et al* propose that the RPGRIP1L/MKS1 band may serve as a recruitment or storage site for TMEM67 and TCTN2, which they found to be present at a similar axial level (on the proximal-distal axis from the base to the tip of the cilium) but a distinct radial position: while RPGRIP1 is localised close to the microtubules at the TZ core, TMEM67 and TCTN2 are close to the ciliary membrane (and ciliary necklace), consistent with the transmembrane anchoring role proposed for these proteins (Yang *et al*, 2015), suggesting they may be components of the membrane-associated outer ends of the Y-links. MKS1 is found in between (Yang *et al*, 2015) and may serve as a bridge between the membrane-associated and MT-associated parts of the complex. Pratt *et al* found that deletion of an N-terminal region of *Mks1* in *Drosophila* abolished TZ localisation of MKS protein orthologues B9D1, B9D2, TMEM216, CC2D2, and Tectonic, but did not affect localisation of CEP290 (Pratt *et al*, 2016), suggesting that MKS1 is critical for recruiting MKS module proteins to the TZ. Furthermore, deletion of *B9D1* also led to abolishment of TZ localisation of MKS1 and B9D2 (and, while not specifically shown, presumably loss of the other proteins dependent on MKS1

for recruitment) (Pratt *et al*, 2016), indicating that the MKS module is interdependent; loss of any one component may disrupt recruitment of the entire complex. These results also suggest that CEP290, while an MKS protein, is not involved in the MKS module (Figure 1.7) but in a separate CEP290 module, which has been proposed to work partially redundantly with the NPHP and MKS modules to organise the TZ (Basiri *et al*, 2014; Schouteden *et al*, 2015; Williams *et al*, 2011).

If ciliopathy proteins are indeed partially redundant components of the Y-links, and the Y-links are essential for ciliary compartmentalisation, then much of the overlapping phenotypic presentation observed in ciliopathy patients can be explained as the result of partial disruption of the Y-link complex leading to failure to control levels of developmental signalling molecules in the cilium, and thus to aberrant developmental signalling. The different severities and symptoms resulting from different mutations would thus represent different degrees of compromised barrier function.

Evidence for non-ciliary phenotypes in MKS

As noted above, there is a growing body of evidence that many ciliopathy proteins have functions not localised to cilia. Within the MKS proteins, TMEM67 is known to interact with filamin A, an actin regulatory protein, and localises to the actin cytoskeleton as well as the cell surface in polarised cells (Dawe *et al*, 2007b, 2009; Adams *et al*, 2012).

Alterations in cell migration can result from absence of ciliopathy proteins; in Inversin (Nephrocystin-2) deficient mouse cells migration is perturbed (Veland *et al*, 2013), potentially downstream of Wnt. In BBS, neural crest cell migration is perturbed leading to developmental abnormalities including mid-facial

hypoplasia and hypognathia (reduced jaw size) (Tobin *et al*, 2008). Since adhesions and the actin cytoskeleton are closely interlinked, and both are central to migration, the alterations in these structures seen frequently in ciliopathies may be at the root of migration defects. An example of such a defect in MKS patients may be occipital encephalocele, which results from failure to close the neural tube during early CNS development. MKS is the most common cause of neural tube defects (Leitch *et al*, 2008), which across all causes affect approximately 1 in 1000 births (Juriloff & Harris, 2000). Closure of the neural tube is a PCP (non-canonical Wnt) signalling dependent process (Wallingford *et al*, 2002; Hamblet *et al*, 2002; Murdoch *et al*, 2014; Juriloff & Harris, 2012; Ybot-Gonzalez *et al*, 2007; Murdoch *et al*, 2001, 2003; Curtin *et al*, 2003; Robinson *et al*, 2012) involving directed mass cell migration by convergent extension, during which cell adhesion is key (Pyrgaki *et al*, 2011; Suzuki *et al*, 2012).

1.3.3 MKS model organism studies

A large number of studies have been published that investigate phenotypes associated with MKS gene homologues in other species. A full review of this work is beyond the scope of this thesis, but the results of these studies are summarised in Table 1.3.

Human gene	Model species	Homologous gene	Alteration + ref	Cellular phenotypes	Developmental phenotypes
MKS1	Mouse	Mks1	Loss of function (Weatherbee *et al*, 2009)	No alteration to BB positioning. Defective ciliation in most tissues. Altered Hh signalling.	Defects in neural tube, biliary duct, limb patterning, skeletal development, kidney.

Human gene	Model species	Homologous gene	Alteration + ref	Cellular phenotypes	Developmental phenotypes
MKS1	*C. elegans*	mks1	B9 domain disrupted (Bialas *et al*, 2009)	No ciliary structural defects. Mislocalisation of MKS1, MKSR1, MKSR2.	Altered insulin signalling led to increased lifespan.
MKS1	*Drosophila melanogaster*	*Mks1*	Deletion of N-terminal region (Pratt *et al*, 2016)	Abolished TZ localisation of B9D1, B9D2, TMEM216, CC2D2, Tectonic. Did not affect localisation of CEP290. Cilium defects in early pupae, but cilia normal at later stage. Shortened spermatocyte axonemes. Subtle perturbation of IFT.	Mutants are viable and fertile. No apparent effect on sensory cilia function.
B9D1	*Drosophila melanogaster*	*B9D1*	Deletion (Pratt *et al*, 2016)	Abolished TZ localisation of MKS1, B9D2.	Mutants are viable and fertile. No apparent effect on sensory cilia function.
TMEM67	Rat	Wpk	Missense (Smith *et al*, 2006; Tammachote *et al*, 2009)	Shortened spermatid flagella Elongated liver ductal cilia	Cystic kidney. Corpus callosum agenesis. Hydrocephalus. Retinal defects.
TMEM67	Mouse	Tmem67	Null (Garcia-Gonzalo *et al*, 2011)	Reduced cilia number in kidney tubules	Survived to birth but died soon after.

Human gene	Model species	Homologous gene	Alteration + ref	Cellular phenotypes	Developmental phenotypes
TMEM67	Mouse	Tmem67	Knockout (Abdelhamed *et al*, 2013)	Loss of primary cilia Diminished Shh signalling Deregulated Wnt. Hyperactive DVL1 at BB.	Exencephaly and encephalocele. Neural tube dorsalisation.
TMEM67	Zebrafish	Mks3	Knockdown (Adams *et al*, 2012)	Basal body positioning disrupted Impaired ciliogenesis in neuroepithelium	Axis defects. Cardiac edema. Auditory and eye defects.
TMEM67	*Parameciu m tetraurelia*	*MKS3*	Knockdown (Picariello, 2015; Picariello *et al*, 2014)	Global shortening and loss of cilia. No effect on BB structure, but alignment disrupted.	
TMEM216	Zebrafish	Tmem216	Knockout (Valente *et al*, 2010)		Gastrulation defects. Body axis shortening. Notochord broadening. Misshapen somites.
TMEM216	Zebrafish	Tmem216	Knockdown (Lee *et al*, 2012)		Pericardial effusion Curved/kinked tail Gastrulation defects. Hydrocephaly.
CEP290	Mouse	Cep290	In-frame deletion (Chang *et al*, 2006)		Retinal degeneration. No CNS or kidney defect.

Human gene	Model species	Homologous gene	Alteration + ref	Cellular phenotypes	Developmental phenotypes
CEP290	Mouse	Cep290	Hypo-morphic mutation (McEwen *et al*, 2007)	Defective ciliary localisation of G proteins Gna1, Gng13	Olfactory dysfunction.
CEP290	Cat	Cep290	SNP causing termination (Menotti-Raymond *et al*, 2007)		Progressive retinal degeneration.
CEP290	Mouse	Cep290	Null (Lancaster *et al*, 2011)		CNS defect: midline fusion
RPGRIP1L	Mouse	Rpgrip1l	Null (Delous *et al*, 2007)		CNS defects including exencephaly, hypoplasia, corpus callosum absence. Eye defects. Cleft lip. Some showed early signs of cystic kidney and liver fibrosis.
RPGRIP1L	Mouse	Rpgrip1l	-/- (Laclef *et al*, 2015)	Neuroepithelia form cilia with no axonemes. Some cells failed to form cilia. Misexpression of guidance molecules. Some symptoms restored by Gli3r.	Ventralisation of telencephalon leading to olfactory defects.
CC2D2A	Zebrafish	Cc2d2a	Null (Gorden *et al*, 2008)	No change in cilium number or morphology.	Cystic kidney. Some had pericardial effusion.

Human gene	Model species	Homologous gene	Alteration + ref	Cellular phenotypes	Developmental phenotypes
CC2D2A	Mouse	Cc2d2a	Null (Garcia-Gonzalo *et al*, 2011)	Cilia defects, but not in embryonic fibroblasts.	Randomised L-R axis. CNS defects. Curved body axis.
NPHP3	Mouse	Nphp3	Substitution in pcy locus (Olbrich *et al*, 2003; Omran *et al*, 2001)	Amenable to treatment with vasopressin-2 receptor antagonist (Gattone *et al*, 2003)	Cystic kidney. Basement membrane defects. Nephropathy.
NPHP3	Mouse	Nphp3	Null (Bergmann *et al*, 2008)		Heterozygotes have no apparent defects, unless heterozygous with pcy. Homozygosity was lethal with lateralisation and *situs* defects.
NPHP3	Zebrafish	Nphp3	Knockdown (Hoff *et al*, 2013)	Common effect with KD of Anks6, Nek8	Cystic kidney. Heart looping defect.
NPHP3	*Xenopus*	Nphp3	Knockdown (Hoff *et al*, 2013)	Common effect with KD of Aks6, Invs	Kidney defect.
TCTN2	Mouse	Tctn2	Null (Garcia-Gonzalo *et al*, 2011)	No nodal cilia. Few, defective neural tube cilia. BB docking normal.	
B9D1	*C. elegans*	mksr1	B9 domain disrupted (Bialas *et al*, 2009)	No ciliary defects. Mislocalisation when disrupted with mks1 and mksr2.	

Human gene	Model species	Homologous gene	Alteration + ref	Cellular phenotypes	Developmental phenotypes
B9D1	Mouse	B9d1	Null (Dowdle *et al*, 2011)	Reduced number of cilia, shortened. Cilia in biliary ducts normal. Nodal cilia absent or defective. BB docking normal but axonemes not built in neural tube. Fibroblasts show normal ciliation, but defective Hh response. TZ complex proteins mislocalised.	Cystic kidney, CNS defects including encephalocele, liver ductal plate malformation; resembles MKS.
B9D1	Mouse	B9d1	Knockout (Chih *et al*, 2012)	Loss of cilia. Altered Shh gene expression.	Lethal. Vascular defects. Polydactyly.
B9D2	Mouse	stumpy	Conditional knockout (Town *et al*, 2008)	Neural and kidney cilia absent or defective.	Hydrocephalus. Cystic kidney.
B9D2	*C. elegans*	mksr2	B9 domain disrupted (Bialas *et al*, 2009)	No ciliary defects. Mislocalisation when disrupted with mks1 and mksr1.	
B9D1	Zebrafish	B9d2	Knockdown (Dowdle *et al*, 2011)	Defects rescued by human B9D2.	Dosage-dependent: Shortened body axes, elongated somites, notochord defects.
JBTS20	Mouse	Tmem231	Knockout (Chih *et al*, 2012)	Loss of cilia. Altered Shh gene expression.	Lethal Vascular defects Polydactyly

Human gene	Model species	Homologous gene	Alteration + ref	Cellular phenotypes	Developmental phenotypes
KIF14	Mouse	Kif14	Laggard (Fujikura *et al*, 2013)	Reduced expression of brain development genes. Increased neural apoptosis.	Growth retardation, Microcephaly. Homozygotes died within 3 weeks of birth with ataxia, tremors.
CSPP1	Zebrafish	cspp1a	Knockdown (Tuz *et al*, 2014)	Cilia appear normal. Reduced ciliary localisation of Arl13b	Curved body axis. Cystic kidney. CNS patterning defects.

Table 1.3: Summary of MKS model studies

This thesis focuses on the MKS genes *TMEM67* (*MKS3*) and *TMEM216* (*MKS2*), which both encode proteins proposed to be involved in the MKS-JBTS module within the ciliary TZ as transmembrane linkers (Figure 1.7) (Garcia-Gonzalo & Reiter, 2012). It is estimated that between them, mutations in these two genes account for over half of MKS cases (Szymanska *et al*, 2012).

1.3.4 TMEM67

TMEM67 was identified in 2006 (Smith *et al*, 2006), and is the most well-studied MKS gene.

Genetics and clinical mutations

TMEM67 is located on chromosome 8 in humans (Smith *et al*, 2006), in a corresponding region to the homologous rat *Wpk* locus, with which it shares >80% sequence identity. In a study of 38 families bearing MKS mutations, 50% of the families had changes to *TMEM67*, indicating that mutations in this gene are the most common cause of MKS (Szymanska *et al*, 2012).

There are multiple disease-causing mutations possible in *TMEM67*, which have variable syndromic presentation: different *TMEM67* mutations have been reported to cause MKS (Smith *et al*, 2006), Joubert syndrome (JBTS) (Baala *et al*, 2007b), Nephronophthisis (NPHP) (Otto *et al*, 2009), and COACH syndrome (Brancati *et al*, 2009). Additionally, one mutation in *TMEM67* was found to be a modifier of Bardet-Biedl syndrome; a zebrafish model showed that this modifier increases probability of gastrulation movement defects when in combination with a mutation in CEP290 (Leitch *et al*, 2008).

Expression and function

TMEM67 has a comparable expression pattern to other ciliopathy proteins. It has two reported major splice variants (UniProt Consortium, 2013), the more prominent of which encodes a protein of 995 amino acids, predicted to contain 7 transmembrane domains. A number of smaller isoforms have also been reported but these have not been characterised (Dawe *et al*, 2007b). It localises to the ciliary membrane, the basal body, basolateral actin cables, the cell surface of polarised cells (Dawe *et al*, 2007b, 2009), and the endoplasmic reticulum, where it is proposed to function in protein degradation (Wang *et al*, 2009). Direct evidence for functional roles outside the cilium and basal body is lacking.

TMEM67 binds at the cytoplasmic C-terminus to filamin A (FLNA) (Adams *et al*, 2012). Loss of either protein leads to alterations in basal body positioning, ciliogenesis, actin organisation, and deregulation of RhoA and Wnt signalling (Adams *et al*, 2012). This indicates that a TMEM67-FLNA complex is involved in Wnt signalling and regulates ciliogenesis, probably by influencing basal body migration or docking. In *C. elegans*, TMEM67, together with other MKS proteins, was found to establish connections between the basal body and TZ

(Williams *et al*, 2011); this process may be important for docking, or it may only be relevant after docking is complete. TMEM67 co-localises with and interacts with the Wnt receptor ROR2 at the TZ, and is required for ROR2 phosphorylation (Abdelhamed *et al*, 2015b), implying that TMEM67 acts as a co-receptor in the Wnt pathway, perhaps influencing its other TZ roles in the MKS/JBTS module and with FLNA.

Genotype/phenotype correlations

The classical diagnostic symptoms of MKS (occipital encephalocele, polydactyly, cystic kidney, and liver fibrosis) may give the false impression that MKS is a single, well defined condition. This is not the case: among the diagnostic symptoms, only occipital encephalocele and cystic kidney are present near-universally in MKS patients (Salonen *et al*, 1984b; Salonen & Paavola, 1998).

Incidence of polydactyly varies depending on genotype: Szymanska *et al* observed polydactyly in only 3 of 19 *TMEM67* patients, a much lower incidence than seen in patients with MKS caused by *RPGRIP1L* or *CC2D2A* mutations (Szymanska *et al*, 2012). Since polydactyly is most easily explained as a consequence of disruption to the Hh signalling pathway, this implies that *TMEM67* mutation is less disruptive to Hh than other MKS mutations. *TMEM67* patients in this sample also exhibited none of the *situs* or intestinal malrotation defects which are seen in other forms of MKS (Szymanska *et al*, 2012). These defects may result from lack of left-right patterning established by cilia during early development, though the aetiology of intestinal malrotation is not well understood (Stringer, 2009). Since *TMEM67* patient cells are defective in ciliogenesis, it is difficult to explain lack of *situs* and malrotation defects in these patients. It may be that defective ciliogenesis is only present in certain cell types

or at certain developmental stages in patients with this genotype, or that other mechanisms of left-right patterning are able to compensate. Left-right patterning exhibits robust error-correcting mechanisms, able to achieve correct axis determination despite serious disruptions such as reversed expression patterns of key genes (McDowell *et al*, 2016). Many of these mechanisms are cilium-independent (reviewed by McDowell *et al* (2016); an example is serotonin asymmetry, which has been shown in *Xenopus* to establish left-right patterning early in development independent of cilia (Vandenberg *et al*, 2013).

In NPHP, liver fibrosis is reported only in patients with *TMEM67* mutations (Otto *et al*, 2009). Since most liver cells do not make cilia (Wheatley, 1995), this implies a non-ciliary role. *TMEM67* MKS patients exhibit increased frequency of liver ductal plate malformation (Szymanska *et al*, 2012), usually caused by arrest of biliary system development as part of the common pattern of fibrotic changes to the liver (Sergi *et al*, 2000; Clotman *et al*, 2008). Bile duct epithelial cells, unlike most liver cells, are ciliated (Masyuk *et al*, 2008), so this does not necessarily require a non-ciliary explanation, but it is still difficult to explain why other MKS genotypes are less correlated with this symptom without invoking non-ciliary roles for TMEM67.

It has been suggested that truncating mutations in *TMEM67* tend to cause MKS, while missense mutations cause less severe phenotypes (Iannicelli *et al*, 2010). This correlation has yet to be systematically verified, but appears to be consistent with the TZ hypothesis for MKS aetiology where the degree of disruption to the TZ complex correlates with the developmental consequences.

1.3.5 TMEM216

TMEM216 was identified more recently than *TMEM67* (Valente *et al*, 2010), and has been the subject of only limited published research thus far.

Genetics and clinical mutations

The *TMEM216* gene is located on chromosome 11 in humans, and is associated with clinical mutations causing MKS2 and Joubert syndrome 2 (JBTS2), both in an autosomally recessive inheritance pattern (Hamosh *et al*, 2005). In a study of 38 families with MKS mutations, only one family had alterations in *TMEM216*, indicating that mutations in this gene are a comparatively rare cause of MKS (Szymanska *et al*, 2012).

Seven distinct mutations in *TMEM216* causing MKS2 have been identified (Valente *et al*, 2010), but these have not been studied in enough detail to make firm conclusions about genotype-phenotype correlations in MKS2.

The R73L mutation, which has a high incidence in individuals of Ashkenazi heritage, is the most common *TMEM216* mutation to cause JBTS2 (Edvardson *et al*, 2010; Hamosh *et al*, 2005). A different mutation in the same codon (R73H) was reported to cause a Joubert-related disorder in one sibling and MKS in another within the same family, implying a very closely related aetiology for the two syndromes. The different patient outcomes despite identical mutations can be assumed to have resulted from interactions with other genetic or environmental factors that have not been identified. Among other symptoms, JBTS2 is associated with CNS, retinal, and renal defects (Edvardson *et al*, 2010), phenotypically overlapping with MKS.

Mutations in *TMEM216* are responsible for approximately half of Joubert syndrome 2 (JBTS2) cases; the remainder, while phenotypically

indistinguishable, are caused by mutations in the neighbouring *TMEM138* gene, which does not display sequence or domain similarity to *TMEM216* but is part of a co-regulated expression module with *TMEM216* that appears to have an evolutionary origin at the amphibian to reptile transition (Venkatesh *et al*, 2012), and has been conserved across the higher vertebrates (Lee *et al*, 2012), though the association was lost in *Xenopus* and zebrafish lineages (Venkatesh *et al*, 2012). Lee *et al* investigated *TMEM138* expression in multiple tissues and found it to parallel that of *TMEM216* (Lee *et al*, 2012), confirming co-expression of the module. This pattern, where adjacent nonparalogous genes form a combined genetic locus with mutations in either gene causing phenotypically identical genetic disorders, is rare but not unique: another example is the cystic kidney disease (ADPKD) caused by mutation in either *PKD1* or *TSC2* (Kleymenova *et al*, 2001). *TMEM138* mutations can also cause OFD(Li *et al*, 2016); two *TMEM216* JBTS 2 patients presented with additional symptoms resembling OFD (Valente *et al*, 2010). Despite this evidence of close genetic association and complementarity of function between *TMEM216* and *TMEM138*, mutations in *TMEM138* have not been reported to cause MKS (Szymanska *et al*, 2014), though this may indicate only that it is an uncommon cause of the phenotype (Szymanska *et al*, 2012). The relevance of *TMEM138* to the pathology of MKS therefore remains unclear, though the protein product localises to the ciliary TZ, where it may form part of the MKS-JBTS module (Li *et al*, 2016) so it is likely to be at least a modifier of ciliopathies that have an aetiology involving TZ complex disruption. The lack of evidence for *TMEM138* involvement in MKS, in contrast to other ciliopathies, may therefore be an indication that TZ disruption is not sufficient to cause MKS.

Expression and function

The human *TMEM216* gene contains multiple exons; authors differ on their interpretation of the sequence data, reporting the presence of 3 (Edvardson *et al*, 2010), 5(Lee *et al*, 2012), or 6 (Valente *et al*, 2010) exons. The gene produces a transcript processed to at least four major splice variants, the longest and most prevalent of which encodes a protein predicted to contain 148 amino acids and four transmembrane domains (Valente *et al*, 2010). In addition to the major variants, alternative splicing produces many very short protein products (Valente *et al*, 2010); the importance of these remains unclear. The expression pattern (Table 1.2) is broadly similar to that of other ciliopathy genes, and the protein localises to the base of the cilium, consistent with the TZ and/or the basal body, as well as to the mitotic spindle (Valente *et al*, 2010), implying an association with the microtubule cytoskeleton. TMEM216 is required for ciliogenesis and for basal body docking to the cell surface (Valente *et al*, 2010).

In *TMEM216* fibroblasts, filamin A localises to actin stress fibres, a localisation pattern not seen in control fibroblasts (Valente *et al*, 2010), implying *TMEM216* regulates the distribution of this important actin-binding protein. When *TMEM216* expression is absent or attenuated, RhoA signalling becomes hyperactivated without an alteration in overall RhoA level (Valente *et al*, 2010). This is similar to the effect of *TMEM67* on RhoA signalling, suggesting that the two proteins function non-redundantly to regulate this pathway. The Dishevelled (Dvl) pathway, responsible for mediation of Rho activation at the apical cell surface required for ciliogenesis, was also altered, with increased phosphorylation of Dvl (Valente *et al*, 2010), and Valente *et al* further suggest

that TMEM216, RhoA, and Dvl may be part of a single complex associated with the centrosome that regulates docking to the cell surface.

1.3.6 Interaction between TMEM67 and TMEM216

The TMEM67 protein physically interacts with TMEM216 to form a complex (Valente *et al*, 2010). It has been proposed that the two function together as a cell surface receptor/coreceptor complex in the non-canonical Wnt pathway (Valente *et al*, 2010), a model made more plausible by the evidence linking TMEM67 to ROR2 in the Wnt pathway (Abdelhamed *et al*, 2015b). Alterations to PCP/RhoA signalling downstream of this receptor activity may be responsible for organising apical actin cytoskeletal remodelling to enable basal body docking to the apical cell surface, and thus initiation of ciliogenesis (Valente *et al*, 2010). RhoA activity has been shown to be required for actin reorganisation during ciliogenesis (Pan *et al*, 2007), and Rho and Dvl are proposed to act together as part of a module of PCP signalling components, required for basal body docking and other ciliary regulatory functions (Park *et al*, 2008), so this signalling role could be an upstream explanation for ciliogenesis defects.

A cell surface receptor role for the TMEM67/TMEM216 complex prior to ciliogenesis would imply plasma membrane localisation, which has been shown for TMEM67 (Dawe *et al*, 2007b, 2009), but not for TMEM216. This may be simply due to the lack of published research on TMEM216.

1.4 Summary and aims

As recently as five years ago, ciliopathy pathologies were thought to stem entirely from ciliary dysfunction. Recent studies have challenged this model: many ciliopathy proteins are now known to have roles away from the cilium in processes including actin organisation and cell adhesion. Adhesions and actin

interact and mutually regulate (Defilippi *et al*, 1999); and the organisation of the actin cytoskeleton is critical for ciliogenesis (Pitaval *et al*, 2010; Boisvieux-Ulrich *et al*, 1990; Boisvieux Ulrich *et al*, 1987; Kim *et al*, 2015, 2010; Klotz *et al*, 1986; Lemullois *et al*, 1988, 1987; Pan *et al*, 2007; Park *et al*, 2008; Yan & Zhu, 2013). It is therefore unclear whether developmental malformations seen in ciliopathy patients are due to signalling defects downstream of cilium defects, or due to defects in other cellular processes such as cytoskeletal organisation, cell migration, and cell adhesion, which are also at the root of ciliogenesis defects.

While much can be said about the genetic basis of MKS and the other ciliopathies, and their clinical presentation in patients, we still know very little about the causal relationships responsible on a cellular and developmental level. While the role of ciliopathy proteins in the ciliary transition zone provides a possible explanation for some patient phenotypes, especially given the importance of the cilium in developmental signalling, it is unsatisfactory to explain all symptoms. The observation of apparently unrelated cellular phenotypes, and roles for ciliopathy proteins outside the cilium that have been recently reported, as well as the findings suggesting MKS proteins act as receptors and are present on the plasma membrane, raise the question: is MKS truly a disease with an entirely ciliary aetiology, or is there a more complex causal relationship involving processes outside the cilium that has yet to be identified?

This thesis will investigate the hypothesis that MKS proteins are involved in the regulation of cell-substrate interaction, which influences cytoskeletal organisation and developmental signalling, and may therefore provide an alternative explanation for MKS patient phenotypes and reveal new therapeutic approaches.

This thesis will demonstrate that the TMEM67 protein is involved in the cell-substrate focal adhesion complex, and using a combination of transcriptomic and proteomic approaches, will show that *TMEM67* patient cells have major alterations to cell-substrate interaction, including changes to the extracellular matrix and to focal adhesions. It will also be shown that defective extracellular matrix is upstream of both cytoskeletal alterations and failure to build cilia in *TMEM67* patient cells, revealing for the first time a dependency relationship between cellular phenotypes in MKS. It will furthermore be shown that these alterations can be restored by antagonising the Wnt or TGF-β developmental signalling pathways, which may be viable drug targets with the potential to improve patient outcomes. Finally, ECM-independent alterations to MKS patient cells will be investigated to identify possible causes of the ECM defect.

Chapter 2

Materials and Methods

Chapter 2: Materials and Methods

2.1 Cell culture

Neonatal patient fibroblasts (hTERT-immortalised *MKS3*/*TMEM67* [c.653G>T p.R217X]+[c.785T>C p.M261T] and *MKS2*/*TMEM216* c.253C>T p.R85X) and age-matched controls (also hTERT-immortalised) were obtained from Colin Johnson (Leeds Institute for Molecular Medicine). Cells were cultured in Dulbecco's Modified Eagle's Medium: Nutrient Mixture F-12 (DMEM-F12; Gibco) supplemented with 20% Fibroblast Growth Medium (FGM; AMS Biotech), 10% foetal calf serum (Gibco), and 500 μg ml^{-1} G418 to select for cells with the hTERT immortalisation plasmid. Cells were grown at 37°C with 5% CO_2, and split to sub-passage in TrypLE Express cell dissociation reagent (Gibco) at approximately 70% confluency. All experiments were performed with cells between passages 11 and 22.

2.2 Surface coating with extracellular matrix protein

ECM protein was diluted to 10 μg ml^{-1} in PBS, or for collagens I and IV, in 0.02 N acetic acid, then the solution was sterilised by passage through a 0.2 micron filter. Glass surfaces were coated by covering with a thin layer of ECM solution. The covered surface was then incubated for 1 hour at room temperature (for cell spreading microscopy) or overnight at 4°C (for all other experiments) before washing with PBS to remove excess protein.

All ECM protein was obtained from Sigma-Aldrich. Collagen I solution from rat tail: product code C3867. Collagen IV derived from human placenta: product code C5533. Recombinant human vitronectin: product code SRP3186. Human plasma fibronectin: product code F2006. Laminin derived from human placenta: product code L6274.

2.3 Cell-derived matrix isolation

To strip cells and purify cell-derived matrix (CDM), a method based on (Rashid *et al*, 2012) was used. Cells were grown to confluency in adherent culture, then left for 4 days post-confluency to synthesise mature ECM. Growth media was removed, cells were washed with PBS, then lysed for 4 minutes at room temperature in a solution of 20 mM ammonium hydroxide (Sigma-Aldrich), 0.5% Triton X-100 in PBS. After a final PBS wash to remove debris and residual lysis solution, the remaining ECM material (the CDM) was either used directly in further experiments, fixed *in situ* for SEM imaging (see below), or recovered into solution mechanically with a cell scraper (Fisher). For western blot analysis, the CDM was recovered in Laemmli reducing sample buffer and used immediately or stored at -20°C.

2.4 Antibodies and probes

Antigen	Host species	Supplier	Clone ID / cat no.	IF fix	IF dilution	WB dilution
Primary antibodies						
acetylated alpha tubulin	mouse	AbCam	6-11B-1	MeOH	1:200	N/A
TMEM67 (MKS3)	rabbit	ProteinTech	13975-1-AP	2% FA	1:500	1:5000
Vinculin	mouse	Millipore	MAB3574	2% FA	1:400	1:5000
VDAC1	rabbit	Santa Cruz	FL-283	N/A	N/A	1:1000
Filamin A	goat	AbCam	ab11074	4% FA	1:100	1:1000
Actin clone c4	mouse	Sigma	C4	MeOH	1:200	1:2000
Laminin	mouse	DSHB	2E8	N/A	N/A	1:25
Collagen 4	mouse	DSHB	M3F7	N/A	N/A	1:100
Secondary antibodies						
anti-rabbit AlexaFluor 488 Fab fragment	goat	Molecular Probes			1:1000	
anti-rabbit AlexaFluor 594 Fab fragment	goat	Molecular Probes			1:1000	
anti-mouse AlexaFluor 488 Fab fragment	goat	Molecular Probes			1:1000	
anti-mouse AlexaFluor 594 Fab fragment	goat	Molecular Probes			1:1000	
anti-rabbit HRP	donkey	Jackson				1:20 000
anti-mouse HRP	donkey	Jackson				1:20 000
anti-goat HRP	donkey	Jackson				1:20 000

Table 2.2: Primary and secondary antibodies used in this thesis

The actin-binding phallotoxin phalloidin, conjugated to Alexa fluor 594 (Molecular Probes), was used to label filamentous actin at a dilution of 1:500.

Anti-collagen IV was deposited to the DSHB by Furthmayr, H. (DSHB Hybridoma Product M3F7), and anti-laminin was deposited to the DSHB by Engvall, E.S. (DSHB Hybridoma Product 2E8).

2.5 Western blotting

Polyacrylamide gels were made with 10% or 8% acrylamide depending on expected band size.

Samples were reduced by boiling in Laemmli reducing sample buffer at 95°C for 5 minutes, then loaded alongside either ColourPlus prestained protein marker (New England Biosciences) or PageRuler Plus prestained protein ladder (Thermo Scientific). Protein was separated by electrophoresis at 75-150 volts for 1-2 hours, and transferred to a nitrocellulose membrane using either a wet transfer system (Mini-Protean 3, BioRad) at 150 mA for 1 hour, or a semi-dry transfer system (Trans-Blot SD, BioRad) at 25 volts for 1 hour.

Membranes were blocked with continuous rotation at room temperature for 1 hour in PBS with 0.1% Tween-20 (Fisher Scientific) and 5% Marvel milk powder (Premier Foods Group, UK), or in PBS with 0.1% Tween-20 and 5% BSA. To probe membranes, antibodies were diluted in blocking solution, and membranes were incubated in primary antibody with continuous rotation at room temperature for 1 hour or at 4°C overnight, washed for 3 x 20 minutes in PBS with 0.1% Tween-20, incubated in secondary antibody with rotation at room temperature for 30 minutes to 1 hour, and washed for 3 x 20 minutes in PBST. To visualise protein, the membrane was treated with ECL reagent and exposed to X-ray film (Super RX, FujiFilm).

Membranes were stripped for re-probing by incubation in stripping buffer (100 mM glycine, 2% SDS, pH 2.0) for 2 x 10 minutes at room temperature, washed with PBS for 3 x 10 minutes, then re-blocked, treated with ECL, and exposed to check for residual signal before re-probing.

2.6 Immunofluorescence and phalloidin staining

For formaldehyde fixation, cells were fixed in 2% or 4% formaldehyde in cytoskeleton buffer (10 mM MES pH 6.1, 138 mM KCl, 3 mM MgCl, 19 mM

EGTA pH 7.0) with sucrose at room temperature for 20 minutes, washed with PBS, then permeabilised in PBS with 0.5% Triton X-100 for 10 minutes.

For methanol fixation, cells were fixed in -20°C methanol for 10 minutes, rehydrated in PBS at room temperature for 10 minutes, then further rehydrated in fresh PBS for another 10 minutes.

Cells were blocked in AbDil (PBS with 2% BSA) for 15 minutes or more before incubation with the primary antibody for 1 hour. Cells were then incubated with the secondary antibody for 30 minutes, and for some experiments stained with DAPI (1 μg ml^{-1}) for 1-2 minutes. After each incubation the cells were washed with PBS. Finally, the coverslips were mounted onto glass slides with Vectashield (Vector Laboratories) and sealed with clear nail polish (Boots, UK).

While phalloidin is not an antibody, its staining protocol is similar to that for immunofluorescence. Labelled phalloidin is used in the place of a primary antibody and requires no secondary.

2.7 Transfection

Cells were transfected using an Amaxa Nucleofector electroporation device with transfection kit R (Lonza), according to the manufacturer's instructions. For each transfection, a subconfluent T-25 flask of cells were dissociated from the culture surface, pelleted, and resuspended in 80 μl of transfection buffer. The transfection buffer contained 65 μl nucleofector solution R (Lonza), 15μl supplement 1 (Lonza), and 1 μg of plasmid DNA. The resulting cell suspension was loaded into an electroporation cuvette (Lonza) and electroporated with program D-023. After electroporation, the suspension was immediately transferred into a T-25 flask with 3 ml of fresh media. Since all transfections

described here involved only transient expression, experiments were performed with cells between 48 and 96 hours post- transfection.

2.8 Light microscopy

For cell spreading, cell volume measurement, and immunofluorescence experiments, samples were imaged using a Zeiss Axio Observer Z1 inverted microscope, controlled by AxioVision (Carl Zeiss). Images were acquired by a CoolSnap HQ2 camera (Photometrics) and processed in AxioVision, ImageJ/FIJI (National Institutes of Health), and MetaMorph (Molecular Devices). The microscope was equipped with high-efficiency filters which have steep cut-offs and high transmittance, and therefore represent the tightest excitation and emission efficiency available from the manufacturer. Single-fluorophore control experiments with fluorescent microbeads (Fisher) could detect no bleedthrough between the channels even at high exposures.

Filter set	Product ID	Manufacturer	Excitation (nm)	Emission (nm)
49 DAPI shift free	488049-9901-000	Carl Zeiss	365	445/50
38 HE eGFP shift free	489038-9901-000	Carl Zeiss	470/40	525/50
43 HE Cy 3 shift free	489043-9901-000	Carl Zeiss	550/25	605/70

Table 2.1: Filter sets used in Zeiss Axio Observer Z1 microscope. Excitation and emission values are given as peak and spread – for example, filter set 38 has an excitation peak at 470 nm with a spread 20 nm to either side, for a total spread of 40 nm.

2.9 Scanning electron microscopy

Samples for SEM were fixed in 2.5% glutaraldehyde, 1% formaldehyde, 0.1 M sodium cacodylate pH 7.1 or in 2.5% glutaraldehyde, 2% formaldehyde, 0.1% picric acid, 100 mM phosphate pH 6.5, then post-fixed in osmium tetroxide, dehydrated through a graded ethanol series, critical point dried and gold coated

with an Alto 2100 chamber (Gatan, Oxfordshire). Samples were imaged with a JSM-6390LV scanning electron microscope (JEOL, Tokyo).

2.10 Cell spreading analysis

For cell spreading experiments, imaging took place within a heated environment chamber at 37°C. Cells were dissociated from the cell culture surface then plated onto pre-warmed ECM-coated glass-bottom dishes 1-2 minutes before the time series began, and imaged at multiple z-axis planes every minute for 90 minutes; or for logarithmic analysis, every 5 seconds for 20 minutes. When processing these time series, out-of-focus planes were discarded. Cell area was measured using the freehand drawing tool in ImageJ/FIJI. At least three cells were measured for each combination of cell line and substrate across at least two biological repeats.

2.11 Cell volume measurement

Control and *TMEM67* cells were dissociated from the culture surface with trypLE Express, then plated still in dissociation buffer onto a glass-bottom dish. Under these conditions, the cells could not spread or form adhesions and remained spherical. The cells were imaged, and from these images, measurements were taken of the cell diameters with the line tool in ImageJ/FIJI, and the cell volumes were calculated. Over 100 cells were measured for each cell line across three biological repeats.

2.12 Adhesion measurement

Cells were plated on ECM-coated coverslips for 20 minutes at 37°C, 5% CO_2, then fixed in 2% formaldehyde and immunostained for vinculin as described above to label adhesions. Images were acquired, then using ImageJ/FIJI's rectangular selection tool, a 10 μm by 10 μm region at the right edge of the cell

was selected as the region of interest. Since the circular coverslip was randomly rotated during mounting, this was effectively a randomly chosen region of the cell periphery. The fluorescently labelled adhesions within this region were manually counted, and measured using the line and freehand measurement tools in ImageJ for area, length, and width. A figure for coverage was derived by dividing the sum of the areas of adhesions in the region by the total region size (100 μm^2) to give the proportion of the region covered by adhesions. At least 25 cells were imaged for each combination of cell line and substrate over two biological repeats.

2.13 Micropipette aspiration

Glass micropipettes were pulled from borosilicate glass capillaries (outer diameter 1.5 mm, inner diameter 0.86 mm, Clark Electromedical Instruments, Reading, UK) with an element puller (Model P-87, Sutter Instrument Co., California, USA), then mounted on a micromanipulator on the stage of a brightfield microscope (Laborlux 12HL, Ernst Leitz, Wetzlar, Germany) and manually forged with a heated filament until a smooth aperture was produced. Prior to use, the micropipette tips were incubated in 1% BSA overnight at 4°C. To create observation chambers, a glass slide and coverslip were assembled together, held approximately one millimetre apart by a parafilm spacer. The chambers were filled with cell suspension and observed with an inverted microscope (IX-51, Olympus, Hamburg, Germany) under DIC illumination.

Micropipettes were back-filled with cell culture medium using a syringe with a fine-gauge needle, and attached to a pressure-generating apparatus controlled by the height of an adjustable water column. All water in the system was replaced at the start of each session with ultrapure water degassed in a vacuum chamber, and the system was checked for leaks or air bubbles. The

micropipette was mounted on a micromanipulator (PT3A/M, Thorlabs, New Jersey, USA) and the tip of the micropipette introduced into the chamber. An individual cell was captured and held at the aperture of the micropipette by minimal aspirating pressure (< 50 Pa). Aspirating pressure was increased to 500 Pa and the resulting change in projection length as the cell moved into the micropipette barrel was imaged. Images were acquired by an AVT Stingray F-145B CCD camera. From these movies, projection lengths were measured every 20 seconds relative to the length at *t* = 0. Measurements were taken with the line tool in ImageJ/FIJI. At least 7 cells were analysed per cell line across three biological repeats. Since micropipette apertures were inconsistent due to the manual forging method, each micropipette was used to aspirate at least one cell of each cell line to ensure a direct comparison was possible.

2.14 Micropipette data analysis

Projection lengths were analysed according to the standard linear solid (SLS) model. This models the cell as a viscoelastic solid (Jones *et al*, 1999; Sato *et al*, 1990; Theret *et al*, 1988), and can be expressed:

$$\mathrm{L}(t) = \frac{\varphi a \Delta P}{\pi k_1}\left[1 - \frac{k_2}{k_1 + k_2} e^{-\frac{t}{\tau}}\right]$$

where

$$\mu = \frac{\tau \cdot k_1 k_2}{k_1 + k_2}$$

and where L(t) is the length of the cellular projection into the micropipette at time *t*, *φ* is a dimensionless parameter representing the wall thickness effect

(derived from the ratio of inner radius to wall thickness), *a* is the inner radius of the micropipette, and *ΔP* is the step change in aspirating pressure.

The elastic parameters k_1 and k_2, and the apparent viscosity μ, were determined for each cell using Scilab (Scilab Enterprises). Parameter values were found by fitting each set of observed projection lengths to the SLS expression via Scilab's *lsqrsolve()* function, which implements a Levenberg-Marquardt algorithm to minimise the sum of squares of the difference between the enumeration of the expression and the experimental result for each data point (Gill & Murray, 1978). This yielded approximations to the parameter values k_1, k_2, and μ. A cellular equilibrium Young's modulus E_∞, which quantifies the mechanical stiffness of the cell, was thus derived from k_1:

$$E_\infty = \frac{3}{2} k_1$$

2.15 Actin co-sedimentation

This method was adapted from the method of Brainard et al (2005) with advice from James Wakefield.

Approximately 10^7 human fibroblasts (10 confluent T-25 flasks) were resuspended in PBS after dissociation with TrypLE Express. The cells were pelleted by centrifugation at 2000 RPM for 3 minutes, washed by resuspension in PBS, and pelleted again. The pellet was snap-frozen in liquid nitrogen and stored at -80°C.

Keeping all tubes and reagents on ice, the cell pellet was resuspended in 0.5 ml C-buffer (50 mM HEPES pH 7.4, 50 mM KCl, 1 mM MgCl, 1 mM EGTA, 0.1%

Triton X-100, protease inhibitor). The suspension was transferred to a Dounce homogeniser tube (Wheaton, USA) and homogenised for 3 x 5 second bursts with a pestle attached to a power drill (KR500RE; Black & Decker, UK). The homogenate was transferred to an ultracentrifuge tube and centrifuged for 30 minutes, at 4°C, 100 000 g (55 000 rpm) with a TLA-120.1 rotor in an Optima MAX Ultracentrifuge (Beckman Coulter, USA). The clear phase was recovered using a syringe and fine-gauge needle, and the pellet was discarded. 20 µl of the clear phase was taken and stored as a total lysis sample in Laemmli reducing sample buffer at -20°C. The remainder was split into positive and negative samples. The negative sample was treated with 100 µM nocodazole, 50 µM latrunculin B, and kept on ice. The positive sample was treated with 100 µM nocodazole and 2 mM ATP (Melford), incubated at 37°C for 10 minutes to promote polymerisation of actin, then treated with 20 nM phalloidin at 37°C for 10 minutes to stabilise polymerised actin.

Samples were layered in ultracentrifuge tubes above a 400 µl cushion of C-buffer/glycerol (C-buffer as above, without inhibitors, with 40% glycerol) and centrifuged for 1 hour at 4°C, 100 000 g. The clear supernatant above the C-buffer/glycerol layer was retrieved and stored at -20°C. The top of the C-buffer/glycerol layer was washed with fresh C-buffer to remove residue of supernatant, then all remaining solution was removed. The pellet was resuspended in Laemmli reducing sample buffer and stored at -20°C.

Total lysis, supernatant, and pellet samples were analysed for protein content via western blot. The experiment was repeated twice, giving the same result both times.

2.16 Total mRNA isolation

For RNA-sequencing differential expression analysis, total mRNA was isolated from control and TMEM67 fibroblasts using a Dynabeads mRNA DIRECT Kit (Ambion/Life Technologies) according to the manufacturer's instructions. A DynaMag-2 magnetic rack (Life Technologies) was used to pellet the Dynabeads. After the final wash, mRNA was eluted and recovered in 13 µl elution buffer (10 mM Tris-HCl pH 7.5). The mRNA was split into a 3 µl quality control sample and a 10 µl sample for sequencing. Both samples were snap-frozen in liquid nitrogen and stored at -80°C before RNA-sequencing.

2.17 Differential expression analysis and gene set enrichment analysis

Differential expression analysis was performed on an Illumina RNA-seq platform. The mRNA was reverse transcribed and quality assessed with a BioAnalyzer (Agilent). Illumina barcoding was performed using the ScriptSeq v2 RNA-seq Library Preparation Kit (Epicentre) and sequencing was performed using a HiSeq 2500 sequencer (Illumina). Data quality was assessed using FastQCReads, low-quality reads filtered out and adaptor sequences removed using RobiNA. Trimmed reads were aligned against the human genome using Tophat2 (Center for Computational Biology, Johns Hopkins University), and Cufflinks (Cole Trapnell, University of Washington) was used for initial processing and automated annotation of data. The online DAVID resource was employed for gene set enrichment and functional annotation clustering analysis.

2.18 Focal adhesion isolation

Adapting the method of Kuo et al (2012), cells were grown to confluency in 10 cm diameter cell culture dishes then left for 4 days post-confluency to

synthesise ECM and form mature adhesions. Culture medium was removed by aspiration and PBS washing. Cells were hypotonically shocked with triethanolamine-containing low ionic strength buffer (2.5 mM triethanolamine, pH 7.0) for 15 minutes to induce rounding, then washed off the surface with hydrodynamic force applied by a WaterPik dental water jet (Interplak dental water jet WJ6RW, Conair) at pressure setting 3. The WaterPik was loaded with PBS supplemented with broad-spectrum protease inhibitor tablets (Fisher) to minimise degradation of material. The jet was applied to the culture surface from a distance of approximately 1 centimetre, at a 90° angle, and moved around the surface in repeated cross-hatch and spiral patterns over approximately 30 seconds per dish to ensure even coverage. The remaining material containing adhesion and ECM protein was then recovered from the surface by scraping in RIPA buffer with mass-spectrometry grade protease and phosphatase inhibitors (MS-SAFE; Sigma-Aldrich), snap frozen in liquid nitrogen, and stored at -80°C.

2.19 Tandem mass tag mass spectrometry

Six 100 µl samples of adhesion fraction (isolated as described above), representing three biological repeats of control and *TMEM67* cells, were submitted to TMT MS/MS analysis. The samples were digested with trypsin and labelled with Tandem Mass Tag reagents according to the manufacturer's protocol (Thermo Fisher Scientific). After labelling, the samples were combined, and the pooled sample was fractionated with an Ettan LC system (GE Healthcare). NanoLC-MS/MS analysis was performed using a Thermo LTQ-Orbitrap Velos mass spectrometer. Data was processed and quantified with Proteome Discoverer 1.2 (Thermo Scientific) and searched against the Uniprot human proteome and analysed for quality with Mascot (Matrix Science).

2.20 Statistical analysis

Numerical and statistical analyses were performed using Excel (Microsoft Corporation), QuickCalcs (GraphPad), Prism (GraphPad), and Scilab (Scilab Enterprises). For all data, D'Agostino's K^2 test was used to assess normality.

Differential expression datasets were aligned to the human genome with Tophat2 and quantification and statistical analysis performed with Cufflinks. Significantly altered transcripts were identified in Cufflinks by multiple-comparison *t*-tests corrected for false discovery rate to account for the large number of tests. Functional annotation clustering was performed using the online DAVID resource.

Mass spectrometry data was analysed by a similar approach, where significantly altered abundance of proteins was assessed by multiple-comparison *t*-tests corrected for false-discovery rate.

Data for adhesion size, number, and coverage were analysed in a one-way ANOVA test comparing each measurement between control and MKS cells, with Bonferroni post-hoc analysis to determine which factor was significantly altered. A parametric test was preferred for this analysis because the data was normally distributed.

Cell volume measurements and ciliogenesis of cells in experiments with only two groups were analysed with Student's *t* test, appropriate for simple comparison of two groups which are normally distributed, as was the case in these datasets. Ciliogenesis of cells in experiments with more than two groups was analysed with Pearson's χ^2 test. This test is appropriate for comparison of non-continuous data such as counts of population (in this case, ciliated cells vs non-ciliated cells). Ciliogenesis of cells plated on collagen IV or laminin involved

a large number of factors that could be responsible for any observed effect (three cell lines and six substrates), so was analysed by one-way ANOVA with Bonferroni post-hoc analysis for multiple comparisons. Parametric tests were chosen because the data was normally distributed.

For analysis of actin organisation in MEFs, since the data was not normally distributed, the non-parametric Kruskal-Wallis test was used. Since four groups were to be compared to a single control, Dunn's post-hoc correction for multiple comparisons was used to determine which groups were significantly altered.

For analysis of micropipette-derived cellular equilibrium Young's moduli, a one-way ANOVA was used with Dunnet's post-hoc analysis, which is appropriate when data is normally distributed and multiple groups are to be compared with a single control group.

Chapter 3

TMEM67 is a focal adhesion protein required for adhesion complex and extracellular matrix morphology and composition

Chapter 3: TMEM67 is a focal adhesion protein required for adhesion complex and extracellular matrix morphology and composition

3.1 Introduction

TMEM67 has been reported in many subcellular localisations including basolateral actin (Adams *et al*, 2012). Basolateral actin is typically in close association with adhesions. Given that TMEM67 is a predicted transmembrane protein proposed to serve a role in membrane tethering as part of the MKS/JBTS module in the cilium (Craige *et al*, 2010; Smith *et al*, 2006), it is plausible that TMEM67 may also be involved in cell surface interactions at focal adhesions.

Adhesions are complex signalling platforms involving a large number of proteins; recent studies have proposed numbers of candidate adhesion proteins in the thousands (Kuo *et al*, 2011; Zaidel-Bar *et al*, 2007; Horton *et al*, 2015). Adhesion-dependent interactions and signalling are key to the organisation of the extracellular matrix (ECM), and to the transduction of ECM-mediated signals which are essential for development (Boudreau & Jones, 1999). Therefore, alterations to adhesions in *TMEM67* patient cells could underlie patient phenotypes, such as the excess ECM secretion in liver fibrosis.

In this chapter, quantitative transcriptomics reveals that mRNA transcripts associated with ECM and adhesion functions are significantly altered in patient cells compared to controls, suggesting a possible role for TMEM67 in ECM organisation that could be important for disease aetiology. The association of TMEM67 with actin and focal adhesions is investigated, and changes to the *TMEM67* patient cell adhesion proteome (adhesome) and extracellular matrix

proteome (matrisome) are quantified. Finally, the morphology of adhesions and ECM of MKS patient cells are shown to be altered.

3.2 *TMEM67* patient cells exhibit altered expression of ECM-associated genes

To investigate the global changes to cellular processes in MKS, Illumina RNA-seq differential transcriptional profiling of *TMEM67* patient fibroblasts, together with age-matched control fibroblasts, was performed. The experiment was replicated across two biological repeats for each cell line. 1376 transcripts were found to be significantly altered in abundance, with $q < 0.05$ (*t*-tests with multiple comparisons: *q* is a false discovery rate-adjusted *p* that corrects for large multiple comparisons). For a full list of significantly altered transcripts, see Appendix 1, table 1. The list of differentially expressed transcripts was submitted for gene set enrichment analysis with functional annotation clustering using the online DAVID resource, revealing disproportionately altered expression of ECM and adhesion genes (Figure 3.1 A). In particular, the single most enriched cluster detected by DAVID represented genes associated with the extracellular matrix, and among the most enriched was a cluster associated with cell-substrate junctions (Figure 3.1 A). Moving from this high-level analysis to investigating individual genes, it was found that among the genes within the dataset annotated as ECM-associated (Figure 3.1 B), laminin (Figure 3.1 B, purple) and collagen transcripts were altered, with expression of laminin α2 in particular almost abolished, and two collagen IV transcripts (Figure 3.1 B, yellow) substantially under-expressed compared to control cells. Additionally, metallopeptidases (Figure 3.1 B, green), which degrade and remodel the extracellular matrix, had predominantly increased expression.

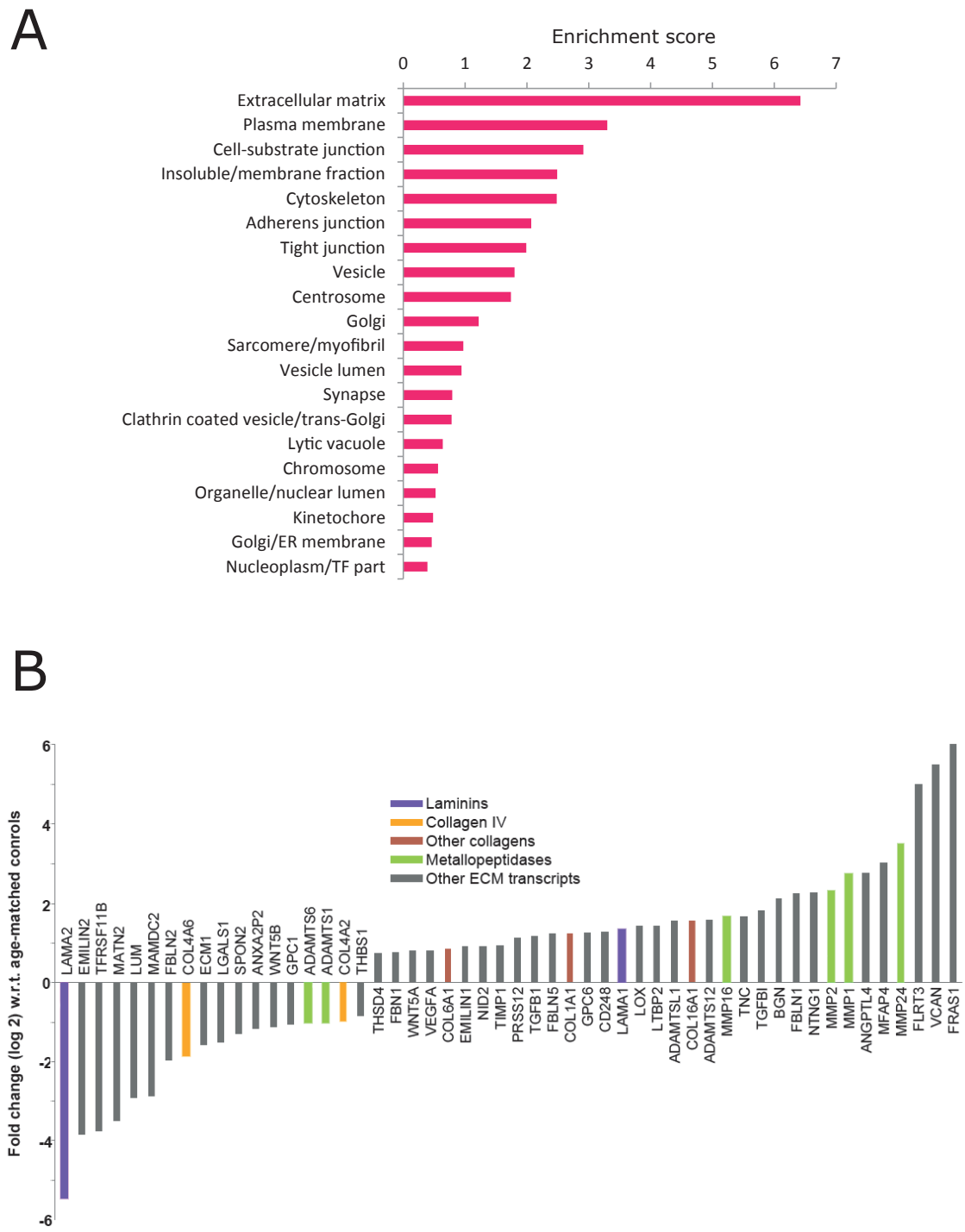

Figure 3.1: *TMEM67* patient cells exhibit altered expression of ECM- and adhesion-associated genes.

A: The top 20 enriched clusters identified by functional annotation clustering analysis (based on Cellular Component GO annotations) of Illumina RNA-seq differential expression data from *TMEM67* patient cells (with respect to age-matched control cells).

B: Fold change in expression of ECM-associated genes in *TMEM67* patient cells from the same dataset.

To determine whether these expression changes were reflected in changes to actual protein levels in the ECM, cell-derived matrix (CDM) was purified from control and *TMEM67* patient cells at 2, 4, 6, 8, and 10 days after plating. These samples were probed via Western blot for collagen IV and laminin (Figure 3.2, A), showing that while control CDM had high levels of collagen IV from day 6 onward, and high levels of laminin on day 2 that diminished in subsequent days, *TMEM67* patient CDM contained reduced levels of both in comparison at each timepoint. A Coomassie stain showed that the samples contained comparable total protein levels (Figure 3.2 B).

3.3 TMEM67 is a focal adhesion protein

Regulation of ECM synthesis and composition is dependent on signalling through the focal adhesion complex (Humphrey *et al*, 2014). Disruption of both ECM and adhesion gene expression in *TMEM67* patient cells might be explained if TMEM67 has a function in the focal adhesion complex. To investigate the localisation of TMEM67, human fibroblasts were fixed and labelled to visualise TMEM67 and actin via immunofluorescence (Figure 3.3 A). In agreement with the findings of Adams *et al* (2012), TMEM67 co-localised with F-actin near the basolateral cell surface. To confirm a physical association between TMEM67 and F-actin, a co-sedimentation assay was performed with human fibroblast cell homogenate in the presence and absence of phalloidin to stabilise F-actin (Figure 3.3 B). TMEM67 was found to co-sediment with the F-actin pellet, consistent with a (direct or indirect) physical interaction. Three TMEM67 bands were observed, of approximate molecular mass 45, 50, and 55, possibly representing the smaller, uncharacterised TMEM67 isoforms identified by Dawe *et al* (2009) that are found only in subconfluent, non-ciliated cells.

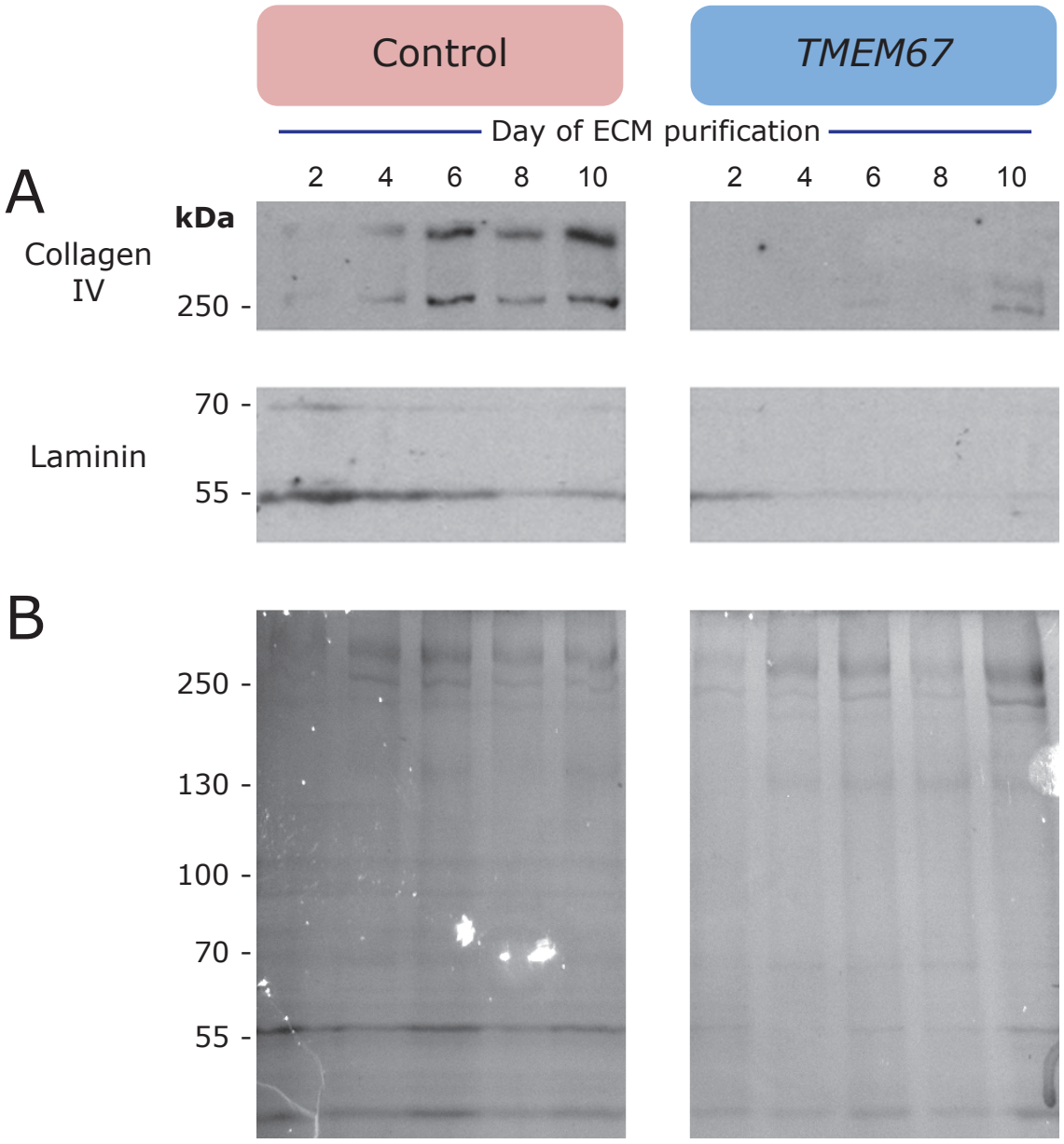

Figure 3.2: *TMEM67* patient cell-derived ECM contains reduced levels of collagen IV and laminin protein.

A: Western blots of purified ECM deposited over time by control and *TMEM67* patient cell cultures, probed for collagen IV and laminin. B: Coomassie stains showing total protein over the same time series.

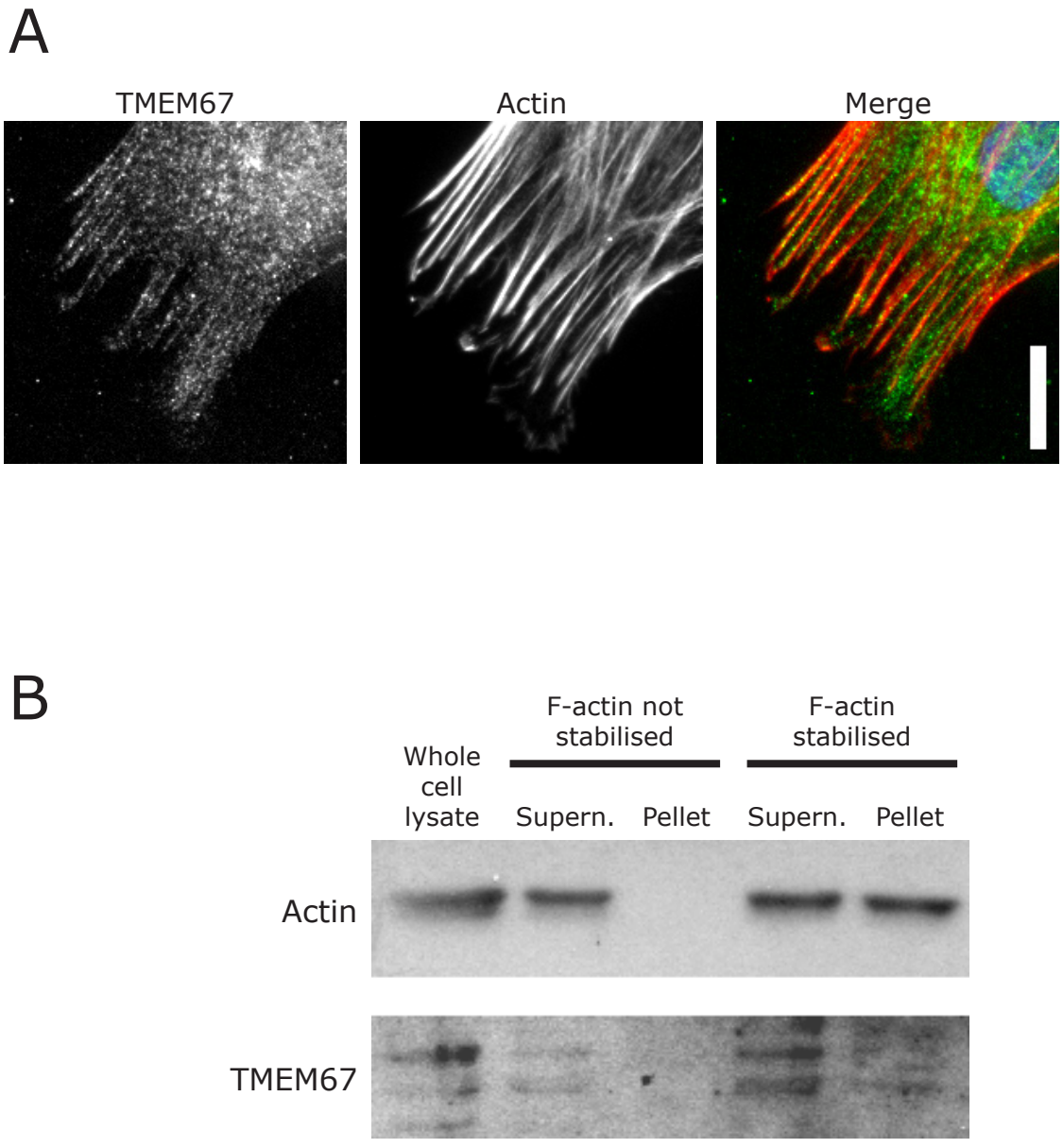

Figure 3.3: TMEM67 localises to basolateral actin filaments and co-sediments with stabilised F-actin.

A: TMEM67 localises to basolateral actin filaments. Human fibroblasts were immunolabelled for TMEM67 (green), stained for actin with phalloidin (red), and for nuclei with DAPI. Bar: 20 μm. Single fluorophore control experiments showed no bleedthough between these channels even at high exposures.

B: Western blot of samples from an actin co-sedimentation assay, showing TMEM67 physically associates with F-actin in human fibroblasts.

Given that basolateral actin cables often directly overlay and connect to adhesions (Xu *et al*, 2012), it was next investigated whether TMEM67 was present in the focal adhesion complex. Human fibroblasts were fixed and immunolabelled for TMEM67 and the adhesion marker vinculin (Figure 3.4 A). TMEM67 was found to co-localise with vinculin adhesion patches (Figure 3.4 A, blue arrows). To confirm the presence of TMEM67 at cell surface adhesions, two different focal adhesion preparations were performed (Figure 3.4 B). Prep 1 was based on the method of Kuo *et al* (2012) using hypotonic treatment and hydrodynamic force. Prep 2 was based on the method of Rashid *et al*, (2012), using high alkaline treatment. In both preparations, vinculin was detected by western blot alongside TMEM67 and filamin A, a known direct TMEM67 interactor (Adams *et al*, 2012) and focal adhesion protein (Kuo *et al*, 2011). VDAC1, a mitochondrial porin not associated with adhesions or the cell surface, was found to be excluded from the preparations, indicating successful removal of cytoplasmic material. In contrast to the three TMEM67 bands observed in whole cell lysate (Figure 3.4 B) and actin co-sedimentation assays (Figure 3.3 B), only a single band was observed in focal adhesions prepared by either method, suggesting isoform-specific functions.

3.4 Tandem mass tag proteomics reveal major alterations to the *TMEM67* patient cell adhesome

To determine the effect of the absent TMEM67 protein on adhesions in *TMEM67* patient cells, tandem mass tag comparative mass spectrometry (TMT-MS/MS) was performed (Figure 3.5) to quantitatively determine differences in the adhesome and matrisome in patient cells compared with age-matched controls grown under identical conditions. The adhesion/ECM fraction was isolated from control and *TMEM67* patient cells, and relative protein content

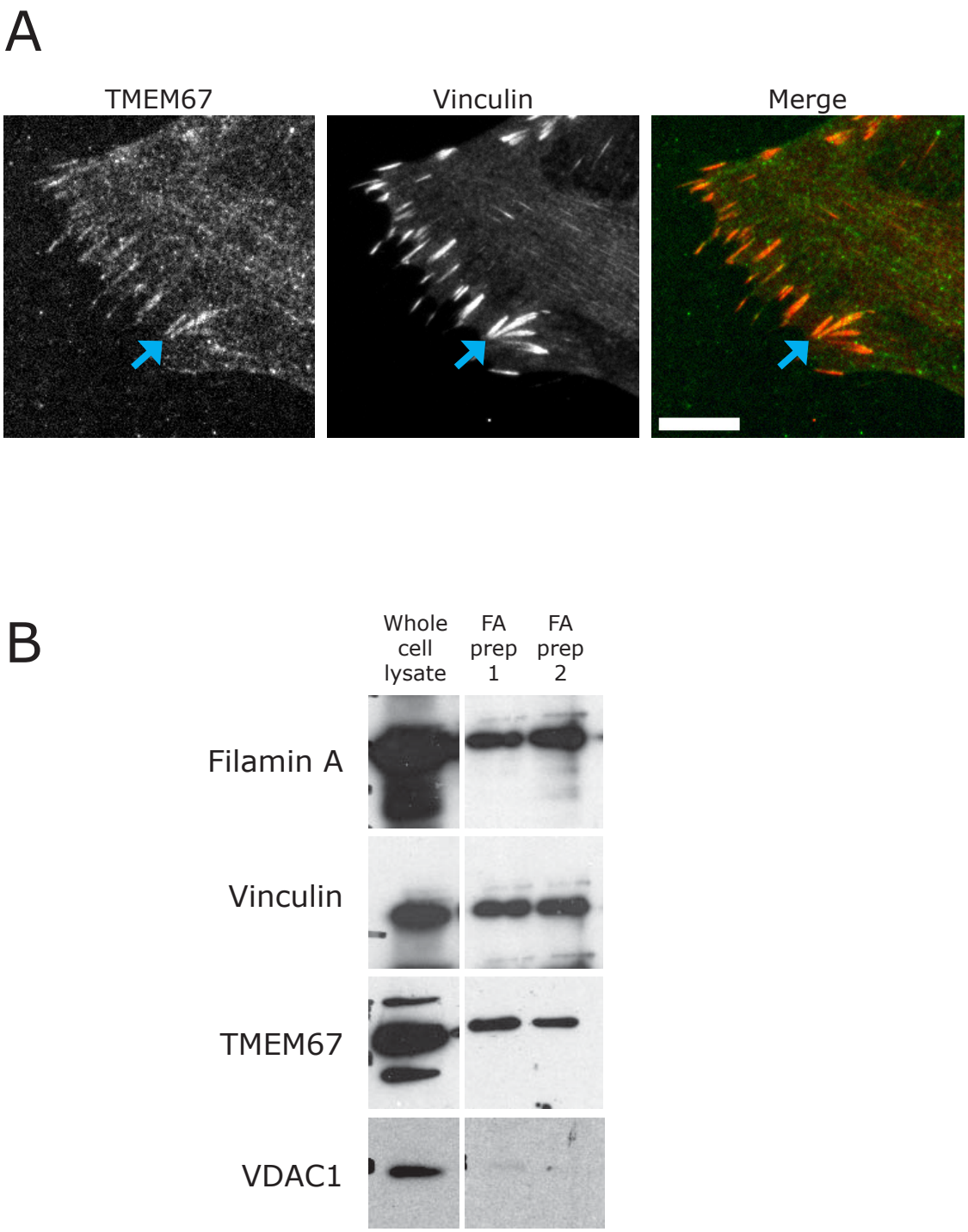

Figure 3.4: TMEM67 is a focal adhesion protein.

A: TMEM67 co-localises with the focal adhesion marker vinculin. Human fibroblasts were immunolabelled for TMEM67 (green) and vinculin (red). Single fluorophore control experiments showed no bleedthough between these channels even at high exposures. Arrows: an area of co-localisation. Bar: 20 μm. B: Western blot showing TMEM67 and filamin A present along with vinculin in two different focal adhesion preparations, while VDAC1 is excluded.

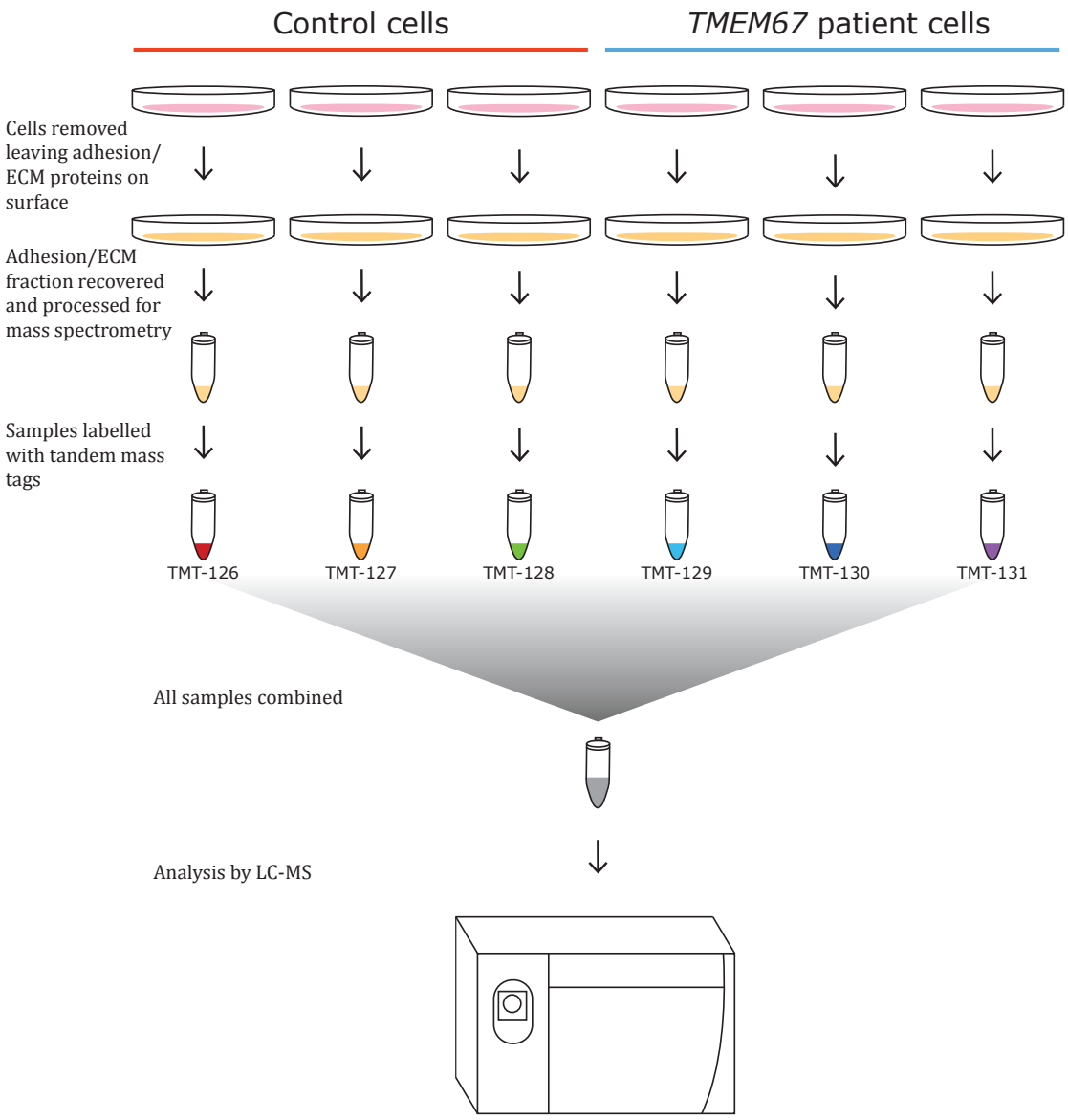

Figure 3.5: Workflow for Tandem Mass Tag (TMT) quantitative mass spectrometry of the adhesion/ECM fraction.

TMEM67 patient cells and age-matched controls were plated until mature adhesions had been formed, then the cells were removed by hypotonic treatment and hydrodynamic force. The residue remaining after cell removal is enriched in adhesion and ECM proteins. This fraction is recovered and processed for mass spectrometry. Each sample is labelled with a different tandem mass tag, after which the samples are combined and analysed in a single liquid chromatography mass spectrometry (LC-MS) experiment.

quantified over three biological repeats for each cell line. A Mascot score was assigned to each detected protein, derived from a combination of criteria including number and size of matching peptides against the expected human proteome. Since lower Mascot score represents proteins with higher probability of erroneous detection, results with Mascot score < 30 (representing a probability of erroneous detection > 10^{-3}) were excluded from further analysis. This threshold is arbitrary, but is widely used in the literature (for example, (Hughes *et al*, 2008; Hauck *et al*, 2010)).

The remaining 1394 proteins were compared to previously published proteomic datasets to assess quality. A previous, methodologically similar study of the adhesion proteome by Kuo *et al.* identified 1917 candidate adhesion proteins (Figure 3.6 A, purple circle), 754 of which were found reproducibly across multiple experimental repeats (Figure 3.6 A, light blue circle) (Kuo *et al*, 2011). Pairwise comparisons showed that the present study had considerable overlap with these results (Figure 3.6 A); of the 1394 proteins detected (Figure 3.6 A, red circle), 797 (57%) matched Kuo *et al*'s full adhesome list. Of their list of 754 reproducible adhesome proteins, 417 were detected in the present study (55%). This overlap, consistent with that found between Kuo *et al*'s three datasets, indicates recovery of the adhesion fraction was successful. (See Appendix 1 for lists of raw data and matching proteins).

The matrisome is less well-studied than the adhesome, but a recent study used a combination of *in silico* and *in vivo* approaches to identify candidate proteins (Naba *et al*, 2011). Working *in silico* (Figure 3.6 B, left), Naba *et al* identified 1062 candidate proteins (Figure 3.6 B left, teal circle), including a "core matrisome" of 281 proteins (Figure 3.6 B left, green circle). Pairwise comparisons with the present study had some overlap with these; of the 1394

A: Adhesome

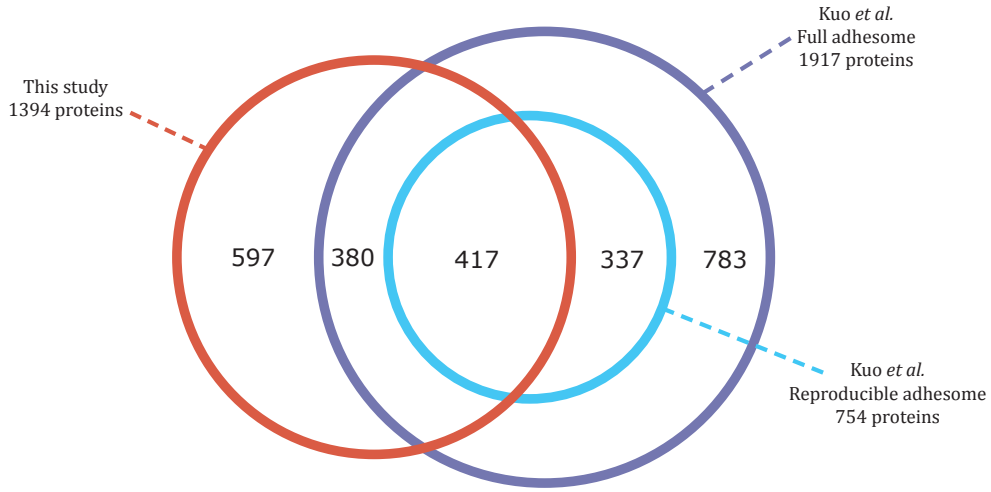

B: Matrisome

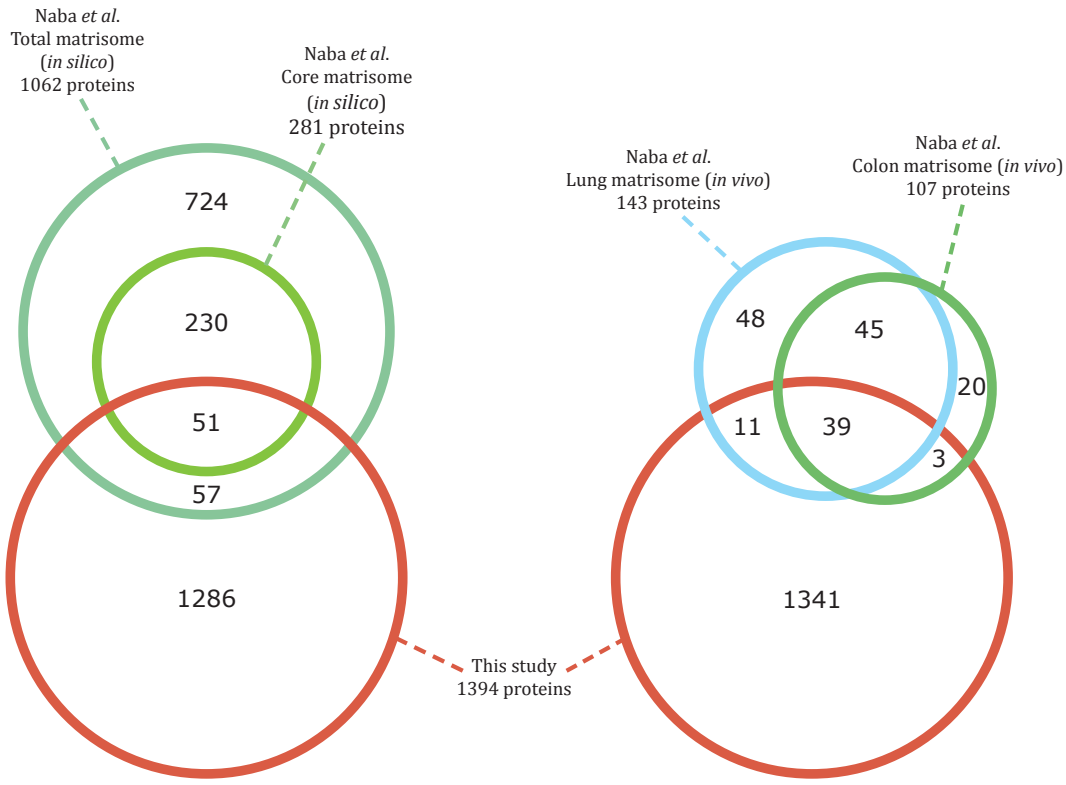

Figure 3.6: The protein content of the recovered adhesion/ECM fraction is consistent with current knowledge of the adhesion and ECM proteomes. Venn diagrams showing overlap between proteins identified by this study and (A) those identified in a methodologically similar adhesome study by Kuo *et al*.; (B) proteins identified in matrisome studies performed both *in silico* and *in vivo* by Naba *et al*.

proteins detected, 108 (8%) matched Naba *et al*'s total matrisome. Of their 281 core matrisome proteins, 51 were detected in the present study (18%). Working *in vivo* (Figure 3.6 B, right), Naba *et al* found 143 and 107 candidate proteins in lung (Figure 3.6 B right, blue circle) and colon (Figure 3.6 B right, green circle) ECM respectively, totalling 166 distinct candidate proteins (with overlap). Of these, 53 were also detected in the present study (32%). This level of overlap indicates that the present study's recovery of ECM proteins, while not as reliable as the recovery of adhesion proteins, is sufficient for analysis.

To analyse the alterations to adhesion and ECM proteins in the recovered fraction, the TMEM67 patient cell protein levels were compared to those of controls. Widespread changes in abundance were found. Of the 1394 proteins detected, 638 had significantly altered abundance. Of these 638, only 30 had increased abundance, with the vast majority (608) reduced. The 608 proteins with reduced abundance included 198 of the "reproducible" adhesome proteins identified by Kuo *et al*, representing 26% of the reproducible adhesome and 47% of the reproducible adhesome proteins also detected in the present study. Only 3 of the 30 proteins with increased abundance were reproducible adhesome proteins (MAP4, P4HB, and tenascin C). In comparison to Kuo *et al*'s full adhesome, 344 proteins were lower in abundance (representing 18% of the full adhesome), while only 14 were increased. These results indicate major reductions in the protein content of adhesions in *TMEM67* patient cells.

To investigate the changes to the adhesome and matrisome, knowledge-based annotation of the list of significantly altered proteins was undertaken. Proteins of interest were identified within six exclusive functional categories (Figures 3.7-3.9): core adhesion components (excluding proteins that fell into any other category) (Figure 3.7 A), transmembrane receptors (including integrins) (Figure

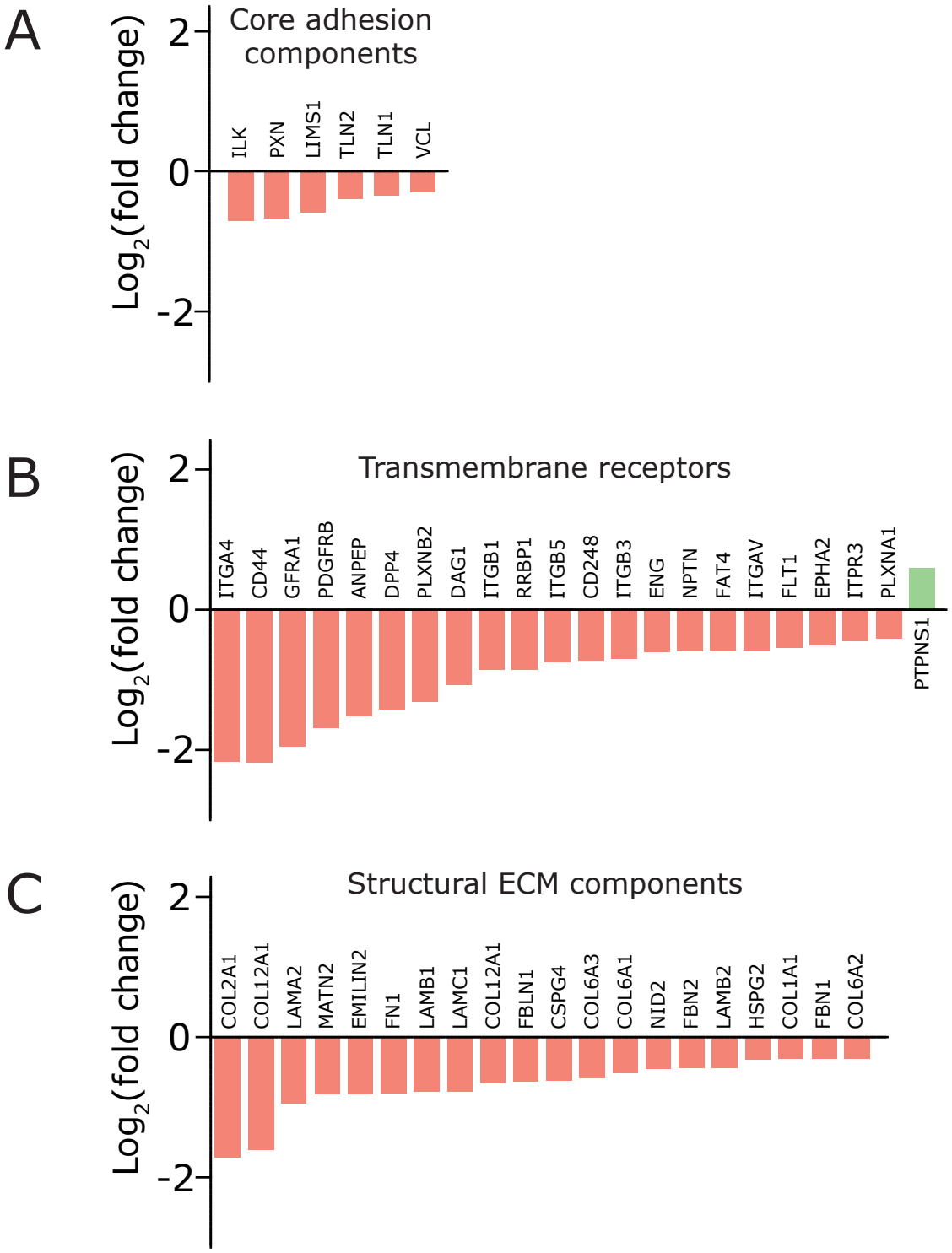

Figure 3.7: Abundance of core adhesion, transmembrane receptor, and structural ECM components are altered in the adhesion/ECM fraction of *TMEM67* patient cells.

Graphs show abundance fold change (on a logarithmic scale) for individual proteins within category, with respect to control cells. Proteins were categorised via knowledge-based annotation.

3.7 B), structural ECM components (including major ECM proteins such as collagen and laminin) (Figure 3.7 C), membrane trafficking proteins (Figure 3.7 A), ECM-associated signalling molecules (which are secreted into and typically sequestered by the ECM) (Figure 3.7 B), ECM remodelling factors (such as matrix metallopeptidases) (Figure 3.7 C), actin binding proteins (Figure 3.9 A), and non-actin-binding actin regulatory proteins (Figure 3.9 B).

Only a few core adhesion components were identified (Figure 3.7 A), which were all present with lower abundance in *TMEM67* patient cells, with fold changes between 0.6 and 0.9.

A total of 22 significantly altered transmembrane receptors were identified, all but one of which were reduced (Figure 3.7 B). Eleven of these were highly reduced with fold changes below 0.5; the most reduced were alpha-4 integrin and CD44, though several other integrins were also represented including beta-1 integrin.

The 20 structural ECM components identified were all reduced in abundance (Figure 3.7 C). This included six collagens and four laminins.

Membrane trafficking proteins were the most highly represented group; 41 were identified, all of which were reduced (Figure 3.8 A). This category included the most reduced protein in the dataset, caveolin-1, with fold change < 0.1. An additional isoform of caveolin-1 was also detected with reduced abundance.

A total of 17 ECM-associated signalling molecules were significantly altered (Figure 3.8 B). However, the alterations here were mixed, with 11 proteins decreased and 6 increased, across a wide range of fold changes from 0.14 to 2.4.

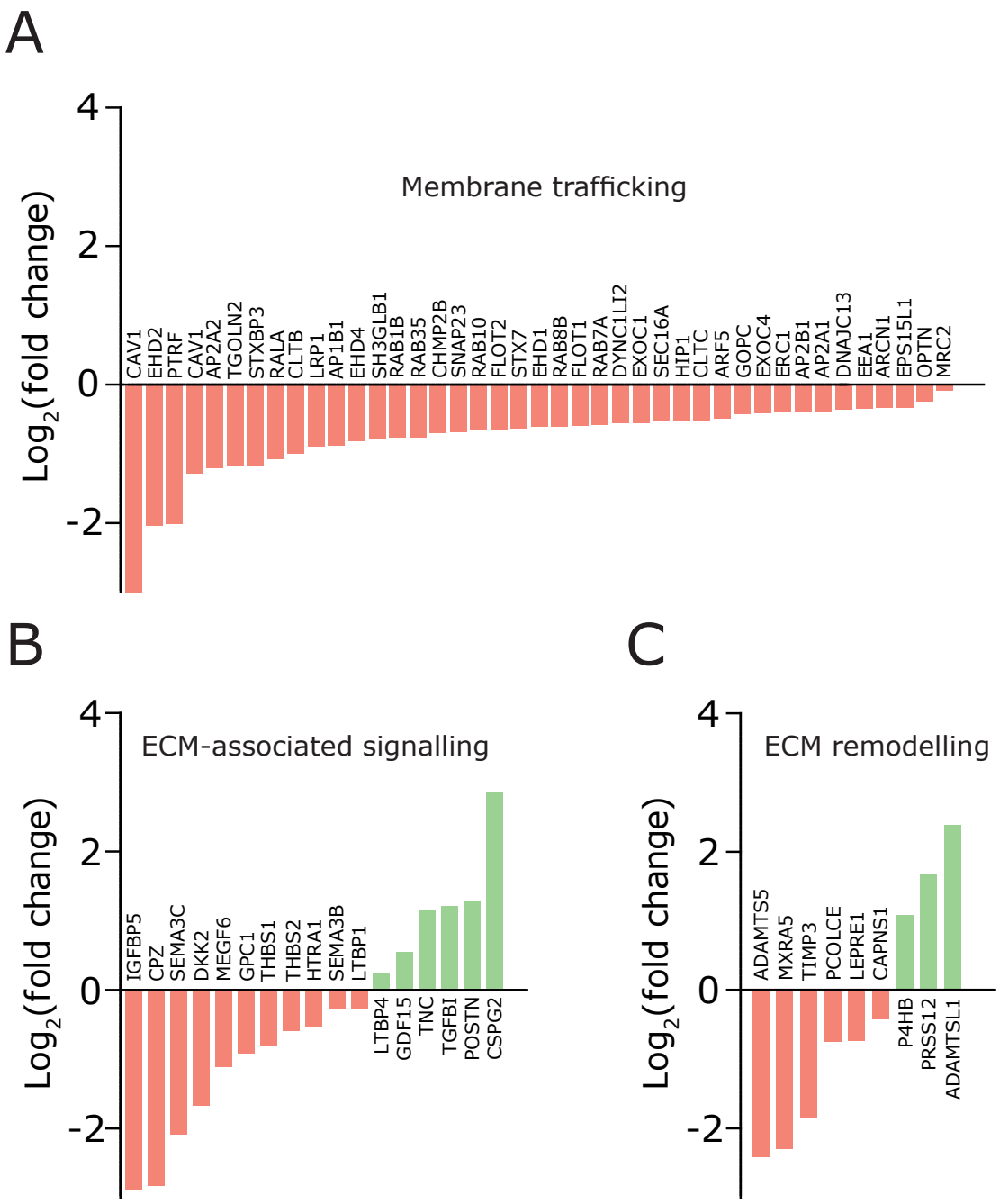

Figure 3.8: Abundance of membrane trafficking, ECM-associated signalling, and ECM remodelling proteins in the adhesion/ECM fraction are altered in *TMEM67* patient cells.

Graphs show abundance fold change (on a logarithmic scale) for individual proteins within category, with respect to control cells. Proteins were categorised via knowledge-based annotation.

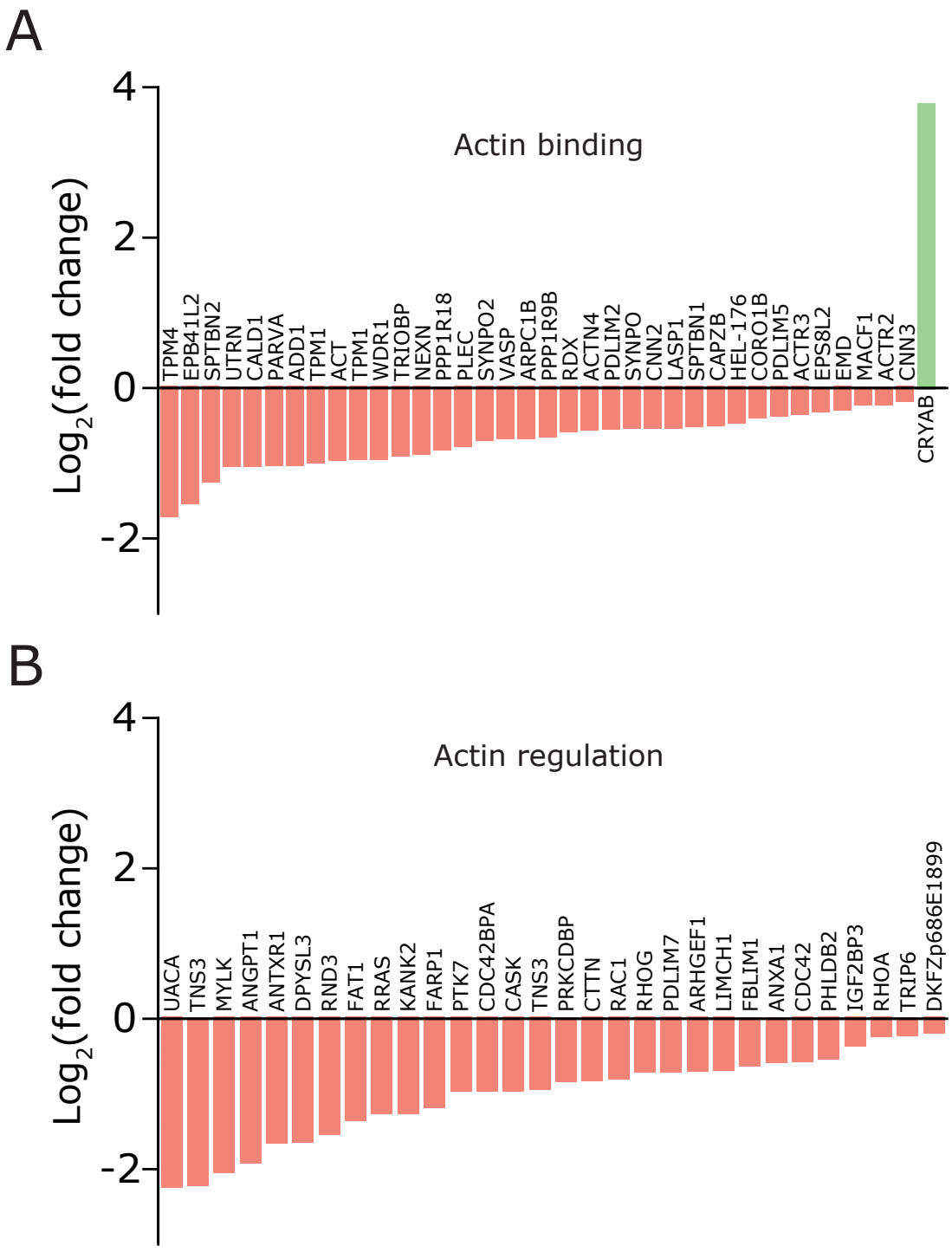

Figure 3.9: Abundance of actin binding and actin regulatory proteins is altered in the adhesion/ECM fraction of *TMEM67* patient cells.

Graphs show abundance fold change (on a logarithmic scale) for individual proteins within category, with respect to control cells. Proteins were categorised via knowledge-based annotation.

ECM remodelling proteins showed a similar mixed pattern, with six decreased and three increased (Figure 3.8 C).

Actin-binding proteins and actin regulatory proteins were a large component of the dataset, with 68 proteins represented between them. Of the 38 actin-binding proteins significantly altered, all but one was reduced in abundance (Figure 3.9 A). The sole increased actin-binding protein was alpha-B crystallin, which was the most increased protein in the dataset with a fold change of 13.6. The 30 actin regulatory proteins were all decreased in abundance (Figure 3.9 B).

3.5 Adhesion morphology is altered in MKS patient fibroblasts

Given the evidence of alterations to adhesion transcripts and proteins in MKS patient cells, the next question addressed was whether these changes led to alterations in the morphology and distribution of adhesions in MKS cells. To investigate changes in distribution of adhesions within spreading cells, control, *TMEM67*, and *TMEM216* cells were plated for 20 minutes on ECM substrates, then fixed and immunolabelled for vinculin, a major component of the cell-substrate adhesion complex. For all cell lines, the population at this timepoint was morphologically heterogeneous. Six categories of combined overall cellular and vinculin adhesion morphology were observed, with examples of each morphology category seen in all three cell lines (Figure 3.10).

These morphology categories (Figure 3.10 A) were:

Early: cells that had not initiated lamellipodial spreading, which were small and usually close to circular. These cells had a ring of vinculin staining, either continuous or punctate, around their periphery but few or no elongated “fibrillar” adhesions. These cells often showed brighter, diffuse vinculin staining within the

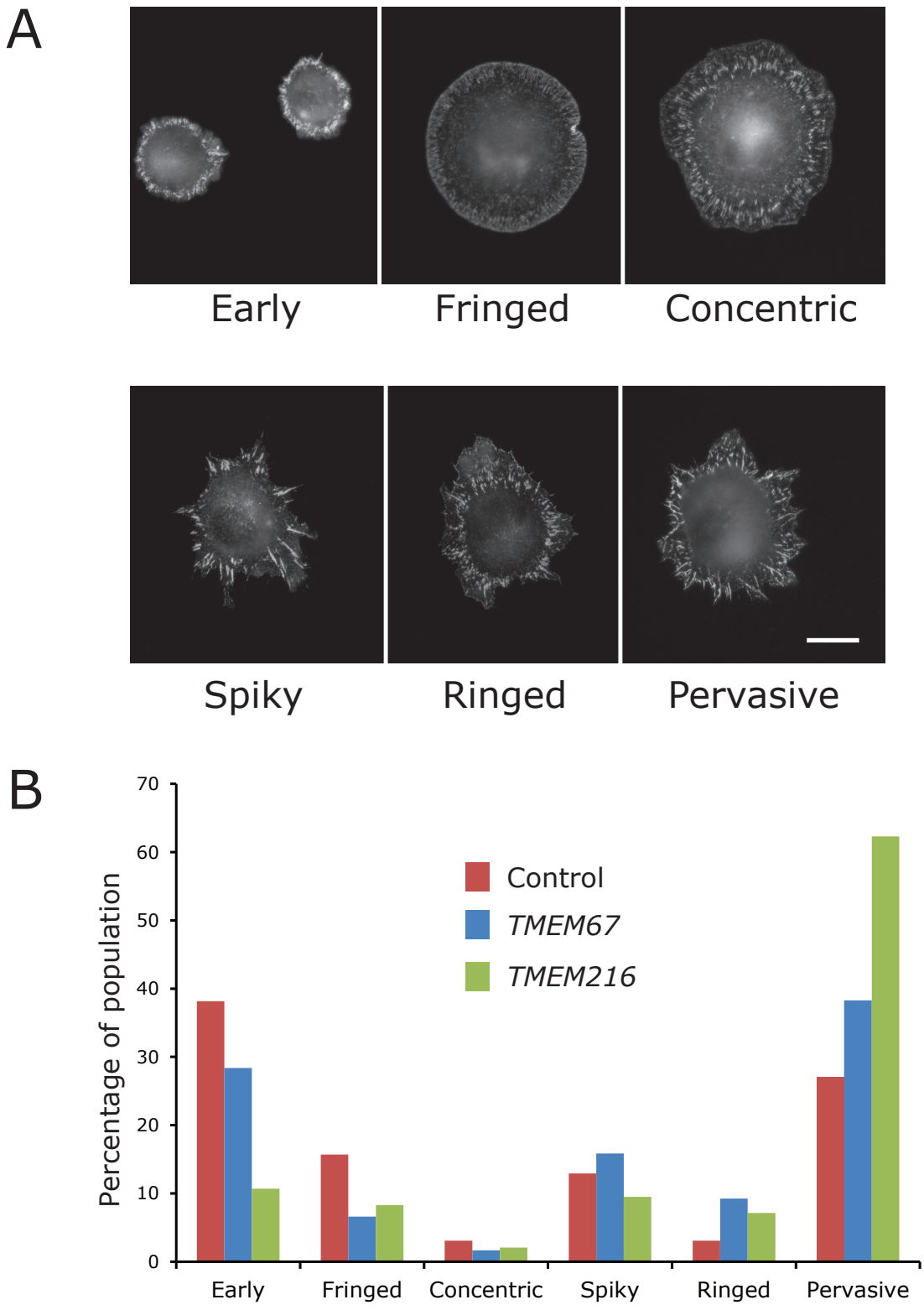

Figure 3.10: MKS patient cells exhibit alterations to adhesion patterning. Cells were plated for 20 minutes on ECM substrates, then fixed and immunostained with anti-vinculin to label focal adhesions. Based on observed adhesion distribution, cells were assigned to one of six categories. A: example cells representing each category. Bar: 20 μm. B: Percentages of control and MKS patient calls that match each category (*n* = at least 56 cells per line).

cell body than other morphologies, likely indicating cytoplasmic reserves of vinculin not yet assembled into adhesion complexes.

Fringed: cells that were spread and highly circular, with a fringe of vinculin staining near the periphery, consisting of a continuous ring of staining at the very edge of the lamella and a region of constant width inward from the cell edge decorated by punctate adhesions. These cells had few or no fibrillar adhesions.

Concentric: cells that were spread and moderately circular, with multiple rings of vinculin staining not confined to the cell periphery. These cells exhibited larger adhesion patches than fringed cells, but still few or no fibrillar adhesions.

Spiky: cells that were highly irregular and stellated in shape, with strongly fibrillar adhesions typically extending along the interior of the stellations. These adhesion “spikes” were prominent and elongated in comparison to the fibrillar adhesions of other morphologies, and few smaller or more punctate adhesions were present.

Ringed: cells that were irregular, but less so than “spiky” cells, and showed a ring of moderately fibrillar adhesions and punctate adhesions around the cell body, but also some large regions of lamella undecorated by adhesions.

Pervasive: cells that were as irregular in shape as “ringed” cells, but which showed adhesions pervading the entire lamella, leaving no undecorated regions other than the cell body. These adhesions ranged from punctate to fibrillar.

Having identified descriptive adhesion morphology categories, prevalence of these morphologies was quantified. For each cell line the percentage of cells that conformed to each category was recorded (Figure 3.10 B). The most

prevalent morphologies in control cells were “Early” and “Pervasive”. In comparison to controls, in the *TMEM67* and *TMEM216* cell lines fewer cells matched the “Early” category, and more cells were seen which matched the “Pervasive” category; with *TMEM216* cells in both cases showing greater deviation from control cells.

Having observed differing cell-wide adhesion patterning, next the patterning of individual adhesions was investigated in more detail. In cells immunolabelled for vinculin after plating for 20 minutes, a 10 μm by 10 μm square region of interest was chosen (without bias) at the cell periphery adjacent to the cell edge (Figure 3.11 A). This region was manually examined to identify individual adhesions (Figure 3.11 B, C) which were counted, and measured for perimeter, area, length, and width (Figure 3.11 D). A ratio of length to width was calculated for each adhesion to quantify roundness, and the total coverage of the area was determined by the percentage of adhesion area to total area. These measurements were taken for cells on fibronectin, collagen I, collagen IV, laminin, and vitronectin substrates. It was found that *TMEM67* patient cells spreading on a collagen IV substrate had significantly fewer adhesions per area than control cells (Figure 3.12), and that *TMEM216* cells spreading on a laminin substrate had significantly more adhesions per area, and greater coverage of the region with adhesions, than control cells (Figure 3.13). Neither MKS cell line exhibited significant alterations to adhesion size (Figures 3.12, 3.13), or to length, width, roundness, or perimeter (data not shown).

3.6 MKS patient cells have defective extracellular matrix

Given the changes to ECM gene expression (Figure 3.1) and ECM protein content (Figures 3.2, 3.7, 3.8, 3.9) found in *TMEM67* cells, together with the alterations to cell-ECM interaction implied by the focal adhesion alterations in

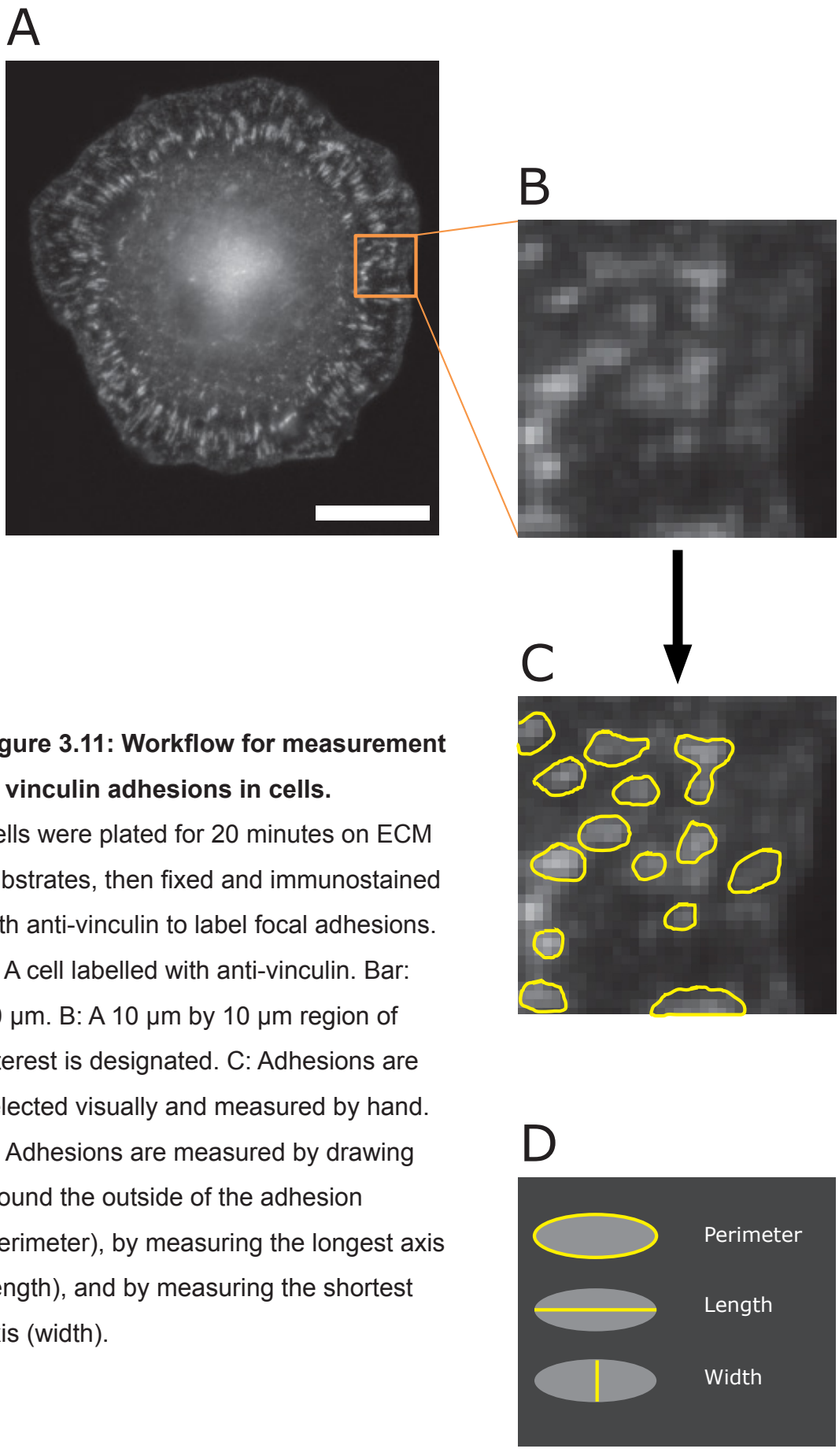

Figure 3.11: Workflow for measurement of vinculin adhesions in cells.
Cells were plated for 20 minutes on ECM substrates, then fixed and immunostained with anti-vinculin to label focal adhesions. A: A cell labelled with anti-vinculin. Bar: 20 μm. B: A 10 μm by 10 μm region of interest is designated. C: Adhesions are selected visually and measured by hand. D: Adhesions are measured by drawing around the outside of the adhesion (perimeter), by measuring the longest axis (length), and by measuring the shortest axis (width).

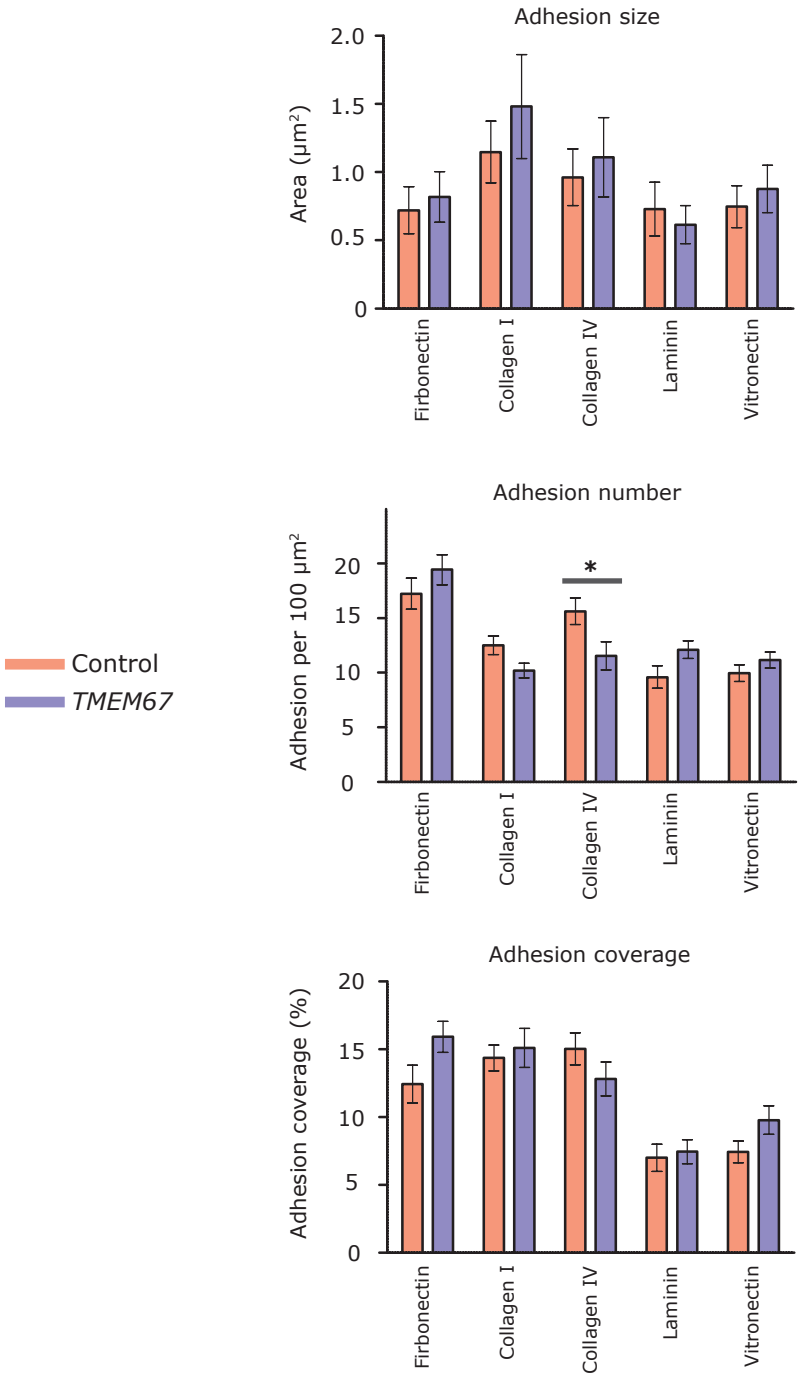

Figure 3.12: *TMEM67* patient cells exhibit reduced adhesion number on a Collagen IV substrate. Error bars: SEM. *: $p < 0.05$, ANOVA with Bonferroni post-tests; *n* = 25 cells per line per condition over 2 experiments.

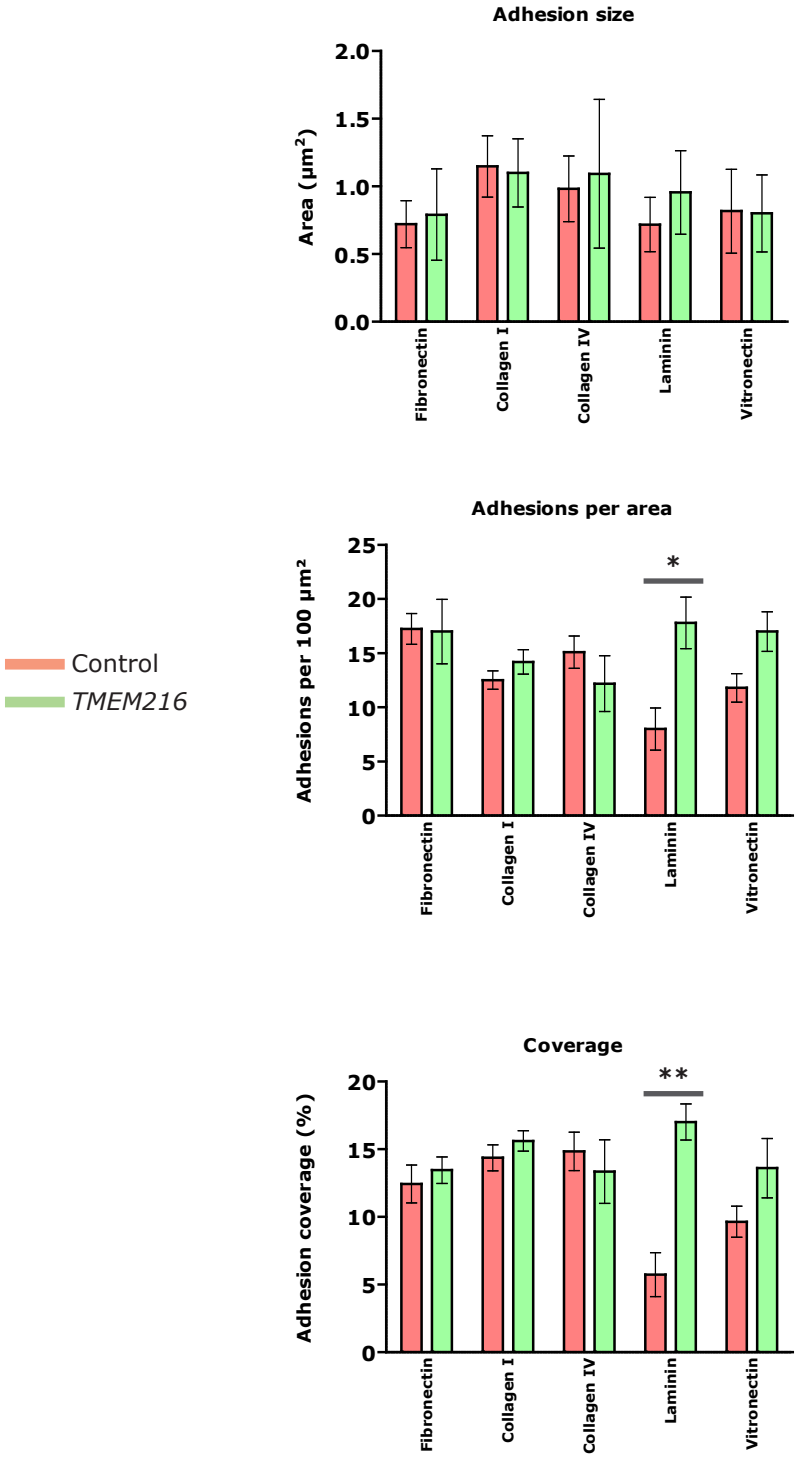

Figure 3.13: *TMEM67* patient cells exhibit increased adhesion number and coverage on a laminin substrate. Error bars: SEM. *: $p < 0.05$, **: $p < 0.01$; ANOVA with Bonferroni post-tests; *n* = 25 cells per line per condition over 2 experiments.

TMEM67 (Figure 3.12) and *TMEM216* cells (Figure 3.13), the next question investigated was whether the MKS patient cell ECM was morphologically defective. MKS patient cells were allowed to synthesise ECM on glass coverslips for four days, then the cell layer was stripped via high alkaline treatment and the remaining cell-derived matrix (CDM) layer was fixed and processed for scanning electron microscopy (SEM). The electron micrographs (Figure 3.14) revealed that *TMEM67* CDM was markedly less dense, contained fewer fibrillar structures, and was less interconnected than the CDM of control cells. *TMEM216* CDM showed an even more severe phenotype: there was little material of any kind, and no evidence of an interconnected ECM network.

3.7 Discussion

In this chapter it has been shown that TMEM67 is a focal adhesion protein, and that the absence of TMEM67 is associated with major alterations to the expression of genes, and to the abundance of proteins, associated with adhesions and the extracellular matrix; as well as a marked morphological alteration to the extracellular matrix and substrate-specific alterations to adhesion patterning. *TMEM216* patient cells showed a more extreme version of the ECM phenotype, as well as an alteration in substrate-specific adhesion patterning.

The proteomics of the focal adhesion complex have been studied for some time, so the identification of TMEM67 as an adhesion protein in this chapter (Figure 3.4) raises the question: why was TMEM67 not detected at adhesions before now? Methods for isolating adhesion proteins for proteomic studies have varied: Plopper *et al* used trypsin treatment and resuspension of the whole culture followed by incubation with RGD-coated beads (Plopper & Ingber, 1993), which was likely to degrade many proteins and only recover those

strongly bound to the subset of integrins with RGD-binding activity; whereas Kuo *et al* introduced a method (used in the present chapter) to recover adhesion proteins via isotonic treatment and hydrodynamic force (Kuo *et al*, 2012), which, while less chemically aggressive than Plopper *et al*'s method, is liable to wash away loosely attached proteins. Furthermore, proteomic studies generally have low repeatability; for example, a meta-analysis of flagellar proteomes found only 25 proteins shared between three different proteomic studies which had each detected >100 proteins (Broadhead *et al*, 2006). Within studies of the adhesome, Horton *et al* defined a consensus adhesome and found that it excluded 90% of the candidate adhesion proteins suggested in a previous analysis (Geiger & Zaidel-Bar, 2012; Horton *et al*, 2015), which they attributed to tissue and isoform specificity of some protein adhesion associations. In Kuo *et al*'s study of the adhesome, only 754 proteins were shared between three methodologically identical repeats which identified a total of 1917 proteins (summarised in Figure 3.6) (Kuo *et al*, 2011). The adhesome presented in this chapter, which was methodologically similar to Kuo *et al*'s but employed different cell lines, had an overlap of 797 proteins (Figure 3.6) with Kuo *et al*'s total out of 1394 detected; and likewise failed to detect TMEM67. Given the high variability of these studies, it is likely that many adhesion associated proteins remain to be detected, especially if their abundance is low or their association with the adhesion is conditional, tissue specific, or transient, any of which may be true for TMEM67.

A cell-substrate adhesion role for TMEM67 places it alongside a number of other ciliopathy proteins that have recently been found to associate with adhesions. NPHP1 localises to cell-matrix and cell-cell adhesions (Benzing *et al*, 2001), and the polycystic kidney disease protein PKD1 is a transmembrane

protein with adhesion domains that is involved in integrin recycling to nascent adhesions (Palsson *et al*, 1996; Woods *et al*, 2004), and also has an essential role in cell-cell adhesion at adherens junctions (Streets *et al*, 2003; Huan & van Adelsberg, 1999; Ibraghimov-Beskrovnaya *et al*, 2000). PKD2 is predicted to be an adhesion protein, and PKD1 and PKD2 regulate extracellular matrix formation (Mangos *et al*, 2010). Since cystic kidney is a common pathology in MKS patients there may be a shared aetiology in dysregulation of the ECM.

The widespread disruption to focal adhesion protein content (Figures 3.7-3.9) may have many downstream effects. Loss of core adhesion components (Figure 3.7 A) such as the talins, major integrin-actin linking and tension-sensing proteins, could further disrupt cell adhesion and actin organisation by preventing the establishment of the ECM-adhesion-actin mechanotransduction axis. Reduction in levels of transmembrane receptors (Figure 3.7 B), including multiple integrins which are essential adhesion receptors, could impact the ability of the cell to sense and respond to its environment; this disruption could be upstream of the ECM defect, since the ECM is regulated through an integrin-mediated feedback mechanism (Gjorevski & Nelson, 2009). ECM structural components are also depleted (Figure 3.7 C), with collagens and laminins prominent, although interestingly collagen IV is not detected as reduced in abundance despite this being indicated by Western blot (Figure 3.2 A); in fact, it was not detected in the fraction at all, even in control cells (Appendix 1, Table 2). Given the unreliable detection of specific proteins by this experimental approach, however (see above), this is not necessarily meaningful.

Widespread disruption to the membrane trafficking machinery is also in evidence (Figure 3.8 A), with two isoforms of caveolin-1 especially reduced in abundance. A defect in trafficking could indicate a loss of delivery and recycling

to the adhesion complex, which might explain the protein depletion observed, and a reduction in ECM secretion. This is reminiscent of the finding that PKD1 promotes recycling of components to the adhesion, including integrins (Woods *et al*, 2004): TMEM67 may have a similar function.

No overall pattern of change to ECM-associated signalling molecules (Figure 3.8 B) or ECM remodelling factors (Figure 3.8 C) was observed, though there were disruptions to individual proteins. Actin binding (Figure 3.9 A) and regulatory proteins (3.9 B) were (with a single exception discussed below) all depleted. This may reflect a loss of actin filament association with the adhesions, which given the bidirectional feedback that drives adhesion and actin cable assembly (Kuo *et al*, 2011; Defilippi *et al*, 1999; Hynes, 2002), could originate in either structure.

Given these large changes to the protein content of adhesions, it is surprising that when visualised and measured (Figures 3.10-3.13), the changes to morphology of adhesions are relatively minor, with only small substrate-specific alterations that barely pass a statistical significance test. However, these results were obtained in cells shortly after plating, whereas the proteomic dataset was acquired from cells that had been plated for >4 days (which was necessary for ECM to be synthesised). By this point an actin defect characterised by dense actin bundles appears in TMEM67 patient cells (McIntosh, 2016; Adams *et al*, 2012; Dawe *et al*, 2007b; Valente *et al*, 2010) (discussed in more detail below). The defective ECM phenotype likely emerges at some point in between; it may be informative to repeat the adhesion measurements in cells at 4 days to determine what the effect of a mature cell-derived ECM is on adhesion morphology in MKS patient cells.

Adhesions and actin filaments are physically connected and work cooperatively to transduce mechanical signals along the ECM-adhesion-actin axis, which regulates adhesion assembly and turnover as well as influencing actin stress fibre formation (Xu *et al*, 2012; Wehrle-Haller, 2012; Tomasek *et al*, 2002; Grinnell, 2003), depending on ECM stiffness and Rho GTPase signalling (Ridley & Hall, 1992). Given the findings in this chapter that in *TMEM67* patient cells, adhesion protein content is widely diminished, with many actin-binding and actin regulatory factors among those reduced in abundance including members of the Rho family (Rho A, Rho G, Rac1, and Cdc42) (Figure 3.9), and that the ECM secreted by these cells is defective (Figure 3.14), effects on the organisation of the actin cytoskeleton are almost inevitable. Actin organisation defects have been reported in *TMEM67* and *TMEM216* patient cells (Adams *et al*, 2012; Dawe *et al*, 2009; Valente *et al*, 2010; McIntosh, 2016). In *TMEM67,* actin bundle density is significantly increased 4 days after plating, with bundles appearing thicker and more intense via immunofluorescence, accompanied by a decreased G- to F-actin ratio (McIntosh, 2016). *TMEM216* cells exhibit earlier dense actin formation arising as quickly as 40 minutes after plating, and, contrary to *TMEM67*, an increased G- to F-actin ratio (McIntosh, 2016). Actin defects have also been reported in other ciliopathies (Gakovic *et al*, 2011; Hernandez-Hernandez *et al*, 2013; Yin *et al*, 2009; Kim *et al*, 2010; Pitaval *et al*, 2010), and other ciliopathy proteins that localise to actin have been identified, including BBS proteins (Hernandez-Hernandez *et al*, 2013; May-Simera *et al*, 2015). Disruption of BBS4, BBS6, or BBS8 proteins lead to abnormal actin morphology (Hernandez-Hernandez *et al*, 2013). This evidence all suggests a general role for ciliopathy proteins in regulation of the actin cytoskeleton. Specifically in the case of TMEM67, its interaction with the adhesion protein and

actin regulator Filamin A (FLNA) (Adams *et al*, 2012) is particularly interesting; the two proteins may cooperate to organise actin both in the cytoplasm and at adhesions; and the absence of TMEM67 in patient cells may lead to aberrant localisation or function of FLNA. Loss of FLNA causes many of the same cellular phenotypes as loss of TMEM67, including actin organisation defects, basal body positioning and ciliogenesis defects, and deregulation of signalling (Adams *et al*, 2012), and has been linked to patient pathologies including pulmonary cysts (Emiralioglu *et al*, 2015), and pulmonary dysplasia (Lord *et al*, 2014), which is the cause of death in most MKS patients (Kenny & Beales, 2013).

In light of this relationship between TMEM67 and FLNA, the massive increase in abundance of the small heat shock protein alpha-B crystallin (CRYAB) in the adhesion/ECM fraction (Figure 3.9 A, green bar) is especially interesting: CRYAB has a conserved actin-binding domain, and also binds to FLNA (Wójtowicz *et al*, 2015). CRYAB's abundance was increased by a factor of 13; it was the single most increased protein in the dataset, and was the only actin-binding or actin-regulatory protein to be increased. Whether this represents a cell-wide increase in CRYAB levels, or merely a redistribution of CRYAB to the ECM, adhesions or adhesion-associated actin is not clear. CRYAB is mostly known as one of the highly stable crystallins that make up the lens of the eye, but it has widespread expression outside the eye, and its actin-binding activity is known to be important for the stabilisation of myofibrils in muscle tissue (Wójtowicz *et al*, 2015; Goldfarb & Dalakas, 2009). This actin stabilising function may have a role in the aberrant dense actin bundles seen in *TMEM67* cells (Adams *et al*, 2012; Dawe *et al*, 2009; Valente *et al*, 2010; McIntosh, 2016). Given the interaction between actin, FLNA, and TMEM67 (Adams *et al*, 2012), a

possible model to explain the increased abundance of CRYAB in the adhesion/ECM fraction is that in the absence of TMEM67, FLNA is free to be bound by CRYAB, leading to increased recruitment of CRYAB to the adhesion complex in place of TMEM67. Alternatively, the increased level of CRYAB may be a stress response to one of the various defects in *TMEM67* patient cells; as a molecular chaperone, this is one of its predicted functions (Morimoto, 1998).

Alterations to the actin cytoskeleton have knock-on effects on ciliogenesis, since actin remodelling is required for basal body migration and docking (Gray *et al*, 2009; Pan *et al*, 2007; Park *et al*, 2006; Carvajal-Gonzalez *et al*, 2016; Song *et al*, 2010; Gray *et al*, 2011; Borovina *et al*, 2010; Epting *et al*, 2015; Boisvieux-Ulrich *et al*, 1990; Boisvieux- Ulrich *et al*, 1987; Kim *et al*, 2015, 2010; Klotz *et al*, 1986; Lemullois *et al*, 1988, 1987; Pitaval *et al*, 2010; Yan & Zhu, 2013). Disruption to actin regulation downstream of the defects found in this chapter may therefore explain ciliation defects leading to signalling disruption and patient phenotypes. This may take place through activated YAP/TAZ signalling downstream of ECM rigidity and stress fibre formation, which inhibits ciliogenesis by preventing actin reorganisation (Kim *et al*, 2015; Halder *et al*, 2012; Wada *et al*, 2011; Zhao *et al*, 2012; Dupont *et al*, 2011). This suggests a model where in MKS patient cells, defective ECM synthesis leads to a more rigid substrate, which activates YAP/TAZ signalling and therefore inhibits ciliogenesis. A cautionary note regarding the relationship between substrate stiffness and ciliation is merited, however: cell culture glass and plastic are several orders of magnitude more stiff than most tissue (Lu *et al*, 2012). It is possible that defective ciliogenesis in MKS cells may be partially caused by the artificial cell culture surface which they are unable to coat with a

functional pliant ECM of their own, and therefore might not represent a fully physiological phenotype.

The influence of adhesions on the microtubule (MT) cytoskeleton is less clear than for actin. MTs can enter the lamella and interact with the actin cytoskeleton to regulate migration (Lindberg *et al*, 1981; Theisen & Straube, 2016). MTs appear to target adhesions, and can regulate adhesions, since contact of a MT plus-end with an adhesion is a stimulus for adhesion disassembly (Stehbens & Wittmann, 2012; Ezratty *et al*, 2005; Kaverina *et al*, 1999). However, adhesions also capture and stabilise MTs (Kaverina *et al*, 1998), leading to regulation of MT dynamics, so causal relationships could run in either direction (Akhmanova *et al*, 2009). It is plausible that the general loss of adhesion protein content found in this chapter would influence these interactions, but it is not clear how. There is a MT defect in MKS cells involving loss of a single focus for the MT cytoskeleton and altered MT maturation (McIntosh, 2016), however this defect is consistent with defective tethering at the minus ends (possibly downstream of a role for TMEM67 as an organiser or linker at the centrosome), and appears rapidly (within 20 minutes) after plating (McIntosh, 2016), so presumably cannot be downstream of an ECM defect (which would not arise in such a short time), and is unlikely to be downstream of an interaction of MT plus-ends with adhesions. The causal relationship may run the other way: could the MT defect underlie changes to adhesions and the ECM by disrupting adhesions, perhaps due to aberrant stimulation of adhesion disassembly, leading to the depleted adhesion proteome found in this chapter? The MT defect was found not to underlie the actin defect or other cellular defects in MKS cells (McIntosh, 2016), but this has not yet been tested for the adhesion or ECM defects found in the present study, so this remains a possibility. Given the influence of MTs on

migration, an alteration to the interaction between MTs and adhesions could be responsible for migration defects in MKS cells, which may underlie patient phenotypes which arise from failure of neural crest cells to migrate to correct sites during development, such as midline defects and heart defects.

The increased expression of matrix metallopeptidases (MMPs) found in this chapter (Figure 3.1 B) might be expected to result in increased ECM degradation, which could explain the reduced ECM density observed in MKS cells (Figure 3.14). However, matrix remodelling enzymes are typically closely regulated at the translational and post-translational levels, via mechanisms such as inhibitory domains, likely due to their potentially destructive effect on tissue if they were to become dysregulated (Page-McCaw *et al*, 2007; Aitken & Bägli, 2009). Therefore a change in expression of these proteins is, even more than for most proteins, not necessarily evidence for a change in abundance or activity. None of the upregulated matrix remodelling transcripts identified in Figure 3.1 were found to have increased abundance in the adhesion/ECM fraction (Figure 3.8 C), though since these proteins are typically soluble they would not be expected to have been retained in this sample. Elevated MMP activity is implicated in inflammatory and vascular disease (Hu *et al*, 2007); these are not reminiscent of any MKS phenotypes, although, in the wider ciliopathies, vascular lesions are seen in PKD (Griffin *et al*, 1997) and airway inflammation is a feature of primary ciliary dyskinesia (Bush *et al*, 2007). Experimentally testing the MMP activity in MKS patient cell cultures would help to determine the importance of this factor in the ECM defect.

ECM stiffness determines cell fate; for example, the differentiation of mesenchymal stem cells into brain (determined by soft ECM), muscle (intermediate ECM), or bone tissue (stiff ECM) (Engler *et al*, 2006). ECM

stiffness is not sufficient for specification, however, as some tissues have similar ECM elasticity (Watt & Hogan, 2000).The ECM has a major influence on cell shape (Ingber, 1991), which is in turn a regulator of growth and differentiation (Folkman & Moscona, 1978) responsible for development of, for example, myocardial organisation (Manasek *et al*, 1972). Correct ECM protein composition also affects cell fate: it is essential for differentiation of endothelia (Wang *et al*, 2013), and control of hepatic stellate cell activation in the liver, which may underlie liver fibrosis in MKS (for more detail on this point, see Chapter 6). Alterations to ECM composition can thus lead to widespread tissue specification defects.

The ECM defect (Figure 3.14) found in this chapter is the most prominent defect yet observed in MKS patient cells and is likely to have profound cellular and developmental consequences. The next chapter will investigate this defect and its downstream effects on cellular phenotypes in MKS patient cells.

Chapter 4

The extracellular matrix defect in MKS is upstream of defective ciliation

Chapter 4: The extracellular matrix defect in MKS is upstream of defective ciliation

4.1 Introduction

Multiple MKS proteins have been shown to be required for ciliogenesis and for docking of the basal body to the cell surface, including TMEM67 (Lee *et al*, 2012; Dawe *et al*, 2007b). Since basal body docking is required for ciliogenesis, it has been suggested that failure to build a cilium in MKS cells is a consequence of disrupted docking. However, docking failure is not always implicated in ciliogenesis defects (Garcia-Gonzalo *et al*, 2011; Singla *et al*, 2010), and MKS proteins including TMEM67 are known to have extra-ciliary roles; among other localisations, TMEM67 has been shown to localise to actin cables (Dawe *et al*, 2009). A number of ciliopathy proteins have been reported to regulate or interact with adhesions (Donaldson *et al*, 2000, 2002; Wilson *et al*, 1999; Markoff *et al*, 2007; Li *et al*, 2005; Hernandez-Hernandez *et al*, 2013), and adhesion and cytoskeletal signalling have been implicated in control of ciliogenesis. It is thus plausible that alterations elsewhere in MKS cells are upstream of ciliogenesis defects.

In this chapter, the causal relationships between absence of the TMEM67 protein, defective ECM, defective ciliogenesis, and disrupted signalling in *TMEM67* cells are investigated.

Both the ciliation and actin defect in *TMEM67* patient cells are shown to be a downstream consequence of defective ECM, and ciliation can be rescued by expression of full-length TMEM67 protein or by inhibition of the TGF-β or canonical Wnt signalling pathways.

4.2 Plating on *TMEM67* cell-derived ECM is necessary and sufficient for defective ciliogenesis

To investigate the role of defective extracellular matrix in ciliogenesis, cell-derived matrix (CDM) from both control and *TMEM67* patient cells was prepared, then control and *TMEM67* patient cells were plated reciprocally on each CDM substrate. The cells were grown under serum-starvation conditions that induce ciliation in normal cells, then cilia were imaged (Figure 4.1 A). Approximately 30% of control cells on control matrix were ciliated, and fewer (< 15%) *TMEM67* cells plated on *TMEM67* CDM were ciliated (Figure 4.1 B), in line with the results of previous studies (Adams *et al*, 2012; Dawe *et al*, 2009). However, when *TMEM67* cells were plated onto control CDM, ciliation was rescued; when control cells were plated on *TMEM67* CDM, ciliation was reduced to a percentage similar to that of *TMEM67* cells on *TMEM67* CDM (Figure 4.1 B). These results indicate that the ciliation defect in *TMEM67* cells is a downstream consequence of defective ECM. To determine whether this was specific to *TMEM67* or might be general to MKS, *TMEM216* patient cells were plated on control and *TMEM216* CDM; control CDM was found to rescue ciliogenesis of *TMEM216* cells (Figure 4.1 C).

4.3 TMEM67 protein is required for a morphologically normal extracellular matrix

Having determined that the ECM defect is upstream of ciliation defects in *TMEM67* cells, it was next asked whether defective ECM morphology (shown in Chapter 3, Figure 3.14) could be attributed to a function of the TMEM67 protein. Cell-derived matrices were prepared from controls, *TMEM67* cells expressing full-length TMEM67, and cells expressing TMEM67-919delF (a deletion in the C-terminal region which abolishes filamin A binding (Adams *et al*,

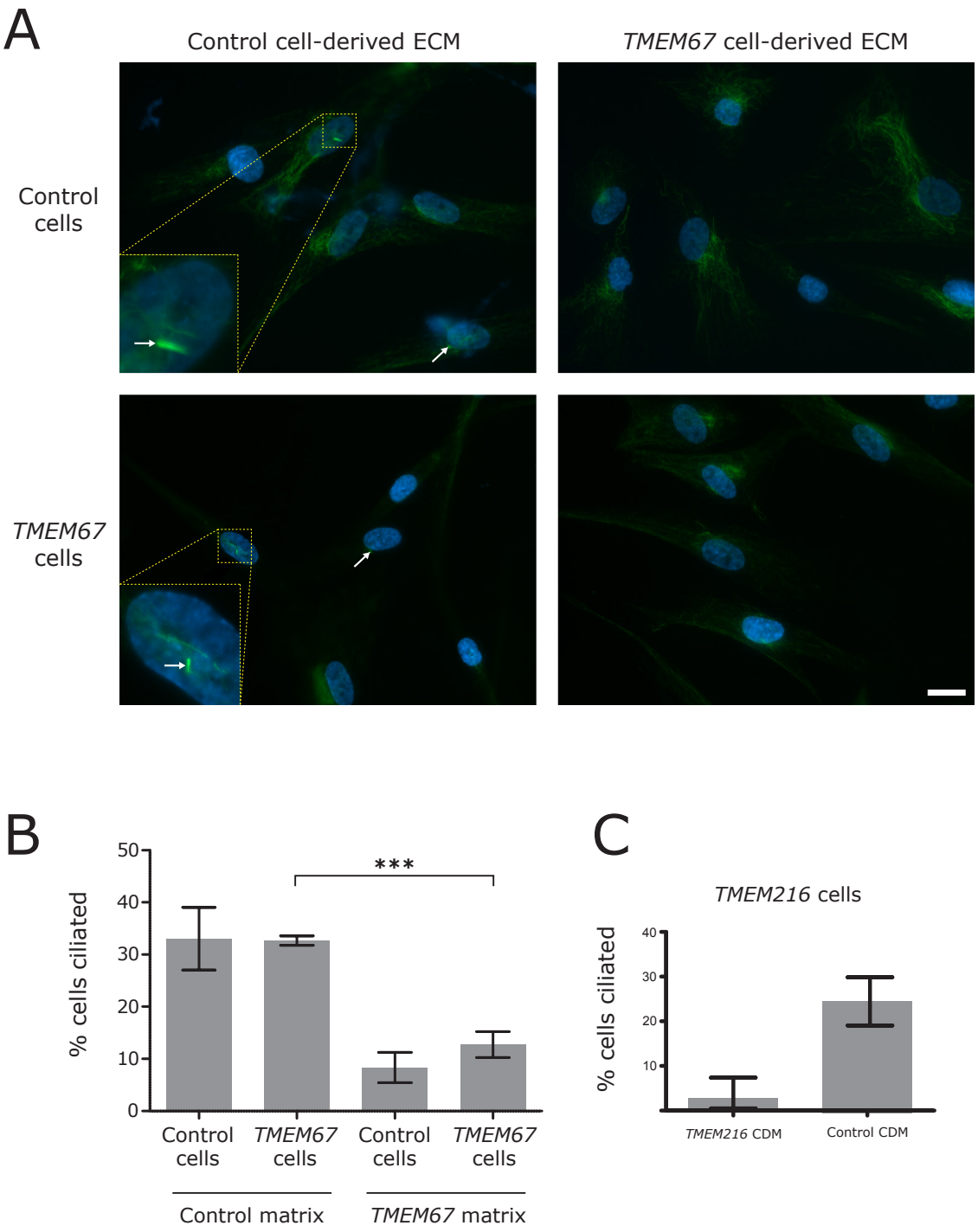

Figure 4.1: Plating on MKS cell-derived matrix is necessary and sufficient for defective ciliogenesis. A: Cells were replated onto control or *TMEM67* cell-derived matrix (CDM), serum-starved for 48 hours to induce ciliation, then fixed and labelled for cilia (acetylated alpha-tubulin, green) and nuclei (DAPI, blue). Micrographs showing representative cells. Arrows: cilia. Bar: 20 μm. B: Percentage of cells ciliated under each condition. Error bars: SEM. ***: $p < 0.001$, χ^2 test, n = at least 200 cells per condition over 4 experiments. C: *TMEM216* cell ciliogenesis was also rescued by replating on control CDM.

2012)). These CDMs were imaged via SEM and the morphology of the ECM examined (Figure 4.2). As previously shown (Figure 3.14), *TMEM67* cells (Figure 4.2, left middle) produce matrix that is sparse in comparison to control cells (Figure 4.2, top). This defect was rescued in cells transfected with full length TMEM67 (Figure 4.2, right middle). Cells transfected with TMEM67-919delF, however, did not rescue matrix morphology (Figure 4.2, bottom row), indicating that the C-terminal region of TMEM67 required for filamin A binding activity is also required for normal matrix morphology.

4.4 Wnt and TGF-β pathway antagonists rescue defective ECM morphology, ciliogenesis, and actin organisation in *TMEM67* patient cells

It has been shown in this chapter that loss of TMEM67 leads to defective ECM morphology, which leads to defective ciliogenesis; however, the causal chain linking these defects, and the connection to the actin defect, is not clear. TGF-β signalling is required for ciliary localisation of MKS proteins (Tozser *et al*, 2015), and Wnt signalling is disrupted in *TMEM67* patient cells and *TMEM67* models (Abdelhamed *et al*, 2013; Adams *et al*, 2012; Dawe *et al*, 2009). To investigate whether these signalling pathways have a role in the cellular defects, *TMEM67* cells were treated with antagonists to the TGF-β and Wnt signalling pathways, and the effect on ECM morphology (Figure 4.3 A), ciliation (Figure 4.3 B), and actin bundle density (Figure 4.3 C) were assessed.

Inhibition of TGF-β signalling with TGF-β receptor 1 kinase inhibitor II (TRIKinII) completely restored matrix morphology (Figure 4.3 A) and ciliogenesis (Figure 4.3 B), but had no effect on actin morphology (Figure 4.3 C). Inhibition of the same pathway with SIS3 partially restored matrix morphology (Figure 4.3 A),

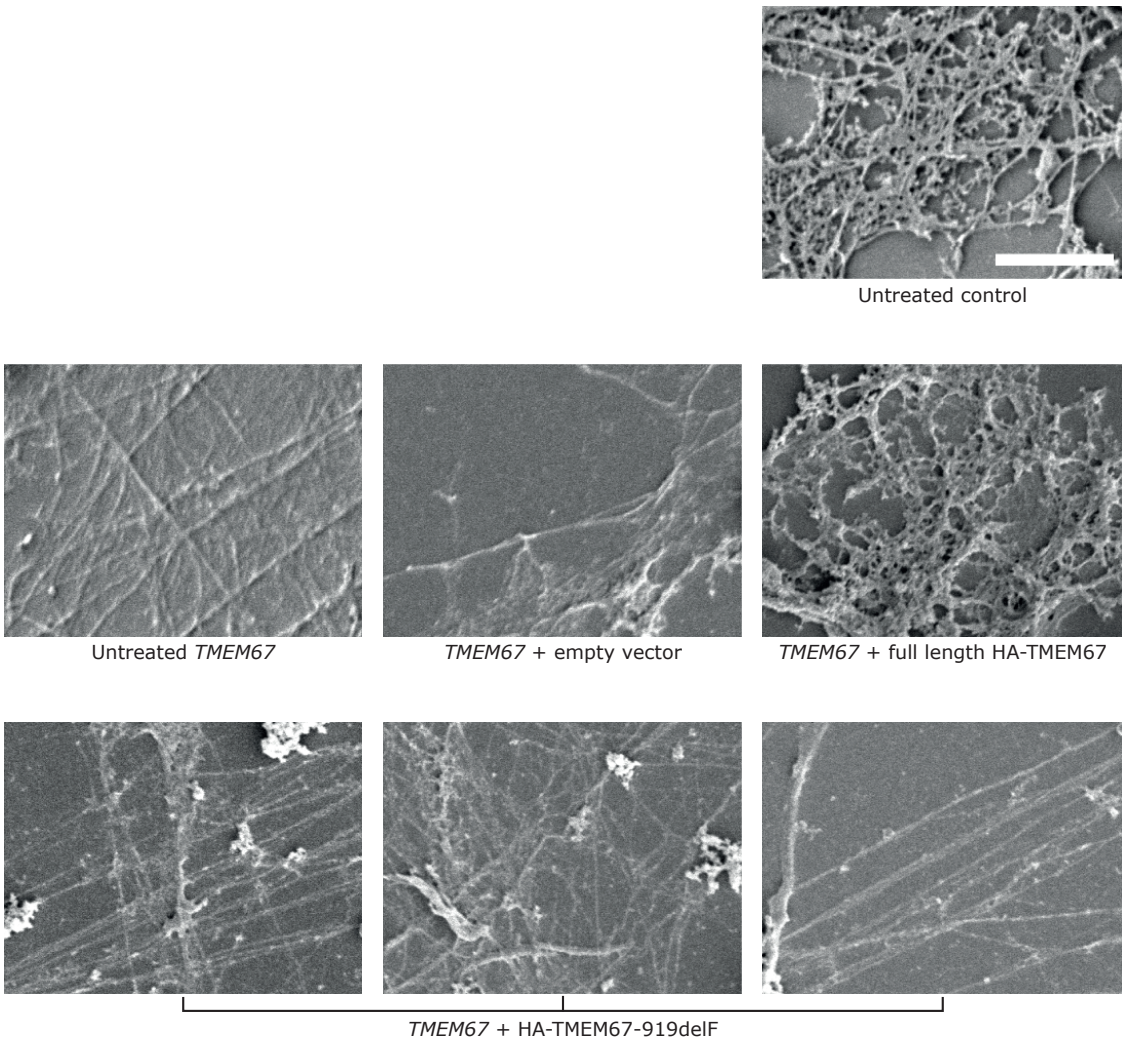

Figure 4.2: *TMEM67* patient cell-derived matrix morphology is rescued by expression of full-length TMEM67, but not by the TMEM67-919delF mutant. Cells were plated (untreated samples) or transfected then plated (all other samples) and allowed to synthesise ECM for 48 hours. Cells were then stripped and CDMs were processed and imaged via scanning electron microscopy. Bar: 5 μm.

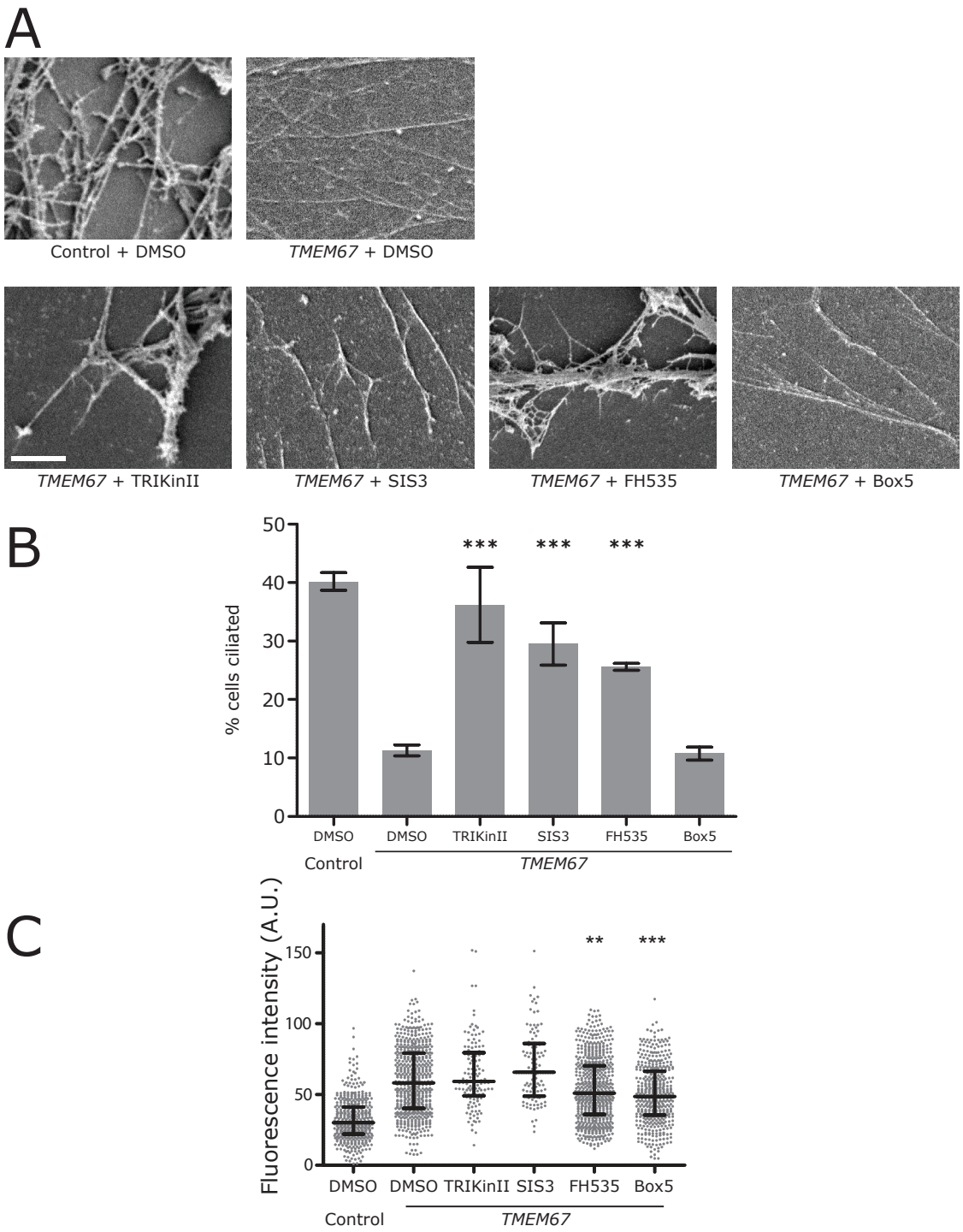

Figure 4.3: *TMEM67* patient cell-derived matrix morphology, ciliogenesis, and actin organisation are restored by treatment with Wnt or TGF-β pathway antagonists. Cells were drug-treated for 48 hours. A: SEM of CDMs. Bar: 2 μm. B: Cells were serum-starved, fixed and labelled for acetylated alpha-tubulin and nuclei, and cilia were counted. Error bars: SEM. ***: $p < 0.001$, χ^2 test; $n = 5$ experiments (at least 200 cells per experiment) C: Cells were fixed and labelled for actin and actin bundle fluorescence intensity was measured. Error bars: interquartile range. **: $p < 0.01$; ***: $p < 0.001$, χ^2 test. $n = 3$ experiments (at least 100 cells per experiment).

and restored ciliogenesis (Figure 4.3 B), but again had no rescue effect on actin morphology (Figure 4.3 C).

The canonical Wnt antagonist FH535 fully restored matrix morphology (Figure 4.3 A), restored ciliogenesis (Figure 4.3 B), and partially restored actin bundle density (Figure 4.3 C). However, the Wnt/planar cell polarity (PCP) pathway inhibitor Box5 had no effect on either ECM morphology (Figure 4.3 A) or ciliogenesis (Figure 4.3 B), though it did partially restore the actin defect (Figure 4.3 C).

These results suggest that signalling through the TGF-β and canonical Wnt pathways, but not the Wnt/PCP pathway, are upstream of defective ECM and ciliogenesis in *TMEM67* cells, while both canonical and non-canonical Wnt/PCP may be involved in the actin defect.

4.5 *TMEM67* knockout mouse cells can be rescued via the same interventions as *TMEM67* patient cells

Having shown that the ciliation and actin defects in *TMEM67* patient cells could be rescued, it was next asked whether these interventions would be effective beyond a single patient cell line. To this end, mouse embryonic fibroblasts (MEFs) with both copies of the *TMEM67* gene knocked out were subjected to the same analyses. These cells exhibited the same sparse ECM phenotype seen in *TMEM67* patient cells (Figure 4.4 A), and their ciliation defect could be rescued by plating on control CDM (Figure 4.4 B). Treatment with pathway antagonists rescued ciliogenesis in a similar pattern to TMEM67 patient cells: TRIKiinII again produced the largest response, but unlike in patient cells, Box5 did partially restore ciliation (Figure 4.4 C). Unlike the patient cells, treatment

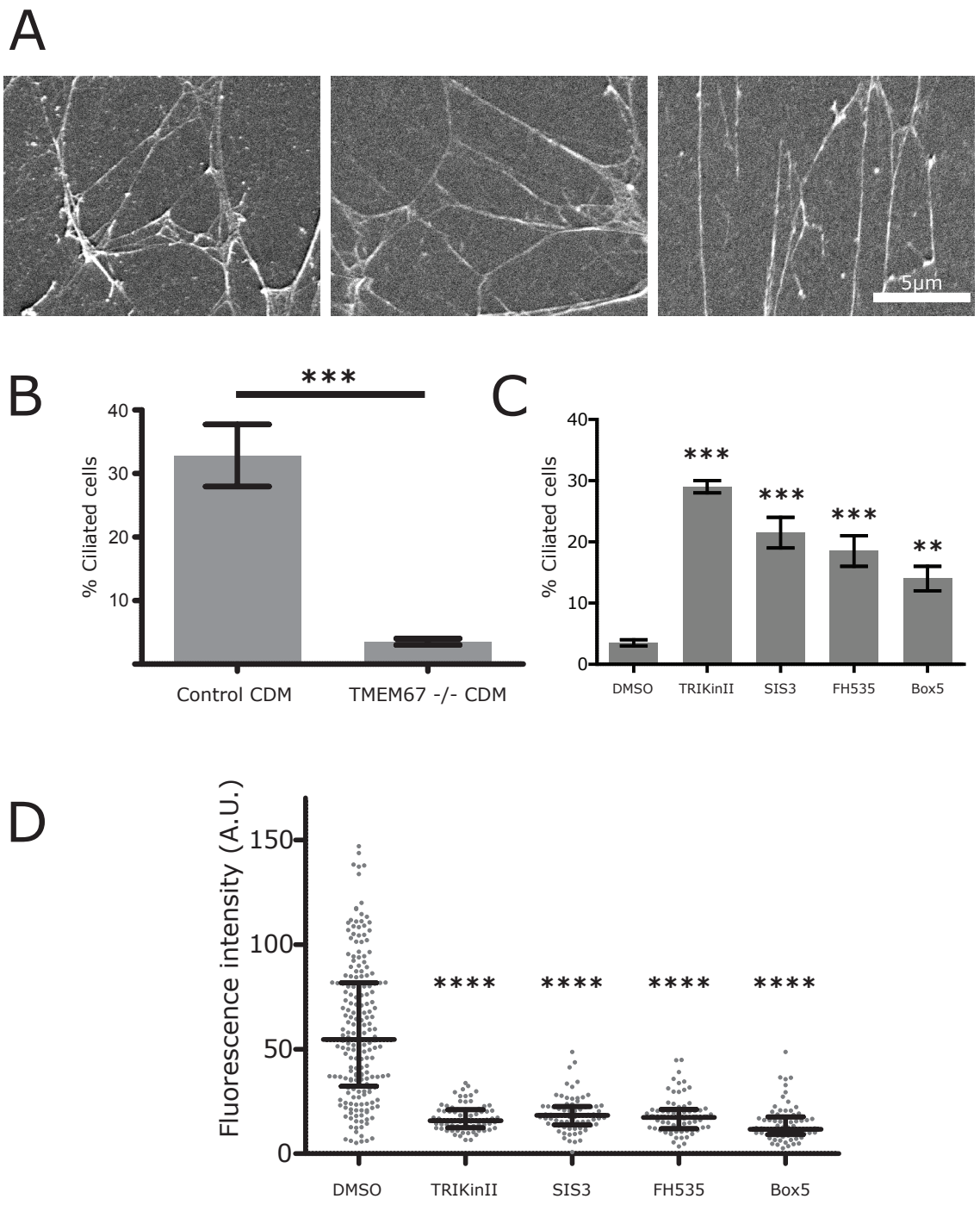

Figure 4.4: *TMEM67* -/- mouse embryonic fibroblasts exhibit the same phenotypes and rescue responses as MKS patient fibrolasts. Cells were treated as for previous experiments. A: SEM of *TMEM67* -/- mouse embryonic fibroblast (MEF) CDM shows sparse ECM. B: *TMEM67* -/- MEF ciliation can be rescued by plating on control CDM (Error bars: SEM; ***: $p < 0.001$, *t*-test), or (C) by treating with Wnt or TGF-β pathway antagonists (Error bars: SEM; **: $p < 0.01$; ***: $p < 0.001$; χ^2 test). C: *TMEM67* -/- MEF actin organisation can be rescued by Wnt or TGF-β antagonists (Error bars: interquartile range. ****: $p < 0.0001$, Kruskal-Wallis test with Dunn's correction for multiple comparisons).

with any of the pathway antagonists reduced the density of actin bundles within the knockout MEFs (Figure 4.4 D).

4.6 *TMEM67* patient cell ciliation can be rescued by plating on collagen IV or laminin

Having shown that plating on a morphologically normal ECM is sufficient to restore MKS patient cell ciliogenesis (Figure 4.1 B), and that drug intervention was sufficient to restore ECM morphology and ciliogenesis in *TMEM67* patient cells, it was next asked: is there a specific component of the ECM which is deficient in MKS patient cells? To investigate this, *TMEM67* and *TMEM216* patient cells were plated onto purified ECM component substrates, or their own CDM as a control, and ciliation was induced by serum-starvation, then cilia were counted as before. *TMEM67* cells had significantly increased ciliation on collagen IV and laminin (Figure 4.5). *TMEM216* cells showed some rescue of ciliation on collagen IV, but this was not statistically significant. For both cell lines, plating on collagen I, fibronectin, or vitronectin had negligible impact on ciliation.

4.5 Discussion

In this chapter, it has been shown that absence of the TMEM67 protein, or its C-terminal filamin A binding region, leads to a chain of events in which, possibly downstream of disrupted TGF-β and/or Wnt signalling, defective ECM causes defective actin organisation and defective ciliogenesis.

The extracellular matrix has diverse roles as both a mechanical substrate and a site for sequestration of signalling molecules , so there are multiple plausible mechanisms whereby defective ECM could lead to defective ciliogenesis. Multiple signalling pathways regulate ciliogenesis (Santos & Reiter, 2008), but

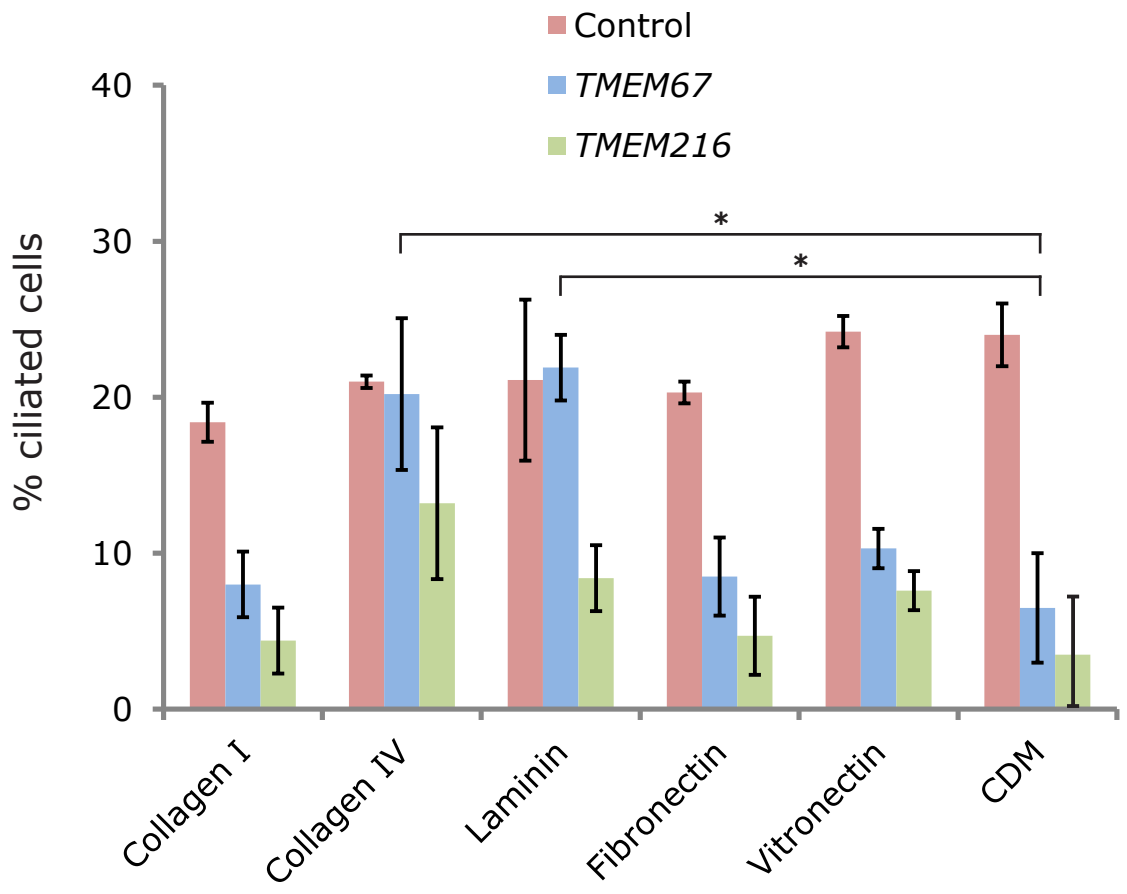

Figure 4.5: Plating on collagen IV or laminin substrates rescues the ciliation defect in *TMEM67* patient cells. Cells were plated onto purified ECM or their own CDM and serum-starved after adhesion. Cilia were counted after 48 hours. Error bars: SEM; *: $p < 0.05$, one-way ANOVA with multiple comparisons post-test. *n* = at least 100 cells per line per condition over 2 experiments.

ciliation also depends on cell shape control: RPE1 cells grown on small fibronectin-coated micropatterns built cilia readily, while those on wide micropatterns did not, leading to the conclusion that spatial confinement is necessary for ciliogenesis (Pitaval *et al*, 2010). However, there is no obvious cell morphology defect in adherent *TMEM67* patient cells, and plating *TMEM67* cells on fibronectin micropatterns did not rescue the ciliation defect (H. Dawe, unpublished observations), so altered spatial confinement of the cell does not appear to be an explanation for the failure of these cells to ciliate. Ciliation is also dependent on cortical contractility (Pitaval *et al*, 2010); aberrant cortical tension could arise due to alterations in adhesion-actin cytoskeleton interaction downstream of cell-ECM interaction. The finding that plating *TMEM67* cells on collagen IV or laminin partially rescues ciliogenesis (Figure 4.5) could therefore indicate that the ECM defect is primarily absence of these components, rather than the other components tested (collagen I, fibronectin, vitronectin). This is consistent with the findings in Chapter 3 that laminin and collagen IV expression (Figure 3.1 B) and protein level in the ECM (Figure 3.2 A) are reduced. A further development of the experiment in Figure 4.5 would be to plate MKS cells on a substrate coated with both laminin and collagen IV; this might completely rescue ciliogenesis.

Restoration of the ECM defect by full-length TMEM67, but not by the TMEM67-919delF mutant that abolishes the filamin A (FLNA)-binding C-terminal region (Figure 4.2), indicates that this region is of critical importance for normal ECM morphology. TMEM67-919delF has previously been shown to not rescue ciliogenesis (Adams *et al*, 2012), which is consistent with the present finding that this defect is downstream of the ECM. The 919delF mutation results in deletion of the last 77 residues of the 995 amino acid protein sequence of

TMEM67, a relatively small sequence with no known domains or function except FLNA binding. It must be presumed therefore that it is the TMEM67-FLNA interaction that is necessary for correct ECM morphology.

FLNA is an actin-binding and adhesion protein, but also binds to integrins, and to TMEM67 in an interaction essential for ciliogenesis (Adams *et al*, 2012). As shown in Chapter 3 (Figure 3.4 B), TMEM67 and FLNA both physically associate with the adhesion fraction. In the absence of TMEM67, FLNA's recruitment to adhesions at the cell surface may be disrupted leading to altered signalling. FLNA has been linked to ECM regulation through control of matrix metallopeptidases (Baldassarre *et al*, 2012), and influences tension response by interacting with β1 integrin (Gehler *et al*, 2009), so its role in the adhesion complex may be key to MKS defects; this will be discussed fully in chapter 6.

The finding that antagonists to the TGF-β and Wnt signalling pathways rescue defects in *TMEM67* patient cells is consistent with a model where disruption to TGF-β and Wnt signalling is an upstream contributor to defective ciliogenesis. It is difficult to interpret the influence of these pathways on ciliogenesis since most studies have investigated the inverse: the effect of disruption to cilia on signalling pathways (Gerdes *et al*, 2007; Corbit *et al*, 2008; McDermott *et al*, 2010; Voronina *et al*, 2009; Huang & Schier, 2009; Ocbina *et al*, 2009).

Signalling via the TGF-β family has broad roles controlling development and homeostasis of tissues throughout the body, including adhesion, cytoskeleton organisation (Weiss & Attisano, 2013), and extracellular matrix production (Sugiyama *et al*, 2013). The effects of TGF-β signalling can differ depending on cell type and context: for example, in wound healing, TGF-β induces proliferation of fibroblasts but inhibits proliferation of keratinocytes (Ashcroft *et*

al, 1999; Zambruno *et al*, 1995). In the absence of TGF-β signalling, the MKS protein B9D1 fails to localise to the ciliary TZ and cilia are shortened (Tozser *et al*, 2015). The finding in this chapter that attenuation of TGF-β restores ciliogenesis in *TMEM67* patient cells (Figure 4.3 B) implies therefore that the native levels of TGF-β are aberrantly high, to the point that inhibition serves to restore a balance of TGF-β signalling required for proper ciliary assembly. In the differential expression and mass spectrometry data shown in Chapter 3, TGFB1 was detected to be increased in both expression (Appendix 1, Table 1) and abundance in the adhesion/ECM fraction (Figure 3.8 B) in *TMEM67* patient cells, supporting this model.

Normally when TGF-β signalling is activated, the core of the signalling pathway is transduced when TGF-β receptor 1 (TGFβRI) phosphorylates Smad3, which enters the nucleus (in conjunction with Smad4) to affect gene expression. TGF-β receptor 1 kinase inhibitor II (TRIKinII) inhibits the TGF-β pathway at the receptor level, while SIS3 selectively inhibits Smad3 phosporylation and interaction with Smad4 (Jinnin *et al*, 2006). The different degrees of rescue observed between these two inhibitors (Figures 4.3, 4.4 C) indicate that when the whole pathway is inhibited from TGFβRI, defects are more strongly alleviated than when just the part of the pathway downstream of Smad3 is inhibited; this implies that *TMEM67* patient cell defects are not solely downstream of Smad3, but other parts of the TGF-β pathway or crosstalk to other pathways branching from TGFβRI are involved; other branches from TGFβRI include Ras and RhoA pathways (Derynck & Zhang, 2003).

TGF-β signalling generally increases production of ECM (Sugiyama *et al*, 2013), so it is strange that inhibition of TGF-β in *TMEM67* patient cells would rescue a lack of ECM production. This may be another example of context-sensitive

regulatory roles for TGF-β, or of restoring a balance of signalling. TGF-β does not universally stimulate ECM synthesis: while treatment of fibroblasts with TGF-β stimulates production of various ECM components including collagen (Roberts *et al*, 1986), vitronectin, fibronectin, and tenascin C, it was reported to have no effect on production of laminins (Sugiyama *et al*, 2013). In fact, presence of basement membrane (BM) proteins such as laminin or collagen IV inhibit TGF-β activity (Streuli *et al*, 1993; Roskelley *et al*, 1995). It was shown in Chapter 3 that *TMEM67* patient cells have lower expression (Figure 3.1 B) and secretion (Figure 3.2 A) of collagen IV and laminin. This could suggest a model where, downstream of low levels of collagen IV and laminin in *TMEM67* ECM, TGF-β signalling is aberrantly activated.

FH535 antagonises the nuclear receptors PPARγ and PPARδ and inhibits GRIP1 and β-catenin recruitment, thus inhibiting canonical Wnt (Handeli & Simon, 2008). Caron *et al* reported that in zebrafish, attenuation of canonical Wnt signalling was upstream of ciliogenesis via *foxj1*, with defects leading to cystic kidney reminiscent of MKS (Caron *et al*, 2012), so activation of this pathway may block ciliogenesis. *TMEM67* patient cells exhibit a hyperactivation response to Wnt ligand (Adams *et al*, 2012). This is consistent with the finding in this chapter that inhibition of canonical Wnt with FH535 rescues ciliogenesis (Figure 4.4 B). FH535 treatment also rescued ECM morphology, which is difficult to interpret given the role of canonical Wnt activation in stimulating ECM deposition in fibrosis (Wei *et al*, 2011; Bergmann *et al*, 2011), which can be in cooperation with TGF-β signalling (Akhmetshina *et al*, 2012); if these pathways are aberrantly activated in *TMEM67* patient cells, the presence of the ECM defect indicates they not stimulating ECM deposition in this context.

Box5 is a stabilised peptide derived from Wnt5a that inhibits the non-canonical Wnt5a/planar cell polarity (PCP) pathway (Jenei *et al*, 2009), upstream of Rho family signalling that controls cell polarity and cytoskeletal rearrangement (Veeman *et al*, 2003). The PCP protein Wdpcp (which is also a BBS protein) is required for ciliogenesis, and modulates the actin cytoskeleton (Cui *et al*, 2013). Box5 treatment did not rescue ECM morphology (Figure 4.3 A) or significantly rescue ciliogenensis in *TMEM67* patient cells (Figure 4.3 B), while both were rescued by inhibition of canonical Wnt with FH535. Wnt/PCP signalling has been linked to control of fibronectin ECM organisation (Dzamba *et al*, 2009), but evidently this is not a major factor in the *TMEM67* ECM defect. Failure to rescue ciliation indicates that this pathway to ciliogenesis may not be disrupted (or as severely disrupted), though a significant rescue (albeit still with smaller effect than other inhibitors) was found in *TMEM67* knockout MEFs (Figure 4.4 C). Box5 treatment did rescue actin morphology (Figure 4.3 C), suggesting that PCP mediated control of the cytoskeleton is disrupted, but this is not as major an influence on ciliation as the pathways affected by other inhibitors.

Analysing the impact of these pathways is complicated by widespread cross-talk between Wnt and TGF-β signalling, as well as other pathways such as YAP/TAZ (Attisano & Wrana, 2013). For example, non-canonical Wnt5a has been shown to be both activated by and a regulator of TGF-β-dependent production of collagen and fibronectin (Kumawat *et al*, 2013). The two pathways converge on RhoA, which in *TMEM67* patient cells is upregulated, influencing actin organisation (Adams *et al*, 2012; Dawe *et al*, 2009). The finding that Wnt antagonists were able to restore actin density, while TGF-β antagonists did not, may reflect greater influence of Wnt on the RhoA pathway; however, the sample size was much lower for the TGF-β component of this experiment, so this result

must be regarded with some caution, especially since when the experiment was repeated in *TMEM67* knockout MEFs all inhibitors had highly significant effects. The possible roles of RhoA in MKS will be discussed in more detail in Chapter 6.

This chapter has shown that the ECM defect is upstream of multiple cellular defects in MKS. However, it is not sufficient to explain all cellular defects found in MKS patient cells. The next chapter will investigate defects that are independent of the ECM, in order to shed further light on the possible causes of the ECM defect and the pattern of causation in MKS.

Chapter 5

Alterations to cell spreading dynamics in MKS patient cells

This chapter incorporates some material prepared by Annie Toynbee, an undergraduate project student who worked under my supervision to assist in analysis of logarithmic cell spreading data. Where included, this has been acknowledged (Figures 5.6-5.8).

Chapter 5: Alterations to cell spreading dynamics in MKS patient cells

5.1 Introduction

Cell adhesion to extracellular substrates is dependent on interactions between cell surface adhesion receptors and their extracellular binding partners. Integrins, the major adhesion receptors, are transmembrane proteins with extracellular domains that couple primarily to the extracellular matrix (Hynes, 1987, 2002). Within the cell, integrins link to a proteomically diverse adhesion complex which couples primarily to the actin cytoskeleton, though it also interacts with microtubules, intermediate filaments, and other structural cell components.

A mature focal adhesion forms a strong physical connection between the actin cytoskeleton and the extracellular ligand, and integrates multiple bidirectional signals as well as serving as a mechanosensor, typically by increasing adhesion protein recruitment in response to increased tension, and disassembly in response to decreased tension (Xu *et al*, 2012; Wehrle-Haller, 2012). Integrin adhesion complex formation requires the presence of extracellular matrix ligands, and Rho family GTPase signalling at the membrane (Hotchin & Hall, 1995).

Adhesions are essential for the migration of cells on both 2D substrates and in physiological 3D environments (Nagano *et al*, 2010; Kubow & Horwitz, 2011) as they represent the points at which cells attach to and exert traction forces on the substrate. Cell spreading follows the initial attachment of a cell to a substrate.

During spreading, a leading edge followed by a thin sheet of membrane and cytoplasm (the lamella) extends from the cell body over the substrate, often initially in an isotropic (unpolarised) pattern giving the cell a circular shape when viewed from above. This process is similar in underlying mechanism to cell migration, except that the leading edge in migration is polarised (Vasiliev, 1982).

The advancement of the leading edge is driven by polymerisation of actin into bundled arrays which undergo retrograde flow away from the leading edge (Small *et al*, 2016). This process is regulated by Rac, one of the Rho family GTPases (Hall, 1998; Ridley, 2001; Brancolini *et al*, 1999). Actin also drives early formation of adhesions at the leading edge. Slower spreading has been observed in cells treated with microtubule-destabilising drugs (Ivanova *et al*, 1976), implying some role for the microtubule cytoskeleton in spreading. However, this role is minimal compared to that of actin. Fragments of lamella disconnected from a cell are capable of leading-edge formation and motility (Euteneuer & Schliwa, 1984), indicating that this process is autonomous to the machinery within the lamella and does not require cell-wide cytoskeletal organisation or signalling.

Biophysical studies of the dynamics of cell spreading have identified three phases of spreading, each characterised by a spreading rate governed by a logarithmic power law, separated by dynamic phase transitions (Döbereiner *et al*, 2004), with each phase proposed to represent a different underlying biological mechanism, and the phase transitions the points at which the cell "switches" from one mechanism to another. Dubin-Thaler *et al* (2008) propose that these three phases correspond to 1: initial contact formation; 2: rapid spreading; and 3: periodic actin-dependent contractions and stable adhesion

formation. The actin cytoskeleton may only be involved in force generation during the third phase, but cortical actin flow is likely rate-limiting throughout (Cuvelier *et al*, 2007). An alteration to the spreading behaviour of a cell may impact any one of these phases or multiple phases, depending on the underlying mechanisms that are disrupted.

In this chapter, the spreading behaviour and pattern of adhesion formation of MKS patient cells is investigated in relation to different extracellular matrix substrates. Having previously shown that MKS patient cells have altered adhesion composition (Chapter 3, Figures 3.7-3.9), including depletion of many key adhesion components, and that the TMEM67 protein is a component of adhesions in non-diseased cells, it was hypothesised that MKS patient cells would exhibit defective adhesion formation and, consequentially, defective cell-ECM interaction. Since adhesion formation is influenced by the extracellular matrix environment, cells were plated onto surfaces artificially coated with individual ECM component proteins so that comparisons could be made of adhesion formation in the same extracellular environment. To minimise secretion and remodelling of the ECM by cells within the timeframe of observation, these experiments were necessarily conducted shortly after seeding cells onto the artificial ECM substrate, and therefore were focused on the cell spreading process.

It was found that MKS patient cells have altered spreading behaviour characterised by faster spreading, greater cell area, and alterations to spreading dynamics, with substrate-dependence.

5.2 Cell spreading is altered in MKS patient fibroblasts

To investigate the morphology of spreading MKS patient cells, *TMEM67*, *TMEM216*, and age-matched control fibroblasts were plated onto a collagen I substrate, and imaged under phase contrast illumination for up to 90 minutes (Figure 5.1).

Control cells (Figure 5.1, left column) exhibited morphology typical of fibroblasts in 2D cell culture, characterised by an irregular shape with long (10 μm or greater) cytoplasmic protrusions emanating from a main cell body containing the nucleus and the bulk of intracellular compartments visible under phase contrast.

TMEM67 patient fibroblasts exhibited similar morphology to control fibroblasts (Figure 5.1, centre column). *TMEM216* fibroblasts (Figure 5.1, right column) were morphologically altered in a number of ways: the vast majority were spread over a larger surface area; many cells had large lamella-like thin, smooth regions, and a number of cells (approximately 10 to 15%) were observed to fragment, leaving multiple patches of membrane disconnected from the cell body.

Having observed altered morphology in MKS patient fibroblasts spreading on a collagen I substrate, quantitative investigation of how spreading progresses over time on this substrate was undertaken. Phase contrast movies were acquired of cells spreading on collagen I (Figure 5.2 A). Cell area was measured at regular timepoints. Since not all cells initiated spreading at the same time, for the purposes of analysis $t = 0$ was assigned for each cell individually. This was defined as the frame prior to the first observation of smooth, lamellipodial spreading. Small changes in cell area due to formation of

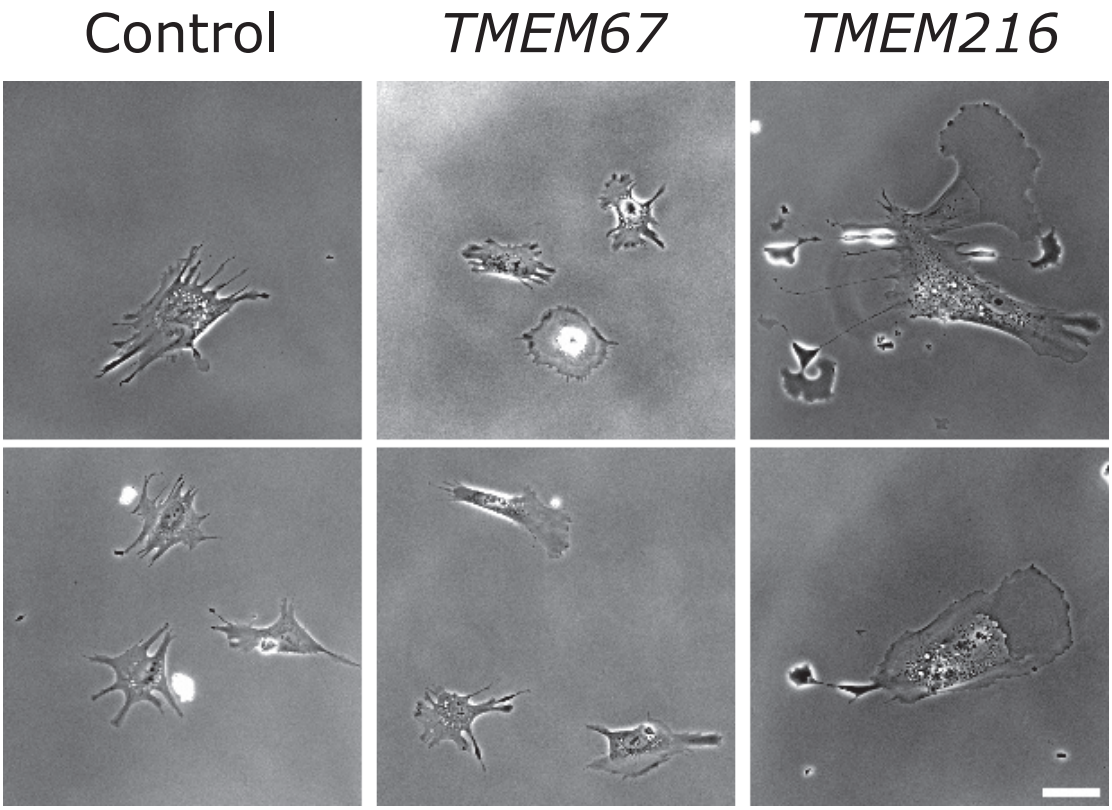

Figure 5.1: *TMEM216* patient fibroblast morphology is altered.
Control fibroblasts (left) exhibit normal morphology. *TMEM67* patient fibroblasts (centre) exhibit similar morphology to controls. *TMEM216* fibroblasts (right) spread over a larger area, and some cells were observed to fragment (top right). Cells shown are representative of the population observed. Cells were plated for 90 minutes on a collagen I substrate and imaged under phase contrast illumination. Bar: 40 μm.

transient protrusions such as blebs and microspikes were often observed earlier than this point; these were not included in this analysis. Cells were measured across 30 minutes of the time series from their individual $t = 0$. Cells that began to spread, but then retracted and rounded up within this timeframe were excluded from the analysis. A mean area was calculated for each cell line at each timepoint (Figure 5.2 B). In line with the first observations, *TMEM216* fibroblasts had a greater area at all timepoints and showed faster spreading, while control and *TMEM67* fibroblasts had very similar areas at all timepoints. Most spreading occurred during the first 10 minutes, with only minor change in cell area between the 10 minute and 30 minute timepoints.

Having observed altered spreading behaviour for MKS patient cells on one substrate, we proceeded to investigate other substrates to determine whether these alterations were substrate-specific. Phase-contrast movies were acquired and analysed as before, for cells spreading on collagen IV (Figure 5.3), fibronectin (Figure 5.4), and laminin (Figure 5.5).

On collagen IV, fewer of the plated cells spread; of over 20 *TMEM67* cells imaged, only3 spread without retracting for the 30 minutes required to be included in the analysis. Those *TMEM67* cells that did spread exhibited faster spreading and a larger area than controls (Figure 5.3 B), even outpacing *TMEM216* cells. This is in contrast to *TMEM67* cells on collagen I, which spread in a similar manner to controls. *TMEM216* cells on collagen IV, as on collagen I, spread over a larger area than controls; however, the area of *TMEM216* cells at 30 minutes was lower than the same cell line on collagen I, and spreading continued after the 10 minute timepoint, unlike on collagen I where most spreading occurred during the first 10 minutes. *TMEM67* and control cells on

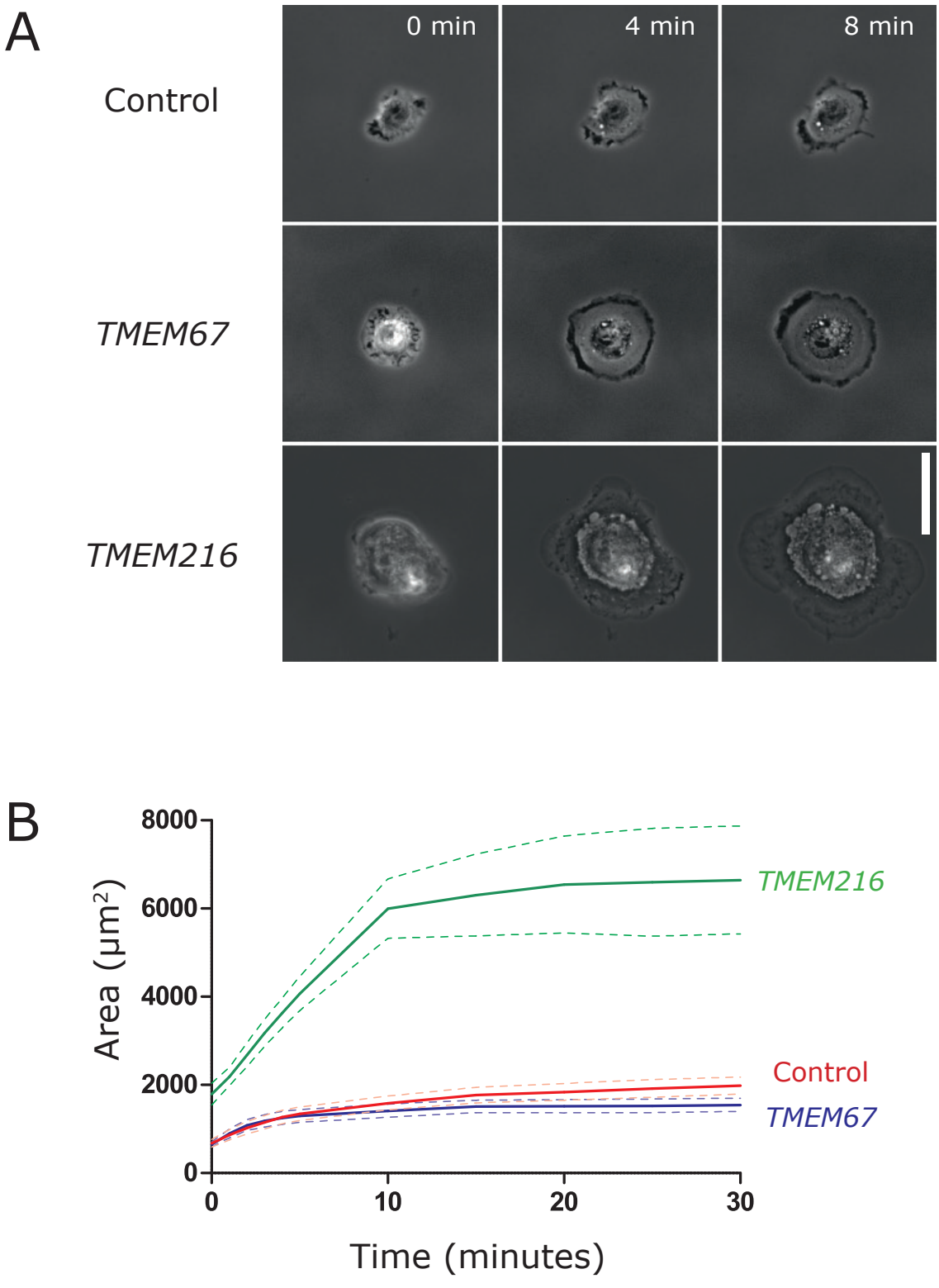

Figure 5.2: *TMEM216* fibroblasts exhibit greater cell area when spreading on collagen I.

A: Images from phase contrast time-lapse movies of cells spreading on a collagen I substrate. Bar: 40 µm. B: Spreading area over time on collagen I. Solid lines: Mean cell area; Dotted lines: SEM; *n* = at least 8 cells per cell line.

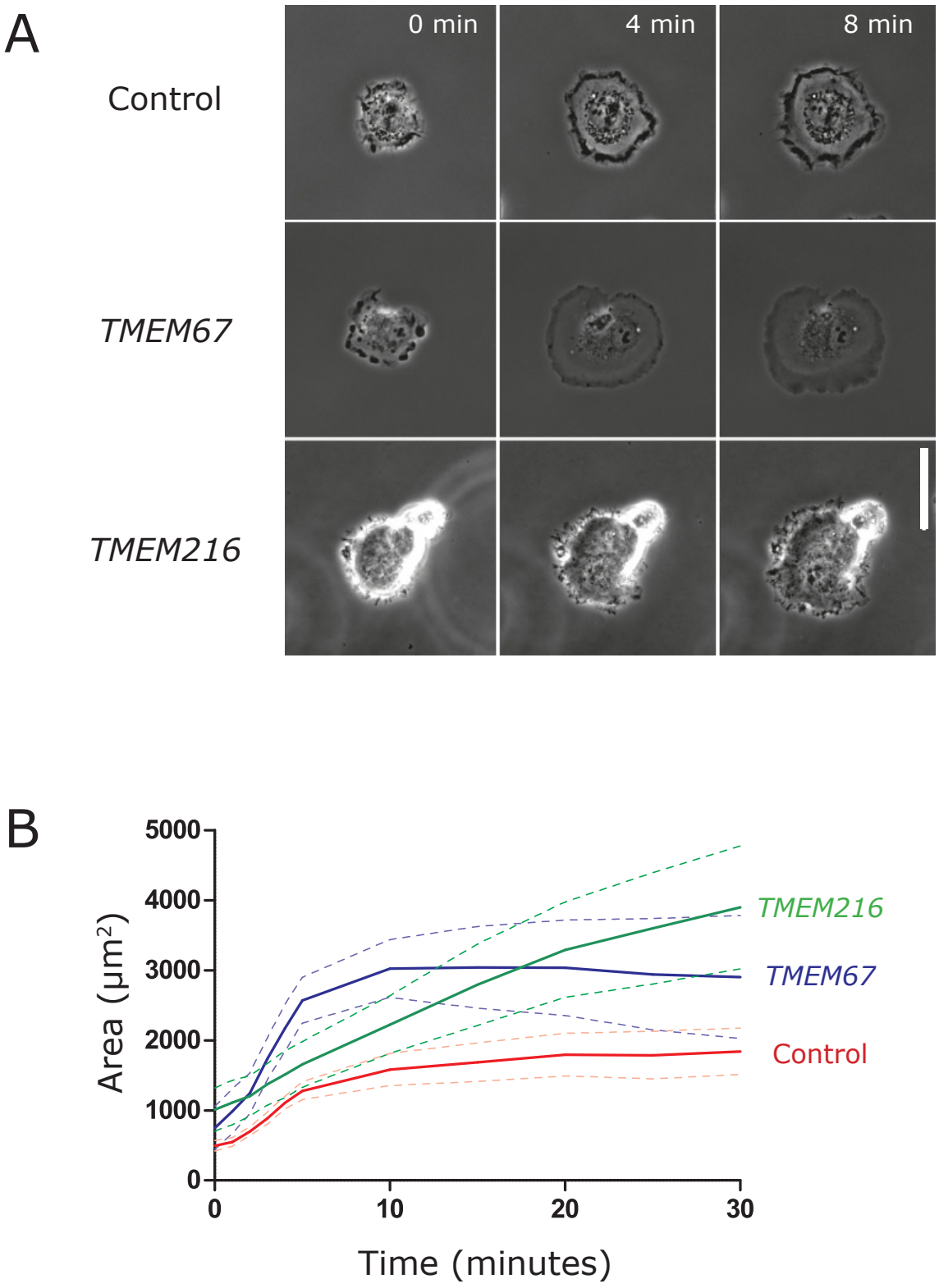

Figure 5.3: *TMEM67* and *TMEM216* fibroblasts exhibit greater cell area when spreading on collagen IV.

(A) Images from phase contrast time-lapse movies of cells spreading on a collagen IV substrate. Bar: 40 µm. (B) Spreading area over time on collagen IV. Solid lines: Mean cell area; Dotted lines: SEM; *n* = at least 3 cells per cell line.

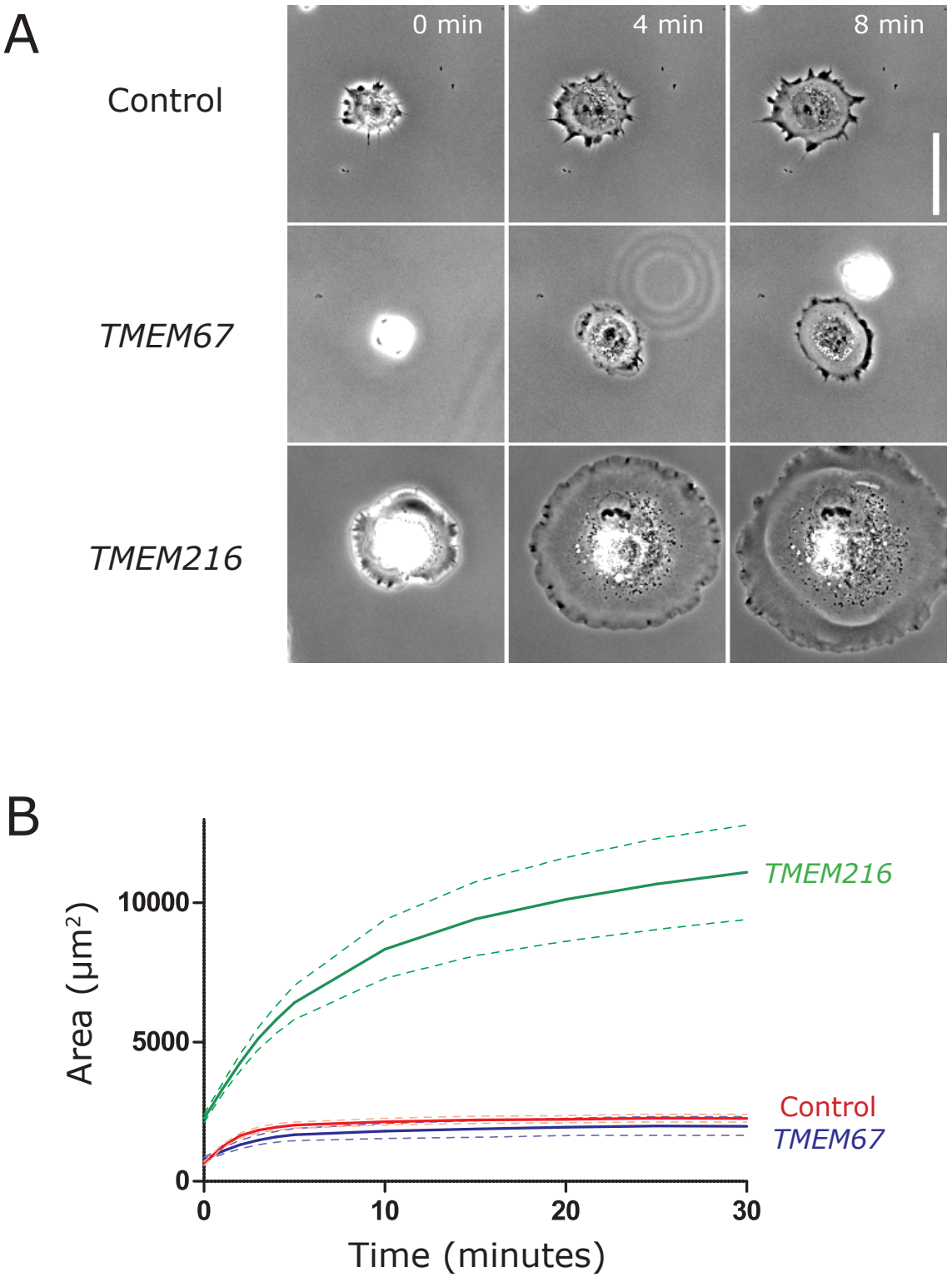

Figure 5.4: *TMEM216* fibroblasts exhibit greater cell area when spreading on fibronectin.

(A) Images from phase contrast time-lapse movies of cells spreading on a fibronectin substrate. Bar: 40 µm. (B) Spreading area over time on fibronectin. Solid lines: Mean cell area; Dotted lines: SEM; *n* = at least 8 cells per cell line.

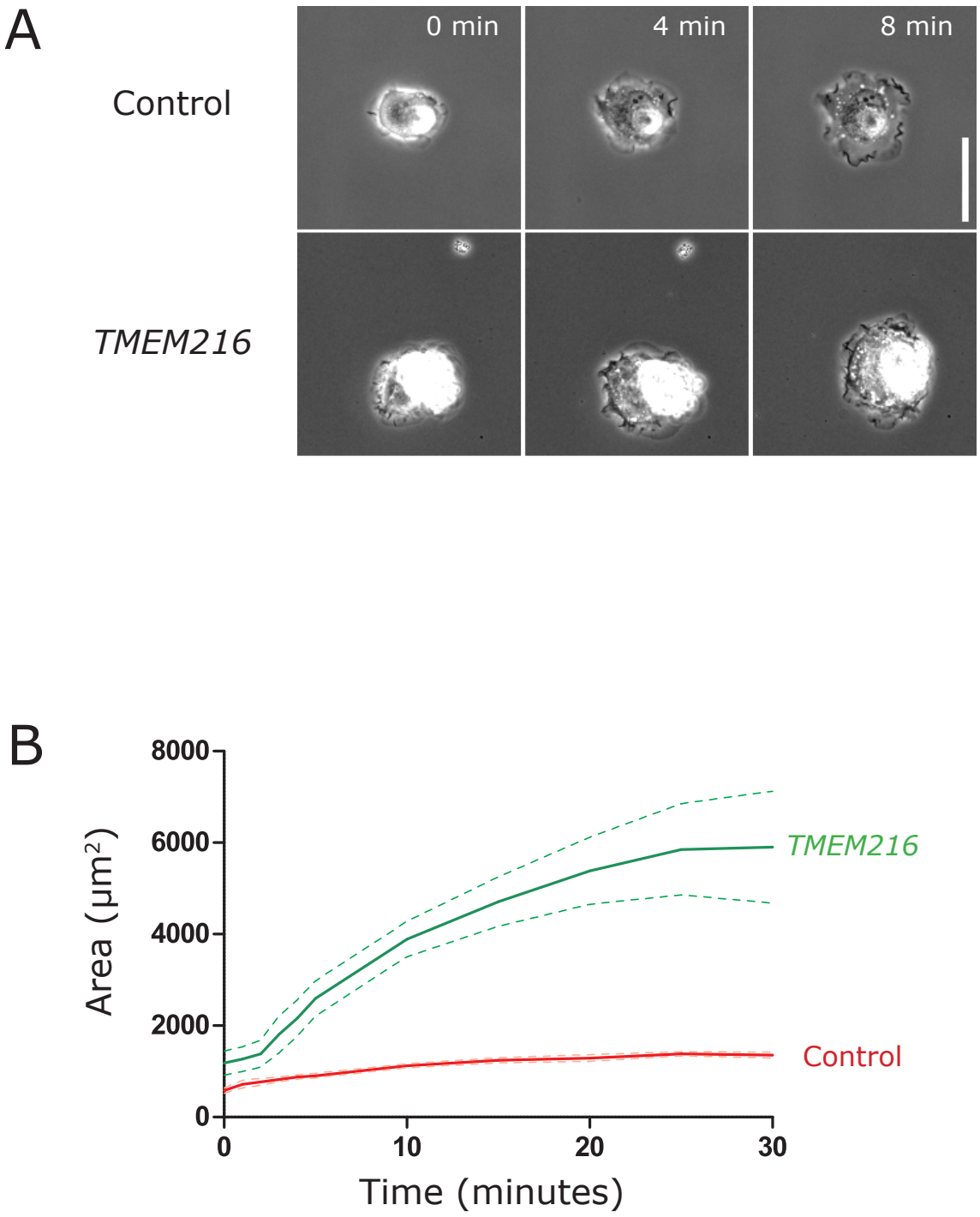

Figure 5.5: *TMEM216* fibroblasts exhibit greater cell area when spreading on laminin.

(A) Images from phase contrast time-lapse movies of cells spreading on a laminin substrate. Bar: 40 µm. (B) Spreading area over time on laminin. Solid lines: Mean cell area; Dotted lines: SEM; *n* = at least 3 cells per cell line.

collagen IV, as on collagen I, reached near maximum area within 10 minutes of spreading initiation.

On fibronectin (Figure 5.4), the overall pattern of spreading observed was similar to that on collagen I, with control and *TMEM67* cells exhibiting very similar morphology (Figure 5.4 A) and area at all timepoints (Figure 5.4 B), while *TMEM216* cells spread faster and over a wider area. In comparison to their spreading area on collagen I, *TMEM216* cells had spread even further on fibronectin at the 30 minute timepoint, and continued to spread beyond the 10 minute timepoint.

On laminin (Figure 5.5), control cells spread at a similar rate to the other substrates, and *TMEM216* cells again spread faster and further than controls, though they showed a small lag period within the first two minutes where their rate of spreading was similar to that of controls. Out of 20 *TMEM67* cells imaged, none were observed to spread even transiently on a laminin substrate; therefore *TMEM67* cells were not included in this analysis.

A limitation of cell spreading analysis is that measurement of planar cell area in two-dimensional images does not provide information about cell shape changes in the z-axis. It may be that MKS patient cells have a larger volume, and this contributes to their ability to spread over a wider area. A previous study assessed the volume of control, *TMEM67*, and *TMEM216* cells via confocal imaging and detected no obvious difference in cell volume (McIntosh, 2016), however this was based on a small sample size and amorphous, highly spread cells which makes measurement of volume difficult. An experiment was designed to improve on this methodology: control and *TMEM67* cells were dissociated from the culture surface with TrypLE Express cell dissociation

reagent and, while still suspended in the reagent, imaged. Under these conditions the cells would be prevented from spreading or forming adhesions and remain spheroid, and therefore their volume could be estimated from diameter measurements. No significant difference was found between the volumes of control and *TMEM67* cells (Student's *t*-test, $p > 0.05$, $n = 3$ biological repeats, at least 100 cells per line).

5.3 Logarithmic analysis of cell spreading

Having found altered spreading area and rate in MKS patient cells, next the spreading process was examined in more depth via logarithmic analysis of spreading rates. Control and MKS fibroblasts were plated as before, on collagen I, collagen IV, and laminin substrates, and imaged at a higher frequency (one image every five seconds for 30 minutes) to generate a dataset with improved temporal resolution. Cell area was measured over time and plotted on double-logarithmic graphs so spreading conforming to exponential power laws could be visualised as straight lines, and dynamic phase transitions between such exponential spreading phases visualised as changes in gradient (Figure 5.6), following the approach of Döbereiner *et al* (2004).

The majority (>70%, $n = 7$) of control cells exhibited three phases of spreading on collagen I; the remainder exhibited two phases. On collagen IV ($n = 3$) and laminin ($n = 3$), control cells all exhibited three spreading phases. A double logarithmic plot of a representative cell for each substrate is shown in Figure 5.7 A.

TMEM67 cells spreading on collagen I all exhibited three phases of spreading ($n = 5$) (Figure 5.7 B, top). On collagen IV, 80% ($n = 5$) exhibited three phases of spreading, while the remainder spread in two phases (Figure 5.7 B, middle).

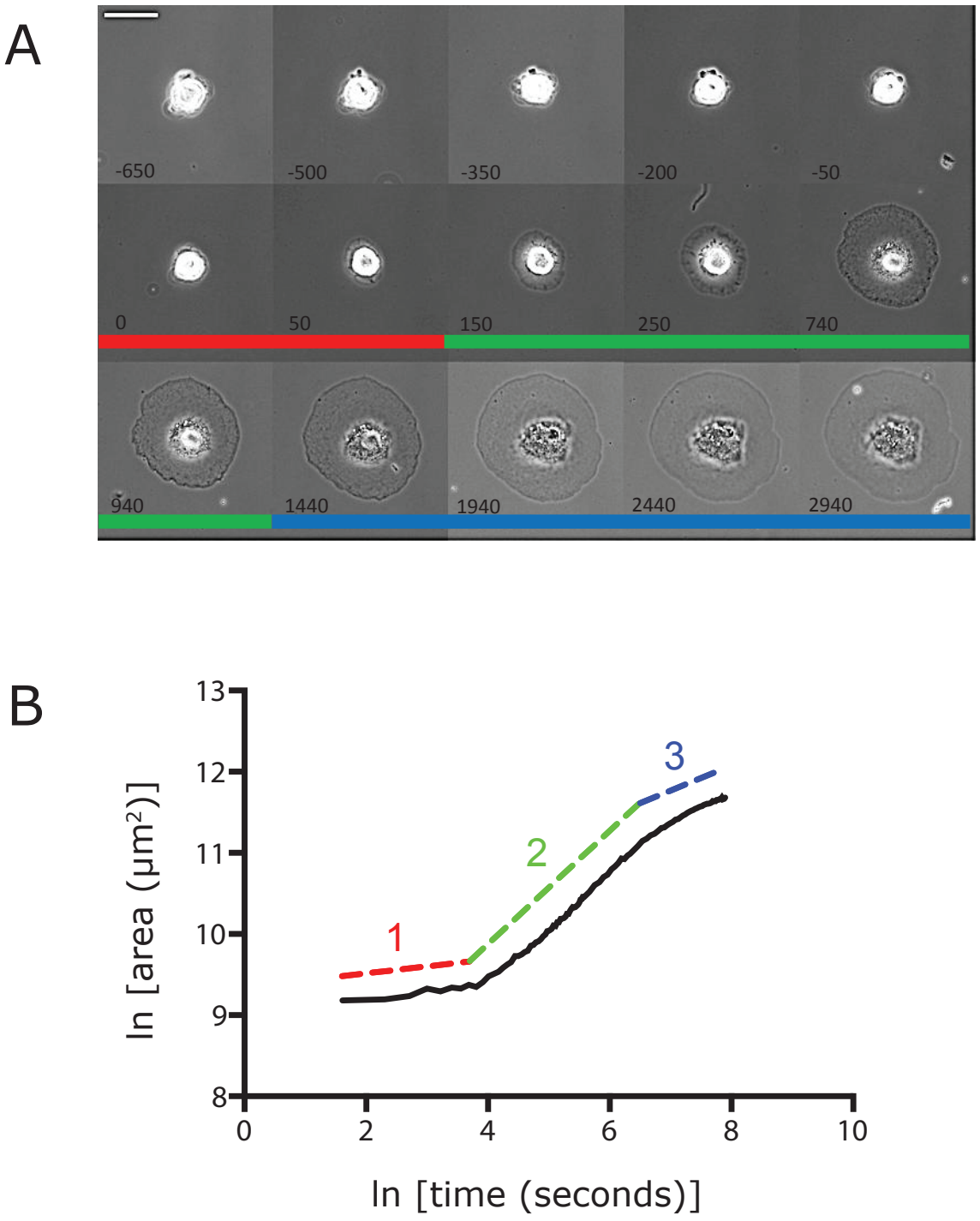

Figure 5.6: The three phases of isotropic cell spreading. A: A control fibroblast spreading normally on a collagen I substrate (phase contrast). The three spreading phases are denoted by colour (red: intial contact formation; green: rapid spreading;, blue: actin contractions and stable adhesions). Images labelled with time in seconds. Bar: 20 μm. B: Spreading area over time represented on a double logarithmic plot reveals the three phases (red, green, blue) governed by different power laws, recognisable as phases of approximately constant gradient. (Figure prepared by A. Toynbee).

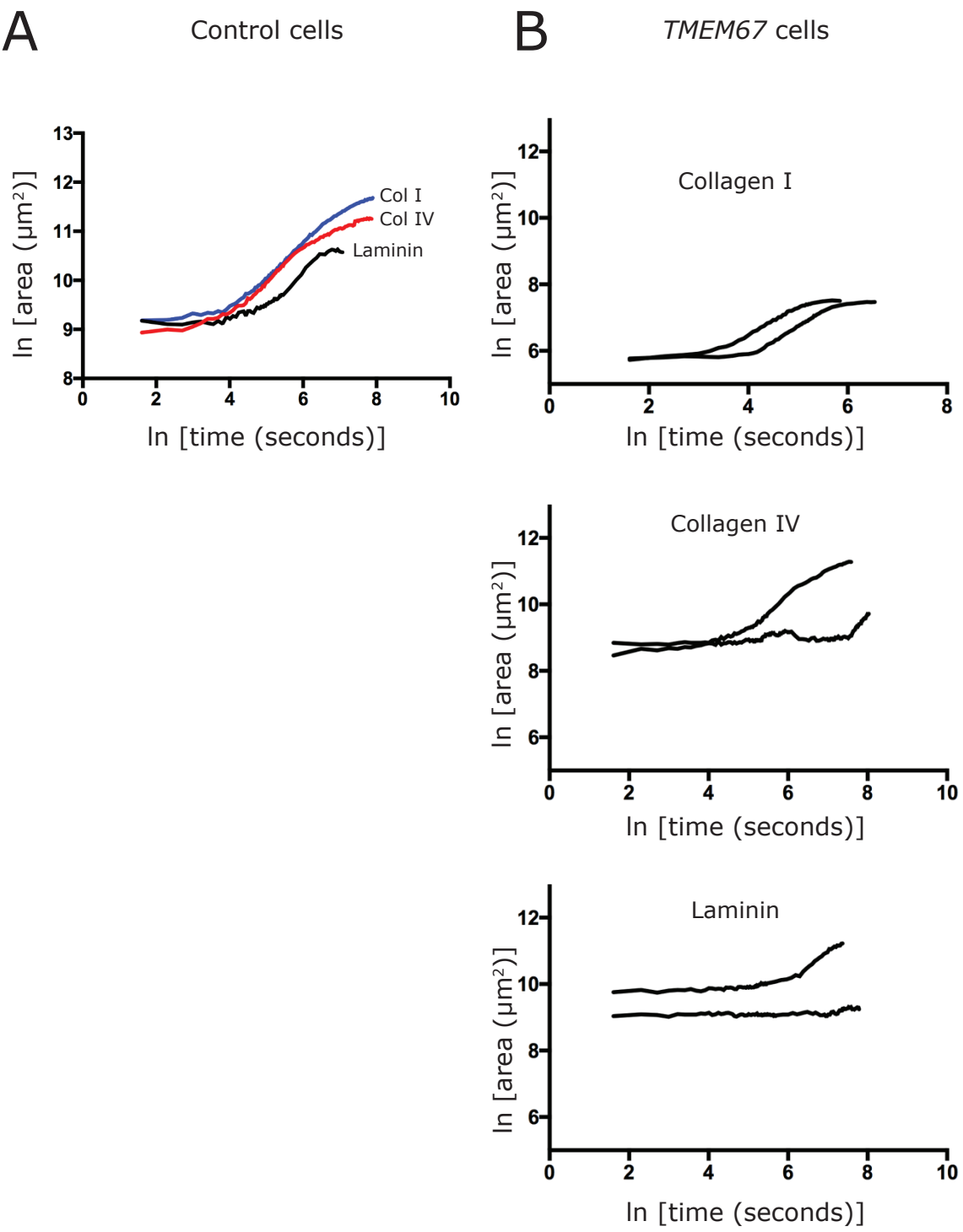

Figure 5.7: *TMEM67* patient cells exhibit disrupted spreading dynamics on collagen IV and laminin. Each line on a double logarithmic plot represents a single cell; cells representative of the observed population have been chosen. A: control cells undergo spreading with similar power laws, especially for the second, rapid spreading phase, on all three substrates. B: *TMEM67* cells exhibit three phases of spreading on collagen I, but on collagen IV some cells spread in only two phases, and on laminin cells only appear to spread in two phases. (Measurements taken by A. Toynbee).

TMEM67 cells would not readily spread on laminin, resulting in sparse data – over four separate experiments, only two cells were observed spreading, with neither showing three phases (Figure 5.7 B, bottom).

A slight majority of *TMEM216* cells on collagen I exhibited three phases (54%, *n* = 13), while the remainder spread in two phases (Figure 5.8 B, top). All *TMEM216* cells spread on collagen IV in only two phases (*n* = 4) (Figure 5.8 B, middle). On laminin, only two cells were observed, but both spread with three phases (Figure 5.8 B, bottom).

5.4 *TMEM67* cells are less resistant to deformation

Spreading speed, especially during the second, fast phase (Cuvelier *et al*, 2007), is limited by the mechanical properties of a cell, especially the resistance to deformation of the cortex and the cytoskeleton. The alterations to spreading behaviour in MKS cells could be explained by changes in the tension or stiffness of the cell caused by alterations in these cellular components.

Micropipette aspiration can be used to determine the mechanical properties of cells under the assumption that cells behave as viscoelastic solids (Jones *et al*, 1999; Sato *et al*, 1990; Theret *et al*, 1988). To investigate whether MKS patient cells had altered mechanical properties, micropipette aspiration of individual cells was undertaken. In this process, aspirating pressure is applied to a cell through a glass micropipette with an aperture smaller than the diameter of the cell, forcing a change in shape as the cell is aspirated inside the micropipette barrel (Figure 5.9 A). The increase in projection length over time in response to 500 Pa of aspirating pressure was measured and used to determine the equilibrium Young's modulus (mechanical stiffness) E_∞ of the cell via a standard linear solid (SLS) viscoelastic model. This model assumes intrinsic

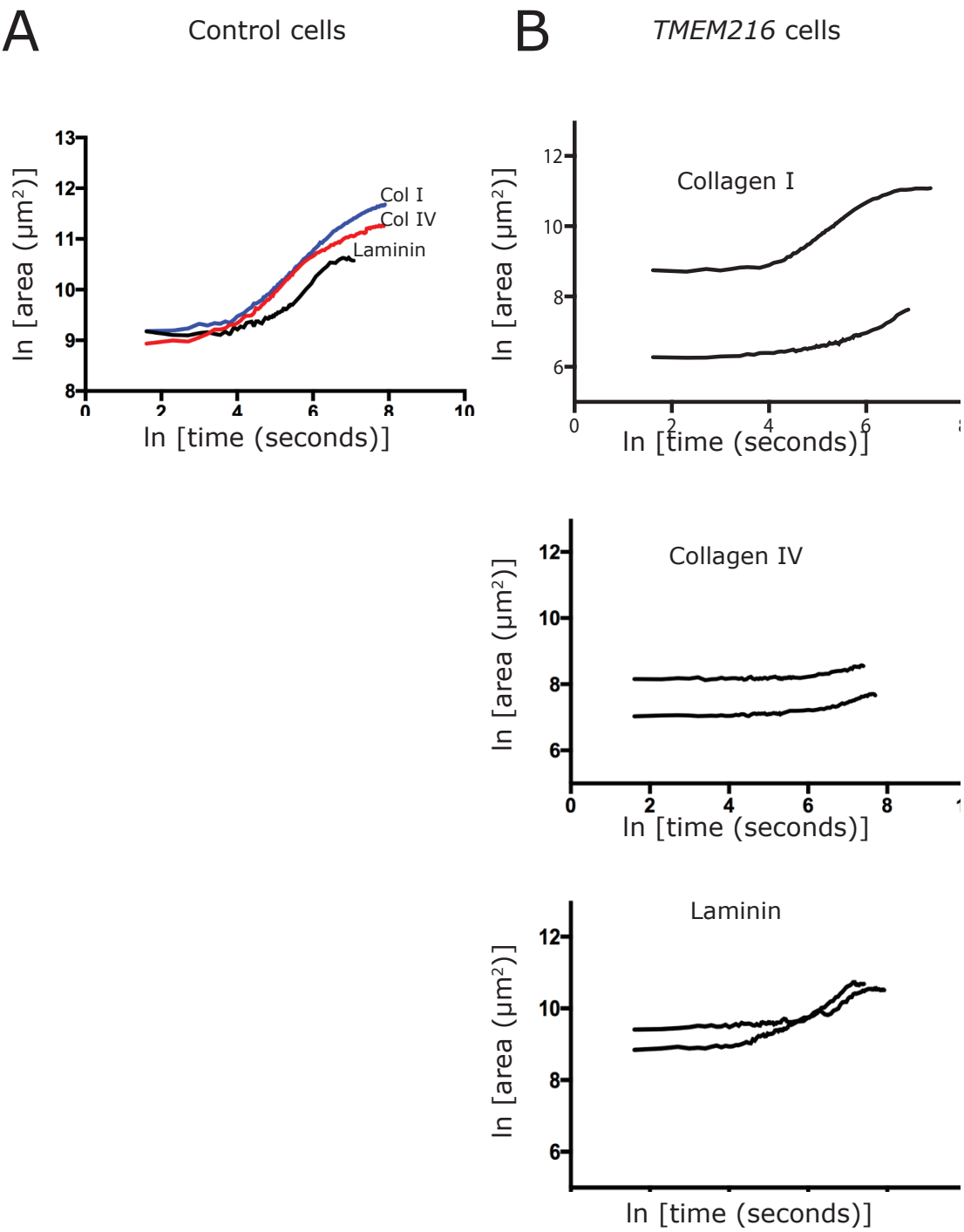

Figure 5.8: *TMEM216* patient cells exhibit disrupted spreading dynamics on collagen I, IV, and laminin. Each line represents a single cell; cells representative of the observed population have been chosen. A: Reproduced from Figure 5.7 for ease of comparison. Control cells undergo spreading with similar power laws, especially for the second, rapid spreading phase, on all three substrates. B: *TMEM216* cells exhibit two patterns of spreading on collagen I; either in three or two phases. On collagen IV only two phases are observed, while on laminin *TMEM216* cells spread in three phases. (Measurements taken by A. Toynbee).

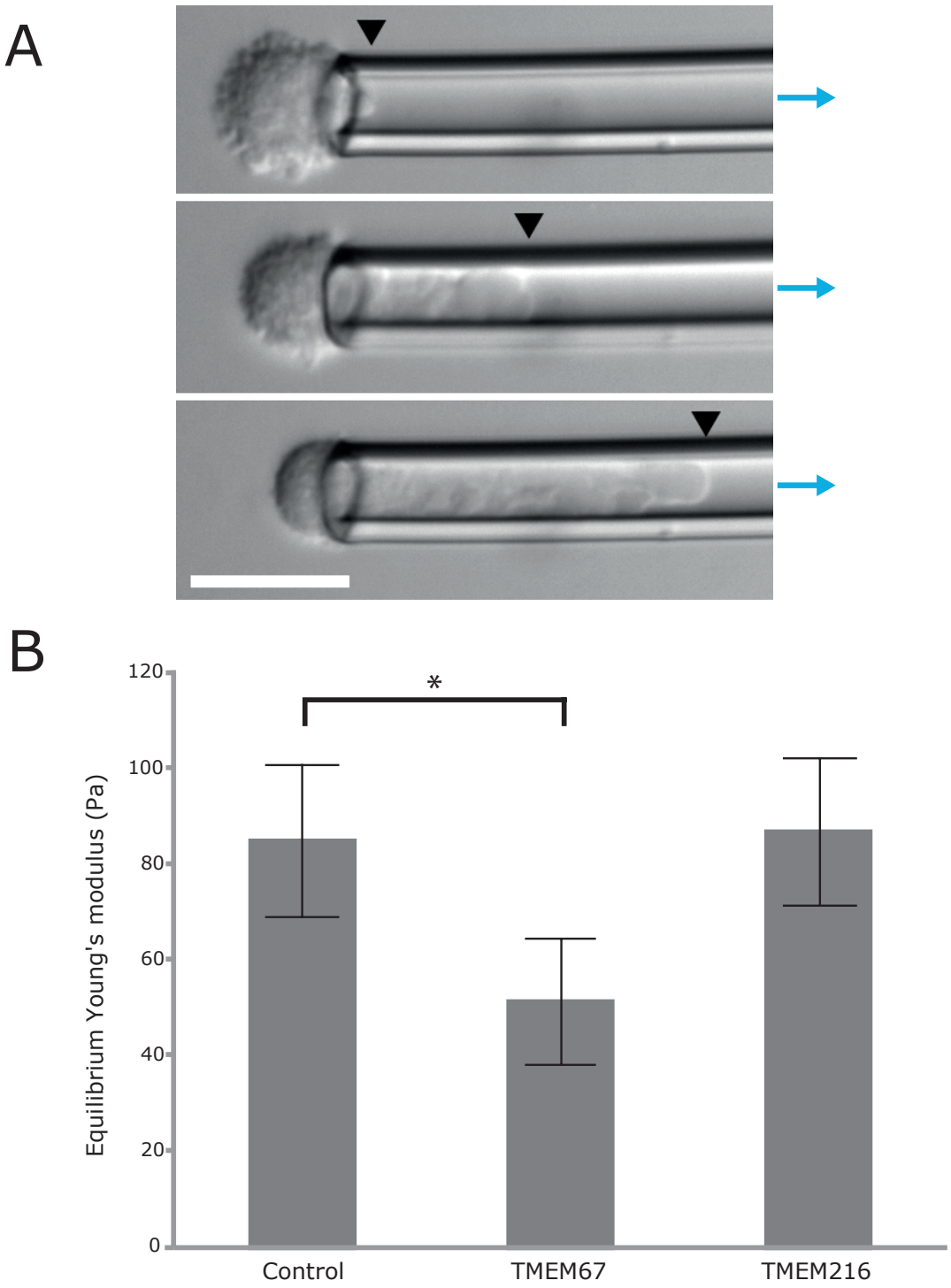

Figure 5.9: TMEM67 patient cells are less resistant to deformation under aspirating pressure than control or TMEM216 cells. A: Example of a cell being aspirated into a micropipette, imaged under DIC. Note the projection of membrane into the micropipette barrel (black arrowheads). Blue arrows: aspiration direction. Bar: 20 µm. B: Mean equilibrium modulus calculated via the standard linear solid (SLS) viscoelastic model for control and MKS cell lines based on response to micropipette aspiration. Error bars: SEM; *n* = at least 7 cells per cell line; *: $p < 0.05$ (One-way ANOVA with Dunnet's post-test).

incompressibility of the cell and instantaneously applied aspiration pressure (Jones *et al*, 1999; Guilak *et al*, 1999). (For technical details of the SLS model, see Chapter 3.) Control and *TMEM216* cells exhibited similar mechanical stiffness, but *TMEM67* cells were found to have significantly reduced mechanical stiffness in comparison to controls (Figure 5.9 B).

5.5 Discussion

MKS patient cells are defective in ciliation, and cells that are highly spread are prevented from forming cilia (Pitaval *et al*, 2010), so defective control of cell spreading is a possible explanation for ciliation defects. As previously shown (Chapter 3, Figure 3.14), MKS patient cells are defective in extracellular matrix synthesis. Due to the complex, bidirectional nature of integrin adhesion signalling, this may either cause alterations in cell spreading or be a downstream consequence of an alteration in cell spreading. Examining the cell-ECM interaction of cells on artificially coated substrates, therefore, might reveal defects that could underlie ECM synthesis defects.

TMEM67 patient cells were found to have altered spreading on collagen IV (Figure 5.3), one of the ECM components for which they exhibited reduced expression and secretion (Chapter 3, Figures 3.1 B, 3.2 A). This may reflect a defective cell-ECM signalling response in collagen IV-binding integrins. A possible model to explain both findings would be that collagen IV-binding integrins are non-competent to bind extracellular collagen IV, and simultaneously, send aberrant signalling to the cell indicating the presence of extracellular collagen IV (and therefore negatively regulating its synthesis). *TMEM216* patient cells exhibited altered spreading on all substrates (Figures 5.2-5.5). This probably indicates that the spreading defect in *TMEM216* is not

dependent on substrate-specific integrin interactions, but on a dysregulation of the cell spreading process itself.

Investigating the dynamics of cell spreading revealed that spreading of non-diseased control fibroblasts proceeds in three phases of growth driven by distinct power laws, in agreement with the findings of Cuvelier *et al* (2007). Where Cuvelier *et al* investigated spreading on fibronectin, here spreading was examined on collagen I, collagen IV, and laminin substrates, but on all three, control cells exhibited the expected three distinct growth phases (Figure 5.7 A). In contrast, MKS patient cells exhibited altered spreading dynamics (Figures 5.7 B, 5.8 B).

Actin defects has been observed in MKS patient cells and models (Dawe *et al*, 2009; Valente *et al*, 2010; Adams *et al*, 2012; McIntosh, 2016). Since the actin cytoskeleton is a key regulator of cell shape and force generator during cell spreading, Cuvelier *et al* predicted that disruption to actin would lead to disrupted spreading (Cuvelier *et al*, 2007). However, the initiation and progress of spreading is also contingent on recognition of the substrate by integrins and subsequent signalling (Maheshwari *et al*, 2000), so a disruption to integrins or integrin signalling could also underlie spreading defects in MKS patient cells. Since the influence of actin and integrins are at least partially temporally separated during the spreading process, it is possible to infer which process might be defective on the basis of the precise timing of alterations to the spreading process.

Control cells exhibited similar power law growth for phase 2 on each of the three ECM substrates (Figure 5.7 A). This suggests that spreading during phase 2 is driven by a substrate-independent mechanism. Morphologically,

during phase 2 a smooth lamella undergoes rapid isotropic growth (Figure 5.6 A, green). Talin-1 is a protein that couples integrins to contractile actin in the adhesion complex and thus mediates traction force transmission through the ECM-adhesion-actin physical assembly. Knockdown of Talin-1 has been shown to reduce formation of adhesions and development of traction force in spreading cells, but does not prevent initial spreading (Zhang *et al*, 2008). This indicates that the early stage of spreading, corresponding to the first and/or second exponential spreading phase as identified by Döbereiner *et al*, is independent of mechanical traction forces generated by actin. Phase 2 is still likely to be dependent on remodelling of of cortical actin (Cuvelier *et al*, 2007). If there are alterations to spreading control in MKS patient cells during this phase, a different power law would be expected. However, when gradients were measured no differences to the power law in phase two were found between MKS and control cells; this suggests that the mechanism driving substrate-independent spreading in phase 2 is not disrupted in MKS, though the loss of phase 2 in some of the observed cells (Figures 5.7 B, 5.8 B) may indicate a failure to initiate this mechanism.

In the logarithmic analysis of *TMEM216* patient cells, greater spreading rate and cell area was not seen (Figure 5.8), in contrast to the dramatic increase in spreading rate found for these cells earlier (Figures 5.2, 5.3, 5.4, 5.5). However, the analysis was different: with the higher temporal resolution of the logarithmic analysis, the spreading initiation point could be determined more accurately, which may tend to place it earlier. Additionally, the logarithmic analysis did not image cells for longer than 30 minutes, whereas the earlier cell spreading analysis covered up to 90 minutes. 30 minutes was sufficient for control cells to undergo all three spreading phases, but *TMEM216* patient cells have prolonged

phase one spreading (Figure 5.8 B), so it may be that *TMEM216* cells take so long to transition to phase 2 after initiation of spreading that it was not seen within the timespan analysed. If the logarithmic analysis was extended further they might eventually be seen to enter phase 2; longer time series imaging should be considered as an extension of this work.

A limitation of the cell spreading analysis presented here is that differences in initial cell volume may contribute to differences in cell spreading behaviour without requiring any other alterations to the spreading machinery. A previous study found no difference in volume between control and MKS cells (McIntosh, 2016), and this was supported by the finding in this chapter that there was no significant difference in cell volume between rounded control and *TMEM67* cells. However, since the lamella represents a very small proportion of the cell by volume, even a small difference in initial volume could have a large impact on spreading behaviour, so it is still possible that a difference in volume below the sensitivity of these experiments may explain some of the altered spreading in MKS cells. Nevertheless, an alteration to spreading behaviour purely driven by different initial volume would be unlikely to exhibit substrate-dependence, which is seen in the present study.

The timing of spreading phase 1 has been established as approximately two minutes in non-diseased cells (Döbereiner *et al*, 2004), and the control cells used here conform to this. Phase one in both MKS cell lines spreading on collagen IV and laminin was extended, however, delaying initiation of phase 2. Phase 2 initiation is contingent on ECM-dependent integrin signalling reaching a threshold (Dubin-Thaler *et al*, 2004), so extension of phase 1 may indicate that MKS patient cells are deficient in cell-ECM signalling. An actin cytoskeleton dependent spreading defect would be expected to delay spreading evenly

across different substrates, whereas the alterations observed in this chapter have been substrate-dependent; integrins are substrate-specific receptors. These factors suggest that the spreading defect is a result of defective cell-ECM interaction through integrin signalling rather than a direct consequence of altered actin dynamics.

Cell-surface integrin density is a critical factor in initiation and progress of rapid phase 2 spreading (Maheshwari *et al*, 2000; Cavalcanti-Adam *et al*, 2007). Reduced integrin density (and therefore increased integrin spacing) delays adhesion complex formation and transition to phase 2 spreading (Cavalcanti-Adam *et al*, 2007). This delay has also been linked to ECM concentration: lower ECM density results in less integrin engagement with the ECM, increased spacing between integrins, and slower integrin clustering, adhesion complex formation, and spreading phase 2 initiation (Dubin-Thaler *et al*, 2004). Since integrins are substrate-specific, the substrate-specific spreading defects could thus be due to lower concentration of only certain integrins on the cell surface, or a failure to cluster these types of integrins.

The existing literature on the cell spreading process either takes a top-down biophysical approach to modelling the dynamics of spreading without considering underlying biology (Dubin-Thaler *et al*, 2004; Döbereiner *et al*, 2004; Cuvelier *et al*, 2007; Dubin-Thaler *et al*, 2008; Döbereiner *et al*, 2005), or focuses on biological mechanisms (Defilippi *et al*, 1999; Maheshwari *et al*, 2000; Loosli *et al*, 2010; Xiong *et al*, 2010), but there is little research that makes links between the two. The molecular and cell biological processes that actually drive the dynamic spreading phases therefore remain somewhat unclear, and the low replication of the experiments presented in this chapter mean that caution must be used when interpreting the results. However, this

evidence does suggest that alterations to integrin-based adhesions may be at the root of the MKS cell spreading defect. Given the placement of *TMEM67* at the adhesion (Chapter 1, Figure 3.4), this may represent one of the core phenotypic alterations in *TMEM67* patient cells.

The rate of cell spreading is determined by a combination of active force generation by actin polymerisation, cell-ECM interactions, and the mechanical resistance of the cell to shape change influenced primarily by the stiffness of the cortex (Cuvelier *et al*, 2007; Carvalho *et al*, 2013; Clark *et al*, 2013). *TMEM67* cells exhibit a reduced resistance to shape change when aspirated by micropipette (Figure 5.9 B), suggesting that their cortical stiffness is lower than that of control cells. *TMEM216* patient cells exhibited no alteration to deformation resistance, a surprising result since *TMEM216* cells have shown a more extreme phenotype than *TMEM67* cells in almost every other experiment. To assess the role of the actin cytoskeleton in cortical stiffness in these cells, imaging of fluorescently labelled f-actin at the cortex in rounded cells would be informative. It might also be informative to repeat the micropipette experiments with cells containing fluorescently labelled actin. Alterations to the actin cortex or failure of the actin cortex to adhere to the plasma membrane when subjected to micropipette aspiration, as observed in MKS1-deficient *Paramecium* (Campillo *et al*, 2012), could indicate a defective connection between the cortex and the membrane, which may explain cell shape control defects. Ciliopathy proteins such as *TMEM67* may be involved in this connection.

Chapter 6

General discussion

Chapter 6: General discussion

6.1 Summary

Despite a well-established genetic basis, the aetiology of MKS, in common with many other ciliopathies, is poorly understood. It is unclear how patient or cellular phenotypes emerge from single gene mutations, and even the function of many of the affected proteins remains unknown. MKS cells are defective in ciliogenesis; however, while MKS proteins have been linked to a functional complex in the cilium, they are also often reported in cellular locations distant from the cilium, and both ciliopathy models and patient cells show many cellular defects that are not easily explained if the primary defect is in ciliation. In this thesis, it has been shown that defective extracellular matrix made by MKS patient cells is the cause of the ciliation defect. This altered extracellular matrix is accompanied by depleted focal adhesion protein content and alterations to the actin cytoskeleton; alterations which can be rescued in *TMEM67* patient cells by treatment with Wnt or TGF-β pathway antagonists.

6.2 Known and proposed functions of MKS proteins

MKS proteins function as part of a diffusion barrier at the ciliary TZ

The MKS protein TMEM67 is a transmembrane protein that functions as part of a network of MKS and other ciliopathy proteins at the ciliary transition zone (TZ), where it is involved in the connection between the basal body and the TZ (Williams *et al*, 2011). This network is composed of two large modules: the NPHP module, and the MKS/JBTS module which includes TMEM67. The ciliopathy protein network is a component of the Y-links which connect the ciliary axoneme doublet microtubules to the ciliary membrane within the TZ, and contribute to a diffusion barrier which maintains separation between the ciliary

lumen and the cytoplasm, as well as between the ciliary membrane and the plasma membrane (Williams *et al*, 2011; Sang *et al*, 2011; Reiter *et al*, 2012; Garcia-Gonzalo *et al*, 2011). Compartmentalisation is essential for correct signalling through the cilium (Reiter *et al*, 2012; Hu *et al*, 2010). Since TMEM67 is a transmembrane protein, and is found within the MKS/JBTS module in close physical association with TCTN1 and TMEM216 (Garcia-Gonzalo & Reiter, 2012), which are also transmembrane proteins, it is likely that these have shared responsibility for connecting the outer ends of the Y-links to the ciliary membrane.

While TMEM216 is less-studied than TMEM67, it is placed within the transition zone complex alongside TMEM67 (Garcia-Gonzalo *et al*, 2011; Garcia-Gonzalo & Reiter, 2012), with which it physically interacts (Valente *et al*, 2010). It likely also serves as a membrane linker since it has been predicted to contain four transmembrane domains (Valente *et al*, 2010).

MKS proteins may be adhesion proteins

In this thesis, it has been shown that TMEM67 is an adhesion protein, and that the focal adhesions of *TMEM67* patient cells are depleted of many proteins. These results suggest that MKS cells have defective control of adhesion formation in response to the substrate, perhaps due to failure of recruitment or retention. The molecular pathways controlling adhesion formation are complex, with the conserved “adhesome” associated with integrin consisting of over 100 proteins (Zaidel-Bar, 2009). Among these are a number of ciliopathy proteins. Fibrocystin-1 is normally present in focal adhesions, but in the ciliopathy polycystic kidney disease, fibrocystin-1 is lost from adhesions. Fibrocystin-1 knockdown cells show longer paxillin-labelled adhesions, which were

associated with actin rearrangement and increased levels of β1-integrin and Src (Israeli *et al*, 2010). Other NPHP proteins have been found to localise to adhesion complexes or to interact with proteins that are components of adhesion complexes (Donaldson *et al*, 2000, 2002; Wilson *et al*, 1999; Markoff *et al*, 2007; Li *et al*, 2005). Polycystin-1 may function as an ECM receptor at focal adhesions, in a role similar to that of integrin (Wilson, 2001). Ciliopathy proteins can therefore be directly involved in regulation of the focal adhesion complex, its composition, and its morphology – MKS proteins may be performing a similar role, which would explain the alterations in adhesion morphology observed in MKS cells. Given its physical interaction with TMEM67, TMEM216 may also be a focal adhesion protein as part of a functional complex with TMEM67, as may other as yet undetected MKS and ciliopathy proteins, perhaps in a large complex with some similarities to the TZ ciliopathy network.

MKS proteins function as cell-surface receptors

TMEM67 has structural resemblance to the Frizzled family of transmembrane receptors, and it has been identified as a receptor in non-canonical Wnt signalling mediated by Wnt5a and ROR2 (Abdelhamed *et al*, 2015b). ROR2 co-localises and physically interacts with TMEM67 at the TZ (Abdelhamed *et al*, 2015b). Consequences of this signalling include inhibition of Shh and canonical Wnt and downstream changes reminiscent of pulmonary dysplasia (a frequent MKS patient symptom), which could be rescued by RhoA activation (Abdelhamed *et al*, 2015b). The finding in this thesis that inhibition of canonical Wnt can restore patient cell phenotypes can be understood in this context: in the absence of TMEM67, canonical Wnt is not inhibited and so becomes aberrantly activated, leading to various downstream defects which inhibition

rescues. This model does not explain why inhibition of Wnt/PCP was able to rescue some phenotypes.

TMEM67 has been reported to localise to the basal body/centrosome, basolateral actin cables, the cell surface of polarised cells (Dawe *et al*, 2007b, 2009), and the endoplasmic reticulum (Wang *et al*, 2009). Its function in these locations is not clear, though Wang *et al* propose a role in protein degradation at the ER. In this thesis, TMEM67 was additionally shown to localise to focal adhesions. The role of TMEM67 at the focal adhesion complex is also unclear. One of the proposed roles for TMEM67 in the ciliary transition zone is as a membrane anchor (Garcia-Gonzalo *et al*, 2011; Williams *et al*, 2011), so it may serve a similar function at the adhesion complex: as a membrane-bound recruiter of other proteins, including filamin A (FLNA). FLNA is not a transmembrane protein, so to be retained at the cell surface it must bind to some other factor. TMEM67's receptor function in cooperation with ROR2 for Wnt/PCP (Abdelhamed *et al*, 2015a) may also take place at adhesions. Cilia are considered to be important for Wnt/PCP signalling, but this is based on the involvement of BBS proteins and IFT88. These are cilium-associated, but BBS and IFT proteins have roles elsewhere in the cell (Hernandez-Hernandez *et al*, 2013; Finetti *et al*, 2009; Qin *et al*, 2007; Wood *et al*, 2012; Boehlke *et al*, 2015), so the involvement of the cilium itself is not necessarily supported by this evidence. Core PCP proteins including Dvl are required for actin reorganisation preceding ciliogenesis (Valente *et al*, 2010; Park *et al*, 2008), so the relationship may be that the cilium depends on PCP components rather than the other way around.

MKS proteins may act as membrane linkers

One of the proposed roles for TMEM67 in the ciliary transition zone is as a membrane anchor (Garcia-Gonzalo *et al*, 2011; Williams *et al*, 2011), so it may serve a similar function elsewhere in the cell. When MKS1 expression is silenced in *Paramecium*, the cortical cytoskeleton detached from the plasma membrane (Campillo *et al*, 2012), and in this thesis it was shown that *TMEM67*, but not *TMEM216*, patient cells have reduced deformation resistance, which could be a consequence of less stable cortical actin attachment. This appears to support a role for some MKS proteins as membrane-cortex linkers, and is consistent with the interaction between TMEM67 and filamin A, which has a tethering activity to actin but no transmembrane domains (Calderwood *et al*, 2001). It may be that the two act together as a complex in tethering roles in multiple contexts. TMEM67 may also act as an actin-dependent tether during ciliogenesis, when attenuation of TMEM67 causes basal body misalignment (Boisvieux-Ulrich *et al*, 1990; Dawe *et al*, 2007a; Lemullois *et al*, 1987; Picariello *et al*, 2014).

6.3 Proposed model for MKS cellular defects

Figure 6.1 shows a model for the causal relationships that might exist between the cellular processes that are defective in *TMEM67* cells, on the basis of the evidence shown in this thesis and previously published work. In non-diseased cells (Figure 6.1 A), TMEM67 and filamin A interact at cell surface focal adhesions, modulating cell-ECM interaction and ECM organisation. Adhesions modulate the actin cytoskeleton through recruitment of actin and actin binding proteins, and mechanotransduction. Correct cell-ECM interaction at the adhesion triggers signalling leading to basal body recruitment to the cell surface and ciliogenesis, possibly through tension signalling along the ECM-actin-

A: Non-diseased cell

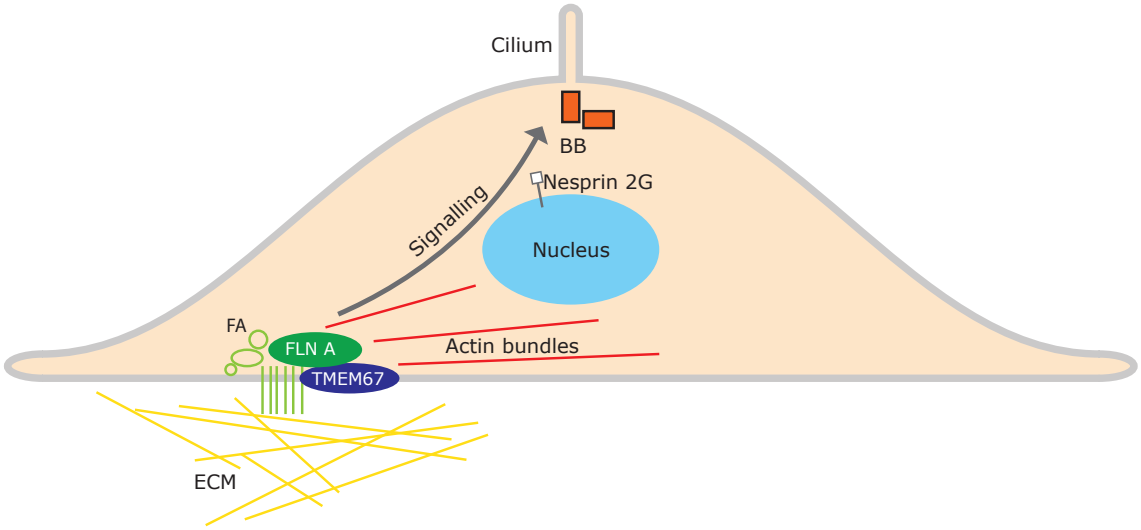

B: *TMEM67* patient cell

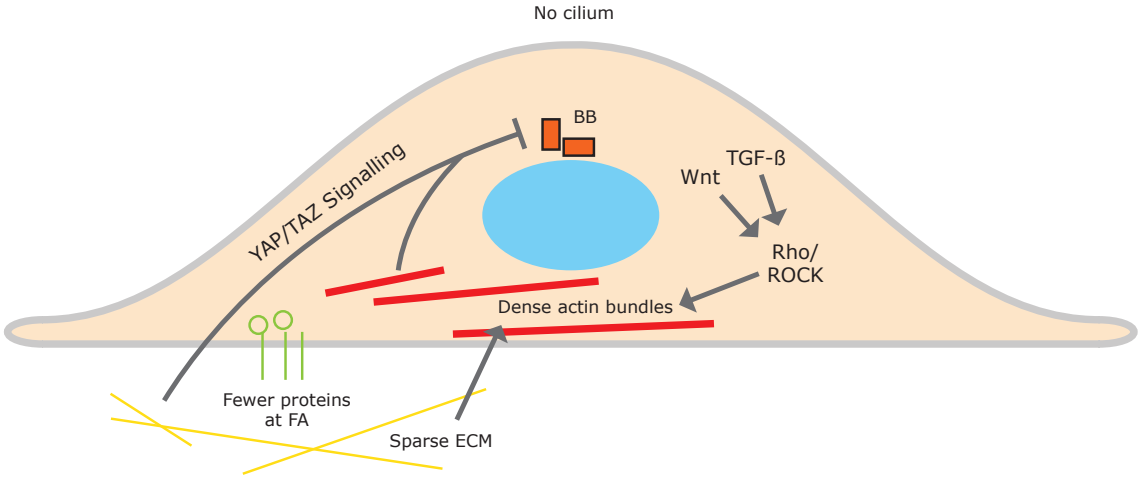

Figure 6.1: Model of possible alterations underlying defects in *TMEM67* patient cells.

A: In a non-diseased cell, TMEM67 interacts with FLNA at sites of cell-substrate adhesion, recruiting adhesion proteins and initiating tension signalling through the actin-nesprin 2G axis to promote basal body migration, docking, and ciliogenesis.

B: In a *TMEM67* patient cell, absence of TMEM67 leads to broad loss of protein at the cell-matrix adhesion, reduced ECM density, and dense actin bundles (downstream of substrate rigidity and/or Wnt/TGF-β/Rho/ROCK signalling). Actin density and/or substrate rigidity may activate YAP/TAZ signalling, which inhibits BB migration/docking and ciliogenesis.

nucleus axis involving nesprin 2G, which is a known TMEM67 binding partner (Dawe *et al*, 2009; Arsenovic *et al*, 2016). In *TMEM67* patient cells (Figure 6.1 B), the absence of TMEM67 at adhesions results in reduced activation of integrins, aberrant assembly of adhesions, and sparse ECM. Downstream of the changes to the ECM, or downstream of TGF-β or Wnt/Rho/ROCK signalling, actin bundles become denser, and either downstream of the reduced ECM pliancy (Dupont *et al*, 2011) or the actin stress fibre formation, the YAP/TAZ pathway may activate and negatively regulate ciliogenesis (Kim *et al*, 2015).

Possible roles of Wnt signalling

Wnt5a has a highly context-dependent effect on canonical Wnt signalling: in the presence of ROR2, Wnt5a inhibits canonical Wnt; however in the absence of ROR2 and the presence of frizzled 4, Wnt5a can activate canonical Wnt signalling (Mikels & Nusse, 2006). Therefore, a possible extension to the model in figure 6.1 would be that in *TMEM67* patient cells, the absence of TMEM67 leads to a failure to recruit its binding partner ROR2 to the cell surface, and as a consequence canonical Wnt is aberrantly activated. Aberrant Wnt activation has been reported previously in *TMEM67* mouse models (Abdelhamed *et al*, 2013), and as shown in this thesis (Figure 5.3), inhibition of canonical Wnt rescues multiple *TMEM67* patient cell phenotypes, lending credence to this model. Aberrant ROR2/Wnt5a signalling could explain multiple defects as ROR2/Wnt5a is involved in regulation of centrosome positioning, lammelipodia formation, cell migration, and convergent extension (Nomachi *et al*, 2008). Abdelhamed *et al.* only report TMEM67 and ROR2 co-localising at the ciliary transition zone, so it is possible that disruption to this signalling pathway is downstream of failure to build cilia, and therefore the loss of the receptor site, rather than directly due to absence of TMEM67. However, inhibition of canonical Wnt rescues ciliation

(Figure 5.3 B), which indicates that aberrant activation of canonical Wnt is an upstream cause of the ciliation defect and thus must be cilium-independent. This implies that ROR2/Wnt5a interaction is disrupted elsewhere in *TMEM67* patient cells. Since TMEM67 is found at multiple cellular sites including adhesions, it is quite plausible that the TMEM67/ROR2 interaction may also occur at adhesions. In this case aberrant activation of the canonical Wnt pathway could be a primary defect, in line with the successful rescue by inhibition. This model is further complicated as ROR2/Wnt5a interaction also activates filamin A by direct physical interaction between ROR2 and filamin A (Nomachi *et al*, 2008). As both of these proteins are reported to bind to TMEM67, it may be that TMEM67 plays a key role in regulating this interaction as well.

Possible roles of the filamins

What is the role of filamins at adhesions? Filamins are a family of multifunctional actin-binding proteins with over 30 known binding partners, many of which are cell surface receptors involved in adhesion (Stossel *et al*, 2001; Feng & Walsh, 2004). Filamins can recruit proteins to the plasma membrane, and are involved in the linking of adhesions to actin, modulating the actin cytoskeleton's spatial organisation and thus influencing cell shape and cell migration (Calderwood *et al*, 2001; Tu *et al*, 2003).

Knockdown of filamins has been shown to impair cell spreading and initiation of motility, which is rescued by full length filamin A but not by a filamin A mutant lacking IgG domains 19 to 21 (Baldassarre *et al*, 2009). Baldassare *et al.* further propose that interaction of FLNA with other proteins mediated by the 19-21 region is important for spreading and migration initiation. Conversely, increased

filamin binding to β-integrin at the adhesion complex inhibits cell migration and matrix protrusions (Calderwood *et al*, 2001). These apparently contradictory results indicate that filamins have complex roles controlling cell shape change that are likely to be regulated by tight control of localisation and specific binding partners. Filamin A is known to physically interact with TMEM67, and this interaction is required for ciliogenesis (Adams *et al*, 2012). It was proposed that this interaction took place at the centrosome; however, in this thesis it has been shown that TMEM67 is also present at adhesions.

The interaction with TMEM67 may be important for recruitment of FLNA to the adhesion complex; however, in the adhesion/ECM fraction investigated by mass spectrometry in Chapter 3, FLNA was detected but was not significantly altered in abundance in *TMEM67* patient cells (Appendix 1, Table 2). It may instead be that TMEM67 is a necessary cofactor or linker to recruit other proteins into a functional complex or subcomplex with FLNA at the adhesion, perhaps involving other MKS/JBTS module proteins which are known binding partners of TMEM67 such as TMEM216, and in the absence of these factors FLNA's activity is dysregulated.

FLNA knockdown has been shown to increase matrix metallopeptidase (MMP) activity and consequent degradation of the ECM (Baldassarre *et al*, 2012). Mutations in FLNA's CHD2 domain can cause otopalatodigital (OPD) spectrum disorders, which typically present symptoms including cleft palate, deafness, skeletal dysplasia, digital malformations, and microcephaly (Robertson *et al*, 2003; Dudding *et al*, 1967; Stratton & Bluestone, 1991; Stoll & Alembik, 1993). These symptoms are reminiscent of those seen in ciliopathies. The CHD2 domain mutations in FLNA are predicted to alter actin binding; mutations in the homologous CHD2 domain of alpha-actinin have been found to increase actin

binding activity (Kaplan *et al*, 2000), suggesting that the ciliopathy-like symptoms of OPD may be downstream of increased actin binding by FLNA. Furthermore, when FLNA expression is knocked down, the observed cellular phenotypes are identical to those caused by *TMEM67* knockdown (Adams *et al*, 2012). Some data also suggest that FLNA mutation is associated with connective tissue fragility (Feng & Walsh, 2004), potentially as a result of alterations to the ECM. These phenotypes are consistent with a role for filamin A as a component or upstream effector of the same signalling pathways that are disrupted in ciliopathies. Adams *et al* (2012) showed that interaction between filamin A and TMEM67 is essential for ciliogenesis, and in this thesis it has been shown to be essential for correct extracellular matrix morphology upstream of ciliation. In Chapter 5 it was shown that cell spreading is disrupted in MKS cells. A possible model to explain multiple MKS cellular defects is that the absence of MKS proteins leads to altered localisation or activity of filamins, disrupting control of actin, spreading, and the extracellular matrix, with the ciliation defect downstream.

Possible roles of TGF-β signalling

How is TGF-β signalling involved in MKS? It has been reported that in the absence of TGF-β signalling, at least one MKS protein, B9D1, fails to localise to the ciliary transition zone (Tozser *et al*, 2015), suggesting that TGF-β signalling may be necessary for the recruitment of components of the transition zone complex. This mis-localisation does not help to explain the non-ciliary phenotypes in patient cells, however. In this thesis, inhibition of TGF-β signalling was shown to rescue ECM morphology in *TMEM67* patient cells upstream of ciliogenesis independently of rescue by inhibition of canonical Wnt. This suggests that defective ECM synthesis in MKS is downstream of combined

activation of both canonical Wnt and TGF-β. TGF-β1 was among the few proteins to have significantly increased abundance in the adhesion/ECM fraction of *TMEM67* patient cells (Figure 4.6 B), further evidencing upregulation of this pathway. TGF-β activation is associated with increased ECM synthesis and reduced matrix metallopeptidase ECM degradation (Gressner *et al*, 2002); thus TGF-β pathway activation is difficult to reconcile with the sparse ECM made by MKS patient cells. A possible explanation could be that while loss of TMEM67 leads to activation of TGF-β signalling, it also blocks the pathways that would increase ECM synthesis downstream of TGF-β. TGF-β itself can also become activated downstream of the ECM: when cells are cultured on a normal matrix, TGF-β1 expression is downregulated, but cells cultured without endogenous or exogenous matrix have elevated TGF-β1 expression (Streuli *et al*, 1993). This cannot explain an elevation of TGF-β in *TMEM67* cells, however, as ECM morphology was rescued by inhibition of TGF-β signalling (figure 5.3 A), placing the ECM defect downstream of elevated TGF-β signalling, in defiance of the normal role of TGF-β in ECM synthesis.

Possible roles of the Rho family GTPases

The Rho family, of which the most well-studied members are RhoA, Rac1, and Cdc42, control various cellular processes including actin organisation and cell shape (Hall, 1998; Schmitz *et al*, 2000).

A number of signalling pathways converge on the GTPase RhoA, including both the TGF-β pathway and the Wnt pathway (Derynck & Zhang, 2003), as well as force transmission via cell-matrix and cell-cell interactions (Lessey *et al*, 2012). RhoA promotes contractility of actomyosin leading to stress fibre and focal adhesion formation, with consequent effects on cell shape and cell-substrate

adhesion (Wennerberg & Der, 2004). ROCK is one of the major downstream effectors of Rho signalling (Leung *et al*, 1995).

In *TMEM216* patient cells, RhoA is hyperactivated, leading to increased ROCK which may be upstream of dense actin bundle formation (Valente *et al*, 2010; McIntosh, 2016), and of the cell spreading defect described in this thesis.

RhoA is downstream of both the pathways which have been shown to rescue defects in *TMEM67* patient cells when inhibited, and various MKS cellular phenotypes are plausibly downstream of altered Rho signalling, including dense actin bundle formation and cell spreading alterations. RhoA in *TMEM67* patient cells has previously been found to be hyperactivated (Adams *et al*, 2012; Dawe *et al*, 2009). While RhoA activation was not investigated in the present study, in Chapter 3 of this thesis, total levels of RhoA were found to be somewhat diminished in the adhesion/ECM fraction, while levels of Rho family members Cdc42, Rac1, RhoG, ARHGEF1, and FARP1 were even more attenuated, as part of the overall pattern of loss of actin regulatory protein from the adhesion. This may reflect a redistribution of these proteins away from adhesions in *TMEM67* patient cells rather than a cell-wide loss of abundance. Given the confluence of signalling and regulatory roles it still seems likely that RhoA has an impact on *TMEM67* patient cell defects, but no clear evidence for such a role was acquired in this thesis.

6.4 Causal relationships in MKS

What is the primary defect in *TMEM67* patient cells? It remains unclear how exactly ciliogenesis is impaired in *TMEM67* cells. Previous studies have proposed factors upstream of ciliogenesis including TMEM67/filamin A interaction-dependent failure to migrate or dock the basal body to initiate

ciliogenesis, which may be due to failure of nucleus rotation, failure to transfer the basal body to the vicinity of the cell surface, or failure to clear a path through the cortical actin to effect docking (Adams *et al*, 2012; Dawe *et al*, 2009).

Given the finding that cellular phenotypes including ECM synthesis and ciliation are rescued by inhibition of developmental signalling pathways, it is tempting to conclude that aberrant activation of these pathways is one of the earlier steps in the causal chain. This may be directly downstream of alterations to cell-surface receptors, especially in the light of TMEM67's proposed role as a Wnt pathway receptor (Abdelhamed *et al*, 2013, 2015a). While developmental signalling pathways have profound effects on multiple cellular components, it is not necessarily the case that alterations in signalling cause all *TMEM67* cell phenotypes directly, since ciliogenesis was rescued by plating on non-disease ECM; at the very least, signalling is taking place through the ECM.

The causal chain linking absence of *TMEM67* to patient symptoms is still unclear. Developmental defects may be caused directly by the activation of Wnt and/or TGF-β signalling, or downstream of these, by alterations to the ECM, or further downstream, by failure to build cilia and thus transduce cilium-dependent developmental signalling. Studying a disease with organism-wide consequences in individual cells, derived from a single tissue in a single individual, inherently limits confidence in the data acquired. To investigate these causal links more thoroughly, tissue-level or whole-organism developmental models would be valuable in future work.

While the ECM defect is upstream of ciliary and actin defects, there remain multiple alterations in *TMEM67* patient cells independent of the ECM, as has been shown in Chapter 5 of this thesis. The altered cell spreading dynamics

and deformation resistance may result from multiple underlying alterations, but if interpreted in line with the model in Figure 6.1, are probably a result of altered actin cytoskeleton regulation or tension sensing, either throughout the cell or specifically in the cortex. These results suggest that these defects are not a result of altered ECM leading to reduced tension or adhesion signalling, but that the causal relationship runs the other way: altered tension/adhesion signalling leads the cell to make an aberrant ECM. This is plausible given that ECM synthesis and maintenance is an actively regulated process dependent on the cell correctly sensing the condition of the ECM in its vicinity, through outside-in integrin signalling and tension sensing by adhesion components.

6.5 Impact on MKS patient symptoms

Cystic kidney dysplasia

Cystic kidney is seen in 100% of MKS patients (Salonen *et al*, 1984a; Salonen & Paavola, 1998). Kidney cysts can be attributed to impaired canonical or non-canonical (PCP) Wnt signalling (Pinson *et al*, 2000; Lancaster *et al*, 2009), and non-canonical Wnt/calcium signalling has been implicated in kidney development (Burn *et al*, 2011) so may also have an impact. Since TMEM67 is a Wnt/PCP receptor, its loss likely impacts the Wnt/PCP pathway upstream of cystic kidney. It is not clear how Wnt/PCP impacts kidney development, but it may involve convergent extension or oriented cell division, both of which are involved in kidney tubule development and are dependent on Wnt/PCP (Lancaster & Gleeson, 2010; Ybot-Gonzalez *et al*, 2007; Jessen *et al*, 2002). Kidney branching morphogenesis is dependent on precise expression of ECM and MMPs, both of which have been shown in this thesis to have altered

abundance in *TMEM67* patient cells; these changes may be a more proximal cause of the cysts (Shah *et al*, 2004).

The reduced laminin production in *TMEM67* patient cells found in this thesis may indicate another possible mechanism driving kidney cysts, as laminin α5 (LAMA5) regulates kidney cell proliferation, and mutation in LAMA5 can cause PKD (Shannon *et al*, 2006; Joly *et al*, 2006) (although LAMA5 was not one of the laminins that was significantly lower in abundance in the present study). The alterations found in collagen IV secretion are not likely to be involved in cystic kidney because collagen IV overexpression, rather than underexpression, is implicated in PKD (Schäfer *et al*, 1993).

Occipital encephalocele

The major CNS defect occipital encephalocele is seen in 85-90% of MKS patients (Salonen *et al*, 1984a, 1984b). Encephalocele results from failure to close the neural tube, which is a process requiring convergent extension of the midline dependent on Wnt/PCP signalling (Wallingford *et al*, 2002; Hamblet *et al*, 2002; Murdoch *et al*, 2014; Juriloff & Harris, 2012; Ybot-Gonzalez *et al*, 2007; Murdoch *et al*, 2001, 2003; Curtin *et al*, 2003; Robinson *et al*, 2012). Again, the role of *TMEM67* as a Wnt/PCP receptor is likely to be important in this pathology. Cell-cell adhesion is key during convergent extension (Pyrgaki *et al*, 2011; Suzuki *et al*, 2012). While in this thesis the focus has been on cell-ECM adhesion, cell-cell adhesion through the adherens junction is also of interest since the ciliopathy proteins NPHP1 (Donaldson *et al*, 2000) and PKD1 (Streets *et al*, 2003) are involved in adherens junctions, as well as both being focal adhesion proteins. It is possible that MKS proteins have roles in these

structures as well, which may influence the convergent extension phenotypes in MKS.

Polydactyly

Polydactyly, a limb patterning defect that results in supernumerary digits, is found in 80% of patients (Salonen & Paavola, 1998). Of all symptoms of MKS, polydactyly may be the simplest to explain, as the developmental patterning of the digits is well understood. Sonic hedgehog (Shh) signalling establishes posterior polarity in the limb bud, with digits specified by Shh concentration. Cilia and IFT are required for Hh signalling (Eggenschwiler, 2012), so this patient symptom is very likely a result of the ciliation defect leading to disrupted Shh signalling in the limb bud.

Liver fibrosis

Liver fibrosis has been estimated to be present in 100% of MKS cases (Salonen & Paavola, 1998). Liver fibrosis is an aberrant overproduction of ECM, while in this thesis it has been shown that MKS patient fibroblasts synthesise a less dense ECM (Figure 3.14), a finding that at first glance is difficult to reconcile. However, liver fibrosis is proximally caused when hepatic stellate cells (HSCs) become activated, transdifferentiating into myofibroblast-like cells, which then initiate ECM production (Puche *et al*, 2013). The HSCs reside in the spaces of Disse within the liver, which contain a selection of basement membrane (BM)-associated ECM proteins (though no apparent structural BM) including collagen IV and laminin, which are thought to be essential for maintaining HSC quiescence (Bissell *et al*, 1987; Burt *et al*, 1990; Friedman *et al*, 1989). The reduced expression and abundance of collagen IV and laminin in *TMEM67* patient cell ECM shown in Chapter 3 (Figures 3.1 B, 3.2), therefore, suggest a

possible aetiology for liver fibrosis in MKS where reduced levels of BM proteins in the spaces of Disse lead to HSC activation and consequent fibrotic overproduction of ECM in the liver.

Elevated levels of TGF-β in MKS would also explain liver fibrosis, as TGF-β activates HSCs and stimulates secretion of ECM. TGF-β activity is implicated in many forms of fibrosis (Leask & Abraham, 2004)

6.6 Evolutionary context

Why would ciliopathy proteins have dual roles at cell-substrate adhesions and at cilia? Many classical adhesion proteins such as paxillin and vinculin have been detected associated with the ciliary basal body, connecting to the actin cytoskeleton, leading Antoniades *et al* (2014) to propose that the adhesion complex may have originated in primitive eukaryotes as a linking module at the ciliary base, and later became co-opted to serve a similar role at cell-substrate adhesions. Ciliopathy proteins such as TMEM67 would have been closely associated, as they have served as highly conserved components of the ciliary TZ for at least as long (Barker *et al*, 2014). An evolutionary model may therefore be proposed where the ciliary base adhesion complex interacted with the TZ ciliopathy protein complex to serve as a cytoskeleton/cilium interface early in eukaryotic evolution, and when the majority of this structure was co-opted to serve as a cytoskeleton/ECM interface (a proto-focal adhesion), TMEM67 and other ciliopathy proteins were included, retaining their function at a new location and becoming integrated into the signalling networks at adhesions. It is possible that TMEM67 has diverged into functional isoforms which are differentially localised to these different sites; indeed, in this thesis, only one isoform of TMEM67 was recovered from focal adhesions (Figure 3.4 B) whereas three isoforms of distinct molecular weight were detected in whole cell lysate and

associated with actin (Figure 3.3 B). These are potentially the same small isoforms of TMEM67 that only appear in subconfluent, non-ciliated cells reported by Dawe *et al* (2009). Investigation of the functional differences between these isoforms may further inform conclusions about the evolutionary relationship between different roles for ciliopathy proteins. It is quite plausible that the single gene mutations that underlie MKS have such complex effects on a cellular and developmental level because they actually abolish a set of homologous but functionally divergent isoforms, each of which may have a tethering or receptor role at a different cellular site.

6.7 Therapeutic outlook

The findings presented here that inhibition of Wnt or TGF-β signalling can rescue major cellular phenotypes may indicate potential for antagonists of these pathways to be used therapeutically. Some such drugs are already licensed; for example, losartan, which antagonises the TGF-β pathway through AT1, is used to treat high blood pressure and slow kidney damage, and it has been proposed as a therapeutic intervention in Marfan syndrome, a connective tissue disorder (Matt *et al*, 2008). Neural tube defects, of which MKS is the most common cause (Leitch *et al*, 2008), are an active area of medical research. Although folic acid supplementation can alleviate symptoms in some patients, many neural tube defects do not respond to this intervention, leading to trials of other therapeutics such as inositol (Greene *et al*, 2016). Since in this thesis many of the defects in *TMEM67* patient cells have been shown to be amenable to rescue via TGFβ or Wnt antagonists, it is possible that the MKS neural tube defect could also be rescued by similar interventions, opening a new category of treatments for neural tube defects.

Further identification of disrupted upstream effectors of the pathways in MKS patient cells would also be relevant to identification of drug targets. Since inhibition of either pathway appeared to independently rescue phenotypes, it may be that multiple different therapeutic strategies are viable. As this thesis was concerned with defects on a cellular level, no direct evidence is shown here for rescue of developmental defects; however the developmental pathways leading to many of the common MKS clinical symptoms are plausibly downstream of altered Wnt and TGF-β signalling, ECM synthesis, or disruption to ciliary signalling, all of which have been shown to be amenable to drug treatment. An obvious next step would be to test these interventions in an animal model.

6.8 Conclusion

This thesis presents the first comprehensive analysis of cell adhesion and the extracellular matrix in a ciliopathy, the first evidence of dependency relationships between cellular defects in Meckel-Gruber syndrome, and therefore a key step forward in our understanding of the aetiology of this phenotypically complex disease. The finding that developmental signalling pathway antagonists can rescue cellular defects raises the hope that new therapeutic approaches may be found following this work, and point toward future work which could further unravel the defects in ciliopathies. If a thorough understanding of the intra- and extracellular signalling pathways that impact on ciliopathies can be achieved, not only could we gain new insight into these complex processes, but also work towards effective treatment for deleterious and lethal diseases.

References

Abdelhamed Z, Natarajan S, Inglehearn C, Toomes C, Johnson C & Jagger D (2015a) The Meckel-Gruber Syndrome protein TMEM67 (meckelin) regulates basal body planar polarization and non-canonical Wnt signalling via Wnt5a and ROR2. *Cilia* **4:** P40

Abdelhamed ZA, Natarajan S, Wheway G, Inglehearn CF, Toomes C, Johnson CA & Jagger DJ (2015b) The Meckel-Gruber syndrome protein TMEM67 controls basal body positioning and epithelial branching morphogenesis in mice via the non-canonical Wnt pathway. *Dis. Model. Mech.* **8:** 527–541

Abdelhamed ZA, Wheway G, Szymanska K, Natarajan S, Toomes C, Inglehearn C & Johnson CA (2013) Variable expressivity of ciliopathy neurological phenotypes that encompass Meckel–Gruber syndrome and Joubert syndrome is caused by complex de-regulated ciliogenesis, Shh and Wnt signalling defects. *Hum. Mol. Genet.* **22:** 1358–1372

Abercrombie M, Heaysman JEM & Pegrum SM (1971) The locomotion of fibroblasts in culture: IV. Electron microscopy of the leading lamella. *Exp. Cell Res.* **67:** 359–367

Adams GMW, Huang B & Luck DJL (1982) Temperature-sensitive, assembly-defective flagella mutants of Chlamydomonas reinhardtii. *Genetics* **100:** 579–586

Adams M, Simms RJ, Abdelhamed Z, Dawe HR, Szymanska K, Logan C V, Wheway G, Pitt E, Gull K & Knowles MA (2012) A meckelin–filamin A interaction mediates ciliogenesis. *Hum. Mol. Genet.* **21:** 1272–1286

Aitken KJ & Bägli DJ (2009) The bladder extracellular matrix. Part I: architecture, development and disease. *Nat. Rev. Urol.* **6:** 596–611

Akhmanova A, Stehbens SJ & Yap AS (2009) Touch, Grasp, Deliver and Control: Functional Cross-Talk Between Microtubules and Cell Adhesions. *Traffic* **10:** 268–274

Akhmetshina A, Palumbo K, Dees C, Bergmann C, Venalis P, Zerr P, Horn A, Kireva T, Beyer C & Zwerina J (2012) Activation of canonical Wnt signalling is required for TGF-β-mediated fibrosis. *Nat. Commun.* **3:** 735

Albrecht-Buehler G (1977) Phagokinetic tracks of 3T3 cells: parallels between the orientation of track segments and of cellular structures which contain actin or tubulin. *Cell* **12:** 333–339

Alby C, Piquand K, Huber C, Megarbané A, Ichkou A, Legendre M, Pelluard F, Encha-Ravazi F, Abi-Tayeh G & Bessières B (2015) Mutations in KIAA0586 cause lethal ciliopathies ranging from a hydrolethalus phenotype to short-rib polydactyly syndrome. *Am. J. Hum. Genet.* **97:** 311–318

Alexiev BA, Lin X, Sun C-C & Brenner DS (2006) Meckel-Gruber syndrome: pathologic manifestations, minimal diagnostic criteria, and differential diagnosis. *Arch. Pathol. Lab. Med.* **130:** 1236–1238

van Amerongen R & Nusse R (2009) Towards an integrated view of Wnt signaling in development. *Development* **136:** 3205–3214

Anastas JN & Moon RT (2013) WNT signalling pathways as therapeutic targets in cancer. *Nat. Rev. Cancer* **13:** 11–26

Andersen RA, Barr DJS, Lynn DH, Melkonian M, Moestrup Ø & Sleigh MA (1991) Terminology and nomenclature of the cytoskeletal elements associated with the flagellar/ciliary apparatus in protists. *Protoplasma* **164:** 1–8

Ansley SJ, Badano JL, Blacque OE, Hill J, Hoskins BE, Leitch CC, Kim JC, Ross AJ, Eichers ER & Teslovich TM (2003) Basal body dysfunction is a likely cause of pleiotropic Bardet–Biedl syndrome. *Nature* **425:** 628–633

Antoniades I, Stylianou P & Skourides PA (2014) Making the connection: ciliary adhesion complexes anchor basal bodies to the actin cytoskeleton. *Dev. Cell* **28:** 70–80

Arnaiz O, Malinowska A, Klotz C, Sperling L, Dadlez M, Koll F & Cohen J (2009) Cildb: a knowledgebase for centrosomes and cilia. *Database* **2009:** bap022

Arsenovic PT, Ramachandran I, Bathula K, Zhu R, Narang JD, Noll NA, Lemmon CA, Gundersen GG & Conway DE (2016) Nesprin-2G, a Component of the Nuclear LINC Complex, Is Subject to Myosin-Dependent Tension. *Biophys. J.* **110:** 34–43

Ashcroft GS, Yang X, Glick AB, Weinstein M, Letterio JJ, Mizel DE, Anzano M, Greenwell-Wild T, Wahl SM & Deng C (1999) Mice lacking Smad3 show accelerated wound healing and an impaired local inflammatory response. *Nat. Cell Biol.* **1:** 260–266

Attisano L & Wrana JL (2013) Signal integration in TGF-β, WNT, and Hippo pathways. *F1000Prime Rep.* **5:**

Aumailley M (2013) The laminin family. *Cell Adh. Migr.* **7:** 48–55

Baala L, Audollent S, Martinovic J, Ozilou C, Babron M-C, Sivanandamoorthy S, Saunier S, Salomon R, Gonzales M & Rattenberry E (2007a) Pleiotropic Effects of CEP290 (NPHP6) Mutations Extend to Meckel Syndrome. *Am. J. Hum. Genet.* **81:** 170–179

Baala L, Romano S, Khaddour R, Saunier S, Smith UM, Audollent S, Ozilou C, Faivre L, Laurent N & Foliguet B (2007b) The Meckel-Gruber syndrome gene, MKS3, is mutated in Joubert syndrome. *Am. J. Hum. Genet.* **80:** 186–194

Bachmann-Gagescu R, Phelps IG, Dempsey JC, Sharma VA, Ishak GE, Boyle EA, Wilson M, Marques Lourenço C, Arslan M & Shendure J (2015) KIAA0586 is mutated in joubert syndrome. *Hum. Mutat.* **36:** 831–835

Badano JL, Mitsuma N, Beales PL & Katsanis N (2006) The ciliopathies: an emerging class of human genetic disorders. *Annu. Rev. Genomics Hum. Genet.* **7:** 125–148

Baldassarre M, Razinia Z, Brahme NN, Buccione R & Calderwood DA (2012) Filamin A controls matrix metalloproteinase activity and regulates cell invasion in human fibrosarcoma cells. *J. Cell Sci.* **125:** 3858–3869

Baldassarre M, Razinia Z, Burande CF, Lamsoul I, Lutz PG & Calderwood DA (2009) Filamins regulate cell spreading and initiation of cell migration. *PLoS One* **4:** e7830

Bangs F, Antonio N, Thongnuek P, Welten M, Davey MG, Briscoe J & Tickle C (2011) Generation of mice with functional inactivation of talpid3, a gene first identified in chicken. *Development* **138:** 3261–3272

Barczyk M, Carracedo S & Gullberg D (2010) Integrins. *Cell Tissue Res.* **339:** 269–280

Barisic I, Boban L, Loane M, Garne E, Wellesley D, Calzolari E, Dolk H, Addor M-C, Bergman JEH & Braz P (2015) Meckel–Gruber Syndrome: a population-based study on prevalence, prenatal diagnosis, clinical features, and survival in Europe. *Eur. J. Hum. Genet.* **23:** 746–752

Barker AR, McIntosh K V & Dawe HR (2015) Centrosome positioning in non-dividing cells. *Protoplasma* **253:** 1–15

Barker AR, Renzaglia KS, Fry K & Dawe HR (2014) Bioinformatic analysis of ciliary transition zone proteins reveals insights into the evolution of ciliopathy networks. *BMC Genomics* **15:** 531

Basiri ML, Ha A, Chadha A, Clark NM, Polyanovsky A, Cook B & Avidor-Reiss T (2014) A migrating ciliary gate compartmentalizes the site of axoneme assembly in Drosophila spermatids. *Curr. Biol.* **24:** 2622–2631

Beales PL, Bland E, Tobin JL, Bacchelli C, Tuysuz B, Hill J, Rix S, Pearson CG, Kai M & Hartley J (2007) IFT80, which encodes a conserved intraflagellar transport protein, is mutated in Jeune asphyxiating thoracic dystrophy. *Nat. Genet.* **39:** 727–729

Ben J, Elworthy S, Ng ASM, van Eeden F & Ingham PW (2011) Targeted mutation of the talpid3

gene in zebrafish reveals its conserved requirement for ciliogenesis and Hedgehog signalling across the vertebrates. *Development* **138:** 4969–4978

Benzing T, Gerke P, Höpker K, Hildebrandt F, Kim E & Walz G (2001) Nephrocystin interacts with Pyk2, p130Cas, and tensin and triggers phosphorylation of Pyk2. *Proc. Natl. Acad. Sci.* **98:** 9784–9789

Bergmann C, Akhmetshina A, Dees C, Palumbo K, Zerr P, Beyer C, Zwerina J, Distler O, Schett G & Distler JHW (2011) Inhibition of glycogen synthase kinase 3β induces dermal fibrosis by activation of the canonical Wnt pathway. *Ann. Rheum. Dis.* **70:** 2191–2198

Bergmann C, Fliegauf M, Brüchle NO, Frank V, Olbrich H, Kirschner J, Schermer B, Schmedding I, Kispert A & Kränzlin B (2008) Loss of nephrocystin-3 function can cause embryonic lethality, Meckel-Gruber-like syndrome, situs inversus, and renal-hepatic-pancreatic dysplasia. *Am. J. Hum. Genet.* **82:** 959–970

Bialas NJ, Inglis PN, Li C, Robinson JF, Parker JDK, Healey MP, Davis EE, Inglis CD, Toivonen T & Cottell DC (2009) Functional interactions between the ciliopathy-associated Meckel syndrome 1 (MKS1) protein and two novel MKS1-related (MKSR) proteins. *J. Cell Sci.* **122:** 611–624

Del Bigio MR (2010) Ependymal cells: biology and pathology. *Acta Neuropathol.* **119:** 55–73

Bissell DM, Arenson DM, Maher JJ & Roll FJ (1987) Support of cultured hepatocytes by a laminin-rich gel. Evidence for a functionally significant subendothelial matrix in normal rat liver. *J. Clin. Invest.* **79:** 801

Bloodgood RA (2010) Sensory reception is an attribute of both primary cilia and motile cilia. *J. Cell Sci.* **123:** 505–509

Boehlke C, Janusch H, Hamann C, Powelske C, Mergen M, Herbst H, Kotsis F, Nitschke R & Kuehn EW (2015) A cilia independent role of Ift88/Polaris during cell migration. *PLoS One* **10:** e0140378

Boisvieux Ulrich E, Laine MC & Sandoz D (1987) In vitro effects of benzodiazepines on ciliogenesis in the quail oviduct. *Cell Motil. Cytoskeleton* **8:** 333–344

Boisvieux-Ulrich E, Laine M & Sandoz D (1987) In vitro effects of benzodiazepines on ciliogenesis in the quail oviduct. *Cell Motil. Cytoskeleton* **8:** 333–344

Boisvieux-Ulrich E, Lainé M-C & Sandoz D (1990) Cytochalasin D inhibits basal body migration and ciliary elongation in quail oviduct epithelium. *Cell Tissue Res.* **259:** 443–454

Bolvar J, Huynh J-R, Lpez-Schier H, Gonzlez C, St Johnston D & Gonzlez-Reyes A (2001) Centrosome migration into the Drosophila oocyte is independent of BicD and egl, and of the organisation of the microtubule cytoskeleton. *Development* **128:** 1889–1897

Boquist L (1970) Cilia and vesicular particles in the endocrine pancreas of the Mongolian gerbil. *J. Cell Biol.* **45:** 532–541

Borovina A, Superina S, Voskas D & Ciruna B (2010) Vangl2 directs the posterior tilting and asymmetric localization of motile primary cilia. *Nat. Cell Biol.* **12:** 407–412

Boudreau NJ & Jones PL (1999) Extracellular matrix and integrin signalling: the shape of things to come. *Biochem. J.* **339:** 481–488

Brancati F, Iannicelli M, Travaglini L, Mazzotta A, Bertini E, Boltshauser E, D'Arrigo S, Emma F, Fazzi E & Gallizzi R (2009) MKS3/TMEM67 mutations are a major cause of COACH Syndrome, a Joubert Syndrome related disorder with liver involvement. *Hum. Mutat.* **30:** E432–E442

Brancolini C, Marzinotto S, Edomi P, Agostoni E, Fiorentini C, Müller HW & Schneider C (1999) Rho-dependent regulation of cell spreading by the tetraspan membrane protein Gas3/PMP22. *Mol. Biol. Cell* **10:** 2441–2459

Bray SJ (2006) Notch signalling: a simple pathway becomes complex. *Nat. Rev. Mol. cell Biol.* **7:** 678–689

Bremer K, Humphries CJ, Mishler BD & Churchill SP (1987) On cladistic relationships in green plants. *Taxon* **36:** 339–349

Breslow DK, Koslover EF, Seydel F, Spakowitz AJ & Nachury M V (2013) An in vitro assay for entry into cilia reveals unique properties of the soluble diffusion barrier. *J. Cell Biol.* **203:** 129–147

Broadhead R, Dawe HR, Farr H, Griffiths S, Hart SR, Portman N, Shaw MK, Ginger ML, Gaskell SJ & McKean PG (2006) Flagellar motility is required for the viability of the bloodstream trypanosome. *Nature* **440:** 224–227

Buehler MJ (2006) Nature designs tough collagen: explaining the nanostructure of collagen fibrils. *Proc. Natl. Acad. Sci.* **103:** 12285–12290

Burakov A, Nadezhdina E, Slepchenko B & Rodionov V (2003) Centrosome positioning in interphase cells. *J. Cell Biol.* **162:** 963–969

Burn SF, Webb A, Berry RL, Davies JA, Ferrer-Vaquer A, Hadjantonakis AK, Hastie ND & Hohenstein P (2011) Calcium/NFAT signalling promotes early nephrogenesis. *Dev. Biol.* **352:** 288–298

Burt AD, Griffiths MR, Schuppan D, Voss B & Macsween RNM (1990) Ultrastructural localization of extracellular matrix proteins in liver biopsies using ultracryomicrotomy and immuno-gold labelling. *Histopathology* **16:** 53–58

Bush A, Chodhari R, Collins N, Copeland F, Hall P, Harcourt J, Hariri M, Hogg C, Lucas J & Mitchison HM (2007) Primary ciliary dyskinesia. *Arch. Dis. Child.* **92:** 1136–1140

Busk M, Pytela R & Sheppard D (1992) Characterization of the integrin alpha v beta 6 as a fibronectin-binding protein. *J. Biol. Chem.* **267:** 5790–5796

Calderwood DA, Huttenlocher A, Kiosses WB, Rose DM, Woodside DG, Schwartz MA & Ginsberg MH (2001) Increased filamin binding to β-integrin cytoplasmic domains inhibits cell migration. *Nat. Cell Biol.* **3:** 1060–1068

Campillo C, Jerber J, Fisch C, Simoes-Betbeder M, Dupuis-Williams P, Nassoy P & Sykes C (2012) Mechanics of membrane–cytoskeleton attachment in Paramecium. *New J. Phys.* **14:** 125016

Canty EG & Kadler KE (2002) Collagen fibril biosynthesis in tendon: a review and recent insights. *Comp. Biochem. Physiol. Part A Mol. Integr. Physiol.* **133:** 979–985

Cao Y, Park A & Sun Z (2010) Intraflagellar transport proteins are essential for cilia formation and for planar cell polarity. *J. Am. Soc. Nephrol.* **21:** 1326–1333

Caron A, Xu X & Lin X (2012) Wnt/β-catenin signaling directly regulates Foxj1 expression and ciliogenesis in zebrafish Kupffer's vesicle. *Development* **139:** 514–524

Carvajal-Gonzalez JM, Roman A-C & Mlodzik M (2016) Positioning of centrioles is a conserved readout of Frizzled planar cell polarity signalling. *Nat. Commun.* **7:** 11135

Carvalho K, Tsai F-C, Lees E, Voituriez R, Koenderink GH & Sykes C (2013) Cell-sized liposomes reveal how actomyosin cortical tension drives shape change. *Proc. Natl. Acad. Sci.* **110:** 16456–16461

Castillo K, Restrepo D & Bacigalupo J (2010) Cellular & molecular Ca2+ microdomains in olfactory cilia support low signaling amplification of odor transduction. *Eur. J. Neurosci.* **32:** 932–938

Cavalcanti-Adam EA, Volberg T, Micoulet A, Kessler H, Geiger B & Spatz JP (2007) Cell spreading and focal adhesion dynamics are regulated by spacing of integrin ligands. *Biophys. J.* **92:** 2964–2974

Cavalier-Smith T (2002) The phagotrophic origin of eukaryotes and phylogenetic classification of Protozoa. *Int. J. Syst. Evol. Microbiol.* **52:** 297–354

Chang B, Khanna H, Hawes N, Jimeno D, He S, Lillo C, Parapuram SK, Cheng H, Scott A & Hurd RE (2006) In-frame deletion in a novel centrosomal/ciliary protein CEP290/NPHP6 perturbs its interaction with RPGR and results in early-onset retinal degeneration in the rd16 mouse. *Hum. Mol. Genet.* **15:** 1847–1857

Chen H (2006) Meckel-Gruber Syndrome. In *Atlas of Genetic Diagnosis and Counseling* pp 636–638. Springer

Cherny RC, Honan MA & Thiagarajan P (1993) Site-directed mutagenesis of the arginine-glycine-aspartic acid in vitronectin abolishes cell adhesion. *J. Biol. Chem.* **268:** 9725–9729

Chih B, Liu P, Chinn Y, Chalouni C, Komuves LG, Hass PE, Sandoval W & Peterson AS (2012) A ciliopathy complex at the transition zone protects the cilia as a privileged membrane domain. *Nat. Cell Biol.* **14:** 61–72

Le Clainche C & Carlier M-F (2008) Regulation of actin assembly associated with protrusion and adhesion in cell migration. *Physiol. Rev.* **88:** 489–513

Clark AG, Dierkes K & Paluch EK (2013) Monitoring actin cortex thickness in live cells. *Biophys. J.* **105:** 570–580

Clotman F, Libbrecht L, Killingsworth MC, Loo CCK, Roskams T & Lemaigre FP (2008) Lack of cilia and differentiation defects in the liver of human foetuses with the Meckel syndrome. *Liver Int.* **28:** 377–384

Cole DG, Diener DR, Himelblau AL, Beech PL, Fuster JC & Rosenbaum JL (1998) Chlamydomonas kinesin-II–dependent intraflagellar transport (IFT): IFT particles contain proteins required for ciliary assembly in Caenorhabditis elegans sensory neurons. *J. Cell Biol.* **141:** 993–1008

Collin GB, Marshall JD, Ikeda A, So WV, Russell-Eggitt I, Maffei P, Beck S, Boerkoel CF, Sicolo N & Martin M (2002) Mutations in ALMS1 cause obesity, type 2 diabetes and neurosensory degeneration in Alström syndrome. *Nat. Genet.* **31:** 74–78

Corbit KC, Shyer AE, Dowdle WE, Gaulden J, Singla V & Reiter JF (2008) Kif3a constrains β-catenin-dependent Wnt signalling through dual ciliary and non-ciliary mechanisms. *Nat. Cell Biol.* **10:** 70–76

Craft JM, Harris JA, Hyman S, Kner P & Lechtreck KF (2015) Tubulin transport by IFT is upregulated during ciliary growth by a cilium-autonomous mechanism. *J. Cell Biol.* **208:** 223–237

Craige B, Tsao C-C, Diener DR, Hou Y, Lechtreck K-F, Rosenbaum JL & Witman GB (2010) CEP290 tethers flagellar transition zone microtubules to the membrane and regulates flagellar protein content. *J. Cell Biol.* **190:** 927–940

Cui C, Chatterjee B, Lozito TP, Zhang Z, Francis RJ, Yagi H, Swanhart LM, Sanker S, Francis D & Yu Q (2013) Wdpcp, a PCP protein required for ciliogenesis, regulates directional cell migration and cell polarity by direct modulation of the actin cytoskeleton. *PLoS Biol* **11:** e1001720

Curtin JA, Quint E, Tsipouri V, Arkell RM, Cattanach B, Copp AJ, Henderson DJ, Spurr N, Stanier P & Fisher EM (2003) Mutation of Celsr1 disrupts planar polarity of inner ear hair cells and causes severe neural tube defects in the mouse. *Curr. Biol.* **13:** 1129–1133

Cuvelier D, Théry M, Chu Y-S, Dufour S, Thiéry J-P, Bornens M, Nassoy P & Mahadevan L (2007) The Universal Dynamics of Cell Spreading. *Curr. Biol.* **17:** 694–699 Available at: http://www.sciencedirect.com/science/article/pii/S096098220701069X

Czarnecki PG & Shah J V (2012) The ciliary transition zone: from morphology and molecules to medicine. *Trends Cell Biol.* **22:** 201–210

Danen EHJ, Sonneveld P, Brakebusch C, Fässler R & Sonnenberg A (2002) The fibronectin-binding integrins α5β1 and αvβ3 differentially modulate RhoA–GTP loading, organization of cell matrix adhesions, and fibronectin fibrillogenesis. *J. Cell Biol.* **159:** 1071–1086

Davey MG, Paton IR, Yin Y, Schmidt M, Bangs FK, Morrice DR, Smith TG, Buxton P, Stamataki D & Tanaka M (2006) The chicken talpid3 gene encodesa novel protein essentialfor Hedgehog signaling. *Genes Dev.* **20:** 1365–1377

Dawe HR, Adams M, Wheway G, Szymanska K, Logan C V, Noegel AA, Gull K & Johnson CA (2009) Nesprin-2 interacts with meckelin and mediates ciliogenesis via remodelling of the actin cytoskeleton. *J. Cell Sci.* **122:** 2716–2726

Dawe HR, Farr H & Gull K (2007a) Centriole/basal body morphogenesis and migration during ciliogenesis in animal cells. *J. Cell Sci.* **120:** 7–15

Dawe HR, Smith UM, Cullinane AR, Gerrelli D, Cox P, Badano JL, Blair-Reid S, Sriram N, Katsanis N, Attie-Bitach T & others (2007b) The Meckel--Gruber syndrome proteins MKS1 and meckelin interact and are required for primary cilium formation. *Hum. Mol. Genet.* **16:** 173–186

De A (2011) Wnt/Ca2+ signaling pathway: a brief overview. *Acta Biochim. Biophys. Sin. (Shanghai).* **43:** 745–756

Deane JA, Cole DG, Seeley ES, Diener DR & Rosenbaum JL (2001) Localization of intraflagellar transport protein IFT52 identifies basal body transitional fibers as the docking site for IFT particles. *Curr. Biol.* **11:** 1586–1590

Defilippi P, Olivo C, Venturino M, Dolce L, Silengo L & Tarone G (1999) Actin cytoskeleton organization in response to integrin-mediated adhesion. *Microsc. Res. Tech.* **47:** 67–78

Delling M, Indzhykulian AA, Liu X, Li Y, Xie T, Corey DP & Clapham DE (2016) Primary cilia are not calcium-responsive mechanosensors. *Nature* **531:** 656–660

Delous M, Baala L, Salomon R, Laclef C, Vierkotten J, Tory K, Golzio C, Lacoste T, Besse L & Ozilou C (2007) The ciliary gene RPGRIP1L is mutated in cerebello-oculo-renal syndrome (Joubert syndrome type B) and Meckel syndrome. *Nat. Genet.* **39:** 875–881

Derynck R & Zhang YE (2003) Smad-dependent and Smad-independent pathways in TGF-β family signalling. *Nature* **425:** 577–584

Dingle AD & Fulton C (1966) Development of the flagellar apparatus of Naegleria. *J. Cell Biol.* **31:** 43–54

Dishinger JF, Kee HL, Jenkins PM, Fan S, Hurd TW, Hammond JW, Truong YN-T, Margolis B, Martens JR & Verhey KJ (2010) Ciliary entry of the kinesin-2 motor KIF17 is regulated by importin-β2 and RanGTP. *Nat. Cell Biol.* **12:** 703–710

Döbereiner H-G, Dubin-Thaler B, Giannone G, Xenias HS & Sheetz MP (2004) Dynamic phase transitions in cell spreading. *Phys. Rev. Lett.* **93:** 108105

Döbereiner H-G, Dubin-Thaler BJ, Giannone G & Sheetz MP (2005) Force sensing and generation in cell phases: analyses of complex functions. *J. Appl. Physiol.* **98:** 1542–1546

Domogatskaya A, Rodin S & Tryggvason K (2012) Functional diversity of laminins. *Annu. Rev. Cell Dev. Biol.* **28:** 523–553

Donaldson JC, Dempsey PJ, Reddy S, Bouton AH, Coffey RJ & Hanks SK (2000) Crk-Associated Substrate p130< sup> Cas</sup> Interacts with Nephrocystin and Both Proteins Localize to Cell–Cell Contacts of Polarized Epithelial Cells. *Exp. Cell Res.* **256:** 168–178

Donaldson JC, Dise RS, Ritchie MD & Hanks SK (2002) Nephrocystin-conserved domains involved in targeting to epithelial cell-cell junctions, interaction with filamins, and establishing cell polarity. *J. Biol. Chem.* **277:** 29028–29035

Doolin PF & Birge WJ (1966) Ultrastructural organization of cilia and basal bodies of the epithelium of the choroid plexus in the chick embryo. *J. Cell Biol.* **29:** 333–345

Dowdle WE, Robinson JF, Kneist A, Sirerol-Piquer MS, Frints SGM, Corbit KC, Zaghloul NA, van Lijnschoten G, Mulders L & Verver DE (2011) Disruption of a ciliary B9 protein complex causes Meckel syndrome. *Am. J. Hum. Genet.* **89:** 94–110

Dubin-Thaler BJ, Giannone G, Döbereiner H-G & Sheetz MP (2004) Nanometer analysis of cell spreading on matrix-coated surfaces reveals two distinct cell states and STEPs. *Biophys. J.* **86:** 1794–1806

Dubin-Thaler BJ, Hofman JM, Cai Y, Xenias H, Spielman I, Shneidman A V, David LA, Döbereiner H-G, Wiggins CH & Sheetz MP (2008) Quantification of cell edge velocities and traction forces reveals distinct motility modules during cell spreading. *PLoS One* **3:** e3735

Dudding BA, Gorlin RJ & Langer LO (1967) The oto-palato-digital syndrome: A new symptom-complex consisting of deafness, dwarfism, cleft palate, characteristic facies, and a generalized bone dysplasia. *Am. J. Dis. Child.* **113:** 214–221

Dupont S, Morsut L, Aragona M, Enzo E, Giulitti S, Cordenonsi M, Zanconato F, Le Digabel J, Forcato M & Bicciato S (2011) Role of YAP/TAZ in mechanotransduction. *Nature* **474:** 179–183

Dustin ML (2002) The immunological synapse. *Arthritis Res. Ther.* **4:** 1

Dzamba BJ, Jakab KR, Marsden M, Schwartz MA & DeSimone DW (2009) Cadherin adhesion, tissue tension, and noncanonical Wnt signaling regulate fibronectin matrix organization. *Dev. Cell* **16:** 421–432

Echelard Y, Epstein DJ, St-Jacques B, Shen L, Mohler J, McMahon JA & McMahon AP (1993) Sonic hedgehog, a member of a family of putative signaling molecules, is implicated in the regulation of CNS polarity. *Cell* **75:** 1417–1430

Eckmann-Scholz C, Jonat W, Zerres K & Ortiz-Brüchle N (2012) Earliest ultrasound findings and description of splicing mutations in Meckel–Gruber syndrome. *Arch. Gynecol. Obstet.* **286:** 917–921

Edvardson S, Shaag A, Zenvirt S, Erlich Y, Hannon GJ, Shanske AL, Gomori JM, Ekstein J & Elpeleg O (2010) Joubert syndrome 2 (JBTS2) in Ashkenazi Jews is associated with a TMEM216 mutation. *Am. J. Hum. Genet.* **86:** 93–97

Eggenschwiler J (2012) Hedgehog Signaling and the Cilium: in the Zone. *Dev. Cell* **23:** 677–678

Eggenschwiler JT & Anderson K V (2007) Cilia and developmental signaling. *Annu. Rev. Cell Dev. Biol.* **23:** 345

Ehlen HWA, Buelens LA & Vortkamp A (2006) Hedgehog signaling in skeletal development. *Birth Defects Res. Part C Embryo Today Rev.* **78:** 267–279

Emiralioglu N, Kiper N, Schwerk N, Cinel G, Yalçin E, Ersöz DD & Özçelik U (2015) An insight of lung cysts with filamin A mutation. *Eur. Respir. J.* **46:** PA3833

Engler AJ, Sen S, Sweeney HL & Discher DE (2006) Matrix elasticity directs stem cell lineage specification. *Cell* **126:** 677–689

Epting D, Slanchev K, Boehlke C, Hoff S, Loges NT, Yasunaga T, Indorf L, Nestel S, Lienkamp SS & Omran H (2015) The Rac1 regulator ELMO controls basal body migration and docking in multiciliated cells through interaction with Ezrin. *Development* **142:** 174–184

Ericson J, Briscoe J, Rashbass P, Van Heyningen V & Jessell TM (1997) Graded sonic hedgehog signaling and the specification of cell fate in the ventral neural tube. In *Cold Spring Harbor symposia on quantitative biology* pp 451–466. Cold Spring Harbor Laboratory Press

Essner JJ, Vogan KJ, Wagner MK, Tabin CJ, Yost HJ & Brueckner M (2002) Left–right development: Conserved function for embryonic nodal cilia. *Nature* **418:** 37–38

Euteneuer U & Schliwa M (1984) Persistent, directional motility of cells and cytoplasmic fragments in the absence of microtubules. *Nature* **310:** 58–61 Available at: http://dx.doi.org/10.1038/310058a0

Ezratty EJ, Partridge MA & Gundersen GG (2005) Microtubule-induced focal adhesion disassembly is mediated by dynamin and focal adhesion kinase. *Nat. Cell Biol.* **7:** 581–590

Ezratty EJ, Stokes N, Chai S, Shah AS, Williams SE & Fuchs E (2011) A role for the primary cilium in Notch signaling and epidermal differentiation during skin development. *Cell* **145:** 1129–1141

Feng Y & Walsh CA (2004) The many faces of filamin: a versatile molecular scaffold for cell motility and signalling. *Nat. Cell Biol.* **6:** 1034–1038

Ferrante MI, Romio L, Castro S, Collins JE, Goulding DA, Stemple DL, Woolf AS & Wilson SW (2009) Convergent extension movements and ciliary function are mediated by ofd1, a zebrafish orthologue of the human oral-facial-digital type 1 syndrome gene. *Hum. Mol. Genet.* **18:** 289–303

Filges I, Nosova E, Bruder E, Tercanli S, Townsend K, Gibson WT, Röthlisberger B, Heinimann K, Hall JG & Gregory-Evans CY (2014) Exome sequencing identifies mutations in KIF14 as a novel cause of an autosomal recessive lethal fetal ciliopathy phenotype. *Clin. Genet.* **86:** 220–228

Finet C, Timme RE, Delwiche CF & Marlétaz F (2012) Multigene phylogeny of the green lineage reveals the origin and diversification of land plants. *Curr. Biol.* **22:** 1456–1457

Finetti F, Paccani SR, Riparbelli MG, Giacomello E, Perinetti G, Pazour GJ, Rosenbaum JL & Baldari CT (2009) Intraflagellar transport is required for polarized recycling of the TCR/CD3 complex to the immune synapse. *Nat. Cell Biol.* **11:** 1332–1339

Fliegauf M, Horvath J, von Schnakenburg C, Olbrich H, Müller D, Thumfart J, Schermer B, Pazour GJ, Neumann HPH & Zentgraf H (2006) Nephrocystin specifically localizes to the transition zone of renal and respiratory cilia and photoreceptor connecting cilia. *J. Am. Soc. Nephrol.* **17:** 2424–2433

Folkman J & Moscona A (1978) Role of cell shape in growth control. *Nature* **273:** 345–349

Francis SS, Sfakianos J, Lo B & Mellman I (2011) A hierarchy of signals regulates entry of membrane proteins into the ciliary membrane domain in epithelial cells. *J. Cell Biol.* **193:** 219–233

Freisinger CM, Fisher RA & Slusarski DC (2010) Regulator of g protein signaling 3 modulates wnt5b calcium dynamics and somite patterning. *PLoS Genet.* **6:** e1001020

Friedman SL, Roll FJ, Boyles J, Arenson DM & Bissell DM (1989) Maintenance of differentiated phenotype of cultured rat hepatic lipocytes by basement membrane matrix. *J. Biol. Chem.* **264:** 10756–10762

Fuchs JL & Schwark HD (2004) Neuronal primary cilia: a review. *Cell Biol. Int.* **28:** 111–118

Fujikura K, Setsu T, Tanigaki K, Abe T, Kiyonari H, Terashima T & Sakisaka T (2013) Kif14 mutation causes severe brain malformation and hypomyelination. *PLoS One* **8:** e53490

Gakovic M, Shu X, Kasioulis I, Carpanini S, Moraga I & Wright AF (2011) The role of RPGR in cilia formation and actin stability. *Hum. Mol. Genet.* **20:** 4840–4850

Garcia-Gonzalo FR, Corbit KC, Sirerol-Piquer MS, Ramaswami G, Otto EA, Noriega TR, Seol AD, Robinson JF, Bennett CL & Josifova DJ (2011) A transition zone complex regulates mammalian ciliogenesis and ciliary membrane composition. *Nat. Genet.* **43:** 776–784

Garcia-Gonzalo FR & Reiter JF (2012) Scoring a backstage pass: mechanisms of ciliogenesis

and ciliary access. *J. Cell Biol.* **197:** 697–709

Gattone VH, Wang X, Harris PC & Torres VE (2003) Inhibition of renal cystic disease development and progression by a vasopressin V2 receptor antagonist. *Nat. Med.* **9:** 1323–1326

Gehler S, Baldassarre M, Lad Y, Leight JL, Wozniak MA, Riching KM, Eliceiri KW, Weaver VM, Calderwood DA & Keely PJ (2009) Filamin A–β1 integrin complex tunes epithelial cell response to matrix tension. *Mol. Biol. Cell* **20:** 3224–3238

Geiger B & Bershadsky A (2001) Assembly and mechanosensory function of focal contacts. *Curr. Opin. Cell Biol.* **13:** 584–592

Geiger T & Zaidel-Bar R (2012) Opening the floodgates: proteomics and the integrin adhesome. *Curr. Opin. Cell Biol.* **24:** 562–568

Geimer S & Melkonian M (2004) The ultrastructure of the Chlamydomonas reinhardtii basal apparatus: identification of an early marker of radial asymmetry inherent in the basal body. *J. Cell Sci.* **117:** 2663–2674

George EL, Georges-Labouesse EN, Patel-King RS, Rayburn H & Hynes RO (1993) Defects in mesoderm, neural tube and vascular development in mouse embryos lacking fibronectin. *Development* **119:** 1079–1091

Gerdes JM, Liu Y, Zaghloul NA, Leitch CC, Lawson SS, Kato M, Beachy PA, Beales PL, DeMartino GN & Fisher S (2007) Disruption of the basal body compromises proteasomal function and perturbs intracellular Wnt response. *Nat. Genet.* **39:** 1350–1360

Ghossoub R, Molla-Herman A, Bastin P & Benmerah A (2011) The ciliary pocket: a once-forgotten membrane domain at the base of cilia. *Biol. Cell* **103:** 131–144

Gill PE & Murray W (1978) Algorithms for the solution of the nonlinear least-squares problem. *SIAM J. Numer. Anal.* **15:** 977–992

Gilula NB & Satir P (1972) The ciliary necklace a ciliary membrane specialization. *J. Cell Biol.* **53:** 494–509

Gjorevski N & Nelson CM (2009) Bidirectional extracellular matrix signaling during tissue morphogenesis. *Cytokine Growth Factor Rev.* **20:** 459–465

Goetz SC & Anderson K V (2010) The primary cilium: a signalling centre during vertebrate development. *Nat. Rev. Genet.* **11:** 331–344

Goetz SC, Liem KF & Anderson K V (2012) The spinocerebellar ataxia-associated gene Tau tubulin kinase 2 controls the initiation of ciliogenesis. *Cell* **151:** 847–858

Goldfarb LG & Dalakas MC (2009) Tragedy in a heartbeat: malfunctioning desmin causes skeletal and cardiac muscle disease. *J. Clin. Invest.* **119:** 1806–1813

Gorden NT, Arts HH, Parisi MA, Coene KLM, Letteboer SJF, van Beersum SEC, Mans DA, Hikida A, Eckert M & Knutzen D (2008) < i> CC2D2A</i> Is Mutated in Joubert Syndrome and Interacts with the Ciliopathy-Associated Basal Body Protein CEP290. *Am. J. Hum. Genet.* **83:** 559–571

Gray RS, Abitua PB, Wlodarczyk BJ, Szabo-Rogers HL, Blanchard O, Lee I, Weiss GS, Liu KJ, Marcotte EM & Wallingford JB (2009) The planar cell polarity effector Fuz is essential for targeted membrane trafficking, ciliogenesis and mouse embryonic development. *Nat. Cell Biol.* **11:** 1225–1232

Gray RS, Roszko I & Solnica-Krezel L (2011) Planar cell polarity: coordinating morphogenetic cell behaviors with embryonic polarity. *Dev. Cell* **21:** 120–133

Greene NDE, Leung K-Y, Gay V, Burren K, Mills K, Chitty LS & Copp AJ (2016) Inositol for the prevention of neural tube defects: a pilot randomised controlled trial. *Br. J. Nutr.* **115:** 974–983

Gressner AM, Weiskirchen R, Breitkopf K & Dooley S (2002) Roles of TGF-beta in hepatic fibrosis. *Front Biosci* **7:** d793–807

Griffin MD, Torres VE, Grande JP & Kumar R (1997) Vascular expression of polycystin. *J. Am. Soc. Nephrol.* **8:** 616–626

Grinnell F (2003) Fibroblast biology in three-dimensional collagen matrices. *Trends Cell Biol.* **13:** 264–269

Guilak F, Ting-Beall HP, Baer AE, Trickey WR, Erickson GR & Setton LA (1999) Viscoelastic properties of intervertebral disc cells: identification of two biomechanically distinct cell populations. *Spine (Phila. Pa. 1976).* **24:** 2475

Hagiwara H, Ohwada N, Aoki T, Suzuki T & Takata K (2008) Immunohistochemical and electron microscopic observations of stromal cells in the human oviduct mucosa. *Med. Mol. Morphol.* **41:** 221–226

Halder G, Dupont S & Piccolo S (2012) Transduction of mechanical and cytoskeletal cues by YAP and TAZ. *Nat. Rev. Mol. cell Biol.* **13:** 591–600

Hall A (1998) Rho GTPases and the Actin Cytoskeleton. *Science* **279:** 509–514 Available at: http://science.sciencemag.org/content/279/5350/509.abstract

Hamblet NS, Lijam N, Ruiz-Lozano P, Wang J, Yang Y, Luo Z, Mei L, Chien KR, Sussman DJ & Wynshaw-Boris A (2002) Dishevelled 2 is essential for cardiac outflow tract development, somite segmentation and neural tube closure. *Development* **129:** 5827–5838

Hamosh A, Scott AF, Amberger JS, Bocchini CA & McKusick VA (2005) Online Mendelian Inheritance in Man (OMIM), a knowledgebase of human genes and genetic disorders. *Nucleic Acids Res.* **33:** D514–D517

Han Y-G, Spassky N, Romaguera-Ros M, Garcia-Verdugo J-M, Aguilar A, Schneider-Maunoury S & Alvarez-Buylla A (2008) Hedgehog signaling and primary cilia are required for the formation of adult neural stem cells. *Nat. Neurosci.* **11:** 277–284

Handeli S & Simon JA (2008) A small-molecule inhibitor of Tcf/β-catenin signaling down-regulates PPARγ and PPARδ activities. *Mol. Cancer Ther.* **7:** 521–529

Hao L, Thein M, Brust-Mascher I, Civelekoglu-Scholey G, Lu Y, Acar S, Prevo B, Shaham S & Scholey JM (2011) Intraflagellar transport delivers tubulin isotypes to sensory cilium middle and distal segments. *Nat. Cell Biol.* **13:** 790–798

Harris JA, Liu Y, Yang P, Kner P & Lechtreck KF (2016) Single-particle imaging reveals intraflagellar transport–independent transport and accumulation of EB1 in Chlamydomonas flagella. *Mol. Biol. Cell* **27:** 295–307

Harunaga JS & Yamada KM (2011) Cell-matrix adhesions in 3D. *Matrix Biol.* **30:** 363–368

Hauck SM, Dietter J, Kramer RL, Hofmaier F, Zipplies JK, Amann B, Feuchtinger A, Deeg CA & Ueffing M (2010) Deciphering membrane-associated molecular processes in target tissue of autoimmune uveitis by label-free quantitative mass spectrometry. *Mol. Cell. Proteomics* **9:** 2292–2305

Hernandez V & Beales PL (2010) Ciliopathy-related BBS proteins regulate the actin cytoskeleton independent of ciliary function. In *(Proceedings) British Human Genetics Conference* p S71.

Hernandez-Hernandez V, Pravincumar P, Diaz-Font A, May-Simera H, Jenkins D, Knight M & Beales PL (2013) Bardet–Biedl syndrome proteins control the cilia length through regulation of actin polymerization. *Hum. Mol. Genet.* **22:** 3858–3868

Hierck BP, Van der Heiden K, Alkemade FE, Van de Pas S, Van Thienen J V, Groenendijk BCW, Bax WH, Van der Laarse A, DeRuiter MC & Horrevoets AJG (2008) Primary cilia sensitize endothelial cells for fluid shear stress. *Dev. Dyn.* **237:** 725–735

Hildebrandt F, Attanasio M & Otto E (2009) Nephronophthisis: disease mechanisms of a ciliopathy. *J. Am. Soc. Nephrol.* **20:** 23–35

Hodges ME, Wickstead B, Gull K & Langdale JA (2011) Conservation of ciliary proteins in plants with no cilia. *BMC Plant Biol.* **11:** 1

Hoff S, Halbritter J, Epting D, Frank V, Nguyen T-MT, Van Reeuwijk J, Boehlke C, Schell C, Yasunaga T & Helmstädter M (2013) ANKS6 is a central component of a nephronophthisis module linking NEK8 to INVS and NPHP3. *Nat. Genet.* **45:** 951–956

Hopp K, Heyer CM, Hommerding CJ, Henke SA, Sundsbak JL, Patel S, Patel P, Consugar MB, Czarnecki PG & Gliem TJ (2011) B9D1 is revealed as a novel Meckel syndrome (MKS) gene by targeted exon-enriched next-generation sequencing and deletion analysis. *Hum. Mol. Genet.* **20:** 2524–2534

Horton ER, Byron A, Askari JA, Ng DHJ, Millon-Frémillon A, Robertson J, Koper EJ, Paul NR, Warwood S & Knight D (2015) Definition of a consensus integrin adhesome and its dynamics during adhesion complex assembly and disassembly. *Nat. Cell Biol.* **17:** 1577–1587

Hotchin NA & Hall A (1995) The assembly of integrin adhesion complexes requires both extracellular matrix and intracellular rho/rac GTPases. *J. Cell Biol.* **131:** 1857–1865

Hu J, Van den Steen PE, Sang Q-XA & Opdenakker G (2007) Matrix metalloproteinase inhibitors as therapy for inflammatory and vascular diseases. *Nat. Rev. Drug Discov.* **6:** 480–498

Hu Q, Milenkovic L, Jin H, Scott MP, Nachury M V, Spiliotis ET & Nelson WJ (2010) A septin diffusion barrier at the base of the primary cilium maintains ciliary membrane protein distribution. *Science* **329:** 436–439

Huan Y & van Adelsberg J (1999) Polycystin-1, the PKD1 gene product, is in a complex containing E-cadherin and the catenins. *J. Clin. Invest.* **104:** 1459–1468

Huang P & Schier AF (2009) Dampened Hedgehog signaling but normal Wnt signaling in zebrafish without cilia. *Development* **136:** 3089–3098

Huangfu D & Anderson K V (2005) Cilia and Hedgehog responsiveness in the mouse. *Proc. Natl. Acad. Sci. U. S. A.* **102:** 11325–11330

Huangfu D, Liu A, Rakeman AS, Murcia NS, Niswander L & Anderson K V (2003) Hedgehog signalling in the mouse requires intraflagellar transport proteins. *Nature* **426:** 83–87

Hughes JR, Meireles AM, Fisher KH, Garcia A, Antrobus PR, Wainman A, Zitzmann N, Deane C, Ohkura H & Wakefield JG (2008) A microtubule interactome: complexes with roles in cell cycle and mitosis. *PLoS Biol* **6:** e98

Humphrey JD, Dufresne ER & Schwartz MA (2014) Mechanotransduction and extracellular matrix homeostasis. *Nat. Rev. Mol. Cell Biol.* **15:** 802–812

Humphries JD, Byron A & Humphries MJ (2006) Integrin ligands at a glance. *J. Cell Sci.* **119:** 3901–3903

Hurd TW, Fan S & Margolis BL (2011) Localization of retinitis pigmentosa 2 to cilia is regulated by Importin β2. *J Cell Sci* **124:** 718–726

Hynes RO (1987) Integrins: A family of cell surface receptors. *Cell* **48:** 549–554 Available at: http://www.sciencedirect.com/science/article/pii/0092867487902339

Hynes RO (1992) Integrins: versatility, modulation, and signaling in cell adhesion. *Cell* **69:** 11–25

Hynes RO (2002) Integrins: Bidirectional, Allosteric Signaling Machines. *Cell* **110:** 673–687 Available at: http://www.sciencedirect.com/science/article/pii/S0092867402009716

Hynes RO (2009) The extracellular matrix: not just pretty fibrils. *Science* **326:** 1216–1219

Iannicelli M, Brancati F, Mougou-Zerelli S, Mazzotta A, Thomas S, Elkhartoufi N, Travaglini L, Gomes C, Luigi Ardissino G & Bertini E (2010) Novel TMEM67 mutations and genotype-phenotype correlates in meckelin-related ciliopathies. *Hum. Mutat.* **31:** E1319–E1331

Ibraghimov-Beskrovnaya O, Bukanov NO, Donohue LC, Dackowski WR, Klinger KW & Landes GM (2000) Strong homophilic interactions of the Ig-like domains of polycystin-1, the protein product of an autosomal dominant polycystic kidney disease gene, PKD1. *Hum. Mol. Genet.* **9:** 1641–1649

Ickowicz V, Eurin D, Maugey-Laulom B, Didier F, Garel C, Gubler MC, Laquerriere A & Avni EF (2006) Meckel–Grüber syndrome: sonography and pathology. *Ultrasound Obstet. Gynecol.* **27:** 296–300

Ingber D (1991) Extracellular matrix and cell shape: potential control points for inhibition of angiogenesis. *J. Cell. Biochem.* **47:** 236–241

Ingham PW & McMahon AP (2001) Hedgehog signaling in animal development: paradigms and principles. *Genes Dev.* **15:** 3059–3087

Ishikawa H & Marshall WF (2011) Ciliogenesis: building the cell's antenna. *Nat. Rev. Mol. cell Biol.* **12:** 222–234

Ishikawa H, Thompson J, Yates III JR & Marshall WF (2012) Proteomic analysis of mammalian primary cilia. *Curr. Biol.* **22:** 414–419

Israeli S, Amsler K, Zheleznova N & Wilson PD (2010) Abnormalities in focal adhesion complex formation, regulation, and function in human autosomal recessive polycystic kidney disease epithelial cells. *Am. J. Physiol. Physiol.* **298:** C831

Ivanova OY, Margolis LB, Vasiliev JM & Gelfand IM (1976) Effect of colcemid on the spreading of fibroblasts in culture. *Exp. Cell Res.* **101:** 207–219

Jahed Z, Shams H, Mehrbod M & Mofrad MR (2014) Mechanotransduction pathways linking the extracellular matrix to the nucleus. *Int Rev Cell Mol Biol* **310:** e220

Jenei V, Sherwood V, Howlin J, Linnskog R, Säfholm A, Axelsson L & Andersson T (2009) A t-butyloxycarbonyl-modified Wnt5a-derived hexapeptide functions as a potent antagonist of Wnt5a-dependent melanoma cell invasion. *Proc. Natl. Acad. Sci.* **106:** 19473–19478

Jessen JR, Topczewski J, Bingham S, Sepich DS, Marlow F, Chandrasekhar A & Solnica-Krezel L (2002) Zebrafish trilobite identifies new roles for Strabismus in gastrulation and neuronal movements. *Nat. Cell Biol.* **4:** 610–615

Jinnin M, Ihn H & Tamaki K (2006) Characterization of SIS3, a novel specific inhibitor of Smad3, and its effect on transforming growth factor-β1-induced extracellular matrix expression. *Mol. Pharmacol.* **69:** 597–607

Johnson KA & Rosenbaum JL (1992) Polarity of flagellar assembly in Chlamydomonas. *J. Cell Biol.* **119:** 1605–1611

Johnson MS, Lu N, Denessiouk K, Heino J & Gullberg D (2009) Integrins during evolution: evolutionary trees and model organisms. *Biochim. Biophys. Acta (BBA)-Biomembranes* **1788:** 779–789

Joly D, Berissi S, Bertrand A, Strehl L, Patey N & Knebelmann B (2006) Laminin 5 regulates polycystic kidney cell proliferation and cyst formation. *J. Biol. Chem.* **281:** 29181–29189

Jones WR, Ting-Beall HP, Lee GM, Kelley SS, Hochmuth RM & Guilak F (1999) Alterations in the Young's modulus and volumetric properties of chondrocytes isolated from normal and osteoarthritic human cartilage. *J. Biomech.* **32:** 119–127

Joo K, Kim CG, Lee M-S, Moon H-Y, Lee S-H, Kim MJ, Kweon H-S, Park W-Y, Kim C-H & Gleeson JG (2013) CCDC41 is required for ciliary vesicle docking to the mother centriole.

Proc. Natl. Acad. Sci. **110:** 5987–5992

Juriloff DM & Harris MJ (2000) Mouse models for neural tube closure defects. *Hum. Mol. Genet.* **9:** 993–1000

Juriloff DM & Harris MJ (2012) A consideration of the evidence that genetic defects in planar cell polarity contribute to the etiology of human neural tube defects. *Birth Defects Res. Part A Clin. Mol. Teratol.* **94:** 824–840

Kaplan JM, Kim SH, North KN, Rennke H, Lori A, Tong H-Q, Mathis BJ, Rodríguez-Pérez J-C, Allen PG & Beggs AH (2000) Mutations in ACTN4, encoding α-actinin-4, cause familial focal segmental glomerulosclerosis. *Nat. Genet.* **24:** 251–256

Karska-Basta I, Kubicka-Trzaska A, Filemonowicz-Skoczek A, Romanowska-Dixon B & Kobylarz J (2007) Alstrom syndrome--a case report and literature review. *Klin. Oczna* **110:** 188–192

Kaverina I, Krylyshkina O & Small JV (1999) Microtubule targeting of substrate contacts promotes their relaxation and dissociation. *J. Cell Biol.* **146:** 1033–1044

Kaverina I, Rottner K & Small JV (1998) Targeting, capture, and stabilization of microtubules at early focal adhesions. *J. Cell Biol.* **142:** 181–190

Kee HL, Dishinger JF, Blasius TL, Liu C-J, Margolis B & Verhey KJ (2012) A size-exclusion permeability barrier and nucleoporins characterize a ciliary pore complex that regulates transport into cilia. *Nat. Cell Biol.* **14:** 431–437

Kee HL & Verhey KJ (2013) Molecular connections between nuclear and ciliary import processes. *Cilia* **2:** 1

Kenny TD & Beales PL (2013) Ciliopathies: A reference for clinicians OUP Oxford

Kestler HA & Kühl M (2008) From individual Wnt pathways towards a Wnt signalling network. *Philos. Trans. R. Soc. B Biol. Sci.* **363:** 1333–1347

Khanna H, Davis EE, Murga-Zamalloa CA, Estrada-Cuzcano A, Lopez I, den Hollander AI, Zonneveld MN, Othman MI, Waseem N & Chakarova CF (2009) A common allele in RPGRIP1L is a modifier of retinal degeneration in ciliopathies. *Nat. Genet.* **41:** 739–745

Kilshaw PJ (1999) Alpha E beta 7. *Mol. Pathol.* **52:** 203

Kim J, Jo H, Hong H, Kim MH, Kim JM, Lee J-K, Do Heo W & Kim J (2015) Actin remodelling factors control ciliogenesis by regulating YAP/TAZ activity and vesicle trafficking. *Nat. Commun.* **6:**

Kim J, Lee JE, Heynen-Genel S, Suyama E, Ono K, Lee K, Ideker T, Aza-Blanc P & Gleeson JG (2010) Functional genomic screen for modulators of ciliogenesis and cilium length. *Nature* **464:** 1048–1051

Kishimoto N & Sawamoto K (2012) Planar polarity of ependymal cilia. *Differentiation* **83:** S86–S90

Kleene SJ (2008) The electrochemical basis of odor transduction in vertebrate olfactory cilia. *Chem. Senses* **33:** 839–859

Kleymenova E, Ibraghimov-Beskrovnaya O, Kugoh H, Everitt J, Xu H, Kiguchi K, Landes G, Harris P & Walker C (2001) Tuberin-dependent membrane localization of polycystin-1: a functional link between polycystic kidney disease and the TSC2 tumor suppressor gene. *Mol. Cell* **7:** 823–832

Klinger M, Wang W, Kuhns S, Bärenz F, Dräger-Meurer S, Pereira G & Gruss OJ (2013) The novel centriolar satellite protein SSX2IP targets Cep290 to the ciliary transition zone. *Mol. Biol. Cell***:** mbc–E13

Klotz C, Bordes N, Laine M-C, Sandoz D & Bornens M (1986) Myosin at the apical pole of

ciliated epithelial cells as revealed by a monoclonal antibody. *J. Cell Biol.* **103:** 613–619

Knight CG, Morton LF, Onley DJ, Peachey AR, Messent AJ, Smethurst PA, Tuckwell DS, Farndale RW & Barnes MJ (1998) Identification in collagen type I of an integrin α2β1-binding site containing an essential GER sequence. *J. Biol. Chem.* **273:** 33287–33294

Knight CG, Morton LF, Peachey AR, Tuckwell DS, Farndale RW & Barnes MJ (2000) The Collagen-binding A-domains of Integrins α1β1 and α2β1recognize the same specific amino acid sequence, GFOGER, in native (Triple-helical) collagens. *J. Biol. Chem.* **275:** 35–40

Kozminski KG, Johnson KA, Forscher P & Rosenbaum JL (1993) A motility in the eukaryotic flagellum unrelated to flagellar beating. *Proc. Natl. Acad. Sci.* **90:** 5519–5523

Krock BL & Perkins BD (2008) The intraflagellar transport protein IFT57 is required for cilia maintenance and regulates IFT-particle–kinesin-II dissociation in vertebrate photoreceptors. *J. Cell Sci.* **121:** 1907–1915

Kubow KE & Horwitz AR (2011) Reducing background fluorescence reveals adhesions in 3D matrices. *Nat. Cell Biol.* **13:** 3–5

Kühl M, Sheldahl LC, Malbon CC & Moon RT (2000) Ca2+/calmodulin-dependent protein kinase II is stimulated by Wnt and Frizzled homologs and promotes ventral cell fates in Xenopus. *J. Biol. Chem.* **275:** 12701–12711

Kumawat K, Menzen MH, Bos IST, Baarsma HA, Borger P, Roth M, Tamm M, Halayko AJ, Simoons M & Prins A (2013) Noncanonical WNT-5A signaling regulates TGF-β-induced extracellular matrix production by airway smooth muscle cells. *FASEB J.* **27:** 1631–1643

Kuo J-C, Han X, Hsiao C-T, Yates III JR & Waterman CM (2011) Analysis of the myosin-II-responsive focal adhesion proteome reveals a role for [beta]-Pix in negative regulation of focal adhesion maturation. *Nat. Cell Biol.* **13:** 383–393

Kuo J-C, Han X, Yates JR & Waterman CM (2012) Isolation of focal adhesion proteins for biochemical and proteomic analysis. *Methods Mol. Biol.* **757:** 297–323

Kwon RY, Temiyasathit S, Tummala P, Quah CC & Jacobs CR (2010) Primary cilium-dependent mechanosensing is mediated by adenylyl cyclase 6 and cyclic AMP in bone cells. *FASEB J.* **24:** 2859–2868

Kyttälä M, Tallila J, Salonen R, Kopra O, Kohlschmidt N, Paavola-Sakki P, Peltonen L & Kestilä M (2006) MKS1, encoding a component of the flagellar apparatus basal body proteome, is mutated in Meckel syndrome. *Nat. Genet.* **38:** 155–157

Laclef C, Anselme I, Besse L, Catala M, Palmyre A, Baas D, Paschaki M, Pedraza M, Métin C & Durand B (2015) The role of primary cilia in corpus callosum formation is mediated by production of the Gli3 repressor. *Hum. Mol. Genet.* **24:** 4997–5014

Lamb TD, Collin SP & Pugh EN (2007) Evolution of the vertebrate eye: opsins, photoreceptors, retina and eye cup. *Nat. Rev. Neurosci.* **8:** 960–976

Lancaster MA & Gleeson JG (2010) Cystic kidney disease: the role of Wnt signaling. *Trends Mol. Med.* **16:** 349–360

Lancaster MA, Gopal DJ, Kim J, Saleem SN, Silhavy JL, Louie CM, Thacker BE, Williams Y, Zaki MS & Gleeson JG (2011) Defective Wnt-dependent cerebellar midline fusion in a mouse model of Joubert syndrome. *Nat. Med.* **17:** 726–731

Lancaster MA, Louie CM, Silhavy JL, Sintasath L, DeCambre M, Nigam SK, Willert K & Gleeson JG (2009) Impaired Wnt–β-catenin signaling disrupts adult renal homeostasis and leads to cystic kidney ciliopathy. *Nat. Med.* **15:** 1046–1054

Laufer E, Nelson CE, Johnson RL, Morgan BA & Tabin C (1994) < i> Sonic hedgehog</i> and< i> Fgf-4</i> act through a signaling cascade and feedback loop to integrate growth and patterning of the developing limb bud. *Cell* **79:** 993–1003

Leask A & Abraham DJ (2004) TGF-β signaling and the fibrotic response. *FASEB J.* **18:** 816–827

LeBleu VS, MacDonald B & Kalluri R (2007) Structure and function of basement membranes. *Exp. Biol. Med.* **232:** 1121–1129

Lee JH, Silhavy JL, Lee JE, Al-Gazali L, Thomas S, Davis EE, Bielas SL, Hill KJ, Iannicelli M & Brancati F (2012) Evolutionarily assembled cis-regulatory module at a human ciliopathy locus. *Science* **335:** 966–969

Lee KL, Guevarra MD, Nguyen AM, Chua MC, Wang Y & Jacobs CR (2015) The primary cilium functions as a mechanical and calcium signaling nexus. *Cilia* **4:** 1

Leitch CC, Zaghloul NA, Davis EE, Stoetzel C, Diaz-Font A, Rix S, Alfadhel M, Lewis RA, Eyaid W & Banin E (2008) Hypomorphic mutations in syndromic encephalocele genes are associated with Bardet-Biedl syndrome. *Nat. Genet.* **40:** 443–448

Lemullois M, Boisvieux-Ulrich E, Laine M-C, Chailley B & Sandoz D (1988) Development and functions of the cytoskeleton during ciliogenesis in metazoa. *Biol. Cell* **63:** 195–208

Lemullois M, Klotz C & Sandoz D (1987) Immunocytochemical localization of myosin during ciliogenesis of quail oviduct. *Eur. J. Cell Biol.* **43:** 429–437

Lessey EC, Guilluy C & Burridge K (2012) From mechanical force to RhoA activation. *Biochemistry* **51:** 7420–7432

Leung T, Manser E, Tan L & Lim L (1995) A novel serine/threonine kinase binding the Ras-related RhoA GTPase which translocates the kinase to peripheral membranes. *J. Biol. Chem.* **270:** 29051–29054

Li C, Jensen VL, Park K, Kennedy J, Garcia-Gonzalo FR, Romani M, De Mori R, Bruel A-L, Gaillard D & Doray B (2016) MKS5 and CEP290 Dependent Assembly Pathway of the Ciliary Transition Zone. *PLoS Biol* **14:** e1002416

Li Q, Montalbetti N, Shen PY, Dai X-Q, Cheeseman CI, Karpinski E, Wu G, Cantiello HF & Chen X-Z (2005) Alpha-actinin associates with polycystin-2 and regulates its channel activity. *Hum. Mol. Genet.* **14:** 1587–1603

Lin Y-C, Niewiadomski P, Lin B, Nakamura H, Phua SC, Jiao J, Levchenko A, Inoue T, Rohatgi R & Inoue T (2013) Chemically inducible diffusion trap at cilia reveals molecular sieve–like barrier. *Nat. Chem. Biol.* **9:** 437–443

Lindberg U, Höglund AS & Karlsson R (1981) On the ultrastructural organization of the microfilament system and the possible role of profilactin. *Biochimie* **63:** 307–323

Liu A, Wang B & Niswander LA (2005) Mouse intraflagellar transport proteins regulate both the activator and repressor functions of Gli transcription factors. *Development* **132:** 3103–3111

Loewenstein WR & Kanno Y (1964) Studies on an epithelial (gland) cell junction I. Modifications of surface membrane permeability. *J. Cell Biol.* **22:** 565–586

Logan C V, Abdel-Hamed Z & Johnson CA (2011) Molecular genetics and pathogenic mechanisms for the severe ciliopathies: insights into neurodevelopment and pathogenesis of neural tube defects. *Mol. Neurobiol.* **43:** 12–26

Loosli Y, Luginbuehl R & Snedeker JG (2010) Cytoskeleton reorganization of spreading cells on micro-patterned islands: a functional model. *Philos. Trans. R. Soc. London A Math. Phys. Eng. Sci.* **368:** 2629–2652

Lopes SS, Lourenço R, Pacheco L, Moreno N & Kreiling J (2010) Notch signalling regulates left-right asymmetry through ciliary length control. *Development* **137:** 3625–3632

Lord A, Shapiro AJ, Saint-Martin C, Claveau M, Melançon S & Wintermark P (2014) Filamin A mutation may be associated with diffuse lung disease mimicking bronchopulmonary

dysplasia in premature newborns. *Respir. Care* **59:** 1

Louvi A & Artavanis-Tsakonas S (2006) Notch signalling in vertebrate neural development. *Nat. Rev. Neurosci.* **7:** 93–102

Louvi A & Grove EA (2011) Cilia in the CNS: the quiet organelle claims center stage. *Neuron* **69:** 1046–1060

Lowell S, Benchoua A, Heavey B & Smith AG (2006) Notch promotes neural lineage entry by pluripotent embryonic stem cells. *PLoS Biol.* **4:** e121

Lu P, Weaver VM & Werb Z (2012) The extracellular matrix: a dynamic niche in cancer progression. *J. Cell Biol.* **196:** 395–406

Lüders J & Stearns T (2007) Microtubule-organizing centres: a re-evaluation. *Nat. Rev. Mol. Cell Biol.* **8:** 161–167

Lukashev ME & Werb Z (1998) ECM signalling: orchestrating cell behaviour and misbehaviour. *Trends Cell Biol.* **8:** 437–441

Macca M & Franco B (2009) The molecular basis of oral-facial-digital syndrome, type 1. In *American Journal of Medical Genetics Part C: Seminars in Medical Genetics* pp 318–325. Wiley Online Library

Madara JL & Dharmsathaphorn K (1985) Occluding junction structure-function relationships in a cultured epithelial monolayer. *J. Cell Biol.* **101:** 2124–2133

Maheshwari G, Brown G, Lauffenburger DA, Wells A & Griffith LG (2000) Cell adhesion and motility depend on nanoscale RGD clustering. *J. Cell Sci.* **113:** 1677–1686

Malicdan MC V, Vilboux T, Stephen J, Maglic D, Mian L, Konzman D, Guo J, Yildirimli D, Bryant J & Fischer R (2015) Mutations in human homologue of chicken talpid3 gene (KIAA0586) cause a hybrid ciliopathy with overlapping features of Jeune and Joubert syndromes. *J. Med. Genet.* **52:** 830–839

Malone AMD, Anderson CT, Tummala P, Kwon RY, Johnston TR, Stearns T & Jacobs CR (2007) Primary cilia mediate mechanosensing in bone cells by a calcium-independent mechanism. *Proc. Natl. Acad. Sci.* **104:** 13325–13330

Manasek FJ, Burnside MB & Waterman RE (1972) Myocardial cell shape change as a mechanism of embryonic heart looping. *Dev. Biol.* **29:** 349–371

Mangos S, Lam P, Zhao A, Liu Y, Mudumana S, Vasilyev A, Liu A & Drummond IA (2010) The ADPKD genes pkd1a/b and pkd2 regulate extracellular matrix formation. *Dis. Model. Mech.* **3:** 354–365

Markoff A, Bogdanova N, Knop M, Rüffer C, Kenis H, Lux P, Reutelingsperger C, Todorov V, Dworniczak B & Horst J (2007) Annexin A5 interacts with polycystin-1 and interferes with the polycystin-1 stimulated recruitment of E-cadherin into adherens junctions. *J. Mol. Biol.* **369:** 954–966

Martin-Belmonte F & Perez-Moreno M (2012) Epithelial cell polarity, stem cells and cancer. *Nat. Rev. Cancer* **12:** 23–38

Martins-Green MM & Tokuyasu KT (1988) A pre-embedding immunolabeling technique for basal lamina and extracellular matrix molecules. *J. Histochem. Cytochem.* **36:** 453–458

Masyuk AI, Masyuk T V & LaRusso NF (2008) Cholangiocyte primary cilia in liver health and disease. *Dev. Dyn.* **237:** 2007–2012

Matt P, Habashi J, Carrel T, Cameron DE, Van Eyk JE & Dietz HC (2008) Recent advances in understanding Marfan syndrome: should we now treat surgical patients with losartan? *J. Thorac. Cardiovasc. Surg.* **135:** 389–394

May SR, Ashique AM, Karlen M, Wang B, Shen Y, Zarbalis K, Reiter J, Ericson J & Peterson

AS (2005) Loss of the retrograde motor for IFT disrupts localization of Smo to cilia and prevents the expression of both activator and repressor functions of Gli. *Dev. Biol.* **287:** 378–389

May-Simera HL, Petralia RS, Montcouquiol M, Wang Y-X, Szarama KB, Liu Y, Lin W, Deans MR, Pazour GJ & Kelley MW (2015) Ciliary proteins Bbs8 and Ift20 promote planar cell polarity in the cochlea. *Development* **142:** 555–566

McDermott KM, Liu BY, Tlsty TD & Pazour GJ (2010) Primary cilia regulate branching morphogenesis during mammary gland development. *Curr. Biol.* **20:** 731–737

McDonald JA (1988) Extracellular matrix assembly. *Annu. Rev. Cell Biol.* **4:** 183–207

McDowell GS, Rajadurai S & Levin M (2016) From cytoskeletal dynamics to organ asymmetry: a non-linear, regulative pathway underlies left-right patterning. *bioRxiv***:** 52191

McEwen DP, Koenekoop RK, Khanna H, Jenkins PM, Lopez I, Swaroop A & Martens JR (2007) Hypomorphic CEP290/NPHP6 mutations result in anosmia caused by the selective loss of G proteins in cilia of olfactory sensory neurons. *Proc. Natl. Acad. Sci.* **104:** 15917–15922

McGlashan SR, Jensen CG & Poole CA (2006) Localization of extracellular matrix receptors on the chondrocyte primary cilium. *J. Histochem. Cytochem.* **54:** 1005–1014

McIntosh K V (2016) The extra-ciliary roles of Meckel-Gruber syndrome proteins (Doctoral thesis, University of Exeter, Exeter, United Kingdom).

Menotti-Raymond M, David VA, Schäffer AA, Stephens R, Wells D, Kumar-Singh R, O'Brien SJ & Narfström K (2007) Mutation in CEP290 discovered for cat model of human retinal degeneration. *J. Hered.* **98:** 211–220

Mikels AJ & Nusse R (2006) Purified Wnt5a protein activates or inhibits β-catenin–TCF signaling depending on receptor context. *PLoS Biol* **4:** e115

Mitchell DR (2004) Speculations on the evolution of 9+ 2 organelles and the role of central pair microtubules. *Biol. Cell* **96:** 691–696

Modell B & Darr A (2002) Genetic counselling and customary consanguineous marriage. *Nat. Rev. Genet.* **3:** 225–229

Morimoto RI (1998) Regulation of the heat shock transcriptional response: cross talk between a family of heat shock factors, molecular chaperones, and negative regulators. *Genes Dev.* **12:** 3788–3796

Murdoch JN, Damrau C, Paudyal A, Bogani D, Wells S, Greene NDE, Stanier P & Copp AJ (2014) Genetic interactions between planar cell polarity genes cause diverse neural tube defects in mice. *Dis. Model. Mech.* **7:** 1153–1163

Murdoch JN, Doudney K, Paternotte C, Copp AJ & Stanier P (2001) Severe neural tube defects in the loop-tail mouse result from mutation of Lpp1, a novel gene involved in floor plate specification. *Hum. Mol. Genet.* **10:** 2593–2601

Murdoch JN, Henderson DJ, Doudney K, Gaston-Massuet C, Phillips HM, Paternotte C, Arkell R, Stanier P & Copp AJ (2003) Disruption of scribble (Scrb1) causes severe neural tube defects in the circletail mouse. *Hum. Mol. Genet.* **12:** 87–98

Myageri A, Grampurohit V & Rao R (2013) Meckel gruber syndrome: Report of two cases with review of literature. *J. Fam. Med. Prim. care* **2:** 106

Naba A, Clauser KR, Hoersch S, Liu H, Carr SA & Hynes RO (2011) The matrisome: in silico definition and in vivo characterization by proteomics of normal and tumor extracellular matrices. *Mol. Cell. Proteomics***:** mcp–M111

Nagano M, Hoshino D, Sakamoto T, Kawasaki N, Koshikawa N & Seiki M (2010) ZF21 protein regulates cell adhesion and motility. *J. Biol. Chem.* **285:** 21013–21022

Nauli SM, Jin X, AbouAlaiwi WA, El-Jouni W, Su X & Zhou J (2013) Non-motile primary cilia as fluid shear stress mechanosensors. *Methods Enzym.* **525:** 1–20

Nelson CM & Bissell MJ (2006) Of extracellular matrix, scaffolds, and signaling: tissue architecture regulates development, homeostasis, and cancer. *Annu. Rev. Cell Dev. Biol.* **22:** 287

Nguyen AM & Jacobs CR (2013) Emerging role of primary cilia as mechanosensors in osteocytes. *Bone* **54:** 196–204

Nomachi A, Nishita M, Inaba D, Enomoto M, Hamasaki M & Minami Y (2008) Receptor tyrosine kinase Ror2 mediates Wnt5a-induced polarized cell migration by activating c-Jun N-terminal kinase via actin-binding protein filamin A. *J. Biol. Chem.* **283:** 27973–27981

Noor A, Windpassinger C, Patel M, Stachowiak B, Mikhailov A, Azam M, Irfan M, Siddiqui ZK, Naeem F & Paterson AD (2008) CC2D2A, encoding a coiled-coil and C2 domain protein, causes autosomal-recessive mental retardation with retinitis pigmentosa. *Am. J. Hum. Genet.* **82:** 1011–1018

Norris DP & Grimes DT (2012) Mouse models of ciliopathies: the state of the art. *Dis. Model. Mech.* **5:** 299–312

Ocbina PJR, Tuson M & Anderson K V (2009) Primary cilia are not required for normal canonical Wnt signaling in the mouse embryo. *PLoS One* **4:** e6839

Olbrich H, Fliegauf M, Hoefele J, Kispert A, Otto E, Volz A, Wolf MT, Sasmaz G, Trauer U & Reinhardt R (2003) Mutations in a novel gene, NPHP3, cause adolescent nephronophthisis, tapeto-retinal degeneration and hepatic fibrosis. *Nat. Genet.* **34:** 455–459

Omran H, Häffner K, Burth S, Fernandez C, Fargier B, Villaquiran A, Nothwang H-G, Schnittger S, Lehrach H & Woo D (2001) Human adolescent nephronophthisis: gene locus synteny with polycystic kidney disease in pcy mice. *J. Am. Soc. Nephrol.* **12:** 107–113

Otto EA, Tory K, Attanasio M, Zhou W, Chaki M, Paruchuri Y, Wise EL, Wolf MTF, Utsch B & Becker C (2009) Hypomorphic mutations in meckelin (MKS3/TMEM67) cause nephronophthisis with liver fibrosis (NPHP11). *J. Med. Genet.* **46:** 663–670

Page-McCaw A, Ewald AJ & Werb Z (2007) Matrix metalloproteinases and the regulation of tissue remodelling. *Nat. Rev. Mol. cell Biol.* **8:** 221–233

Palecek SP, Schmidt CE, Lauffenburger DA & Horwitz AF (1996) Integrin dynamics on the tail region of migrating fibroblasts. *J. Cell Sci.* **109:** 941–952

Palsson R, Sharma CP, Kim K, McLaughlin M, Brown D & Arnaout MA (1996) Characterization and cell distribution of polycystin, the product of autosomal dominant polycystic kidney disease gene 1. *Mol. Med.* **2:** 702

Pan D (2010) The hippo signaling pathway in development and cancer. *Dev. Cell* **19:** 491–505

Pan J & Snell WJ (2005) Chlamydomonas Shortens Its Flagella by Activating Axonemal Disassembly, Stimulating IFT Particle Trafficking, and Blocking Anterograde Cargo Loading. *Dev. Cell* **9:** 431–438

Pan J, You Y, Huang T & Brody SL (2007) RhoA-mediated apical actin enrichment is required for ciliogenesis and promoted by Foxj1. *J. Cell Sci.* **120:** 1868–1876

Parisi MA (2009) Clinical and molecular features of Joubert syndrome and related disorders. In *American Journal of Medical Genetics Part C: Seminars in Medical Genetics* pp 326–340. Wiley Online Library

Park TJ, Haigo SL & Wallingford JB (2006) Ciliogenesis defects in embryos lacking inturned or fuzzy function are associated with failure of planar cell polarity and Hedgehog signaling. *Nat. Genet.* **38:** 303–311

Park TJ, Mitchell BJ, Abitua PB, Kintner C & Wallingford JB (2008) Dishevelled controls apical docking and planar polarization of basal bodies in ciliated epithelial cells. *Nat. Genet.* **40:** 871–879

Pazour GJ, Baker SA, Deane JA, Cole DG, Dickert BL, Rosenbaum JL, Witman GB & Besharse JC (2002) The intraflagellar transport protein, IFT88, is essential for vertebrate photoreceptor assembly and maintenance. *J. Cell Biol.* **157:** 103–114

Peterkofsky B (1991) Ascorbate requirement for hydroxylation and secretion of procollagen: relationship to inhibition of collagen synthesis in scurvy. *Am. J. Clin. Nutr.* **54:** 1135S–1140S

Petit V & Thiery J (2000) Focal adhesions: structure and dynamics. *Biol. Cell* **92:** 477–494

Picariello T, Valentine MS, Yano J & Van Houten J (2014) Reduction of meckelin leads to general loss of cilia, ciliary microtubule misalignment and distorted cell surface organization. *Cilia* **3:** 2

Picariello TA (2015) Meckelin Functions in the Guided Movement and Orientation of Basal Bodies Prior to Duplication in Paramecium tetraurelia (Doctoral thesis, University of Vermont, Burlington, Vermont, USA).

Piccolo S, Dupont S & Cordenonsi M (2014) The biology of YAP/TAZ: hippo signaling and beyond. *Physiol. Rev.* **94:** 1287–1312

Pierschbacher MD & Ruoslahti E (1984) Cell attachment activity of fibronectin can be duplicated by small synthetic fragments of the molecule. *Nature* **309:** 30

Pinson KI, Brennan J, Monkley S, Avery BJ & Skarnes WC (2000) An LDL-receptor-related protein mediates Wnt signalling in mice. *Nature* **407:** 535–538

Pitaval A, Tseng Q, Bornens M & Théry M (2010) Cell shape and contractility regulate ciliogenesis in cell cycle–arrested cells. *J. Cell Biol.* **191:** 303–312

Plopper G & Ingber DE (1993) Rapid induction and isolation of focal adhesion complexes. *Biochem. Biophys. Res. Commun.* **193:** 571–578

Plotnikova O V, Golemis EA & Pugacheva EN (2008) Cell Cycle–Dependent Ciliogenesis and Cancer. *Cancer Res.* **68:** 2058–2061

Pollard TD & Cooper JA (2009) Actin, a central player in cell shape and movement. *Science* **326:** 1208–1212

Porter ME & Sale WS (2000) The 9+ 2 axoneme anchors multiple inner arm dyneins and a network of kinases and phosphatases that control motility. *J. Cell Biol.* **151:** F37–F42

Pratt MB, Titlow JS, Davis I, Barker AR, Dawe HR, Raff JW & Roque H (2016) Drosophila sensory cilia lacking MKS-proteins exhibit striking defects in development but only subtle defects in adults. *J Cell Sci* **129:** 3732–3743

Puche JE, Saiman Y & Friedman SL (2013) Hepatic stellate cells and liver fibrosis. *Compr. Physiol.* **3:** 1473–1492

Pugacheva EN, Jablonski SA, Hartman TR, Henske EP & Golemis EA (2007) HEF1-dependent Aurora A activation induces disassembly of the primary cilium. *Cell* **129:** 1351–1363

Pyrgaki C, Liu A & Niswander L (2011) Grainyhead-like 2 regulates neural tube closure and adhesion molecule expression during neural fold fusion. *Dev. Biol.* **353:** 38–49

Pytela R, Pierschbacher MD, Argraves S, Suzuki S & Ruoslahti E (1987) [27] Arginine-glycine-aspartic acid adhesion receptors. *Methods Enzymol.* **144:** 475–489

Qin H, Wang Z, Diener D & Rosenbaum J (2007) Intraflagellar transport protein 27 is a small G protein involved in cell-cycle control. *Curr. Biol.* **17:** 193–202

Ramachandran U, Malla T & Joshi KS (2006) Meckel-Gruber syndrome. *Kathmandu Univ. Med. J.* **4:** 334–336

Rashid ST, Humphries JD, Byron A, Dhar A, Askari JA, Selley JN, Knight D, Goldin RD, Thursz M & Humphries MJ (2012) Proteomic analysis of extracellular matrix from the hepatic stellate cell line LX-2 identifies CYR61 and Wnt-5a as novel constituents of fibrotic liver. *J. Proteome Res.* **11:** 4052–4064

Reese TS (1965) Olfactory cilia in the frog. *J. Cell Biol.* **25:** 209–230

Reiter JF, Blacque OE & Leroux MR (2012) The base of the cilium: roles for transition fibres and the transition zone in ciliary formation, maintenance and compartmentalization. *EMBO Rep.* **13:** 608–618

Renzaglia KS & Garbary DJ (2001) Motile gametes of land plants: diversity, development, and evolution. *CRC. Crit. Rev. Plant Sci.* **20:** 107–213

Reya T & Clevers H (2005) Wnt signalling in stem cells and cancer. *Nature* **434:** 843–850

Ridley AJ (2001) Rho GTPases and cell migration. *J. Cell Sci.* **114:** 2713–2722

Ridley AJ & Hall A (1992) The small GTP-binding protein rho regulates the assembly of focal adhesions and actin stress fibers in response to growth factors. *Cell* **70:** 389–399

Ringo DL (1967) Flagellar motion and fine structure of the flagellar apparatus in Chlamydomonas. *J. Cell Biol.* **33:** 543–571

Riveline D, Zamir E, Balaban NQ, Schwarz US, Ishizaki T, Narumiya S, Kam Z, Geiger B & Bershadsky AD (2001) Focal contacts as mechanosensors externally applied local mechanical force induces growth of focal contacts by an mdia1-dependent and rock-independent mechanism. *J. Cell Biol.* **153:** 1175–1186

Roberson EC, Dowdle WE, Ozanturk A, Garcia-Gonzalo FR, Li C, Halbritter J, Elkhartoufi N, Porath JD, Cope H & Ashley-Koch A (2015) TMEM231, mutated in orofaciodigital and Meckel syndromes, organizes the ciliary transition zone. *J. Cell Biol.* **209:** 129–142

Roberts AB, Sporn MB, Assoian RK, Smith JM, Roche NS, Wakefield LM, Heine UI, Liotta LA, Falanga V & Kehrl JH (1986) Transforming growth factor type beta: rapid induction of fibrosis and angiogenesis in vivo and stimulation of collagen formation in vitro. *Proc. Natl. Acad. Sci.* **83:** 4167–4171

Robertson SP, Twigg SRF, Sutherland-Smith AJ, Biancalana V, Gorlin RJ, Horn D, Kenwrick SJ, Kim CA, Morava E & Newbury-Ecob R (2003) Localized mutations in the gene encoding the cytoskeletal protein filamin A cause diverse malformations in humans. *Nat. Genet.* **33:** 487–491

Robinson A, Escuin S, Doudney K, Vekemans M, Stevenson RE, Greene NDE, Copp AJ & Stanier P (2012) Mutations in the planar cell polarity genes CELSR1 and SCRIB are associated with the severe neural tube defect craniorachischisis. *Hum. Mutat.* **33:** 440–447

Roca C & Adams RH (2007) Regulation of vascular morphogenesis by Notch signaling. *Genes Dev.* **21:** 2511–2524

Rohatgi R, Milenkovic L & Scott MP (2007) Patched1 regulates hedgehog signaling at the primary cilium. *Science* **317:** 372–376

Rohatgi R & Snell WJ (2010) The ciliary membrane. *Curr. Opin. Cell Biol.* **22:** 541–546

Rosenbaum JL & Witman GB (2002) Intraflagellar transport. *Nat. Rev. Mol. Cell Biol.* **3:** 813–825

Roskelley CD, Srebrow A & Bissell MJ (1995) A hierarchy of ECM-mediated signalling regulates tissue-specific gene expression. *Curr. Opin. Cell Biol.* **7:** 736–747

Ross AJ, May-Simera H, Eichers ER, Kai M, Hill J, Jagger DJ, Leitch CC, Chapple JP, Munro PM & Fisher S (2005) Disruption of Bardet-Biedl syndrome ciliary proteins perturbs planar cell polarity in vertebrates. *Nat. Genet.* **37:** 1135–1140

Roume J, Ma HW, Le Merrer M, Cormier-Daire V, Girlich D, Genin E & Munnich A (1997) Genetic heterogeneity of Meckel syndrome. *J. Med. Genet.* **34:** 1003–1006

Rozario T & DeSimone DW (2010) The extracellular matrix in development and morphogenesis: a dynamic view. *Dev. Biol.* **341:** 126–140

Ruiz i Altaba A (1999) Gli proteins and Hedgehog signaling: development and cancer. *Trends Genet.* **15:** 418–425

Ruoslahti E & Pierschbacher MD (1986) Arg-Gly-Asp: a versatile cell recognition signal. *Cell* **44:** 517–518

Salonen R, Norio R, Opitz JM & Reynolds JF (1984a) The Meckel syndrome in Finland: epidemiologic and genetic aspects. *Am. J. Med. Genet.* **18:** 691–698

Salonen R, Opitz JM & Reynolds JF (1984b) The Meckel syndrome: clinicopathological findings in 67 patients. *Am. J. Med. Genet.* **18:** 671–689

Salonen R & Paavola P (1998) Meckel syndrome. *J. Med. Genet.* **35:** 497–501

Sang L, Miller JJ, Corbit KC, Giles RH, Brauer MJ, Otto EA, Baye LM, Wen X, Scales SJ & Kwong M (2011) Mapping the NPHP-JBTS-MKS protein network reveals ciliopathy disease genes and pathways. *Cell* **145:** 513–528

Santos N & Reiter JF (2008) Building it up and taking it down: the regulation of vertebrate ciliogenesis. *Dev. Dyn.* **237:** 1972–1981

Satir P & Christensen ST (2007) Overview of structure and function of mammalian cilia. *Annu. Rev. Physiol.* **69:** 377–400

Satir P & Christensen ST (2008) Structure and function of mammalian cilia. *Histochem. Cell Biol.* **129:** 687–693

Satir P, Mitchell DR & Jékely G (2008) How did the cilium evolve? *Curr. Top. Dev. Biol.* **85:** 63–82

Sato M, Theret D, Wheeler L, Ohshima N & Nerem RM (1990) Application of the micropipette technique to the measurement of cultured porcine aortic endothelial cell viscoelastic properties. *J. Biomech. Eng.* **112:** 263

Schaefer L & Schaefer RM (2010) Proteoglycans: from structural compounds to signaling molecules. *Cell Tissue Res.* **339:** 237–246

Schäfer K, Bader M, Gretz N, Oberbäumer I & Bachmann S (1993) Focal overexpression of collagen IV characterizes the initiation of epithelial changes in polycystic kidney disease. *Exp. Nephrol.* **2:** 190–195

Schlessinger K, Hall A & Tolwinski N (2009) Wnt signaling pathways meet Rho GTPases. *Genes Dev.* **23:** 265–277

Schmidt KN, Kuhns S, Neuner A, Hub B, Zentgraf H & Pereira G (2012) Cep164 mediates vesicular docking to the mother centriole during early steps of ciliogenesis. *J. Cell Biol.* **199:** 1083–1101

Schmitz AAP, Govek E-E, Böttner B & Van Aelst L (2000) Rho GTPases: signaling, migration, and invasion. *Exp. Cell Res.* **261:** 1–12

Schneider L, Clement CA, Teilmann SC, Pazour GJ, Hoffmann EK, Satir P & Christensen ST (2005) PDGFRαα signaling is regulated through the primary cilium in fibroblasts. *Curr. Biol.* **15:** 1861–1866

Schouteden C, Serwas D, Palfy M & Dammermann A (2015) The ciliary transition zone functions in cell adhesion but is dispensable for axoneme assembly in C. elegans. *J. Cell Biol.* **210:** 35–44

Schwartz RS, Hildebrandt F, Benzing T & Katsanis N (2011) Ciliopathies. *N. Engl. J. Med.* **364:** 1533–1543

Schwarzbauer JE & Sechler JL (1999) Fibronectin fibrillogenesis: a paradigm for extracellular matrix assembly. *Curr. Opin. Cell Biol.* **11:** 622–627

Sebé-Pedrós A, Roger AJ, Lang FB, King N & Ruiz-Trillo I (2010) Ancient origin of the integrin-mediated adhesion and signaling machinery. *Proc. Natl. Acad. Sci.* **107:** 10142–10147

Seller MJ (1978) Meckel syndrome and the prenatal diagnosis of neural tube defects. *J. Med. Genet.* **15:** 462–465

Sergi C, Adam S, Kahl P & Otto HF (2000) Study of the malformation of ductal plate of the liver in Meckel syndrome and review of other syndromes presenting with this anomaly. *Pediatr. Dev. Pathol.* **3:** 568–583

Shah MM, Sampogna R V, Sakurai H, Bush KT & Nigam SK (2004) Branching morphogenesis and kidney disease. *Development* **131:** 1449–1462

Shaheen R, Almoisheer A, Faqeih E, Babay Z, Monies D, Tassan N, Abouelhoda M, Kurdi W, Al Mardawi E & Khalil MMI (2015) Identification of a novel MKS locus defined by TMEM107 mutation. *Hum. Mol. Genet.* **24:** 5211–5218

Shaheen R, Ansari S, Mardawi EAL, Alshammari MJ & Alkuraya FS (2013a) Mutations in TMEM231 cause Meckel–Gruber syndrome. *J. Med. Genet.* **50:** 160–162

Shaheen R, Faqeih E, Alshammari MJ, Swaid A, Al-Gazali L, Mardawi E, Ansari S, Sogaty S, Seidahmed MZ & AlMotairi MI (2013b) Genomic analysis of Meckel–Gruber syndrome in Arabs reveals marked genetic heterogeneity and novel candidate genes. *Eur. J. Hum. Genet.* **21:** 762–768

Shaheen R, Faqeih E, Seidahmed MZ, Sunker A, Alali FE, Khadijah A & Alkuraya FS (2011) A TCTN2 mutation defines a novel Meckel Gruber syndrome locus. *Hum. Mutat.* **32:** 573–578

Shaheen R, Shamseldin HE, Loucks CM, Seidahmed MZ, Ansari S, Ibrahim Khalil M, Al-Yacoub N, Davis EE, Mola NA & Szymanska K (2014) Mutations in CSPP1, Encoding a Core Centrosomal Protein, Cause a Range of Ciliopathy Phenotypes in Humans. *Am. J. Hum. Genet.* **94:** 73–79

Shannon MB, Patton BL, Harvey SJ & Miner JH (2006) A hypomorphic mutation in the mouse laminin α5 gene causes polycystic kidney disease. *J. Am. Soc. Nephrol.* **17:** 1913–1922

Sharma AK, Mauer SM, Kim Y & Michael AF (1993) Interstitial fibrosis in obstructive nephropathy. *Kidney Int.* **44:** 774–788

Shoulders MD & Raines RT (2009) Collagen structure and stability. *Annu. Rev. Biochem.* **78:** 929

Shyjan AM, Bertagnolli M, Kenney CJ & Briskin MJ (1996) Human mucosal addressin cell adhesion molecule-1 (MAdCAM-1) demonstrates structural and functional similarities to the alpha 4 beta 7-integrin binding domains of murine MAdCAM-1, but extreme divergence of mucin-like sequences. *J. Immunol.* **156:** 2851–2857

Simons M, Gloy J, Ganner A, Bullerkotte A, Bashkurov M, Krönig C, Schermer B, Benzing T, Cabello OA & Jenny A (2005) Inversin, the gene product mutated in nephronophthisis type II, functions as a molecular switch between Wnt signaling pathways. *Nat. Genet.* **37:** 537–543

Singh P, Carraher C & Schwarzbauer JE (2010) Assembly of fibronectin extracellular matrix. *Annu. Rev. Cell Dev. Biol.* **26:** 397

Singla V & Reiter JF (2006) The primary cilium as the cell's antenna: signaling at a sensory organelle. *Science* **313:** 629–633

Singla V, Romaguera-Ros M, Garcia-Verdugo JM & Reiter JF (2010) < i> Ofd1</i>, a Human Disease Gene, Regulates the Length and Distal Structure of Centrioles. *Dev. Cell* **18:** 410–424

Small JV, Stradal T, Vignal E & Rottner K (2016) The lamellipodium: where motility begins. *Trends Cell Biol.* **12:** 112–120 Available at: http://dx.doi.org/10.1016/S0962-8924(01)02237-1

Smith UM, Consugar M, Tee LJ, McKee BM, Maina EN, Whelan S, Morgan N V, Goranson E, Gissen P & Lilliquist S (2006) The transmembrane protein meckelin (MKS3) is mutated in Meckel-Gruber syndrome and the wpk rat. *Nat. Genet.* **38:** 191–196

Sobeih MM & Corfas G (2002) Extracellular factors that regulate neuronal migration in the central nervous system. *Int. J. Dev. Neurosci.* **20:** 349–357

Song H, Hu J, Chen W, Elliott G, Andre P, Gao B & Yang Y (2010) Planar cell polarity breaks bilateral symmetry by controlling ciliary positioning. *Nature* **466:** 378–382

Sorokin S (1962) Centrioles and the formation of rudimentary cilia by fibroblasts and smooth muscle cells. *J. Cell Biol.* **15:** 363

Sparks AB, Morin PJ, Vogelstein B & Kinzler KW (1998) Mutational analysis of the APC/β-catenin/Tcf pathway in colorectal cancer. *Cancer Res.* **58:** 1130–1134

Starr DA & Fridolfsson HN (2010) Interactions between nuclei and the cytoskeleton are mediated by SUN-KASH nuclear-envelope bridges. *Annu. Rev. Cell Dev. Biol.* **26:** 421

Stehbens S & Wittmann T (2012) Targeting and transport: how microtubules control focal adhesion dynamics. *J. Cell Biol.* **198:** 481–489

Stephen LA, Tawamie H, Davis GM, Tebbe L, Nürnberg P, Nürnberg G, Thiele H, Thoenes M, Boltshauser E & Uebe S (2015) TALPID3 controls centrosome and cell polarity and the human ortholog KIAA0586 is mutated in Joubert syndrome (JBTS23). *Elife* **4:** e08077

Stoll C & Alembik Y (1993) Oto-palato-digital syndrome type II. *Genet. Couns.* **5:** 61–66

Stossel TP, Condeelis J, Cooley L, Hartwig JH, Noegel A, Schleicher M & Shapiro SS (2001) Filamins as integrators of cell mechanics and signalling. *Nat. Rev. Mol. cell Biol.* **2:** 138–145

Stratton RF & Bluestone DL (1991) Oto-palatal-digital syndrome type II with X-linked cerebellar hypoplasia/hydrocephalus. *Am. J. Med. Genet.* **41:** 169–172

Streets AJ, Newby LJ, O'Hare MJ, Bukanov NO, Ibraghimov-Beskrovnaya O & Ong ACM (2003) Functional analysis of PKD1 transgenic lines reveals a direct role for polycystin-1 in mediating cell-cell adhesion. *J. Am. Soc. Nephrol.* **14:** 1804–1815

Streuli CH, Schmidhauser C, Kobrin M, Bissell MJ & Derynck R (1993) Extracellular matrix regulates expression of the TGF-beta 1 gene. *J. Cell Biol.* **120:** 253–260

Stringer MD (2009) Intestinal Malrotation. In *Pediatric Surgery* pp 393–403. Springer

Sugiyama D, Kulkeaw K & Mizuochi C (2013) TGF-beta-1 up-regulates extra-cellular matrix production in mouse hepatoblasts. *Mech. Dev.* **130:** 195–206

Surendran K, Selassie M, Liapis H, Krigman H & Kopan R (2010) Reduced Notch signaling leads to renal cysts and papillary microadenomas. *J. Am. Soc. Nephrol.* **21:** 819–832

Suzuki M, Morita H & Ueno N (2012) Molecular mechanisms of cell shape changes that contribute to vertebrate neural tube closure. *Dev. Growth Differ.* **54:** 266–276

Szymanska K, Berry I, Logan C V, Cousins SRR, Lindsay H, Jafri H, Raashid Y, Malik-Sharif S,

Castle B & Ahmed M (2012) Founder mutations and genotype-phenotype correlations in Meckel-Gruber syndrome and associated ciliopathies. *Cilia* **1:** 18

Szymanska K, Hartill VL & Johnson CA (2014) Unraveling the genetics of Joubert and Meckel-Gruber syndromes. *J. Pediatr. Genet.* **3:** 65–78

Tallila J, Jakkula E, Peltonen L, Salonen R & Kestilä M (2008) Identification of< i> CC2D2A</i> as a Meckel Syndrome Gene Adds an Important Piece to the Ciliopathy Puzzle. *Am. J. Hum. Genet.* **82:** 1361–1367

Tammachote R, Hommerding CJ, Sinders RM, Miller CA, Czarnecki PG, Leightner AC, Salisbury JL, Ward CJ, Torres VE & Gattone VH (2009) Ciliary and centrosomal defects associated with mutation and depletion of the Meckel syndrome genes MKS1 and MKS3. *Hum. Mol. Genet.* **18:** 3311–3323

Tanos BE, Yang H-J, Soni R, Wang W-J, Macaluso FP, Asara JM & Tsou M-FB (2013) Centriole distal appendages promote membrane docking, leading to cilia initiation. *Genes Dev.* **27:** 163–168

Tasouri E & Tucker KL (2011) Primary cilia and organogenesis: is Hedgehog the only sculptor? *Cell Tissue Res.* **345:** 21–40

Theisen U & Straube A (2016) Microtubules regulate cell migration and neuronal pathfinding. In *The Microtubule Cytoskeleton* pp 151–189. Springer

Theret DP, Levesque MJ, Sato R, Nerem RM & Wheeler LT (1988) The application of a homogeneous half-space model in the analysis of endothelial cell micropipette measurements. **110:** 190–199

Timpl R, Rohde H, Robey PG, Rennard SI, Foidart J-M & Martin GR (1979) Laminin--a glycoprotein from basement membranes. *J. Biol. Chem.* **254:** 9933–9937

Tobin JL & Beales PL (2009) The nonmotile ciliopathies. *Genet. Med.* **11:** 386–402

Tobin JL, Di Franco M, Eichers E, May-Simera H, Garcia M, Yan J, Quinlan R, Justice MJ, Hennekam RC & Briscoe J (2008) Inhibition of neural crest migration underlies craniofacial dysmorphology and Hirschsprung's disease in Bardet–Biedl syndrome. *Proc. Natl. Acad. Sci.* **105:** 6714–6719

Tomasek JJ, Gabbiani G, Hinz B, Chaponnier C & Brown RA (2002) Myofibroblasts and mechano-regulation of connective tissue remodelling. *Nat. Rev. Mol. cell Biol.* **3:** 349–363

Torrado B, Graña M, Badano JL & Irigoín F (2016) Ciliary Entry of the Hedgehog Transcriptional Activator Gli2 Is Mediated by the Nuclear Import Machinery but Differs from Nuclear Transport in Being Imp-α/β1-Independent. *PLoS One* **11:** e0162033

Town T, Breunig JJ, Sarkisian MR, Spilianakis C, Ayoub AE, Liu X, Ferrandino AF, Gallagher AR, Li MO & Rakic P (2008) The stumpy gene is required for mammalian ciliogenesis. *Proc. Natl. Acad. Sci.* **105:** 2853–2858

Tozser J, Earwood R, Kato A, Brown J, Tanaka K, Didier R, Megraw TL, Blum M & Kato Y (2015) TGF-b Signaling Regulates the Differentiation of Motile Cilia. *Cell Rep.* **11:** 1000–1007

Tryggvason K (1993) The laminin family. *Curr. Opin. Cell Biol.* **5:** 877–882

Tsang WY, Bossard C, Khanna H, Peränen J, Swaroop A, Malhotra V & Dynlacht BD (2008) CP110 suppresses primary cilia formation through its interaction with CEP290, a protein deficient in human ciliary disease. *Dev. Cell* **15:** 187–197

Tsun A, Qureshi I, Stinchcombe JC, Jenkins MR, de la Roche M, Kleczkowska J, Zamoyska R & Griffiths GM (2011) Centrosome docking at the immunological synapse is controlled by Lck signaling. *J. Cell Biol.* **192:** 663–674

Tu Y, Wu S, Shi X, Chen K & Wu C (2003) Migfilin and Mig-2 link focal adhesions to filamin and

the actin cytoskeleton and function in cell shape modulation. *Cell* **113:** 37–47

Tuz K, Bachmann-Gagescu R, O'Day DR, Hua K, Isabella CR, Phelps IG, Stolarski AE, O'Roak BJ, Dempsey JC & Lourenco C (2014) Mutations in CSPP1 cause primary cilia abnormalities and Joubert syndrome with or without Jeune asphyxiating thoracic dystrophy. *Am. J. Hum. Genet.* **94:** 62–72

UniProt Consortium (2013) Update on activities at the Universal Protein Resource (UniProt) in 2013. *Nucleic Acids Res.* **41:** D43–D47

Valente EM, Logan C V, Mougou-Zerelli S, Lee JH, Silhavy JL, Brancati F, Iannicelli M, Travaglini L, Romani S & Illi B (2010) Mutations in TMEM216 perturb ciliogenesis and cause Joubert, Meckel and related syndromes. *Nat. Genet.* **42:** 619–625

Vandenberg LN, Lemire JM & Levin M (2013) Serotonin has early, cilia-independent roles in Xenopus left-right patterning. *Dis. Model. Mech.* **6:** 261–268

Vasiliev JM (1982) Spreading and locomotion of tissue cells: factors controlling the distribution of pseudopodia. *Philos. Trans. R. Soc. London B Biol. Sci.* **299:** 159–167

Veeman MT, Axelrod JD & Moon RT (2003) A second canon: functions and mechanisms of β-catenin-independent Wnt signaling. *Dev. Cell* **5:** 367–377

Veit G, Kobbe B, Keene DR, Paulsson M, Koch M & Wagener R (2006) Collagen XXVIII, a novel von Willebrand factor A domain-containing protein with many imperfections in the collagenous domain. *J. Biol. Chem.* **281:** 3494–3504

Veland IR, Montjean R, Eley L, Pedersen LB, Schwab A, Goodship J, Kristiansen K, Pedersen SF, Saunier S & Christensen ST (2013) Inversin/Nephrocystin-2 is required for fibroblast polarity and directional cell migration. *PLoS One* **8:** e60193

Velling T, Risteli J, Wennerberg K, Mosher DF & Johansson S (2002) Polymerization of type I and III collagens is dependent on fibronectin and enhanced by integrins α11β1and α2β1. *J. Biol. Chem.* **277:** 37377–37381

Venkatesh B, Ravi V, Lee AP, Warren WC & Brenner S (2012) Basal vertebrates clarify the evolutionary history of ciliopathy-associated genes Tmem138 and Tmem216. *Mol. Biol. Evol.* **30:** 62–65

Vleming LJ, Baelde JJ, Westendorp RG, Daha MR, Van Es LA & Bruijn JA (1995) Progression of chronic renal disease in humans is associated with the deposition of basement membrane components and decorin in the interstitial extracellular matrix. *Clin. Nephrol.* **44:** 211–219

Vorobjev IA & Chentsov YS (1982) Centrioles in the cell cycle. I. Epithelial cells. *J. Cell Biol.* **93:** 938–949

Voronina VA, Takemaru K-I, Treuting P, Love D, Grubb BR, Hajjar AM, Adams A, Li F-Q & Moon RT (2009) Inactivation of Chibby affects function of motile airway cilia. *J. Cell Biol.* **185:** 225–233

Wada K-I, Itoga K, Okano T, Yonemura S & Sasaki H (2011) Hippo pathway regulation by cell morphology and stress fibers. *Development* **138:** 3907–3914

Wallingford JB, Fraser SE & Harland RM (2002) Convergent extension: the molecular control of polarized cell movement during embryonic development. *Dev. Cell* **2:** 695–706

Wallingford JB & Mitchell B (2011) Strange as it may seem: the many links between Wnt signaling, planar cell polarity, and cilia. *Genes Dev.* **25:** 201–213

Wang C-H, Wang T-M, Young T-H, Lai Y-K & Yen M-L (2013) The critical role of ECM proteins within the human MSC niche in endothelial differentiation. *Biomaterials* **34:** 4223–4234

Wang M, Bridges JP, Na C-L, Xu Y & Weaver TE (2009) Meckel-Gruber syndrome protein MKS3 is required for endoplasmic reticulum-associated degradation of surfactant protein

C. *J. Biol. Chem.* **284:** 33377–33383

Wann AKT, Zuo N, Haycraft CJ, Jensen CG, Poole CA, McGlashan SR & Knight MM (2012) Primary cilia mediate mechanotransduction through control of ATP-induced Ca2+ signaling in compressed chondrocytes. *FASEB J.* **26:** 1663–1671

Watt FM & Hogan BLM (2000) Out of Eden: stem cells and their niches. *Science* **287:** 1427–1430

Weatherbee SD, Niswander LA & Anderson K V (2009) A mouse model for Meckel syndrome reveals Mks1 is required for ciliogenesis and Hedgehog signaling. *Hum. Mol. Genet.* **18:** 4565–4575

Wehrle-Haller B (2012) Assembly and disassembly of cell matrix adhesions. *Curr. Opin. Cell Biol.* **24:** 569–581

Wei J, Melichian D, Komura K, Hinchcliff M, Lam AP, Lafyatis R, Gottardi CJ, MacDougald OA & Varga J (2011) Canonical Wnt signaling induces skin fibrosis and subcutaneous lipoatrophy: a novel mouse model for scleroderma? *Arthritis Rheum.* **63:** 1707–1717

Weiss A & Attisano L (2013) The TGFbeta superfamily signaling pathway. *Wiley Interdiscip. Rev. Dev. Biol.* **2:** 47–63

Wennerberg K & Der CJ (2004) Rho-family GTPases: it's not only Rac and Rho (and I like it). *J. Cell Sci.* **117:** 1301–1312

Westlake CJ, Baye LM, Nachury M V, Wright KJ, Ervin KE, Phu L, Chalouni C, Beck JS, Kirkpatrick DS & Slusarski DC (2011) Primary cilia membrane assembly is initiated by Rab11 and transport protein particle II (TRAPPII) complex-dependent trafficking of Rabin8 to the centrosome. *Proc. Natl. Acad. Sci.* **108:** 2759–2764

Wheatley DN (1995) Primary cilia in normal and pathological tissues. *Pathobiology* **63:** 222–238

Wheway G, Schmidts M, Mans DA, Szymanska K, Nguyen T-MT, Racher H, Phelps IG, Toedt G, Kennedy J & Wunderlich KA (2015) An siRNA-based functional genomics screen for the identification of regulators of ciliogenesis and ciliopathy genes. *Nat. Cell Biol.* **17:** 1074–1087

Whittaker CA, Bergeron K-F, Whittle J, Brandhorst BP, Burke RD & Hynes RO (2006) The echinoderm adhesome. *Dev. Biol.* **300:** 252–266

Wierzbicka-Patynowski I & Schwarzbauer JE (2003) The ins and outs of fibronectin matrix assembly. *J. Cell Sci.* **116:** 3269–3276

Williams CL, Li C, Kida K, Inglis PN, Mohan S, Semenec L, Bialas NJ, Stupay RM, Chen N & Blacque OE (2011) MKS and NPHP modules cooperate to establish basal body/transition zone membrane associations and ciliary gate function during ciliogenesis. *J. Cell Biol.* **192:** 1023–1041

Williams CL, Masyukova S V & Yoder BK (2010) Normal ciliogenesis requires synergy between the cystic kidney disease genes MKS-3 and NPHP-4. *J. Am. Soc. Nephrol.* **21:** 782–793

Wilson PD (2001) Polycystin: new aspects of structure, function, and regulation. *J. Am. Soc. Nephrol.* **12:** 834–845

Wilson PD, Geng L, Li X & Burrow CR (1999) The PKD1 gene product,' polycystin-1,' is a tyrosine-phosphorylated protein that colocalizes with alpha2beta1-integrin in focal clusters in adherent renal epithelia. *Lab. Invest.* **79:** 1311–1323

Winter CG, Wang B, Ballew A, Royou A, Karess R, Axelrod JD & Luo L (2001) < i> Drosophila</i> Rho-Associated Kinase (Drok) Links Frizzled-Mediated Planar Cell Polarity Signaling to the Actin Cytoskeleton. *Cell* **105:** 81–91

Wójtowicz I, Jabłońska J, Zmojdzian M, Taghli-Lamallem O, Renaud Y, Junion G, Daczewska M, Huelsmann S, Jagla K & Jagla T (2015) Drosophila small heat shock protein CryAB

ensures structural integrity of developing muscles, and proper muscle and heart performance. *Development* **142:** 994–1005

Wong SY & Reiter JF (2008) The primary cilium: at the crossroads of mammalian hedgehog signaling. *Curr. Top. Dev. Biol.* **85:** 225–260

Wood CR, Wang Z, Diener D, Zones JM, Rosenbaum J & Umen JG (2012) IFT proteins accumulate during cell division and localize to the cleavage furrow in Chlamydomonas. *PLoS One* **7:** e30729

Woods AJ, White DP, Caswell PT & Norman JC (2004) PKD1/PKCμ promotes αvβ3 integrin recycling and delivery to nascent focal adhesions. *EMBO J.* **23:** 2531–2543

Wright JW, Kramár EA, Meighan SE & Harding JW (2002) Extracellular matrix molecules, long-term potentiation, memory consolidation and the brain angiotensin system. *Peptides* **23:** 221–246

Wright KJ, Baye LM, Olivier-Mason A, Mukhopadhyay S, Sang L, Kwong M, Wang W, Pretorius PR, Sheffield VC & Sengupta P (2011) An ARL3–UNC119–RP2 GTPase cycle targets myristoylated NPHP3 to the primary cilium. *Genes Dev.* **25:** 2347–2360

Xiong Y, Rangamani P, Fardin M-A, Lipshtat A, Dubin-Thaler B, Rossier O, Sheetz MP & Iyengar R (2010) Mechanisms controlling cell size and shape during isotropic cell spreading. *Biophys. J.* **98:** 2136–2146

Xu K, Babcock HP & Zhuang X (2012) Dual-objective STORM reveals three-dimensional filament organization in the actin cytoskeleton. *Nat. Methods* **9:** 185–188

Xu Y, Gurusiddappa S, Rich RL, Owens RT, Keene DR, Mayne R, Höök A & Höök M (2000) Multiple binding sites in collagen type I for the integrins α1β1 and α2β1. *J. Biol. Chem.* **275:** 38981–38989

Yadav SP, Sharma NK, Liu C, Dong L, Li T & Swaroop A (2016) Centrosomal protein CP110 controls maturation of the mother centriole during cilia biogenesis. *Development* **143:** 1491–1501

Yan X & Zhu X (2013) Branched F-actin as a negative regulator of cilia formation. *Exp. Cell Res.* **319:** 147–151

Yang TT, Su J, Wang W-J, Craige B, Witman GB, Tsou M-FB & Liao J-C (2015) Superresolution pattern recognition reveals the architectural map of the ciliary transition zone. *Sci. Rep.* **5:** 14096

Ybot-Gonzalez P, Savery D, Gerrelli D, Signore M, Mitchell CE, Faux CH, Greene NDE & Copp AJ (2007) Convergent extension, planar-cell-polarity signalling and initiation of mouse neural tube closure. *Development* **134:** 789–799

Yeatman TJ (2004) A renaissance for SRC. *Nat. Rev. Cancer* **4:** 470–480

Yi J, Wu X, Chung AH, Chen JK, Kapoor TM & Hammer JA (2013) Centrosome repositioning in T cells is biphasic and driven by microtubule end-on capture-shrinkage. *J. Cell Biol.* **202:** 779–792

Yin Y, Bangs F, Paton IR, Prescott A, James J, Davey MG, Whitley P, Genikhovich G, Technau U & Burt DW (2009) The Talpid3 gene (KIAA0586) encodes a centrosomal protein that is essential for primary cilia formation. *Development* **136:** 655–664

Yoshimura S, Egerer J, Fuchs E, Haas AK & Barr FA (2007) Functional dissection of Rab GTPases involved in primary cilium formation. *J. Cell Biol.* **178:** 363–369

Yuan S & Sun Z (2013) Expanding horizons: ciliary proteins reach beyond cilia. *Annu. Rev. Genet.* **47:** 353–376

Zaidel-Bar R (2009) Evolution of complexity in the integrin adhesome. *J. Cell Biol.* **186:** 317–321

Zaidel-Bar R, Itzkovitz S, Ma'ayan A, Iyengar R & Geiger B (2007) Functional atlas of the integrin adhesome. *Nat. Cell Biol.* **9:** 858–867

Zambruno G, Marchisio PC, Marconi A, Vaschieri C, Melchiori A, Giannetti A & De Luca M (1995) Transforming growth factor-beta 1 modulates beta 1 and beta 5 integrin receptors and induces the de novo expression of the alpha v beta 6 heterodimer in normal human keratinocytes: implications for wound healing. *J. Cell Biol.* **129:** 853–865

Zamir E, Katz M, Posen Y, Erez N, Yamada KM, Katz B-Z, Lin S, Lin DC, Bershadsky A & Kam Z (2000) Dynamics and segregation of cell–matrix adhesions in cultured fibroblasts. *Nat. Cell Biol.* **2:** 191–196

Zhang X, Jiang G, Cai Y, Monkley SJ, Critchley DR & Sheetz MP (2008) Talin depletion reveals independence of initial cell spreading from integrin activation and traction. *Nat Cell Biol* **10:** 1062–1068

Zhao B, Li L, Wang L, Wang C-Y, Yu J & Guan K-L (2012) Cell detachment activates the Hippo pathway via cytoskeleton reorganization to induce anoikis. *Genes Dev.* **26:** 54–68

Appendix 1

Data tables

Supplementary Table 1: Illumina differential expression analysis

Official gene Name	Full gene name	log2(fold_change)
ABCA1	ATP-binding cassette, sub-family A (ABC1), membe	1.27666
ABCC5	ATP-binding cassette, sub-family C (CFTR/MRP), m	1.54252
ABCC9	ATP-binding cassette, sub-family C (CFTR/MRP), m	2.39777
ABHD13	abhydrolase domain containing 13	1.16719
ABHD2	abhydrolase domain containing 2	1.33772
ABHD5	abhydrolase domain containing 5	-1.55508
ABI3BP	ABI family, member 3 (NESH) binding protein	-2.23738
ABLIM1	actin binding LIM protein 1	-2.61344
ACAA2	hypothetical LOC648603; acetyl-Coenzyme A acyltra	1.38283
ACADM	acyl-Coenzyme A dehydrogenase, C-4 to C-12 straig	1.00416
ACLY	ATP citrate lyase	0.830769
ACOX1	acyl-Coenzyme A oxidase 1, palmitoyl	1.24279
ACPL2	acid phosphatase-like 2	2.85809
ACSS3	acyl-CoA synthetase short-chain family member 3	-1.86537
ACTA2	actin, alpha 2, smooth muscle, aorta	-2.27376
ACTR2	ARP2 actin-related protein 2 homolog (yeast)	1.09742
ACVRL1	activin A receptor type II-like 1	-4.22295
ACYP1	acylphosphatase 1, erythrocyte (common) type	-1.56813
ADAM10	ADAM metallopeptidase domain 10	1.27091
ADAM12	ADAM metallopeptidase domain 12	1.58166
ADAM19	ADAM metallopeptidase domain 19 (meltrin beta)	3.151
ADAMTS1	ADAM metallopeptidase with thrombospondin type 1	-1.02107
ADAMTS12	ADAM metallopeptidase with thrombospondin type 1	1.58827
ADAMTS6	ADAM metallopeptidase with thrombospondin type 1	-1.0243
ADAMTSL1	ADAMTS-like 1	1.56946
ADCY7	adenylate cyclase 7	1.36317
ADK	adenosine kinase	-1.47022
ADM	adrenomedullin	-1.20007
ADM2	adrenomedullin 2	-2.57051
AGAP11-C10orf116	ankyrin repeat and GTPase domain Arf GTPase acti	-3.17174
AGFG2	ArfGAP with FG repeats 2	2.51403
AGPAT2	1-acylglycerol-3-phosphate O-acyltransferase 2 (lysc	-1.57242
AGPAT5	1-acylglycerol-3-phosphate O-acyltransferase 5 (lysc	0.762837
AGPS	alkylglycerone phosphate synthase	1.55564
AGTR1	angiotensin II receptor, type 1	1.19111
AGTRAP	angiotensin II receptor-associated protein	-2.13317
AHNAK2	AHNAK nucleoprotein 2	1.18451
AIM1	absent in melanoma 1	0.870181
AJUBA	ajuba LIM protein	-1.0314
AK4	adenylate kinase 4	1.22614
AK5	adenylate kinase 5	-0.874911
AKAP12	A kinase (PRKA) anchor protein 12	3.57012
ALDH1A1	aldehyde dehydrogenase 1 family, member A1	4.01852
ALDH1A3	aldehyde dehydrogenase 1 family, member A3	1.83607
ALDH2	aldehyde dehydrogenase 2 family (mitochondrial)	1.49948
ALG10B	asparagine-linked glycosylation 10, alpha-1,2-glucos	1.53345
ALMS1	Alstrom syndrome 1	0.943234
ALPK1	alpha-kinase 1	-2.00555
ALPK2	alpha-kinase 2	-2.04979
AMOT	angiomotin	2.51657
AMOTL1	angiomotin like 1	1.12105
AMPD3	adenosine monophosphate deaminase (isoform E)	1.10696
AMZ2	archaelysin family metallopeptidase 2	-0.917297
ANAPC1	anaphase promoting complex subunit 1; similar to ar	0.957962
ANGPTL4	angiopoietin-like 4	2.77765
ANKDD1A	ankyrin repeat and death domain containing 1A	-1.80711
ANKRD1	ankyrin repeat domain 1 (cardiac muscle)	3.13106
ANKRD33B	ankyrin repeat domain 33B	3.04791
ANO2	anoctamin 2	inf
ANO3	anoctamin 3	2.43375
ANP32A	hepatopoietin PCn127; acidic (leucine-rich) nuclear p	0.772422
ANPEP	alanyl (membrane) aminopeptidase	-2.66581
ANXA2P2	annexin A2 pseudogene 2	-1.21108
ANXA5	annexin A5	0.869039
AP1AR	chromosome 4 open reading frame 16	-0.876568
AP1S2	adaptor-related protein complex 1, sigma 2 subunit p	1.86544
AP1S3	adaptor-related protein complex 1, sigma 3 subunit	3.26998
APAF1	apoptotic peptidase activating factor 1	1.19259
APLP2	amyloid beta (A4) precursor-like protein 2	1.37227
APOBEC3B	apolipoprotein B mRNA editing enzyme, catalytic pol	-1.47971

APOL6	apolipoprotein L, 6	-1.66824
APPL1	adaptor protein, phosphotyrosine interaction, PH dor	0.797917
AR	androgen receptor	-2.59733
ARAP2	ArfGAP with RhoGAP domain, ankyrin repeat and P	inf
ARHGAP29	Rho GTPase activating protein 29	-2.35549
ARHGAP31	Cdc42 GTPase-activating protein 31	1.11631
ARHGDIB	Rho GDP dissociation inhibitor (GDI) beta	3.48463
ARL4C	ADP-ribosylation factor-like 4C	3.42277
ARL6IP4	ADP-ribosylation-like factor 6 interacting protein 4	-0.931122
ARMCX3	armadillo repeat containing, X-linked 3	0.984325
ARMCX4	similar to hCG1792883	-1.18477
ARPP19	cAMP-regulated phosphoprotein 19 pseudogene; cA	0.94993
ARRDC3	arrestin domain containing 3	1.8463
ARSJ	arylsulfatase family, member J	1.22271
ASAH1	N-acylsphingosine amidohydrolase (acid ceramidase	1.15117
ASIC1	acid-sensing (proton-gated) ion channel 1	1.75785
ASNS	asparagine synthetase	-1.58743
ASS1	argininosuccinate synthetase 1	-3.6714
ATF1	activating transcription factor 1	-1.13851
ATF3	activating transcription factor 3	-2.32275
ATF4	activating transcription factor 4 (tax-responsive enha	-1.76969
ATOH8	atonal homolog 8 (Drosophila)	2.95746
ATP13A3	ATPase type 13A3	1.43556
ATP2B1	ATPase, Ca++ transporting, plasma membrane 1	-1.01892
ATP2B4	ATPase, Ca++ transporting, plasma membrane 4	0.755718
ATP5E-SLMO2	ATP synthase, H+ transporting, mitochondrial F1 co	-1.22283
ATP6V1A	ATPase, H+ transporting, lysosomal 70kDa, V1 subu	1.12318
ATRX	alpha thalassemia/mental retardation syndrome X-lir	0.867452
ATXN7L3B	ataxin 7-like 3B	1.6881
AURKA	aurora kinase A; aurora kinase A pseudogene 1	-1.04372
AUTS2	autism susceptibility candidate 2	5.51109
AVPI1	arginine vasopressin-induced 1	-1.23663
B2M	beta-2-microglobulin	-1.27575
B3GALTL	beta 1,3-galactosyltransferase-like	1.21691
B3GNT5	UDP-GlcNAc:betaGal beta-1,3-N-acetylglucosaminy	1.06871
B4GALNT4	beta-1,4-N-acetyl-galactosaminyl transferase 4	2.72013
B4GALT4	UDP-Gal:betaGlcNAc beta 1,4- galactosyltransferas	-0.836808
BAALC	brain and acute leukemia, cytoplasmic	4.1237
BBS2	Bardet-Biedl syndrome 2	1.11735
BCAT1	branched chain aminotransferase 1, cytosolic	2.3425
BCOR	BCL6 co-repressor	1.2503
BCYRN1	brain cytoplasmic RNA 1 (non-protein coding)	-0.949748
BEX1	brain expressed, X-linked 1	1.02303
BEX4	brain expressed, X-linked 4	-1.65998
BGN	biglycan	2.13611
BHLHE41	basic helix-loop-helix family, member e41	0.970513
BHMT2	betaine-homocysteine methyltransferase 2	-2.47987
BICC1	bicaudal C homolog 1 (Drosophila)	-1.03906
BIRC6	baculoviral IAP repeat-containing 6	0.759303
BLCAP	bladder cancer associated protein	0.920888
BNC1	basonuclin 1	-5.01044
BTN2A1	butyrophilin, subfamily 2, member A1	-0.943724
BTN2A2	butyrophilin, subfamily 2, member A2	-1.11174
BTN3A1	butyrophilin, subfamily 3, member A1	-2.15881
BTN3A2	butyrophilin, subfamily 3, member A2	-2.30666
BTN3A3	butyrophilin, subfamily 3, member A3	-3.10287
BZW1	basic leucine zipper and W2 domains 1 pseudogene	1.11785
C11orf63	chromosome 11 open reading frame 63	-3.1193
C11orf9	chromosome 11 open reading frame 9	1.79537
C14orf132	chromosome 14 open reading frame 132	1.67056
C14orf37	chromosome 14 open reading frame 37	2.39154
C1GALT1C1	C1GALT1-specific chaperone 1	1.28177
C1QL4	complement component 1, q subcomponent-like 4	inf
C20orf111	chromosome 20 open reading frame 111	-1.2429
C22orf29-GNB1L	C22orf29 - guanine nucleotide binding protein (G pro	-1.26494
C2orf44	chromosome 2 open reading frame 44	1.44273
C3orf55	chromosome 3 open reading frame 55	-1.73223
C3orf67	chromosome 3 open reading frame 67	-2.22964
C7orf10	chromosome 7 open reading frame 10	1.1556
C7orf41	chromosome 7 open reading frame 41	1.24305
C9orf64	chromosome 9 open reading frame 64	-2.30051
CA12	carbonic anhydrase XII	1.47224

CABYR	calcium binding tyrosine-(Y)-phosphorylation regulat	-1.47529
CADM3	cell adhesion molecule 3	inf
CALCRL	calcitonin receptor-like	-1.89875
CALHM2	calcium homeostasis modulator 2	-1.27149
CAMK1D	calcium/calmodulin-dependent protein kinase ID	2.84135
CAND1	cullin-associated and neddylation-dissociated 1	1.34477
CARD16	caspase recruitment domain family, member 16	-3.28496
CARD6	caspase recruitment domain family, member 6	-2.03093
CARD9	caspase recruitment domain family, member 9	-inf
CARS	cysteinyl-tRNA synthetase	-1.05459
CASP1	caspase 1, apoptosis-related cysteine peptidase (int	-3.3351
CASS4	Cas scaffolding protein family member 4	-3.53058
CAST	calpastatin	-1.06626
CBS	cystathionine-beta-synthase	-1.00927
CBX5	chromobox homolog 5 (HP1 alpha homolog, Drosop	1.09598
CBX7	chromobox homolog 7	-2.96316
CBY1	chibby homolog 1 (Drosophila)	-1.10738
CCDC113	coiled-coil domain containing 113	-1.76335
CCDC130	coiled-coil domain containing 130	-1.56788
CCDC152	coiled-coil domain containing 152	inf
CCDC71L	coiled-coil domain containing 71-like	-1.8226
CCDC8	coiled-coil domain containing 8	1.72829
CCDC85A	coiled-coil domain containing 85A	3.99673
CCNB1	cyclin B1	-0.937324
CCNB2	cyclin B2	-0.887692
CCND1	cyclin D1	1.03973
CCND2	cyclin D2	2.48238
CCT2	chaperonin containing TCP1, subunit 2 (beta)	0.799956
CD109	CD109 molecule	1.27569
CD164	CD164 molecule, sialomucin	0.799539
CD248	CD248 molecule, endosialin	1.29987
CD274	CD274 molecule	0.915163
CD2AP	CD2-associated protein	1.04862
CD55	CD55 molecule, decay accelerating factor for compl	-2.1411
CD58	CD58 molecule	-2.14454
CD59	CD59 molecule, complement regulatory protein	0.898397
CD68	CD68 molecule	-1.09217
CD82	CD82 molecule	-3.15769
CD83	CD83 molecule	-3.815
CD97	CD97 molecule	-1.01691
CDC20	cell division cycle 20 homolog (S. cerevisiae)	-1.31356
CDC25B	cell division cycle 25 homolog B (S. pombe)	-1.3198
CDC42EP1	CDC42 effector protein (Rho GTPase binding) 1	-1.53983
CDCA3	cell division cycle associated 3	-1.45681
CDCA8	cell division cycle associated 8	-0.862716
CDH11	cadherin 11, type 2, OB-cadherin (osteoblast)	1.26243
CDH2	cadherin 2, type 1, N-cadherin (neuronal)	0.947065
CDK11A	similar to cell division cycle 2-like 1 (PITSLRE protei	-0.940209
CDK15	PFTAIRE protein kinase 2	-1.56201
CDK17	PCTAIRE protein kinase 2	1.09715
CDK20	cell cycle related kinase	-2.05691
CDKN1A	cyclin-dependent kinase inhibitor 1A (p21, Cip1)	-1.11063
CDKN1B	cyclin-dependent kinase inhibitor 1B (p27, Kip1)	-1.36325
CDKN2D	cyclin-dependent kinase inhibitor 2D (p19, inhibits C	-1.45961
CDKN3	cyclin-dependent kinase inhibitor 3	-2.28507
CDR1	cerebellar degeneration-related protein 1, 34kDa	1.72713
CDR2	cerebellar degeneration-related protein 2, 62kDa	-0.880281
CDYL	chromodomain protein, Y-like	-0.921214
CEBPB	CCAAT/enhancer binding protein (C/EBP), beta	-1.2911
CEBPD	CCAAT/enhancer binding protein (C/EBP), delta	-1.80966
CEBPG	CCAAT/enhancer binding protein (C/EBP), gamma	-1.24876
CELF2	CUG triplet repeat, RNA binding protein 2	2.73062
CEP170	centrosomal protein 170kDa	1.8749
CEP19	centrosomal protein 19kDa	-1.88973
CEP250	centrosomal protein 250kDa / CNAP1	1.41592
CETN3	centrin, EF-hand protein, 3 (CDC31 homolog, yeast)	-1.09736
CFH	complement factor H	-1.18438
CFL2	cofilin 2 (muscle)	-0.860912
CHAC1	ChaC, cation transport regulator homolog 1 (E. coli)	-2.79477
CHD9	chromodomain helicase DNA binding protein 9	0.780368
CHIC1	cysteine-rich hydrophobic domain 1	0.999948
CHN1	chimerin (chimaerin) 1	-2.47714

CHORDC1	cysteine and histidine-rich domain (CHORD)-contair	0.852996
CHPF	chondroitin polymerizing factor	1.14338
CHST15	carbohydrate (N-acetylgalactosamine 4-sulfate 6-O)	2.59689
CHSY3	chondroitin sulfate synthase 3	2.50189
CISD1	CDGSH iron sulfur domain 1	1.18842
CITED2	Cbp/p300-interacting transactivator, with Glu/Asp-ric	-2.02062
CKAP2	cytoskeleton associated protein 2	-0.707997
CKAP4	cytoskeleton-associated protein 4	0.706704
CKS2	CDC28 protein kinase regulatory subunit 2	-0.892051
CLCN5	chloride channel 5	1.36993
CLDN1	claudin 1	1.84605
CLDN11	claudin 11	4.18892
CLPP	ClpP caseinolytic peptidase, ATP-dependent, protec	-1.23401
CLTB	clathrin, light chain (Lcb)	-1.09621
CLTCL1	clathrin, heavy chain-like 1	-1.7184
CLU	clusterin	3.96023
CMIP	c-Maf-inducing protein	1.06442
CMTM4	CKLF-like MARVEL transmembrane domain contain	1.64097
CNIH3	cornichon homolog 3 (Drosophila)	2.99667
CNN1	calponin 1, basic, smooth muscle	4.18816
CNTNAP2	contactin associated protein-like 2	inf
CNTNAP3B	contactin associated protein-like 3; contactin associa	inf
COA6	cytochrome c oxidase assembly factor 6 homolog (S	-1.23795
COBLL1	COBL-like 1	1.01567
COL16A1	collagen, type XVI, alpha 1	1.57505
COL1A1	collagen, type I, alpha 1	1.2435
COL4A2	collagen, type IV, alpha 2	-0.98649
COL4A6	collagen, type IV, alpha 6	-1.8766
COL6A1	collagen, type VI, alpha 1	0.843068
COLEC12	collectin sub-family member 12	inf
COPS8	COP9 constitutive photomorphogenic homolog subu	0.817848
CORIN	corin, serine peptidase	-2.18769
CORO2B	coronin, actin binding protein, 2B	-1.52726
CPA4	carboxypeptidase A4	2.55071
CPEB2	cytoplasmic polyadenylation element binding protein	2.35014
CPED1	cadherin-like and PC-esterase domain containing 1	-1.82691
CPM	carboxypeptidase M	-1.2285
CPNE8	copine VIII	-inf
CPS1	carbamoyl-phosphate synthetase 1, mitochondrial	3.07178
CPT1A	carnitine palmitoyltransferase 1A (liver)	1.55128
CPXM2	carboxypeptidase X (M14 family), member 2	inf
CRABP2	cellular retinoic acid binding protein 2	3.18615
CRADD	CASP2 and RIPK1 domain containing adaptor with d	-2.3475
CREB5	cAMP responsive element binding protein 5	2.4193
CREG1	cellular repressor of E1A-stimulated genes 1	-1.75744
CRELD1	cysteine-rich with EGF-like domains 1	-1.49636
CRISPLD2	cysteine-rich secretory protein LCCL domain contain	-3.89405
CRNDE	hCG1815491	-1.47427
CRYAB	crystallin, alpha B	2.2337
CSRP2	cysteine and glycine-rich protein 2	-1.63107
CST3	cystatin C	-1.08921
CTNNB1	catenin (cadherin-associated protein), beta 1, 88kDa	0.868635
CTNND2	catenin (cadherin-associated protein), delta 2 (neura	inf
CTSC	cathepsin C	-1.63365
CTSL1	cathepsin L1	-1.37689
CTSZ	cathepsin Z	-0.857053
CUL4B	cullin 4B	1.69546
CXCL1	chemokine (C-X-C motif) ligand 1 (melanoma growth	-2.69854
CXCL12	chemokine (C-X-C motif) ligand 12 (stromal cell-deri	7.47892
CXCL5	chemokine (C-X-C motif) ligand 5	-1.88329
CXXC5	CXXC finger 5	-2.33221
CYB5R2	cytochrome b5 reductase 2	-3.63906
CYFIP2	cytoplasmic FMR1 interacting protein 2	3.16387
CYGB	cytoglobin	-1.29924
CYP4V2	cytochrome P450, family 4, subfamily V, polypeptide	-1.96144
CYR61	cysteine-rich, angiogenic inducer, 61	-1.31188
CYYR1	cysteine/tyrosine-rich 1	3.03389
DBNDD1	dysbindin (dystrobrevin binding protein 1) domain co	2.38699
DCBLD2	discoidin, CUB and LCCL domain containing 2	1.84057
DCHS1	dachsous 1 (Drosophila)	1.34521
DCLK2	doublecortin-like kinase 2	-2.3465
DCP1B	DCP1 decapping enzyme homolog B (S. cerevisiae)	-0.91217

DCTN3	dynactin 3 (p22)	-0.903299
DDIT4	DNA-damage-inducible transcript 4	-2.39062
DDIT4L	DNA-damage-inducible transcript 4-like	-3.11374
DDX19B	DEAD (Asp-Glu-Ala-As) box polypeptide 19B	-0.877952
DDX6	DEAD (Asp-Glu-Ala-Asp) box polypeptide 6	0.800345
DEGS1	degenerative spermatocyte homolog 1, lipid desatura	0.874168
DENND1A	DENN/MADD domain containing 1A	-1.14827
DGKB	diacylglycerol kinase, beta 90kDa	-4.20003
DGKI	diacylglycerol kinase, iota	-1.88613
DHRS3	dehydrogenase/reductase (SDR family) member 3	inf
DHRS7	dehydrogenase/reductase (SDR family) member 7	-1.384
DHX9	DEAH (Asp-Glu-Ala-His) box polypeptide 9	1.12236
DKK3	dickkopf homolog 3 (Xenopus laevis)	-0.772393
DNAJA1	DnaJ (Hsp40) homolog, subfamily A, member 1	0.849068
DNAJA4	DnaJ (Hsp40) homolog, subfamily A, member 4	-2.15521
DNAJC15	DnaJ (Hsp40) homolog, subfamily C, member 15	-3.21689
DNAJC6	DnaJ (Hsp40) homolog, subfamily C, member 6	-1.51549
DNM3OS	DNM3 opposite strand/antisense RNA	1.91143
DNMBP	dynamin binding protein	1.06954
DOCK7	dedicator of cytokinesis 7	1.23904
DOK5	docking protein 5	inf
DPM3	dolichyl-phosphate mannosyltransferase polypeptide	-1.36268
DPP6	dipeptidyl-peptidase 6	inf
DPY19L1	dpy-19-like 1 (C. elegans); similar to hCG1645499	1.25509
DPYSL3	dihydropyrimidinase-like 3	-1.8657
DRAP1	DR1-associated protein 1 (negative cofactor 2 alpha	-1.45234
DRP2	dystrophin related protein 2	3.49499
DSP	desmoplakin	1.43308
DTNA	dystrobrevin, alpha	1.49901
DUSP7	dual specificity phosphatase 7	-0.872847
DYRK3	dual-specificity tyrosine-(Y)-phosphorylation regulate	-1.13724
EBF1	early B-cell factor 1	2.69508
ECE1	endothelin converting enzyme 1	-1.4237
ECH1	enoyl Coenzyme A hydratase 1, peroxisomal	1.06097
ECM1	extracellular matrix protein 1	-1.59787
EDEM3	ER degradation enhancer, mannosidase alpha-like 3	1.18644
EDIL3	EGF-like repeats and discoidin I-like domains 3	3.58966
EDN1	endothelin 1	2.69965
EDNRA	endothelin receptor type A	3.02633
EEA1	early endosome antigen 1	0.748717
EEF2K	eukaryotic elongation factor-2 kinase	1.19295
EFCAB2	EF-hand calcium binding domain 2	-1.14182
EFHA2	EF-hand domain family, member A2	1.37444
EFS	embryonal Fyn-associated substrate	2.32565
EGLN1	egl nine homolog 1 (C. elegans)	0.91977
EGR1	early growth response 1	-2.80541
EIF1	similar to eukaryotic translation initiation factor 1; eul	-0.886446
EIF2B2	eukaryotic translation initiation factor 2B, subunit 2 b	-1.14541
EIF4EBP1	eukaryotic translation initiation factor 4E binding prot	-0.798792
EIF5B	eukaryotic translation initiation factor 5B	0.884016
ELOVL6	ELOVL family member 6, elongation of long chain fa	1.09481
EMB	embigin homolog (mouse)	4.4359
EMILIN1	elastin microfibril interfacer 1	0.91782
EMILIN2	elastin microfibril interfacer 2	-3.85787
EML1	echinoderm microtubule associated protein like 1	-1.3169
EML2	echinoderm microtubule associated protein like 2	-1.35044
EMP1	epithelial membrane protein 1	1.17646
EMR2	egf-like module containing, mucin-like, hormone rec	-1.9149
EMX2	empty spiracles homeobox 2	3.05693
ENAH	enabled homolog (Drosophila)	0.750457
ENC1	ectodermal-neural cortex (with BTB-like domain)	1.6565
ENPP1	ectonucleotide pyrophosphatase/phosphodiesterase	-1.47876
ENY2	enhancer of yellow 2 homolog (Drosophila)	0.79612
EPAS1	endothelial PAS domain protein 1	-2.84778
EPB41L1	erythrocyte membrane protein band 4.1-like 1	1.40027
EPHA5	EPH receptor A5	5.09744
EPHB2	EPH receptor B2	4.86398
EPHB4	EPH receptor B4	1.48017
EPM2AIP1	EPM2A (laforin) interacting protein 1	1.1658
EPSTI1	epithelial stromal interaction 1 (breast)	-1.98292
EPT1	selenoprotein I	0.977814
ERCC1	excision repair cross-complementing rodent repair d	-1.02249

ERN1	endoplasmic reticulum to nucleus signaling 1	-2.61485
ESAM	endothelial cell adhesion molecule	-inf
ESM1	endothelial cell-specific molecule 1	-2.48189
EVA1C	eva-1 homolog C (C. Elegans)	-1.90607
EVL	Enah/Vasp-like	3.28693
EXOC5	exocyst complex component 5	0.826216
EXTL3	exostoses (multiple)-like 3	1.27224
EYA3	eyes absent homolog 3 (Drosophila)	0.932061
F2RL2	coagulation factor II (thrombin) receptor-like 2	2.71598
F3	coagulation factor III (thromboplastin, tissue factor)	-4.65222
F8A1	coagulation factor VIII-associated (intronic transcript	1.80648
FABP5	fatty acid binding protein 5-like 2; fatty acid binding p	0.909151
FADS2	fatty acid desaturase 2	-0.910657
FADS3	fatty acid desaturase 3	-2.46254
FAHD2B	fumarylacetoacetate hydrolase domain containing 2I	-2.41446
FAM100B	family with sequence similarity 100, member B	-1.62775
FAM101B	hypothetical protein LOC100133632; family with seq	0.829994
FAM102B	family with sequence similarity 102, member B	-2.12812
FAM105A	family with sequence similarity 105, member A	-5.04816
FAM115C	family with sequence similarity 115, member C; fami	1.45379
FAM127C	family with sequence similarity 127, member C; hypo	1.08822
FAM149B1	family with sequence similarity 149, member B1	-0.915872
FAM156A	family with sequence similarity 156, member A; fami	3.62284
FAM160B1	family with sequence similarity 160, member B1	0.853713
FAM162B	family with sequence similarity 162, member B	-3.55294
FAM171A1	family with sequence similarity 171, member A1	1.96446
FAM173B	family with sequence similarity 173, member B	1.27539
FAM19A5	family with sequence similarity 19 (chemokine (C-C	inf
FAM206A	family with sequence similarity 206, member A	-1.35426
FAM20B	family with sequence similarity 20, member B	0.992194
FAM210B	family with sequence similarity 210, member B	0.815229
FAM21B	family with sequence similarity 21, member B; family	-inf
FAM3C	family with sequence similarity 3, member C	1.1279
FAM63B	family with sequence similarity 63, member B	1.43031
FAM65A	family with sequence similarity 65, member A	-0.812135
FAM83D	family with sequence similarity 83, member D	-1.1053
FAM98A	family with sequence similarity 98, member A	0.852854
FAM98B	family with sequence similarity 98, member B	0.87878
FANCM	Fanconi anemia, complementation group M	1.23376
FAP	fibroblast activation protein, alpha	2.15828
FARP1	FERM, RhoGEF (ARHGEF) and pleckstrin domain p	-1.09358
FBLN1	fibulin 1	2.24302
FBLN2	fibulin 2	-1.97545
FBLN5	fibulin 5	1.23585
FBN1	fibrillin 1	0.767791
FBXL2	F-box and leucine-rich repeat protein 2	-1.33678
FBXL7	F-box and leucine-rich repeat protein 7	-1.08072
FBXO4	F-box protein 4	-1.46901
FBXW5	F-box and WD repeat domain containing 5	-1.20055
FCHO1	FCH domain only 1	-3.80109
FCHSD1	FCH and double SH3 domains 1	-1.15864
FCHSD2	FCH and double SH3 domains 2	-0.957955
FDXR	ferredoxin reductase	-1.56914
FEN1	flap structure-specific endonuclease 1	1.03001
FER1L4	fer-1-like 4 (C. elegans)	-1.36104
FERMT1	fermitin family homolog 1 (Drosophila)	-2.7883
FGD4	FYVE, RhoGEF and PH domain containing 4	1.29177
FGF2	fibroblast growth factor 2 (basic)	-1.2029
FHL1	four and a half LIM domains 1	-1.74194
FHOD3	formin homology 2 domain containing 3	1.94733
FIBIN	fin bud initiation factor homolog (zebrafish)	2.87582
FILIP1	filamin A interacting protein 1	-3.05188
FKBP9L	FK506 binding protein 9-like	1.44545
FLJ42627	hypothetical LOC645644	3.74231
FLJ45340	hypothetical LOC402483; similar to capicua-like prot	1.39366
FLNC	filamin C, gamma (actin binding protein 280)	0.909861
FLOT1	flotillin 1	-0.980214
FLRT3	fibronectin leucine rich transmembrane protein 3	5.01167
FMN2	formin 2	1.36628
FNBP1L	formin binding protein 1-like	2.49282
FOLR3	folate receptor 3 (gamma)	-inf
FOSL2	FOS-like antigen 2	-1.10946

FOXD1	forkhead box D1	1.278
FOXF2	forkhead box F2	-2.96617
FOXN3	forkhead box N3	1.47012
FOXO3	forkhead box O3; forkhead box O3B pseudogene	1.03703
FRAS1	Fraser syndrome 1	6.00799
FRMD3	FERM domain containing 3	1.00267
FRMD4A	FERM domain containing 4A	0.952147
FRMPD4	FERM and PDZ domain containing 4	-2.14447
FRYL	FRY-like	0.942554
FUS	fusion (involved in t(12;16) in malignant liposarcoma	0.807373
FUT8	fucosyltransferase 8 (alpha (1,6) fucosyltransferase)	1.55209
FXYD5	FXYD domain containing ion transport regulator 5	-1.14422
FYCO1	FYVE and coiled-coil domain containing 1	0.986025
FZD1	frizzled homolog 1 (Drosophila)	1.71073
FZD4	frizzled homolog 4 (Drosophila)	-1.71385
G0S2	G0/G1switch 2	-6.69607
G3BP1	GTPase activating protein (SH3 domain) binding prc	1.04477
GABBR2	gamma-aminobutyric acid (GABA) B receptor, 2	4.68423
GADD45A	growth arrest and DNA-damage-inducible, alpha	-1.09578
GADD45B	growth arrest and DNA-damage-inducible, beta	-1.47781
GALNT1	UDP-N-acetyl-alpha-D-galactosamine:polypeptide N	1.00392
GALNT10	UDP-N-acetyl-alpha-D-galactosamine:polypeptide N	1.52515
GALNT2	UDP-N-acetyl-alpha-D-galactosamine:polypeptide N	0.94851
GALNT3	UDP-N-acetyl-alpha-D-galactosamine:polypeptide N	3.96136
GALNT5	UDP-N-acetyl-alpha-D-galactosamine:polypeptide N	1.00265
GALNT7	UDP-N-acetyl-alpha-D-galactosamine:polypeptide N	1.78008
GALNTL2	UDP-N-acetyl-alpha-D-galactosamine:polypeptide N	1.89482
GANC	glucosidase, alpha; neutral C	1.4026
GAP43	growth associated protein 43	inf
GAS2L3	growth arrest-specific 2 like 3	-1.92197
GAS5	growth arrest-specific 5 (non-protein coding)	-0.926889
GAS6	similar to growth arrest-specific 6; growth arrest-spe	-0.78806
GATAD2B	GATA zinc finger domain containing 2B	0.985028
GBP3	guanylate binding protein 3	-1.10648
GDF15	growth differentiation factor 15	-1.94194
GDNF	glial cell derived neurotrophic factor	3.31722
GGA2	golgi associated, gamma adaptin ear containing, AR	0.995662
GHR	growth hormone receptor	3.52875
GJA1	gap junction protein, alpha 1, 43kDa	1.52568
GLCCI1	glucocorticoid induced transcript 1	1.06217
GLIPR1	GLI pathogenesis-related 1	3.09151
GLIS2	GLIS family zinc finger 2	-1.32179
GLRB	glycine receptor, beta	-1.25349
GLS	glutaminase	0.967195
GLUL	glutamate-ammonia ligase (glutamine synthetase)	-1.20263
GM2A	GM2 ganglioside activator	-0.9274
GMFB	glia maturation factor, beta	1.17835
GNA12	guanine nucleotide binding protein (G protein) alpha	-1.07038
GNAQ	guanine nucleotide binding protein (G protein), q pol	0.879318
GNB4	guanine nucleotide binding protein (G protein), beta	1.22141
GNG2	guanine nucleotide binding protein (G protein), gamr	2.4221
GOLGA8A	golgi autoantigen, golgin subfamily a, 8B; golgi autoa	1.07817
GOLM1	golgi membrane protein 1	1.79907
GOT1	glutamic-oxaloacetic transaminase 1, soluble (aspar	-1.88783
GPBP1	GC-rich promoter binding protein 1	-0.780635
GPC1	glypican 1	-1.05326
GPC6	glypican 6	1.271
GPM6B	glycoprotein M6B	3.14969
GPR155	G protein-coupled receptor 155	1.31649
GPR176	G protein-coupled receptor 176	-0.80256
GPX4	glutathione peroxidase 4 (phospholipid hydroperoxid	-0.976611
GRAMD3	GRAM domain containing 3	-0.92356
GRB14	growth factor receptor-bound protein 14	2.96493
GREM1	gremlin 1, cysteine knot superfamily, homolog (Xenc	-2.99277
GRHPR	glyoxylate reductase/hydroxypyruvate reductase	-0.88368
GRIA1	glutamate receptor, ionotropic, AMPA 1	1.72969
GRSF1	G-rich RNA sequence binding factor 1	0.817898
GSTA4	glutathione S-transferase alpha 4	1.02708
GSTM4	glutathione S-transferase mu 4	-1.72633
GULP1	GULP, engulfment adaptor PTB domain containing 1	-2.47147
GUSB	glucuronidase, beta	-1.05278
GXYLT1	glycosyltransferase 8 domain containing 3	1.04251

GYG2	glycogenin 2	2.5253
H1F0	H1 histone family, member 0	-2.48234
H1FX	H1 histone family, member X	-1.90722
HCFC1R1	host cell factor C1 regulator 1 (XPO1 dependent)	-1.08458
HCLS1	hematopoietic cell-specific Lyn substrate 1	-6.6458
HECTD2	HECT domain containing 2	1.30276
HELZ	helicase with zinc finger	0.995185
HERC2P7	hect domain and RLD 2 pseudogene 7	inf
HERPUD1	homocysteine-inducible, endoplasmic reticulum stre	-0.984702
HEY1	hairy/enhancer-of-split related with YRPW motif 1	-2.36771
HFE	hemochromatosis	-1.21649
HHIP	hedgehog interacting protein	3.63982
HHIP-AS1	HHIP antisense RNA 1	2.30151
HIC1	hypermethylated in cancer 1	-1.4375
HINT1	histidine triad nucleotide binding protein 1	-1.09043
HIPK2	homeodomain interacting protein kinase 2; similar to	0.84467
HJURP	Holliday junction recognition protein	-1.22585
HLA-A	major histocompatibility complex, class I, A	-0.821578
HLA-C	major histocompatibility complex, class I, C; major hi	1.82993
HLA-E	major histocompatibility complex, class I, E	-1.20576
HLX	H2.0-like homeobox	-2.038
HMGA2	high mobility group AT-hook 2	1.89086
HMGB1	high-mobility group box 1; high-mobility group box 1-	0.797918
HNMT	histamine N-methyltransferase	-3.0376
HNRNPL	similar to heterogeneous nuclear ribonucleoprotein L	1.05643
HNRNPM	heterogeneous nuclear ribonucleoprotein M	1.12647
HNRNPU	heterogeneous nuclear ribonucleoprotein U (scaffold	0.977889
HNRPLL	heterogeneous nuclear ribonucleoprotein L-like	1.0212
HOMER1	homer homolog 1 (Drosophila)	1.47924
HOMER3	homer homolog 3 (Drosophila)	-0.988472
HOOK3	hook homolog 3 (Drosophila)	0.992316
HOPX	HOP homeobox	1.89295
HOXA10-HOXA9	homeobox A10 - homeobox A9	-7.13909
HOXA11-AS	HOXA11 antisense RNA	-inf
HOXB-AS3	HOXB cluster antisense RNA 3	inf
HOXB4	homeobox B4	inf
HOXB5	homeobox B5	inf
HOXB6	homeobox B6	inf
HOXB8	homeobox B8	inf
HOXC10	homeobox C10	2.44632
HOXC4-5-6	homeobox C4 - homeobox C5 - homeobox C6	3.82751
HOXC8	homeobox C8	6.85905
HOXC9	homeobox C9	1.22503
HOXD-AS1	HOXD cluster antisense RNA 1	3.33391
HOXD12	homeobox D12	-inf
HOXD13	homeobox D13	-inf
HOXD9	homeobox D9	-2.10587
HPCAL1	hippocalcin-like 1	-2.91195
HSBP1L1	heat shock factor binding protein 1-like	-2.77585
HSPA1A	heat shock 70kDa protein 1A; heat shock 70kDa pro	2.25994
HSPA1B	heat shock 70kDa protein 1A; heat shock 70kDa pro	1.85133
HSPA2	heat shock 70kDa protein 2	-2.1368
HSPD1	heat shock 60kDa protein 1 (chaperonin) pseudoger	0.916597
HSPH1	heat shock 105kDa/110kDa protein 1	1.02258
HTATSF1P2	HIV-1 Tat specific factor 1 pseudogene 2	-4.01519
HTR7P1	5-hydroxytryptamine (serotonin) receptor 7 pseudoge	2.50236
HTRA1	HtrA serine peptidase 1	-1.20197
HYAL3-NAT6	Hyaluronoglucosaminidase 3 - N-acetyltransferase (	-1.47789
HYLS1	hydrolethalus syndrome 1	-2.25236
IAH1	isoamyl acetate-hydrolyzing esterase 1 homolog (S.	-0.999219
ICAM1	intercellular adhesion molecule 1	-4.01889
ICAM5	intercellular adhesion molecule 5, telencephalin	-2.07951
ICK	intestinal cell (MAK-like) kinase	1.14282
ID2	inhibitor of DNA binding 2, dominant negative helix-l	3.01118
IDE	insulin-degrading enzyme	1.13843
IER3	immediate early response 3	-1.50332
IFI27L2	interferon, alpha-inducible protein 27-like 2	-1.28116
IFI35	interferon-induced protein 35	-1.85921
IFI44	interferon-induced protein 44	1.99545
IFIH1	interferon induced with helicase C domain 1	-2.12642
IFITM1	interferon induced transmembrane protein 1 (9-27)	-1.5045
IFITM2	interferon induced transmembrane protein 2 (1-8D)	-1.64381

IFITM3	interferon induced transmembrane protein 3 (1-8U)	-1.38122
IFNAR1	interferon (alpha, beta and omega) receptor 1	1.02002
IFNGR1	interferon gamma receptor 1	-0.984212
IFRD1	interferon-related developmental regulator 1	-0.927675
IGF1R	insulin-like growth factor 1 receptor	0.902806
IGF2BP1	insulin-like growth factor 2 mRNA binding protein 1	2.00907
IGF2BP2	insulin-like growth factor 2 mRNA binding protein 2	-0.79061
IGF2BP3	insulin-like growth factor 2 mRNA binding protein 3	1.06442
IGFBP3	insulin-like growth factor binding protein 3	3.92219
IGFBP5	insulin-like growth factor binding protein 5	3.1166
IGFBP7	insulin-like growth factor binding protein 7	-1.54497
IKZF2	IKAROS family zinc finger 2 (Helios)	1.27753
IL10RB	interleukin 10 receptor, beta	-1.05597
IL32	interleukin 32	-3.03102
IL7R	interleukin 7 receptor	-3.34722
IL8	interleukin 8	-4.37071
IMPAD1	inositol monophosphatase domain containing 1	0.991612
INA	internexin neuronal intermediate filament protein, alp	4.45129
ING2	inhibitor of growth family, member 2	-1.34412
INPP1	inositol polyphosphate-1-phosphatase	-1.32143
INPP4B	inositol polyphosphate-4-phosphatase, type II, 105kD	-2.01152
INSIG1	insulin induced gene 1	-1.69197
IPW	imprinted in Prader-Willi syndrome (non-protein codi	2.33296
IQCB1	IQ motif containing B1	-1.22219
IQGAP1	IQ motif containing GTPase activating protein 1	0.837213
IQGAP3	IQ motif containing GTPase activating protein 3	-1.42997
IRAK3	interleukin-1 receptor-associated kinase 3	-5.15571
IRAK4	interleukin-1 receptor-associated kinase 4	1.30373
IRF1	interferon regulatory factor 1	-1.60238
IRF2	interferon regulatory factor 2	-1.21716
IRX2	iroquois homeobox 2	2.97669
IRX5	iroquois homeobox 5	-2.78844
ITGA1-PELO	integrin, alpha 1 - pelota homolog (Drosophila)	-0.996068
ITGA10	integrin, alpha 10	2.32336
ITGA2	integrin, alpha 2 (CD49B, alpha 2 subunit of VLA-2 r	2.63657
ITGA4	integrin, alpha 4 (antigen CD49D, alpha 4 subunit of	-1.32241
ITGA5	integrin, alpha 5 (fibronectin receptor, alpha polypep	0.852733
ITGAV	integrin, alpha V (vitronectin receptor, alpha polypep	0.981272
ITGBL1	integrin, beta-like 1 (with EGF-like repeat domains)	2.22384
ITPR2	inositol 1,4,5-triphosphate receptor, type 2	1.34505
JAM2	junctional adhesion molecule 2	2.75744
JDP2	Jun dimerization protein 2	-1.36843
JRKL	jerky homolog-like (mouse)	1.05758
JUNB	jun B proto-oncogene	-1.58681
JUND	jun D proto-oncogene	-1.16647
KBTBD6	kelch repeat and BTB (POZ) domain containing 6	1.06208
KBTBD8	kelch repeat and BTB (POZ) domain containing 8	2.92384
KCNE4	potassium voltage-gated channel, Isk-related family,	2.42894
KCNJ8	potassium inwardly-rectifying channel, subfamily J, r	1.73682
KCNK2	potassium channel, subfamily K, member 2	0.888359
KCNQ3	potassium voltage-gated channel, KQT-like subfamil	4.23663
KCNQ5	potassium voltage-gated channel, KQT-like subfamil	1.4318
KCTD12	potassium channel tetramerisation domain containin	2.71563
KCTD16	potassium channel tetramerisation domain containin	2.40081
KDR	kinase insert domain receptor (a type III receptor tyrc	inf
KHDRBS3	KH domain containing, RNA binding, signal transduc	-1.84926
KIAA0391	KIAA0391	0.997664
KIAA0408-SOGA3	KIAA0408 - SOGA family member 3	-1.12752
KIAA1147	KIAA1147	1.31772
KIAA1217	KIAA1217	3.64925
KIAA1456	KIAA1456	-2.33334
KIAA1462	KIAA1462	1.65147
KIAA1549L	KIAA1549L	0.94839
KIAA1598	KIAA1598	2.45778
KIF14	kinesin family member 14	-0.897447
KIF2C	kinesin family member 2C	-0.888528
KIFC3	kinesin family member C3	-1.92175
KIT	similar to Mast/stem cell growth factor receptor precu	2.04094
KITLG	KIT ligand	0.76707
KLF10	Kruppel-like factor 10	0.866038
KLF4	Kruppel-like factor 4 (gut)	-1.87634
KLF5	Kruppel-like factor 5 (intestinal)	-2.44426

KLHL29	kelch-like 29 (Drosophila)	1.4157
KLHL9	kelch-like 9 (Drosophila)	1.35535
KRBOX1	KRAB box domain containing 1	-1.77955
KRCC1	lysine-rich coiled-coil 1	-0.887558
KRR1	KRR1, small subunit (SSU) processome component	1.62807
KRT19	keratin 19	0.890488
KRT34	keratin 34	-3.08787
KRTAP2-3	keratin associated protein 2-1; keratin associated pr	-2.47193
KRTAP3-1	keratin associated protein 3-1	-inf
KRTCAP2	keratinocyte associated protein 2	-0.940404
L3MBTL3	l(3)mbt-like 3 (Drosophila)	1.46059
LAMA1	laminin, alpha 1	1.35974
LAMA2	laminin, alpha 2	-5.47237
LANCL1	LanC lantibiotic synthetase component C-like 1 (bac	1.19459
LCE2A	late cornified envelope 2A	-2.07037
LDOC1	leucine zipper, down-regulated in cancer 1	3.22106
LGALS1	lectin, galactoside-binding, soluble, 1	-1.53186
LHFP	lipoma HMGIC fusion partner	-1.94153
LHPP	phospholysine phosphohistidine inorganic pyrophosp	-2.96725
LIFR	leukemia inhibitory factor receptor alpha	1.63513
LINC00467	long intergenic non-protein coding RNA 467	-2.04789
LINC00657	long intergenic non-protein coding RNA 657	1.02389
LITAF	lipopolysaccharide-induced TNF factor	-4.53655
LOC100134259	similar to hCG1987718	-2.31247
LOC100144602	hypothetical	inf
LOC100190986	hypothetical LOC100190986	inf
LOC100294145	hypothetical protein LOC100294145	1.49293
LOC100505491		4.69634
LOC100506123		1.44719
LOC100506453		inf
LOC100506518		-1.80099
LOC100506548		1.06119
LOC100506844		-1.00058
LOC100506948		1.57331
LOC100507053		3.02992
LOC100507127		-3.28069
LOC100507165		-2.70221
LOC100507420-LOC100507439		1.69455
LOC100996242		inf
LOC100996277		inf
LOC152742	hypothetical protein LOC152742	-3.5702
LOC344595	hypothetical LOC344595	1.71968
LOC375295	hypothetical protein LOC375295	2.21159
LOC388796	hypothetical LOC388796	-2.57018
LOC400027	hypothetical protein LOC400027	1.45189
LOC441528	hypothetical protein LOC441528; similar to hCG198	inf
LOC646329	hypothetical LOC646329	1.27377
LOC646719	hypothetical LOC646719	1.93115
LOC728392	hypothetical protein LOC728392	3.55366
LOC728730	hypothetical LOC728730	-1.46861
LOC730101	hypothetical LOC730101	-0.829729
LOC730102	hypothetical protein LOC730102	-2.44679
LOC90246	hypothetical protein LOC90246	2.43129
LONRF1	LON peptidase N-terminal domain and ring finger 1	-2.13581
LOX	lysyl oxidase	1.43598
LPCAT2	lysophosphatidylcholine acyltransferase 2	2.70662
LPCAT4	lysophosphatidylcholine acyltransferase 4	-1.16844
LPHN2	latrophilin 2	3.35194
LPP	LIM domain containing preferred translocation partne	1.14905
LRBA	LPS-responsive vesicle trafficking, beach and ancho	1.3983
LRFN5	leucine rich repeat and fibronectin type III domain co	-inf
LRIF1	ligand dependent nuclear receptor interacting factor	-1.38102
LRP4	low density lipoprotein receptor-related protein 4	2.68745
LRRC17	leucine rich repeat containing 17	2.62118
LRRC37A4P	leucine rich repeat containing 37, member A4, pseu	2.13854
LRRC8B	leucine rich repeat containing 8 family, member B	3.5717
LRRFIP2	leucine rich repeat (in FLII) interacting protein 2	-0.901066
LTBP2	latent transforming growth factor beta binding protei	1.44772
LTBR	lymphotoxin beta receptor (TNFR superfamily, meml	-1.08803
LUM	lumican	-2.91782
LY6E	lymphocyte antigen 6 complex, locus E	-0.900249
LY75-CD302	lymphocyte antigen 75 - CD302 molecule	-1.24544

MAD2L2	MAD2 mitotic arrest deficient-like 2 (yeast)	-1.68487
MAFF	v-maf musculoaponeurotic fibrosarcoma oncogene h	-1.14794
MAGED1	melanoma antigen family D, 1	0.776822
MAGI1	membrane associated guanylate kinase, WW and P	1.22238
MAGI2-AS3	MAGI2 antisense RNA 3	-1.62109
MAMDC2	MAM domain containing 2	-2.85811
MAN1A1	mannosidase, alpha, class 1A, member 1	2.09409
MAP1A	microtubule-associated protein 1A	1.30931
MAP1B	microtubule-associated protein 1B	0.944347
MAP2K3	mitogen-activated protein kinase kinase 3	-1.01027
MAP7D3	MAP7 domain containing 3	2.80351
MAPK13	mitogen-activated protein kinase 13	-2.9206
MAPK8	mitogen-activated protein kinase 8	-1.01305
MARC2	mitochondrial amidoxime reducing component 2	-3.02562
MARCKS	myristoylated alanine-rich protein kinase C substrate	1.67687
MARCKSL1	MARCKS-like 1	3.36511
MARK1	MAP/microtubule affinity-regulating kinase 1	inf
MARS	methionyl-tRNA synthetase	-0.805528
MASP1	mannan-binding lectin serine peptidase 1 (C4/C2 ac	-3.02318
MAT2A	methionine adenosyltransferase II, alpha	-1.83962
MATN2	matrilin 2	-3.51999
MBOAT2	membrane bound O-acyltransferase domain contain	1.02863
MCAM	melanoma cell adhesion molecule	1.71038
MCTP1	multiple C2 domains, transmembrane 1	-3.05574
MCTP2	multiple C2 domains, transmembrane 2	-2.29342
MDK	midkine (neurite growth-promoting factor 2)	2.49801
MDN1	MDN1, midasin homolog (yeast)	0.862162
MECOM	ecotropic viral integration site 1	1.30286
MED28	mediator complex subunit 28	1.15803
MEF2A	myocyte enhancer factor 2A	0.825775
MEST	mesoderm specific transcript homolog (mouse)	1.58624
METRNL	meteorin, glial cell differentiation regulator-like; simil	-2.01577
METTL9	methyltransferase like 9	0.987785
MEX3A	mex-3 homolog A (C. elegans)	1.55964
MFAP4	microfibrillar-associated protein 4	3.01033
MGARP	mitochondria-localized glutamic acid-rich protein	-2.25983
MGC45800	hypothetical LOC90768	2.47778
MGMT	O-6-methylguanine-DNA methyltransferase	-3.3289
MGP	matrix Gla protein	inf
MGST1	microsomal glutathione S-transferase 1	-1.88079
MID1IP1	MID1 interacting protein 1 (gastrulation specific G12	-1.2981
MID2	midline 2	-2.50339
MIOS	missing oocyte, meiosis regulator, homolog (Drosop	0.86629
MITF	microphthalmia-associated transcription factor	-5.48937
MKI67	antigen identified by monoclonal antibody Ki-67	-1.00064
MKNK1	MAP kinase interacting serine/threonine kinase 1	-1.0802
MKNK2	MAP kinase interacting serine/threonine kinase 2	-1.24334
MKX	mohawk homeobox	-5.70329
MLH3	mutL homolog 3 (E. coli)	2.80764
MLLT11	myeloid/lymphoid or mixed-lineage leukemia (trithora	2.4135
MLLT3	myeloid/lymphoid or mixed-lineage leukemia (trithora	-1.70287
MMP1	matrix metallopeptidase 1 (interstitial collagenase)	2.75702
MMP16	matrix metallopeptidase 16 (membrane-inserted)	1.66101
MMP2	matrix metallopeptidase 2 (gelatinase A, 72kDa gela	2.33847
MMP24	matrix metallopeptidase 24 (membrane-inserted)	3.49951
MOAP1	modulator of apoptosis 1	1.26046
MOB3C	MOB kinase activator 3C	-1.29113
MOCOS	molybdenum cofactor sulfurase	-3.38138
MOK	MOK protein kinase	-2.63255
MOXD1	monooxygenase, DBH-like 1	-0.854693
MPP1	membrane protein, palmitoylated 1, 55kDa	-1.77838
MR1	major histocompatibility complex, class I-related	-2.02344
MRPL23	mitochondrial ribosomal protein L23	-1.19076
MRPL4	mitochondrial ribosomal protein L4	-1.08451
MRPL42	mitochondrial ribosomal protein L42	0.827851
MRPS6-SLC5A3	mitochondrial ribosomal protein S6 - solute carrier f	1.79322
MSL3P1	male-specific lethal 3 homolog (Drosophila) pseudo	-1.37712
MSN	moesin	0.741884
MT1E	metallothionein 1L (gene/pseudogene); metallothion	1.01068
MT1L	metallothionein 1L (gene/pseudogene); metallothion	-1.02695
MT3	metallothionein 3	inf
MTHFD2	methylenetetrahydrofolate dehydrogenase (NADP+	-1.11692

MTPN	myotrophin; leucine zipper protein 6	0.883325
MTRNR2L1	MT-RNR2-like 1	1.22132
MTRNR2L10	MT-RNR2-like 10	inf
MTRNR2L8	MT-RNR2-like 8	8.61338
MTSS1	metastasis suppressor 1	-1.65331
MTSS1L	metastasis suppressor 1-like	-1.24368
MYBL1	v-myb myeloblastosis viral oncogene homolog (avia	-1.21896
MYEF2	myelin expression factor 2	-1.4748
MYO10	myosin X	1.04454
MYO1B	myosin IB	0.997485
MYOZ2	myozenin 2	4.62989
N4BP2	NEDD4 binding protein 2	1.35009
NAA15	NMDA receptor regulated 1	0.891006
NALCN	sodium leak channel, non-selective	2.13203
NAT1	N-acetyltransferase 1 (arylamine N-acetyltransferase	-1.60318
NAV1	neuron navigator 1	1.15644
NBLA00301	Nbla00301	inf
NBPF3	neuroblastoma breakpoint family, member 3	-1.25687
NCAM1	neural cell adhesion molecule 1	-2.75511
NCAM2	neural cell adhesion molecule 2	inf
NCBP1	nuclear cap binding protein subunit 1, 80kDa	0.924867
NCEH1	arylacetamide deacetylase-like 1	-1.00781
NCK1	NCK adaptor protein 1	-1.155
NDE1	nudE nuclear distribution gene E homolog 1 (A. nidu	-1.08489
NDN	necdin homolog (mouse)	3.12353
NDNF	neuron-derived neurotrophic factor	2.78448
NDST1	N-deacetylase/N-sulfotransferase (heparan glucosar	0.812278
NEAT1	non-protein coding RNA 84	1.61578
NEK11	NIMA (never in mitosis gene a)- related kinase 11	-1.37715
NEK2	NIMA (never in mitosis gene a)-related kinase 2	-1.2498
NET1	neuroepithelial cell transforming 1	0.847237
NETO1	neuropilin (NRP) and tolloid (TLL)-like 1	-2.15051
NETO2	neuropilin (NRP) and tolloid (TLL)-like 2	6.14029
NEURL1B	neuralized homolog 1B (Drosophila)	-1.61782
NFE2L2	nuclear factor (erythroid-derived 2)-like 2	-1.09039
NFKB1	nuclear factor of kappa light polypeptide gene enhar	-1.06052
NFKB2	nuclear factor of kappa light polypeptide gene enhar	-1.41833
NFKBIE	nuclear factor of kappa light polypeptide gene enhar	-2.50551
NFXL1	nuclear transcription factor, X-box binding-like 1	-1.6987
NFYA	nuclear transcription factor Y, alpha	1.07557
NID2	nidogen 2 (osteonidogen)	0.934174
NIPAL2	NIPA-like domain containing 2	-1.70044
NLGN1	neuroligin 1	-1.79861
NLGN4Y	neuroligin 4, Y-linked	1.84538
NMT2	N-myristoyltransferase 2	1.12792
NNMT	nicotinamide N-methyltransferase	-1.7006
NOB1	NIN1/RPN12 binding protein 1 homolog (S. cerevisia	-0.96998
NOTCH2	Notch homolog 2 (Drosophila)	0.864433
NOTCH2NL	Notch homolog 2 (Drosophila) N-terminal like	1.14348
NOTCH3	Notch homolog 3 (Drosophila)	-1.67148
NPIPL3	nuclear pore complex interacting protein-like 3; simil	2.56145
NQO1	NAD(P)H dehydrogenase, quinone 1	-3.15695
NR1D2	nuclear receptor subfamily 1, group D, member 2	-1.04063
NR2F1	nuclear receptor subfamily 2, group F, member 1	-1.42756
NRCAM	neuronal cell adhesion molecule	4.2517
NREP	neuronal regeneration related protein	1.96124
NRG1	neuregulin 1	-2.2647
NRGN	neurogranin (protein kinase C substrate, RC3)	-3.11498
NRK	Nik related kinase	10.2053
NRN1	neuritin 1	7.91488
NRP2	neuropilin 2	1.6744
NT5E	5'-nucleotidase, ecto (CD73)	-1.15946
NTF3	neurotrophin 3	2.11497
NTNG1	netrin G1	2.26727
NUDT11	nudix (nucleoside diphosphate linked moiety X)-type	1.47389
NUDT12	nudix (nucleoside diphosphate linked moiety X)-type	-1.62258
NUF2	NUF2, NDC80 kinetochore complex component, hor	-0.879882
NUPR1	nuclear protein, transcriptional regulator, 1	-3.4198
NYNRIN	KIAA1305	1.36406
OAF	OAF homolog (Drosophila)	-2.70124
OAZ1	ornithine decarboxylase antizyme 1	-1.1338
OGFRL1	opioid growth factor receptor-like 1	-2.43307

OLAH	oleoyl-ACP hydrolase	inf
OLFML3	olfactomedin-like 3	2.01766
OPTN	optineurin	-1.35844
OSBPL6	oxysterol binding protein-like 6	-1.19287
OSR1	odd-skipped related 1 (Drosophila)	1.93259
OSR2	odd-skipped related 2 (Drosophila)	-4.18878
OXTR	oxytocin receptor	-2.45369
PAG1	phosphoprotein associated with glycosphingolipid m	-2.00815
PAK4	p21 protein (Cdc42/Rac)-activated kinase 4	-1.28142
PAPPA	PAPPA antisense RNA (non-protein coding); pregna	2.40688
PAR5	Prader-Willi/Angelman syndrome-5	1.72947
PARD3B	par-3 partitioning defective 3 homolog B (C. elegans	-1.43165
PARG	similar to poly (ADP-ribose) glycohydrolase; poly (AD	1.60789
PARP1	poly (ADP-ribose) polymerase 1	0.809193
PARP4	poly (ADP-ribose) polymerase family, member 4	0.786836
PARVB	parvin, beta	-1.27771
PBRM1	polybromo 1	1.21802
PCDH10	protocadherin 10	3.49047
PCDH18	protocadherin 18	-0.779012
PCDHGA1-12	protocadherin gamma subfamily A, 1 – 12	1.11457
PCGF5	polycomb group ring finger 5	1.73758
PCK2	phosphoenolpyruvate carboxykinase 2 (mitochondria	-1.73228
PCOLCE	procollagen C-endopeptidase enhancer	1.13719
PCOLCE2	procollagen C-endopeptidase enhancer 2	inf
PDE12	phosphodiesterase 12	1.16224
PDE1C	phosphodiesterase 1C, calmodulin-dependent 70kD	-2.71687
PDE4D	phosphodiesterase 4D, cAMP-specific (phosphodies	-0.892858
PDE7B	phosphodiesterase 7B	4.06662
PDGFC	platelet derived growth factor C	-0.810702
PDGFRA	platelet-derived growth factor receptor, alpha polype	2.1335
PDK1	pyruvate dehydrogenase kinase, isozyme 1	1.74615
PDLIM4	PDZ and LIM domain 4	1.37014
PDZRN3	PDZ domain containing ring finger 3	2.82411
PEA15	phosphoprotein enriched in astrocytes 15	-0.77804
PEAR1	platelet endothelial aggregation receptor 1	4.22289
PER1	period homolog 1 (Drosophila)	-1.90519
PFN2	profilin 2	0.737425
PGLS	6-phosphogluconolactonase	-1.18503
PGM2	phosphoglucomutase 2	-1.54733
PGM2L1	phosphoglucomutase 2-like 1	3.06574
PHACTR2	phosphatase and actin regulator 2	1.6092
PHB2	prohibitin 2	-0.963147
PHGDH	phosphoglycerate dehydrogenase	-1.18643
PHIP	pleckstrin homology domain interacting protein	0.782513
PHKA1	phosphorylase kinase, alpha 1 pseudogene 1; phosp	0.881072
PHLDA1	pleckstrin homology-like domain, family A, member	-2.05333
PHLDB1	pleckstrin homology-like domain, family B, member	1.52
PHLDB2-PLCXD2	pleckstrin homology-like domain, family B, member 2	1.08416
PHTF2	putative homeodomain transcription factor 2	-0.826681
PIANP	PILR alpha associated neural protein	2.05068
PIGL	phosphatidylinositol glycan anchor biosynthesis, clas	-1.31192
PIGM	phosphatidylinositol glycan anchor biosynthesis, clas	1.2771
PIGW	phosphatidylinositol glycan anchor biosynthesis, clas	1.15497
PIK3C2A	phosphoinositide-3-kinase, class 2, alpha polypeptid	1.17419
PIK3IP1	phosphoinositide-3-kinase interacting protein 1	1.59234
PIK3R3	phosphoinositide-3-kinase, regulatory subunit 3 (gan	1.89917
PION	pigeon homolog (Drosophila)	-2.1709
PIP	prolactin-induced protein	inf
PITX2	paired-like homeodomain 2	inf
PJA2	praja ring finger 2	0.855053
PKD1P1	polycystic kidney disease 1 (autosomal dominant) ps	4.09202
PKI55	DKFZp434H1419	2.25562
PLAU	plasminogen activator, urokinase	1.74962
PLCB1	phospholipase C, beta 1 (phosphoinositide-specific)	2.36883
PLCB4	phospholipase C, beta 4	1.26312
PLCD1	phospholipase C, delta 1	-1.4013
PLK1	polo-like kinase 1 (Drosophila)	-0.833125
PLK1S1	non-protein coding RNA 153	-1.07136
PLSCR4	phospholipid scramblase 4	-2.20324
PLXNA2	plexin A2	2.30799
PLXNB1	plexin B1	1.55739
PM20D2	peptidase M20 domain containing 2	0.984651

PMF1-BGLAP	polyamine-modulated factor 1 - bone gamma-carbox	-1.1237
PMM1	phosphomannomutase 1	-1.23388
PMP22	peripheral myelin protein 22	2.72747
PMS2L2	postmeiotic segregation increased 2-like 5; postmeic	inf
PNMAL1	PNMA-like 1	-4.84834
PODXL	podocalyxin-like	5.50039
POLM	polymerase (DNA directed), mu	-1.46933
POLQ	polymerase (DNA directed), theta	-1.00347
POLR2J	polymerase (RNA) II (DNA directed) polypeptide J, 1	-0.971444
POLR3A	polymerase (RNA) III (DNA directed) polypeptide A,	1.13642
POLR3G	polymerase (RNA) III (DNA directed) polypeptide G (	1.08014
PPA2	pyrophosphatase (inorganic) 2	-1.1693
PPAP2B	phosphatidic acid phosphatase type 2B	2.65679
PPAPDC3	phosphatidic acid phosphatase type 2 domain conta	-inf
PPARA	peroxisome proliferator-activated receptor alpha	-1.57216
PPAT	phosphoribosyl pyrophosphate amidotransferase	1.04012
PPCS	phosphopantothenoylcysteine synthetase	-1.1091
PPIF	peptidylprolyl isomerase F	-0.948192
PPM1D	protein phosphatase 1D magnesium-dependent, del	-1.48589
PPM1M	protein phosphatase 1M (PP2C domain containing)	-1.29229
PPP1CB	protein phosphatase 1, catalytic subunit, beta isoforr	0.921916
PPP1R15A	protein phosphatase 1, regulatory (inhibitor) subunit	-1.7575
PPP1R18	protein phosphatase 1, regulatory subunit 18	-0.745421
PPP1R3B	protein phosphatase 1, regulatory (inhibitor) subunit	1.13274
PPP2R2C	protein phosphatase 2 (formerly 2A), regulatory subu	3.488
PPP2R3B	protein phosphatase 2 (formerly 2A), regulatory subu	-2.053
PPP3CB	protein phosphatase 3 (formerly 2B), catalytic subun	0.78672
PRAF2	PRA1 domain family, member 2	-0.874153
PRDM1	PR domain containing 1, with ZNF domain	-1.54567
PRDM8	PR domain containing 8	-3.25745
PREX1	phosphatidylinositol-3,4,5-trisphosphate-dependent I	1.56677
PRKCA	protein kinase C, alpha	1.07293
PRKCD	protein kinase C, delta	-1.17234
PRKCDBP	protein kinase C, delta binding protein	-1.39898
PRKDC	similar to protein kinase, DNA-activated, catalytic po	1.02512
PRKG1	protein kinase, cGMP-dependent, type I	3.05612
PRPS1	phosphoribosyl pyrophosphate synthetase 1; phospl	0.921169
PRR16	proline rich 16	-1.45895
PRRT2	proline-rich transmembrane protein 2	-2.37809
PRRX1	paired related homeobox 1	1.93215
PRSS12	protease, serine, 12 (neurotrypsin, motopsin)	1.13383
PRSS23	protease, serine, 23	-0.892186
PRUNE2	prune homolog 2 (Drosophila)	7.33773
PSAT1	chromosome 8 open reading frame 62; phosphoseri	-1.00273
PSD3	pleckstrin and Sec7 domain containing 3	3.17911
PSG4	pregnancy specific beta-1-glycoprotein 7; pregnancy	-4.22696
PSG5	pregnancy specific beta-1-glycoprotein 5	-1.02658
PSMB9	proteasome (prosome, macropain) subunit, beta typ	-4.04439
PSME4	proteasome (prosome, macropain) activator subunit	1.08466
PSRC1	proline/serine-rich coiled-coil 1	-1.96313
PTMS	parathymosin	-0.922531
PTP4A1	protein tyrosine phosphatase type IVA, member 1	0.824712
PTPLAD2	protein tyrosine phosphatase-like A domain containi	-0.927615
PTPN14	protein tyrosine phosphatase, non-receptor type 14	0.849229
PTPRD	protein tyrosine phosphatase, receptor type, D	-1.69447
PTPRN	protein tyrosine phosphatase, receptor type, N	4.82647
PTPRQ	protein tyrosine phosphatase, receptor type, Q	-3.12196
PTTG1	pituitary tumor-transforming 1; pituitary tumor-transfo	-1.23832
PUS7L	pseudouridylate synthase 7 homolog (S. cerevisiae)-	1.08501
PXK	PX domain containing serine/threonine kinase	-1.48559
PYCARD	PYD and CARD domain containing	-2.82352
R3HDM2	R3H domain containing 2	-0.801332
RAB27B	RAB27B, member RAS oncogene family	-1.55176
RAB31	RAB31, member RAS oncogene family	0.98328
RAB32	RAB32, member RAS oncogene family	-0.99443
RAB38	RAB38, member RAS oncogene family	-3.23119
RAP1GAP2	GTPase activating Rap/RanGAP domain-like 4	-4.89796
RBBP6	retinoblastoma binding protein 6	-1.25973
RBM12B	RNA binding motif protein 12B	1.59281
RBM24	RNA binding motif protein 24	-1.1389
RBPJ	recombination signal binding protein for immunoglob	1.77958
RCHY1	ring finger and CHY zinc finger domain containing 1	0.936505

RCN1	reticulocalbin 1, EF-hand calcium binding domain	-0.815832
RDH10	retinol dehydrogenase 10 (all-trans)	2.33539
RECQL	RecQ protein-like (DNA helicase Q1-like)	1.01029
RELB	v-rel reticuloendotheliosis viral oncogene homolog B	-2.29375
RGS20	regulator of G-protein signaling 20	-1.66187
RGS3	regulator of G-protein signaling 3	-1.35278
RGS4	regulator of G-protein signaling 4	0.815643
RHBDF2	rhomboid 5 homolog 2 (Drosophila)	-1.71802
RHOU	ras homolog gene family, member U	1.09227
RIMS2	regulating synaptic membrane exocytosis 2	-2.12718
RIN2	Ras and Rab interactor 2	-0.88595
RIPK2	receptor-interacting serine-threonine kinase 2	-1.79775
RN7SK	RNA, 7SK small nuclear	-1.77664
RN7SL1	RNA, 7SL, cytoplasmic 2; RNA, 7SL, cytoplasmic 1	inf
RNASEL	ribonuclease L (2',5'-oligoisoadenylate synthetase-d	-2.17675
RNF130	ring finger protein 130	4.06696
RNF141	ring finger protein 141	0.929311
RNF144B	ring finger protein 144B	2.39479
RNF6	ring finger protein (C3H2C3 type) 6	-0.836501
ROR1	receptor tyrosine kinase-like orphan receptor 1	1.80759
RORA	RAR-related orphan receptor A	2.87465
RPA2	replication protein A2, 32kDa	0.847011
RPL23A	ribosomal protein L23a pseudogene 63; ribosomal p	0.99521
RPL28	ribosomal protein L28	-0.993039
RPL39	ribosomal protein L39 pseudogene 10; ribosomal pr	-1.24042
RPL39L	ribosomal protein L39-like	-1.67747
RPL9	ribosomal protein L9; ribosomal protein L9 pseudoge	-0.794515
RPLP2	ribosomal protein, large, P2 pseudogene 3; ribosom	-0.99474
RPS19	ribosomal protein S19 pseudogene 3; ribosomal pro	-0.98473
RPS26	ribosomal protein S26 pseudogene 38; ribosomal pr	-1.18058
RPS5	ribosomal protein S5	-1.12957
RPS6KA2	ribosomal protein S6 kinase, 90kDa, polypeptide 2; I	2.85769
RPS6KA5	ribosomal protein S6 kinase, 90kDa, polypeptide 5	-2.67941
RPSAP58	ribosomal protein SA pseudogene 9; ribosomal prote	1.11579
RRAS	related RAS viral (r-ras) oncogene homolog	-1.13557
RTEL1-TNFRSF6B	regulator of telomere elongation helicase 1 - tumor	-2.50158
RTN2	reticulon 2	-1.77364
RTTN	rotatin	-1.29541
RUNX1T1	runt-related transcription factor 1; translocated to, 1	-1.44643
RUNX2	runt-related transcription factor 2	-1.19392
RXRA	retinoid X receptor, alpha	1.14779
S100A13	S100 calcium binding protein A13	1.05335
S100A16	S100 calcium binding protein A16	-1.5239
S100A6	S100 calcium binding protein A6	-1.16099
S1PR1	sphingosine-1-phosphate receptor 1	-1.83939
SALL1	sal-like 1 (Drosophila)	-5.38719
SALL2	sal-like 2 (Drosophila)	1.58757
SAMD3	sterile alpha motif domain containing 3	1.79017
SAMD9L	sterile alpha motif domain containing 9-like	-3.62208
SARS	seryl-tRNA synthetase	-1.10212
SAV1	salvador homolog 1 (Drosophila)	-1.20382
SCARA3	scavenger receptor class A, member 3	2.78831
SCD5	stearoyl-CoA desaturase 5	3.07152
SCN9A	sodium channel, voltage-gated, type IX, alpha subur	0.815452
SDC2	syndecan 2	3.60882
SDC3	syndecan 3	1.97575
SDK1	sidekick homolog 1, cell adhesion molecule (chicker	3.53733
SELM	selenoprotein M	-1.36848
SEMA5A	sema domain, seven thrombospondin repeats (type	1.67369
SEPP1	selenoprotein P, plasma, 1	inf
SEPT6	septin 6	2.31958
SEPT9	septin 9	0.811132
SERPINB1	serpin peptidase inhibitor, clade B (ovalbumin), mem	-1.74972
SERPINB2	serpin peptidase inhibitor, clade B (ovalbumin), mem	-3.63219
SERPINB7	serpin peptidase inhibitor, clade B (ovalbumin), mem	-3.77104
SERPINE2	serpin peptidase inhibitor, clade E (nexin, plasminog	0.943321
SESN2	sestrin 2	-1.91658
SGOL1	shugoshin-like 1 (S. pombe)	-1.24328
SH3BP2	SH3-domain binding protein 2	-0.996869
SH3BP5	SH3-domain binding protein 5 (BTK-associated)	1.36917
SH3D19	SH3 domain containing 19	0.88353
SH3KBP1	SH3-domain kinase binding protein 1	0.96157

SH3PXD2B	SH3 and PX domains 2B	1.3853
SH3RF1	SH3 domain containing ring finger 1	1.27164
SHC3	SHC (Src homology 2 domain containing) transformi	1.89107
SHISA9	hypothetical protein LOC729993	3.83112
SHMT2	serine hydroxymethyltransferase 2 (mitochondrial)	-1.0405
SHOX2	short stature homeobox 2	0.965961
SHROOM2	shroom family member 2	-4.70224
SHROOM3	shroom family member 3	-3.04883
SIRPA	signal-regulatory protein alpha	1.8253
SIX1	SIX homeobox 1	1.21462
SKAP2	src kinase associated phosphoprotein 2	-0.976246
SLC11A2	solute carrier family 11 (proton-coupled divalent met	1.03777
SLC12A2	solute carrier family 12 (sodium/potassium/chloride t	1.04783
SLC14A1	solute carrier family 14 (urea transporter), member 1	4.83963
SLC16A1	solute carrier family 16, member 1 (monocarboxylic a	0.889572
SLC16A12	solute carrier family 16, member 12 (monocarboxylic	3.10135
SLC17A9	solute carrier family 17, member 9	-1.81065
SLC1A5	solute carrier family 1 (neutral amino acid transporte	-1.48801
SLC20A1	solute carrier family 20 (phosphate transporter), mer	1.33865
SLC22A15	solute carrier family 22, member 15	-4.05798
SLC25A5	solute carrier family 25 (mitochondrial carrier; adenir	-0.847198
SLC25A6	solute carrier family 25 (mitochondrial carrier; adenir	-1.35326
SLC26A2	solute carrier family 26 (sulfate transporter), membe	0.949979
SLC2A1	solute carrier family 2 (facilitated glucose transporter	0.86242
SLC2A12	solute carrier family 2 (facilitated glucose transporter	1.69976
SLC2A13	solute carrier family 2 (facilitated glucose transporter	-3.87055
SLC35F2	solute carrier family 35, member F2	1.56731
SLC37A2	solute carrier family 37 (glycerol-3-phosphate transp	-2.22524
SLC38A5	solute carrier family 38, member 5	1.46496
SLC39A1	solute carrier family 39 (zinc transporter), member 1	-0.759829
SLC39A4	solute carrier family 39 (zinc transporter), member 4	-2.22172
SLC44A1	solute carrier family 44, member 1	1.31978
SLC4A4	solute carrier family 4, sodium bicarbonate cotranspo	2.86533
SLC6A9	solute carrier family 6 (neurotransmitter transporter,	-2.9411
SLC7A11	solute carrier family 7, (cationic amino acid transport	-1.25931
SLC7A2	solute carrier family 7 (cationic amino acid transporte	1.51301
SLC7A5	solute carrier family 7 (cationic amino acid transporte	-1.2195
SLC7A6	solute carrier family 7 (cationic amino acid transporte	1.76614
SLC8A1	solute carrier family 8 (sodium/calcium exchanger), r	0.824504
SLC9A7	solute carrier family 9 (sodium/hydrogen exchanger)	1.73759
SLC9A9	solute carrier family 9 (sodium/hydrogen exchanger)	-2.4099
SLFN11	schlafen family member 11	-1.86687
SLIT2	slit homolog 2 (Drosophila)	-1.5438
SLIT3	slit homolog 3 (Drosophila)	2.54296
SMAD9	SMAD family member 9	1.50927
SMARCA1	SWI/SNF related, matrix associated, actin depender	0.847674
SMARCC1	SWI/SNF related, matrix associated, actin depender	1.28314
SMC1A	structural maintenance of chromosomes 1A	0.878832
SMCP	sperm mitochondria-associated cysteine-rich protein	inf
SMYD3	SET and MYND domain containing 3	-0.944649
SNAI2	snail homolog 2 (Drosophila)	-0.927921
SNAPC1	small nuclear RNA activating complex, polypeptide 1	-0.886334
SNCAIP	synuclein, alpha interacting protein	-4.77817
SNHG5	small nucleolar RNA host gene 5 (non-protein codin	1.34399
SNRNP27	small nuclear ribonucleoprotein 27kDa (U4/U6.U5)	-1.0426
SNRPG	hypothetical protein LOC100132425; similar to small	-0.886559
SNTB1	syntrophin, beta 1 (dystrophin-associated protein A1	1.57992
SOCS2	suppressor of cytokine signaling 2	-2.83476
SORT1	sortilin 1	1.5178
SOX11	SRY (sex determining region Y)-box 11	6.24776
SOX9	SRY (sex determining region Y)-box 9	2.88432
SPAG7	sperm associated antigen 7	0.832696
SPATA18	spermatogenesis associated 18 homolog (rat)	-1.08419
SPATA6	spermatogenesis associated 6	-3.38969
SPATS2	spermatogenesis associated, serine-rich 2	1.06616
SPCS3	signal peptidase complex subunit 3 homolog (S. cer	1.18504
SPDYE7P	speedy homolog E7 (Xenopus laevis), pseudogene	inf
SPOCD1	SPOC domain containing 1	1.45262
SPOCK3	sparc/osteonectin, cwcv and kazal-like domains prot	inf
SPON2	spondin 2, extracellular matrix protein	-1.31959
SPRED1	sprouty-related, EVH1 domain containing 1	0.878543
SPRY1	sprouty homolog 1, antagonist of FGF signaling (Drc	3.09049

SPRY2	sprouty homolog 2 (Drosophila)	0.800871
SPSB1	splA/ryanodine receptor domain and SOCS box cont	-1.31557
SPTBN1	spectrin, beta, non-erythrocytic 1	0.91976
SPTLC2	serine palmitoyltransferase, long chain base subunit	0.797591
SRD5A3	steroid 5 alpha-reductase 3	1.25099
SREBF2	sterol regulatory element binding transcription factor	-0.896079
SRGN	serglycin	-0.792521
SRPX2	sushi-repeat-containing protein, X-linked 2	1.67759
SSFA2	sperm specific antigen 2	-0.808965
SSTR1	somatostatin receptor 1	-1.68759
SSX2IP	synovial sarcoma, X breakpoint 2 interacting protein	-1.9618
ST3GAL5	ST3 beta-galactoside alpha-2,3-sialyltransferase 5	1.93286
ST3GAL6	ST3 beta-galactoside alpha-2,3-sialyltransferase 6	1.64772
ST6GAL1	ST6 beta-galactosamide alpha-2,6-sialyltranferase 1	2.64226
ST6GALNAC3	ST6 (alpha-N-acetyl-neuraminyl-2,3-beta-galactosyl-	3.31466
ST6GALNAC5	ST6 (alpha-N-acetyl-neuraminyl-2,3-beta-galactosyl-	inf
STAG2	stromal antigen 2	0.992699
STARD8	StAR-related lipid transfer (START) domain containi	-2.43045
STC1	stanniocalcin 1	1.00946
STEAP1	six transmembrane epithelial antigen of the prostate	1.299
STEAP1B	STEAP family member 1B	1.7123
STEAP2	six transmembrane epithelial antigen of the prostate	1.68847
STEAP3	STEAP family member 3	2.4173
STPG1	sperm tail PG rich repeat containing 1	-1.38079
STRBP	spermatid perinuclear RNA binding protein	-1.70057
STX1A	syntaxin 1A (brain)	2.39918
STX1B	syntaxin 1B	1.71436
STX6	syntaxin 6	1.00002
STX8	syntaxin 8	-0.851769
STXBP6	syntaxin binding protein 6 (amisyn)	-1.58601
STYK1	serine/threonine/tyrosine kinase 1	2.26607
SUCLG2	similar to sucb; succinate-CoA ligase, GDP-forming,	-0.959139
SULF1	sulfatase 1	4.47284
SV2A	synaptic vesicle glycoprotein 2A	2.73271
SVIL	supervillin	2.69325
SYNCRIP	synaptotagmin binding, cytoplasmic RNA interacting	0.8697
SYNGR2	synaptogyrin 2	-1.17636
SYNJ2	synaptojanin 2	1.20962
SYNPO	synaptopodin	-2.25653
SYT1	synaptotagmin I	-1.49838
SYT11	synaptotagmin XI	1.62607
SYT14	synaptotagmin XIV	2.45707
SYTL2	synaptotagmin-like 2	-1.04314
SYTL4	synaptotagmin-like 4	1.15812
TACC1	transforming, acidic coiled-coil containing protein 1	-1.23128
TACC2	transforming, acidic coiled-coil containing protein 2	-2.26038
TAF15	TAF15 RNA polymerase II, TATA box binding protei	0.733706
TAGLN	transgelin	1.73003
TANC1	tetratricopeptide repeat, ankyrin repeat and coiled-cc	1.15196
TAOK3	TAO kinase 3	-0.875339
TAP1	transporter 1, ATP-binding cassette, sub-family B (M	-1.97902
TBC1D1	TBC1 (tre-2/USP6, BUB2, cdc16) domain family, me	-0.933769
TBC1D2	TBC1 domain family, member 2	-2.39482
TBC1D9	TBC1 domain family, member 9 (with GRAM domair	0.911988
TBX15	T-box 15	2.81275
TBX2	T-box 2	-1.15613
TBX3	T-box 3	-0.817011
TBX5	T-box 5	-6.23781
TCEA3	transcription elongation factor A (SII), 3	-1.96269
TCEAL3	transcription elongation factor A (SII)-like 3	-1.13643
TCEAL4	transcription elongation factor A (SII)-like 4	-0.955688
TCF4	transcription factor 4	0.91443
TEF	thyrotrophic embryonic factor	-1.80252
TENM2	teneurin transmembrane protein 2	1.93732
TENM3	teneurin transmembrane protein 3	2.08983
TES	testis derived transcript (3 LIM domains)	1.70915
TFAP2A	transcription factor AP-2 alpha (activating enhancer	-4.11888
TFAP2C	transcription factor AP-2 gamma (activating enhance	-2.17584
TGFB1	transforming growth factor, beta 1	1.17719
TGFBI	transforming growth factor, beta-induced, 68kDa	1.81639
TGIF1	TGFB-induced factor homeobox 1	-1.54141
THBS1	thrombospondin 1	-0.848488

THBS2	thrombospondin 2	-3.80012
THNSL1	threonine synthase-like 1 (S. cerevisiae)	1.24158
THSD4	thrombospondin, type I, domain containing 4	0.743909
TIA1	TIA1 cytotoxic granule-associated RNA binding prot	0.872304
TIAM1	T-cell lymphoma invasion and metastasis 1	4.32921
TICAM1	toll-like receptor adaptor molecule 1	-1.2296
TIFA	TRAF-interacting protein with forkhead-associated d	-1.43022
TIMM9	translocase of inner mitochondrial membrane 9 hom	-1.2812
TIMP1	TIMP metallopeptidase inhibitor 1	0.937005
TKT	transketolase	-1.20248
TLE4	transducin-like enhancer of split 4 (E(sp1) homolog,	-1.1314
TMEFF2	transmembrane protein with EGF-like and two follist	2.74258
TMEM106C	transmembrane protein 106C	-1.21627
TMEM11	transmembrane protein 11	-1.14327
TMEM119	transmembrane protein 119	2.92113
TMEM120A	transmembrane protein 120A	-1.58016
TMEM132B	transmembrane protein 132B; hypothetical LOC121	4.28403
TMEM154	transmembrane protein 154	-2.6736
TMEM158	transmembrane protein 158	-1.02546
TMEM200A	transmembrane protein 200A	1.94637
TMEM237	transmembrane protein 237	0.930043
TMEM35	transmembrane protein 35	3.11315
TMEM50A	transmembrane protein 50A	1.05245
TMEM51	transmembrane protein 51	-2.90031
TMEM64	transmembrane protein 64	1.22591
TMEM67	transmembrane protein 67	-1.33112
TMOD2	tropomodulin 2 (neuronal)	3.64525
TMTC3	transmembrane and tetratricopeptide repeat contain	1.03175
TNC	tenascin C	1.66344
TNFAIP8L1	tumor necrosis factor, alpha-induced protein 8-like 1	-0.936313
TNFAIP8L3	tumor necrosis factor, alpha-induced protein 8-like 3	1.95989
TNFRSF10D	tumor necrosis factor receptor superfamily, member	2.33643
TNFRSF11B	tumor necrosis factor receptor superfamily, member	-3.7712
TNFRSF19	tumor necrosis factor receptor superfamily, member	-3.48802
TNFRSF1A	tumor necrosis factor receptor superfamily, member	-0.8253
TNFSF12-TNFSF13	TNFSF12-TNFSF13 readthrough transcript; tumor n	-2.56666
TNIK	TRAF2 and NCK interacting kinase	1.8141
TNPO1	transportin 1	1.0967
TNS1	tensin 1	4.96371
TNS3	tensin 3	-0.974262
TOM1L1	target of myb1 (chicken)-like 1	-1.95748
TOM1L2	target of myb1-like 2 (chicken)	0.874764
TOP1	topoisomerase (DNA) I	1.03574
TP53INP1	tumor protein p53 inducible nuclear protein 1	1.01709
TPCN1	two pore segment channel 1	-1.36474
TPST1	tyrosylprotein sulfotransferase 1	-1.33546
TRIB2	tribbles homolog 2 (Drosophila)	2.35668
TRIB3	tribbles homolog 3 (Drosophila)	-3.16038
TRIM22	tripartite motif-containing 22	-1.17258
TRIM44	tripartite motif-containing 44	0.886195
TRIM66	tripartite motif-containing 66	-1.8556
TRIP10	thyroid hormone receptor interactor 10	-0.836833
TRNT1	tRNA nucleotidyl transferase, CCA-adding, 1	1.16743
TRO	trophinin	2.98963
TRPA1	transient receptor potential cation channel, subfamil	-3.46927
TRPS1	trichorhinophalangeal syndrome I	1.34827
TRPV2	transient receptor potential cation channel, subfamil	2.18497
TSC22D3	TSC22 domain family, member 3; GRAM domain co	-1.87447
TSKU	tsukushin	2.30116
TSPAN14	tetraspanin 14	0.883013
TSPYL1	TSPY-like 1	0.953928
TSPYL4	TSPY-like 4	1.5868
TSPYL5	TSPY-like 5	2.1947
TSTA3	tissue specific transplantation antigen P35B	-1.42023
TTYH3	tweety homolog 3 (Drosophila)	1.11325
TUB	tubby homolog (mouse)	2.334
TUBA1A	tubulin, alpha 1a	1.54122
TUBE1	tubulin, epsilon 1	-1.88458
TUG1	taurine upregulated 1 (non-protein coding)	1.48394
TYW1B	tRNA-yW synthesizing protein 1 homolog B (non-prc	-3.12428
UACA	uveal autoantigen with coiled-coil domains and anky	-0.961539
UBASH3B	ubiquitin associated and SH3 domain containing, B	0.92835

UBE2J2	ubiquitin-conjugating enzyme E2, J2 (UBC6 homolo	-0.929691
UBE2L6	ubiquitin-conjugating enzyme E2L 6	-1.07945
UBE2S	ubiquitin-conjugating enzyme E2S	-1.82296
UBR3	ubiquitin protein ligase E3 component n-recognin 3 (	0.87952
UBR5	similar to E3 ubiquitin protein ligase, HECT domain (	0.959679
UBXN11	UBX domain protein 11	-2.17847
UBXN6	UBX domain protein 6	-0.963097
UHRF1	ubiquitin-like with PHD and ring finger domains 1	1.05284
ULBP1	UL16 binding protein 1	-3.32718
UNC119B	unc-119 homolog B (C. elegans)	-0.944141
USP12	ubiquitin specific peptidase 12	0.820724
VAT1	vesicle amine transport protein 1 homolog (T. califor	-0.811281
VAT1L	vesicle amine transport protein 1 homolog (T. califor	3.75996
VCAN	versican	5.49773
VCL	vinculin	0.899026
VEGFA	vascular endothelial growth factor A	0.803307
VPS13A	vacuolar protein sorting 13 homolog A (S. cerevisiae	1.40538
VPS41	vacuolar protein sorting 41 homolog (S. cerevisiae)	0.921365
VRK1	vaccinia related kinase 1	0.99521
VSNL1	visinin-like 1	inf
WAC-AS1	WAC antisense RNA 1 (head to head)	1.86077
WASF3	WAS protein family, member 3	0.992719
WASH5P	WAS protein family homolog 3 pseudogene; WAS p	inf
WASL	Wiskott-Aldrich syndrome-like	0.855422
WDFY1	WD repeat and FYVE domain containing 1	0.93064
WDR62	WD repeat domain 62	-1.34223
WDR66	WD repeat domain 66	-1.21335
WDR91	WD repeat domain 91	-2.11467
WHAMMP1	WAS protein homolog associated with actin, golgi m	3.42404
WIPI1	WD repeat domain, phosphoinositide interacting 1	-0.935348
WNK4	WNK lysine deficient protein kinase 4	-0.970018
WNT5A	wingless-type MMTV integration site family, member	0.793361
WNT5B	wingless-type MMTV integration site family, member	-1.11355
WWC1	WW and C2 domain containing 1	3.85493
XAF1	XIAP associated factor 1	-3.64019
XBP1	X-box binding protein 1	-0.92707
XIAP	X-linked inhibitor of apoptosis	0.95733
XPC	xeroderma pigmentosum, complementation group C	-1.0346
XRCC5	X-ray repair complementing defective repair in Chine	0.892379
XXYLT1	xyloside xylosyltransferase 1	1.14752
XYLT1	xylosyltransferase I	1.7115
YAP1	Yes-associated protein 1, 65kDa	1.02891
YY1AP1	YY1 associated protein 1; gon-4-like (C. elegans)	-0.851649
ZBED5	zinc finger, BED-type containing 5	1.3742
ZBTB10	zinc finger and BTB domain containing 10	1.42762
ZBTB33	zinc finger and BTB domain containing 33	1.08311
ZBTB38	zinc finger and BTB domain containing 38	-0.883911
ZC3H13	zinc finger CCCH-type containing 13	0.809431
ZDHHC18	zinc finger, DHHC-type containing 18	-1.11042
ZFAND2B	zinc finger, AN1-type domain 2B	-1.10758
ZFHX4	zinc finger homeobox 4	1.27071
ZFP36	zinc finger protein 36, C3H type, homolog (mouse)	-1.29417
ZFP36L1	zinc finger protein 36, C3H type-like 1	-1.96425
ZFP62	zinc finger protein 62 homolog (mouse)	1.01741
ZFPM2	zinc finger protein, multitype 2	-1.86603
ZMAT1	zinc finger, matrin type 1	3.30172
ZNF12	postmeiotic segregation increased 2-like 3; zinc finge	1.20374
ZNF140	zinc finger protein 140	-1.07575
ZNF185	zinc finger protein 185 (LIM domain)	0.996787
ZNF213	zinc finger protein 213	-1.17566
ZNF260	zinc finger protein 260	1.29989
ZNF322	zinc finger protein 322	1.73702
ZNF326	zinc finger protein 326	1.66665
ZNF331	zinc finger protein 331	-1.1428
ZNF33A	zinc finger protein 33A	1.74224
ZNF33B	zinc finger protein 33B	2.52811
ZNF365	zinc finger protein 365	-3.05316
ZNF407	zinc finger protein 407	1.23816
ZNF415	zinc finger protein 415	-2.70783
ZNF434	zinc finger protein 434	-1.05333
ZNF438	zinc finger protein 438	-1.55854
ZNF503	zinc finger protein 503	1.82613

ZNF536	zinc finger protein 536	inf
ZNF593	zinc finger protein 593	-1.57727
ZNF600	zinc finger protein 600	-1.24994
ZNF618	zinc finger protein 618	0.994489
ZNF664-FAM101A	zinc finger protein 664 - family with sequence similar	0.897909
ZNF703	zinc finger protein 703	-2.01008
ZNF711	zinc finger protein 711	4.78613
ZNF780B	zinc finger protein 780B	1.55014
ZNF84	zinc finger protein 84	1.05586
ZNRF2	zinc and ring finger 2	-2.1475

Supplementary Table 2: TMT-MS (1394 proteins with score > 30)

Accession	Gene name	Score	Coverage	# Unique Pe	# Peptides	Fold change (control/ TEMEM67)	p-value (t-test)	Significant
Q09666	AHNAK	2548.291346	77.83	367	372	0.550299976	6.1656E-05	***
P62736	ACTA2	2102.808761	59.42	8	24	1		
P35579	MYH9	1880.956313	69.39	144	181	0.938076642	0.25607624	ns
P21333	FLNA	1661.802431	61.69	121	164	0.871347163	0.07132594	ns
Q15149	PLEC	1618.3484	61.25	309	320	0.591085406	0.00050806	***
K7EM38	ACTG1	1469.717712	86.47	2	12	1		
P02751	FN1	1234.425823	47.53	86	100	0.597819172	0.00087466	***
P08670	VIM	1211.491325	82.4	48	52	1		
Q562R1	ACTBL2	1118.182656	28.46	3	11	1		
V9HVZ7	HEL-176	883.2879592	56.95	1	15	0.732308745	0.03787219	*
Q9Y490	TLN1	876.4000921	61.87	127	153	0.812600631	0.02456296	*
A0A024R884	TNC	732.0419426	44.62	3	91	2.163394224	3.5931E-05	***
Q14315	FLNC	726.4536204	48.77	105	127	1.035549346	0.37390097	ns
A7BI36	RRBP1	721.140589	77.08	5	113	0.569310668	0.00247826	**
Q9P2E9	RRBP1	698.3166647	74.04	1	107		0.37390097	ns
P07355	ANXA2	666.6238135	73.75	4	36	0.605345387	0.05467716	ns
J3QSU6	TNC	665.199635	45.62	1	86	1		
O43707	ACTN4	658.120904	68.61	47	72	0.690474684	0.01181065	*
P02452	COL1A1	641.6736932	64.07	27	78	0.841352423	0.00598474	**
A7MBN2	TNC	634.0634744	47.33	1	81	1		
P12814	ACTN1	601.9220594	68.27	6	65	1.024595437	0.7078428	ns
Q9NZM1	MYOF	598.8537889	52.3	109	109	0.696477111	0.00103697	**
A0A024RAB6	HSPG2	594.6339364	33.87	118	118	0.83294794	0.02155118	*
P02545	LMNA	593.7931058	71.69	58	60	0.632706168	0.00180691	**
A3KC71	okuribin	571.1877854	45.79	54	54	1.3931369	0.08674285	ns
A7XZE4	TPM2b	561.1105729	79.23	0	42		0.37390097	ns
V9HW25	HEL-S-273	560.9230582	79.23	0	42		0.37390097	ns
H9KV75	ACTN1	557.7364188	68.49	2	58	1		
P35555	FBN1	555.4908155	37.58	88	97	0.84174742	0.00463287	**
E7EX44	CALD1	547.7379301	66.07	2	48	0.762641409	0.06701541	ns
P04406	GAPDH	531.0058281	63.58	18	24	1		
O75369	FLNB	522.8687154	49.96	104	120	0.927212849	0.32998714	ns
Q14204	DYNC1H1	519.8988945	31.68	151	154	0.987846459	0.37390097	ns
Q13813	SPTAN1	519.8065332	50.44	128	131	0.92611441	0.291638	ns
A0A024QZN4	VCL	517.4315126	69.23	82	82	0.837731683	0.01554463	*
P07951	TPM2	513.3293515	79.93	0	41		0.37390097	ns
Q5TCU3	TPM2	513.1418368	79.93	0	41		0.37390097	ns
A0A087WTA8	COL1A2	494.0386064	58.43	65	66	1		
A1A5C4	RRBP1	467.6552649	74.09	1	81	0.549480479	0.06428488	ns
Q01082	SPTBN1	457.7369539	48.94	95	113	0.709403508	0.00357674	**
P35580	MYH10	451.1570888	41.75	69	101	0.910526341	0.2028309	ns
Q9NYG1	CALD1	450.7610346	65.9	1	43	0.493158018	0.03887113	*
Q6ZN40	TPM1	448.9174283	82.82	0	47		0.37390097	ns

P12111	COL6A3	445.930968	35.76	91	111	0.691426307	0.00130278	**
P09493	TPM1	436.2237647	78.17	3	43	0.523483864	0.00184149	**
D3DTX7	COL1A1	434.9648905	65.2	2	50	1		
P11021	HSPA5	424.8001866	58.87	42	45	0.785115258	0.01419472	*
D6RGG3	COL12A1	421.1263083	37.43	83	105	0.341581009	0.00010642	***
Q01995	TAGLN	402.038233	88.06	23	24	1		
P11142	HSPA8	397.828596	67.03	27	45	0.835867066	0.14170051	ns
Q9Y6C2	EMILIN1	397.3190974	41.24	40	41	1.107206504	0.12630456	ns
P46939	UTRN	392.6341412	35.22	124	128	0.493121532	0.00017494	***
H3BPE1	MACF1	391.9020389	19.21	119	142	0.867691593	0.00161102	**
E7EVA0	MAP4	388.751092	30.78	42	79	1		
P07437	TUBB	386.5880187	58.33	1	23	0.995536199	0.77219546	ns
A0A024R5W6	TPM1	384.8602352	84.15	2	42	0.910414402	0.37524163	ns
P06733	ENO1	377.330439	61.29	22	32	1		
P68371	TUBB4B	376.8059994	58.2	3	23	0.45733371	0.00081374	***
F8J2B5	LMO7	368.4897411	48.8	15	81	0.781259377	0.00014803	***
Q562L9	ACT	361.6715438	62.14	1	5	0.796645023	0.35608301	ns
P50454	SERPINH1	356.5576262	64.11	29	29	0.965260328	0.12673625	ns
Q6NZI2	PTRF	354.4344435	48.97	25	25	0.257716867	1.0035E-05	***
H0YL33	ANXA2	348.5871323	94.37	1	20	0.998536231	0.99276992	ns
Q07954	LRP1	347.2111082	22.58	97	99	0.556713386	0.00018004	***
Q13885	TUBB2A	347.0562832	48.76	2	21	0.649844794	0.00860867	**
P35556	FBN2	343.9252758	30.39	71	80	0.767000531	0.00067495	***
K7ENT6	TPM4	339.5298222	72.07	4	23	0.966213677	0.11611652	ns
A0A024R5Z9	PKM2	339.2878151	65.35	4	39	1.309466263	0.10839275	ns
P14618	PKM	336.3497125	68.93	4	39	1		
Q9BVA1	TUBB2B	335.5305188	47.87	1	20	1		
P26038	MSN	334.6859671	64.99	39	53	0.856598426	0.06815586	ns
P07900	HSP90AA1	329.1727566	47.4	25	42	0.923318177	0.17734462	ns
H7BYY1	TPM1	328.8078473	77.82	5	33	0.510033044	9.1748E-05	***
P08238	HSP90AB1	324.117381	46.82	20	39	0.99949352	0.97982142	ns
B7Z722	TPM1	314.8596587	76.21	0	33		0.37390097	ns
Q07065	CKAP4	311.6385463	75.25	47	51	0.811086991	0.00813192	**
P07237	P4HB	311.0591892	62.2	19	41	0.659529182	0.00574831	**
A0A087WWU8	TPM3	304.6919378	76.65	0	29		0.37390097	ns
Q00610	CLTC	302.3552299	40.48	46	66	0.720153887	0.02337615	*
F8WE98	FLNA	298.8545407	49.5	1	37	0.358828626	0.1826965	ns
J3KN67	TPM3	298.8268863	74.39	0	35		0.37390097	ns
E9PMP7	LMO7	296.1819879	62.72	1	67	1		
P05556	ITGB1	294.2261002	34.46	32	32	0.568053086	0.00054908	***
P0CG38	POTEI	292.8573812	6.7	2	9	0.385835791	0.00292175	**
Q562Z4	ACT	292.3050373	43.69	2	5	0.521964622	0.00981352	**
P00558	PGK1	287.879802	80.1	31	37	0.969466692	0.45450322	ns
Q5CAQ5	TRA1	286.4381999	49.63	48	50	0.710498413	0.00393027	**
P15144	ANPEP	285.4914589	36.4	40	40	0.358430957	2.0143E-05	***
Q8N6G6	ADAMTSL1	284.8162529	33.14	53	53	5.131836577	0.00689487	**
P04075	ALDOA	275.8095648	52.47	20	26	0.90751017	0.18671031	ns

P08133	ANXA6	274.5942166	69.99	17	54	0.959173066	0.23908694	ns
P68871	HBB	273.1425576	80.27	9	10	1		
Q15746	MYLK	271.9642065	38.45	75	76	0.244756638	2.8425E-08	***
Q15075	EEA1	269.9820769	56.84	85	86	0.814187691	0.02195571	*
P06753	TPM3	266.1630107	58.6	0	29		0.37390097	ns
Q6UVK1	CSPG4	262.7662312	30.62	60	60	0.676220325	6.5054E-05	***
P13639	EEF2	262.6470323	47.55	44	46	0.959360058	0.31285028	ns
P46940	IQGAP1	261.2991457	39.29	65	71	0.830185526	0.09524408	ns
Q13509	TUBB3	251.4441684	46.67	3	19	1		
P07814	EPRS	248.7080508	44.11	66	66	0.921798276	0.29846771	ns
A0A024R4E5	HDLBP	247.0384294	46.29	67	68	0.81753132	0.1086258	ns
Q5VU61	TPM3	246.7296144	73.09	0	27		0.37390097	ns
P07996	THBS1	244.497406	35.3	45	47	0.595028283	0.00094269	***
P78527	PRKDC	241.4075385	22.65	89	90	0.950916787	0.28954462	ns
P37802	TAGLN2	241.0602553	60.8	16	16	1		
H6VRF8	KRT1	240.2438672	53.88	31	37	1.62718057	0.12997129	ns
Q9Y4G6	TLN2	239.5484822	26	40	64	0.780224006	0.00124288	**
Q14766	LTBP1	239.2944666	30.68	16	49	0.863410867	0.0011778	**
B4DDF4	CNN2	236.6205363	64.09	7	19	0.699775552	8.984E-05	***
H0YMT9	ANXA2	236.3209443	74.44	1	12	1		
P05121	SERPINE1	236.1432859	49.75	20	20	2.752676045	0.04821869	*
F5H6E2	MYO1C	232.736766	48.41	10	56	0.707338333		
A0A024RAM4	MAP1B	232.7246077	31.12	71	73	1.697069333	0.04010525	*
P04083	ANXA1	230.1643298	69.08	25	25	0.679745816	0.00295271	**
P68104	EEF1A1	228.2592816	53.25	17	29	0.950384643	0.31745178	ns
O95782	AP2A1	214.3199095	44.01	32	46	0.793206291	0.00637162	**
P00338	LDHA	213.5945603	50.9	18	22	1		
P09382	LGALS1	209.7425601	61.48	9	9	0.873708746	0.02939249	*
P13645	KRT10	206.4215987	48.29	24	29	1.204207305	0.00434723	**
F8W1R7	PDE6H	205.2020943	73.1	10	14	0.66548598	0.01524969	*
Q14847	LASP1	204.1760097	62.84	21	21	0.702306731	0.00013824	***
P13667	PDIA4	202.5469694	56.74	42	42	0.824601601	0.02482868	*
A0A024R316	WNT5A	202.1867456	65.48	21	28	1		
E5RK69	ANXA6	200.6484622	68.91	2	38	1.448222867	0.20235332	ns
P55072	VCP	199.0352004	46.03	37	38	0.732903819	0.0080365	**
Q15582	TGFBI	198.3452414	37.34	28	28	2.260095341	0.03624746	*
P35241	RDX	196.7058394	48.2	23	41	0.675501275	0.00637906	**
P19338	NCL	196.3796581	49.15	52	54	0.764211172	0.00072966	***
P35908	KRT2	195.2749681	59.62	25	36	1.129208342	0.03628783	*
P68366	TUBA4A	195.1068015	51.12	7	22	1		
P23528	CFL1	194.884449	57.23	13	17	0.892138546	0.09048513	ns
P54652	HSPA2	193.9694864	49.45	19	36	0.162704618	1.641E-05	***
P78559	MAP1A	193.2342867	23.72	59	60	1.345043661	0.086733	ns
G3V511	LTBP2	191.0526236	21.14	32	33	1.033457262	0.37390097	ns
A0A024RBC7	ATP2B1	190.6042435	30.98	23	43	0.187261445	3.9452E-05	***
P10412	HIST1H1E	189.460579	50.68	7	21	0.80397553	0.10883412	ns
P63104	YWHAZ	188.4819531	70.61	14	22	0.637164873	0.00606452	**

Q13308	PTK7	188.0309761	41.4	31	39	0.520474371	0.00420134	**
Q14764	MVP	187.6864544	45.58	38	38	1		
Q92743	HTRA1	187.153482	41.67	23	24	0.727502567	0.00179837	**
A0A024R8V0	SEPT9	185.2142369	48.94	30	31	0.871243058	0.08732122	ns
P35527	KRT9	183.7064301	46.07	24	27	1.046352678	0.37390097	ns
H0Y3Z3	P4HB	182.0657699	63.14	1	22	2.05199365	1.4528E-05	***
O00622	CYR61	179.9928662	59.06	8	26	1.322912655	0.09031084	ns
P08758	ANXA5	179.104543	64.38	23	24	0.996805142	0.37390097	ns
H0YNH8	UACA	179.0918717	37.76	58	60	0.214672826	6.8332E-07	***
P69905	HBA1	178.8468475	67.61	1	7	1		
Q99880	HIST1H2BL	177.7797129	75.4	3	12	0.599885351	0.0136029	*
D3DTH7	MYO1C	177.4313129	46.87	1	47	0.829269712	0.22034168	ns
P62258	YWHAE	173.6921875	63.14	16	19	0.991087565	0.37390097	ns
H0UID5	AP2B1	173.0101945	34.8	17	40	0.789548867	0.00711105	**
P04792	HSPB1	172.8352734	68.29	15	15	1		
P34932	HSPA4	172.5974011	60	46	51	0.930702707	0.37390097	ns
A5YM53	ITGAV	172.1697701	39.12	43	43	0.694045701	0.00639968	**
E1NZA1	PRIC295	171.7274282	22.91	59	59	1		
Q9P0K7	RAI14	171.2898729	47.96	15	55	0.61262396	0.10325788	ns
H3BVI6	CNN2	171.189696	55.5	1	12	1		
P12270	TPR	170.6305518	27.3	60	62	0.966004203	0.37390097	ns
Q86UP2	KTN1	170.0112429	38.69	55	55	0.522855356	0.00249309	**
Q16643	DBN1	169.3715217	30.2	19	19	0.984214704	0.16578221	ns
Q15417	CNN3	169.3560406	51.67	12	17	0.892970587	1.2558E-06	***
C9JD84	LTBP1	169.0533299	28.13	2	35	1.182815899	0.19696483	ns
Q16181	SEPT7	169.0110484	56.98	1	32	0.604957685	0.09618452	ns
Q9C0C2	TNKS1BP1	168.9289422	34.82	47	47	0.750989657	0.00182711	**
P06576	ATP5B	168.8537085	43.67	19	19	1		
D3DVC4	NES	168.2278731	36.09	54	55	0.43503887	0.00023324	***
P50990	CCT8	166.9869953	61.5	38	38	1.007056549	0.50216216	ns
A4GYY8	DKFZp686F17268	166.7033601	57.27	1	32	1		
P07737	PFN1	166.4012851	75	14	14	1		
D6RGI3	SEPT11	165.2654428	53.88	21	26	0.936004919	0.23697042	ns
H7C4C5	MAP4	164.8512311	57.61	1	33	1.23850677	0.02352006	*
Q9NZN4	EHD2	163.8736092	55.8	31	36	0.251549884	3.2558E-06	***
Q03001	DST	163.8669878	10.26	18	73	0.936899764	0.21769326	ns
A0A024R968	ATP2B4	163.5945637	31.54	19	39	0.645383043	0.00380248	**
Q14517	FAT1	163.297958	13.58	60	61	0.394805853	0.00032022	***
Q06830	PRDX1	163.1730397	67.84	13	17	0.896887056	0.23218901	ns
P53396	ACLY	162.9876926	42.6	2	43	1		
V9HWK1	HEL-S-49	162.6966738	64.26	16	16	1.039272013	0.37390097	ns
P36578	RPL4	161.7100201	58.31	34	34	0.784286174	0.02405164	*
P23527	HIST1H2BO	160.9403104	75.4	0	12		0.37390097	ns
P42224	STAT1	159.8770468	45.73	33	33	2.166535553	0.08589961	ns
P49588	AARS	159.5166144	37.81	37	38	0.97235105	0.37390097	ns
Q15942	ZYX	159.4029963	38.11	18	18	0.777149879	0.08383182	ns
P12109	COL6A1	159.2365223	33.95	32	32	0.729606246	0.00431815	**

Q14697	GANAB	159.1921918	34.96	6	33	0.691971245	0.00982615	**
Q14247	CTTN	159.1920178	53.09	35	35	0.572716956	0.00021378	***
P16403	HIST1H1C	159.1845506	51.17	6	19	0.674677552	0.00021671	***
Q16555	DPYSL2	158.8813334	47.2	12	25	0.745739574	0.00696558	**
P25705	ATP5A1	158.724646	46.65	27	27	0.818476915	0.12599899	ns
P06899	HIST1H2BJ	158.6156653	75.4	1	12	1		
P62979	RPS27A	158.457484	66.67	3	11	0.875770179	0.10216263	ns
P78371	CCT2	157.7462435	57.57	29	29	0.936226791	0.46434211	ns
O60664	PLIN3	157.69199	47.93	20	20	0.941559051	0.37390097	ns
P33176	KIF5B	156.9906948	47.46	38	47	0.955974352	0.35672256	ns
A0A024R972	LAMC1	156.6201007	28.99	48	48	0.608690509	0.00024581	***
Q15019	SEPT2	155.3444058	64.82	1	18	1.055694582	0.37390097	ns
Q8WX93	PALLD	155.0870602	26.25	29	30	1		
P29401	TKT	154.7412307	43.98	30	30	0.700062357	0.009044	**
P16401	HIST1H1B	154.5475035	46.02	12	18	0.581744128	0.0008482	***
P08107	HSPA1A	154.4033821	42.59	25	31	0.624745661	0.00242907	**
P22314	UBA1	154.173106	32.23	34	34	0.853595007	0.04981382	*
P22626	HNRNPA2B1	154.1225662	62.32	18	21	1		
Q75MT9	MDH2	153.8939714	68.67	20	20	0.877504155	0.00153648	**
Q9Y617	PSAT1	153.1415509	62.7	23	25	0.951885391	0.17798032	ns
P35221	CTNNA1	152.9984876	42.16	40	41	0.930022675	0.15118623	ns
P10809	HSPD1	152.8527744	54.62	34	34	0.862045574	0.04550256	*
P52272	HNRNPM	152.7092085	56.58	41	41	0.739650741	0.00634019	**
Q7Z406	MYH14	150.5499064	7.92	1	21	0.77325912	0.59023817	ns
Q9NR12	PDLIM7	148.8551916	60.61	22	26	0.620734662	0.00108061	**
B5MCX3	SEPT2	148.8292395	67.91	1	18	2.301628569	0.10015173	ns
Q9UMS6	SYNPO2	148.1076521	33.03	2	30	1.356947831	0.10968932	ns
F1T0J2	GOLGB1	147.5332184	18.4	53	58	0.995950288	0.37390097	ns
A0A024R1Y2	ACLY	146.8171654	42.53	1	42	1.090961672	0.37390097	ns
B9EG60	SYNPO2	146.4652463	28.87	2	30	0.624065153	0.0368964	*
Q4W4Y1	DRIP4	145.8285236	42.63	13	41	0.887601181	0.2180873	ns
Q4LE64	NUMA1	145.5194148	23.95	49	51	0.992990326	0.37390097	ns
B1AK87	CAPZB	144.8130934	60	19	19	0.718399859	0.00169186	**
U3PXP0	HBA2	144.4545075	66.67	1	3	1.108423991	0.30417802	ns
Q96AY3	FKBP10	144.1849332	39.86	8	21	0.99751601	0.37390097	ns
J9R021	eIF3a	143.1834774	31.33	46	46	0.857462844	0.15792758	ns
Q562M3	ACT	142.8758645	63.11	1	4	1		
P16402	HIST1H1D	142.34615	55.66	9	21	0.608452782	5.3839E-05	***
P16615	ATP2A2	142.2563137	33.97	23	36	0.886150383	6.5429E-06	***
Q9UBG0	MRC2	141.2125521	22.65	32	32	0.979019885	0.03339527	*
O75083	WDR1	141.1094668	53.96	2	30	0.676098694	0.08138391	ns
P04259	KRT6B	140.9515443	48.23	2	29	8.106084218	0.34159634	ns
P15924	DSP	140.143989	15.67	53	54	1.881798851	0.16705582	ns
Q0ZGT2	NEXN	139.8744437	40.74	8	38	0.549970498	0.00736104	**
P05023	ATP1A1	139.6666487	35.97	37	37	0.586358395	0.00030901	***
Q53GN4	WDR1	139.1673987	53.96	1	29	0.526954373	0.03247766	*
P49327	FASN	139.1655601	19.95	43	44	0.948541019	0.48363166	ns

Q05639	EEF1A2	138.4625857	23.33	1	13	3.831314217	0.00474054	**
P62987	UBA52	138.152216	58.59	1	9	0.502742521	0.00546223	**
B9EGI2	MPRIP	136.9463496	40.79	13	38	0.911360911	0.13667744	ns
Q5VSQ6	P4HA1	136.9330615	44.94	3	30	1.001006803	0.99381623	ns
L0R849	EDARADD	136.6105492	17.01	1	9	0.67248539	0.41945802	ns
Q16891	IMMT	135.3568089	44.06	24	36	0.783639761	1.1026E-07	***
P60981	DSTN	134.8958205	60.61	14	16	0.754255877	0.08708322	ns
P61981	YWHAG	134.6530833	57.89	11	18	0.930446357	0.47399171	ns
C9JZR2	CTNND1	134.6313362	41.58	3	36	0.788917666	0.09391941	ns
B7Z468	CAST	134.2900164	44.16	1	29	0.431365654	0.04250405	*
P09936	UCHL1	134.0906191	55.61	13	13	1.009604458	0.37390097	ns
P61160	ACTR2	132.9217631	40.61	15	16	0.871180146	0.00306342	**
P80723	BASP1	132.9019195	90.75	18	18	1.06482871	0.44862993	ns
Q96FS1	CTNND1	132.7694018	44.94	2	35	0.520736621	0.11945106	ns
F8W9U4	MAP4	132.5353867	23.67	1	24		0.37390097	ns
A0A024RDE8	PDLIM5	132.4792871	44.8	26	26	0.782528053	0.0101845	*
O43175	PHGDH	132.4610718	44.28	23	23	1		
E9PDF6	MYO1B	132.3769262	30.98	31	34	1.004179959	0.9323451	ns
P42704	LRPPRC	132.33355	31.85	48	48	0.652003969	0.02302581	*
P62805	HIST1H4A	132.1132618	59.22	8	8	0.875558779	0.25985011	ns
P11940	PABPC1	132.0747147	36.95	8	27	0.731075341	0.03202648	*
Q9BXX0	EMILIN2	131.7607465	38.27	36	36	0.592634009	0.00151198	**
H3BLZ8	DDX17	131.3434603	39.95	21	30	0.781984795	0.01891577	*
P13674	P4HA1	131.3028356	44.94	1	28	0.836904531	0.75151654	ns
P30041	PRDX6	130.9547349	65.18	14	20	0.512929788	4.8121E-07	***
E9PHM6	DST	130.7590989	10.71	1	56	1		
P13797	PLS3	130.5439528	43.97	28	28	0.936940408	0.43636682	ns
O43491	EPB41L2	130.0160707	36.32	25	37	0.348943113	3.2092E-05	***
P46783	RPS10	129.8825579	61.21	13	14	0.852999138	0.21721834	ns
P40939	HADHA	128.960264	42.07	35	35	0.828693697	0.07988641	ns
Q0VG55	TNS1	128.9290791	27.48	24	39	1.477018259	0.11716346	ns
P23396	RPS3	128.7227206	82.72	21	21	1.123436122	0.16369883	ns
P61158	ACTR3	128.4069434	44.02	21	21	0.796324447	0.02820602	*
P50991	CCT4	127.9244182	50.65	23	24	0.933258935	0.37390097	ns
P54577	YARS	127.8571453	60.98	36	37	0.714808766	0.01434562	*
Q14192	FHL2	127.6310918	69.18	24	24	0.576018491	0.00740547	**
F8W6I7	HNRNPA1	127.1105659	49.51	11	15	1		
E9PKU7	GANAB	127.0304532	33.57	1	28	0.615390063	0.20838233	ns
A0A024RAC0	LUZP1	126.2594339	33.64	36	38	0.744115429	0.02105395	*
P53621	COPA	125.6068113	31.13	39	39	0.883450744	0.30196192	ns
P23246	SFPQ	125.468215	33.24	22	23	0.91933363	0.01624401	*
P51911	CNN1	124.890978	51.18	13	17	1.224789917	0.11830904	ns
P08473	MME	124.8862733	36.13	30	30	0.386951042		
Q04917	YWHAH	124.7699639	61.79	12	19	0.942109911	0.33710753	ns
P12110	COL6A2	123.7901797	26.01	29	29	0.842006315	0.04950592	*
Q13428	TCOF1	123.6172953	26.81	39	40	0.971185432	0.37390097	ns
P46777	RPL5	123.3136277	59.26	24	24	0.684052177	0.01475471	*

P12956	XRCC6	122.537093	47.45	31	32	0.715984763	0.0074175	**
Q92626	PXDN	122.3245876	26.71	37	37	1		
Q6ZMP0	THSD4	121.9858315	32.61	31	31	1.233594018	0.11815306	ns
Q9H4M9	EHD1	121.5936142	49.44	17	25	0.679386672	0.01543007	*
P27348	YWHAQ	121.3325688	55.92	13	21	0.973813013	0.37390097	ns
P98095	FBLN2	120.7940519	22.97	21	21	0.246503518		
Q9Y4L1	HYOU1	120.4799857	32.03	24	34	0.641753491	0.00689286	**
B5BU24	YWHAB	119.317009	49.59	6	15	0.909918912	0.2319738	ns
P61247	RPS3A	119.2561367	59.47	21	21	0.936471066	0.25708173	ns
A0A024R7F1	PRKCSH	118.8073331	34.91	21	22	0.92796777	0.00077078	***
Q9NR99	MXRA5	118.6306386	15.74	42	43	0.206665617	1.4329E-09	***
Q9NYU2	UGGT1	118.0733888	21.67	32	33	0.855884948	0.18423421	ns
V9HWC6	HEL-S-39	117.457016	66.35	16	17	0.629871012	0.00160822	**
P07195	LDHB	117.3477082	43.71	15	17	0.839404235	0.09993236	ns
A0A024RBR1	RSN	117.3324572	28.8	6	42	0.906652315	0.48797657	ns
Q5ZEY3	GAPD	117.3277793	82.56	1	7	1.299733685	0.65076261	ns
Q9Y281	CFL2	117.1565025	53.61	8	12	0.76272253	0.08155423	ns
A0A024R152	hCG_28765	116.9731456	28.2	7	32	0.919182588	0.01016658	*
P08729	KRT7	116.9231068	50.32	19	27	0.499987295	0.00054884	***
A0A087WZH7	MARCKS	116.3047463	37.88	11	11	0.979231104	0.28866214	ns
Q15084	PDIA6	115.7789886	46.36	22	22	1		
P62906	RPL10A	115.5641451	54.84	15	15	0.863494207	0.08750442	ns
P11216	PYGB	115.203419	43.3	31	36	1.023819507	0.50508696	ns
A0A087WTP3	KHSRP	115.2032006	48.1	29	34	0.680161794	0.00469485	**
P08779	KRT16	114.4794499	62.37	18	31	2.395929688	0.37390097	ns
Q10567	AP1B1	113.5890634	27.71	4	33	0.564120778	0.01088418	*
O00468	AGRN	113.3961686	23.51	38	38	1		
Q9H1J7	WNT5B	113.366237	51.25	12	20	1.311476292	0.11886264	ns
P49792	RANBP2	113.0460924	17.21	42	45	0.993696103	0.37390097	ns
B2ZZ86	COL5A1	113.0095174	17.9	2	32	0.873288645	0.26289096	ns
P52209	PGD	112.0586804	41.2	22	22	0.728607945	0.00091616	***
P26640	VARS	111.8930584	28.48	33	34	0.944840466	0.37390097	ns
J3KTA4	DDX5	111.8308004	41.04	19	27	0.948061794	0.1261551	ns
P13647	KRT5	111.7110255	38.81	15	25	1.884037842	0.37390097	ns
P04843	RPN1	111.67961	42.5	27	27	0.68997072	0.00166499	**
O60506	SYNCRIP	111.6434879	36.76	3	25	1		
E7EX90	DCTN1	111.2703466	30.81	29	39	0.985705149	0.24045445	ns
P18669	PGAM1	111.207642	51.18	7	12	0.953396049	0.18255768	ns
P39019	RPS19	110.9174967	62.76	13	13	1		
Q8IX30	SCUBE3	110.7792724	27.39	26	26	0.936476623	0.18124504	ns
Q14008	CKAP5	110.3784194	20.37	42	42	1		
A0A087WXW9	COL5A1	110.291368	17.85	1	31	1.743305974	0.25021365	ns
Q9UID7	CYR61	110.123684	51.8	1	19	1.088048077	0.73001024	ns
A0A024R755	CALU	109.9674361	42.86	2	14	1.16980138	0.60593353	ns
K4DI93	CUL4B	109.9444809	38.22	26	37	0.751655651	0.00886359	**
P55268	LAMB2	109.5432255	22.36	33	34	0.767846399	4.5402E-05	***
E7EPN9	PRRC2C	108.6890309	14.05	20	37	1		

P24844	MYL9	108.4822969	54.65	4	10	1		
A0A024R652	MTHFD1	108.0902104	33.37	32	33	0.737757315	0.02073715	*
Q8N2S1	LTBP4	107.5885618	23.58	32	33	1.142211077	0.00798273	**
Q5T4S7	UBR4	107.2926911	7.81	40	41	1		
P63244	GNB2L1	107.0053422	66.56	21	21	1.007943506	0.37390097	ns
Q01813	PFKP	106.8734899	35.97	24	32	1.368885983	0.0392236	*
Q13418	ILK	106.4220018	48.23	22	22	0.621032374	0.00080987	***
Q03252	LMNB2	105.7580711	48.5	28	33	0.63494303	0.00309776	**
P62424	RPL7A	105.7038603	55.26	19	20	0.756996442	0.06126472	ns
Q13423	NNT	105.2907741	26.7	31	31	0.41526868	3.5721E-05	***
P19105	MYL12A	105.2013487	66.67	5	11	1		
A6XND0	IGFBP3	105.1730219	72.59	19	19	0.898670007	0.11104011	ns
J3KP58	CLIP1	104.7454406	28.42	1	37	1.031706061	0.75975074	ns
P14649	MYL6B	104.0745589	42.79	7	11	0.991927108	0.84154448	ns
P00352	ALDH1A1	103.7933685	43.51	19	21	0.675096897	1.7548E-06	***
Q8WUJ3	CEMIP	103.7649856	26.45	34	34	1.47912209	0.08416036	ns
F5GZS6	SLC3A2	103.7404037	33.89	20	21	0.770250587	0.01611655	*
E9PLK3	NPEPPS	103.7036138	38.25	35	35	0.908742335	0.25866744	ns
Q9NZU5	LMCD1	102.916867	59.45	24	24	0.592002376	0.00013294	***
Q03135	CAV1	102.8381137	39.33	2	8	0.098050003	1.1064E-05	***
P62820	RAB1A	102.1914731	80.98	6	16	1		
O00410	IPO5	101.2415268	27.07	27	27	0.84662973	0.00228706	**
P41252	IARS	101.2162381	26.07	34	34	1		
O43776	NARS	101.0379478	39.05	24	24	0.941515251	0.37390097	ns
Q8IVF2	AHNAK2	100.9883219	21.1	41	43	1.200649495	0.15315104	ns
P50552	VASP	100.8974239	50.53	18	18	0.632921596	0.00277398	**
Q8IUD2	ERC1	100.4879887	29.21	33	34	0.788846403	0.00107459	**
P05362	ICAM1	100.1500107	37.03	21	22	0.808996052	#DIV/0!	#DIV/0!
H0Y2S9	MPRIP	100.0219896	15.66	3	27	1		
B5BUB5	SSB	99.99410915	44.61	25	26	0.845392068	0.00918932	**
P02786	TFRC	99.95833945	37.5	2	26	0.644106022	0.02770189	*
O60763	USO1	99.68557072	31.7	31	31	0.907600035	0.09513308	ns
B5BTY4	DDX3X	99.65425193	44.11	10	29	1.007795825	0.88604212	ns
P02533	KRT14	99.6000005	39.62	4	22	1.344832691	0.37216347	ns
E7ETU9	PLOD2	99.58264327	36.27	2	26	1.02204854	0.84344239	ns
P27824	CANX	99.55334008	35.64	17	25	1		
P15880	RPS2	99.40856874	56.31	13	18	0.953390957	0.21974664	ns
Q9Y678	COPG1	99.09563303	36.5	26	30	0.817281885	0.06016245	ns
O94973	AP2A2	99.04706872	29.82	15	29	0.448924198	0.00022328	***
P26641	EEF1G	98.64518356	36.84	20	20	0.870030381	0.2330113	ns
H0YD13	CD44	98.02377772	47.09	9	9	0.226233389	6.4202E-06	***
Q15365	PCBP1	97.96830523	48.03	8	15	0.983212237	0.37390097	ns
P09619	PDGFRB	97.95063233	22.97	24	26	0.319675337	9.6082E-05	***
P20700	LMNB1	97.92282057	42.66	23	28	0.810974928	0.01727052	*
P48444	ARCN1	97.77234137	40.9	23	23	0.81765081	0.0416616	*
C9JNG9	COL6A3	97.61256146	30.79	1	21	0.942365326	0.37390097	ns
P54136	RARS	97.54465842	41.52	28	28	0.941634699	0.41479073	ns

Q6YHK3	CD109	97.5137459	19.58	28	29	0.982101478	0.23029939	ns
O94979	SEC31A	97.14377224	26.56	32	33	0.901913691	0.16622422	ns
Q12797	ASPH	96.96380341	34.04	28	28	0.42398085	0.00045452	***
P21796	VDAC1	96.82183814	49.82	11	12	1		
B1ANR0	PABPC4	96.78370559	33.98	16	25	0.806116448	0.26764043	ns
P50395	GDI2	96.30039406	50.79	15	22	0.794983057	0.05177516	ns
Q08211	DHX9	96.1631974	24.25	28	28	0.85000148	2.1152E-05	***
O00151	PDLIM1	96.073645	56.23	16	17	0.604644069	0.00087827	***
A0A024RB16	FAM62A	95.8872509	31.42	32	32	0.87212994	0.22692896	ns
A0A024RC87	RNH1	95.79523396	46.27	19	20	0.605761762	0.00018909	***
F5H365	SEC23A	95.70094883	35.73	19	21	1		
E9PRU1	EFEMP2	95.63373756	37.84	15	15	1		
Q5EC54	HNRPK	95.53801703	42.03	1	21	0.614479689	0.13156432	ns
Q9Y2D5	AKAP2	95.42605007	35.51	1	25	1.440149862	0.15801953	ns
Q92896	GLG1	95.08208466	23.49	33	33	0.760052655	0.021968	*
G3V4W0	HNRNPC	95.05706072	56.87	21	21	0.731491562	0.01684258	*
A0A087WUT6	EIF5B	94.7693392	23.2	29	31	0.757927251	0.00164248	**
P13611	VCAN	94.63353288	6.8	3	26	1.160174235	0.37390097	ns
P09972	ALDOC	94.42240787	36.81	9	15	0.927163511	0.37390097	ns
A0A087WY71	AP2M1	94.39802742	44.01	3	20	0.724516912	0.10328021	ns
O95025	SEMA3D	93.91996622	33.2	29	30	0.883157732	0.19437182	ns
P35998	PSMC2	93.60846174	57.74	26	26	0.948298668	0.36142944	ns
O00469	PLOD2	93.55829906	32.29	1	25	1		
P41250	GARS	93.47918344	29.5	25	25	0.95944394	0.45921659	ns
P53618	COPB1	93.44026887	34.52	30	30	0.990932351	0.37390097	ns
Q32Q12	NME1-NME2	93.39006877	56.16	1	12	1.23697253	0.32715043	ns
Q92974	ARHGEF2	93.18259382	30.93	30	30	0.994929124	0.76174362	ns
A0A087WYF1	LAMA2	93.15405285	11.32	33	34	0.539964127	4.1149E-07	***
P36871	PGM1	93.13989377	45.2	25	25	0.982948903	0.80104402	ns
O00425	IGF2BP3	92.44845319	44.21	23	25	0.787271654	0.00775972	**
O43390	HNRNPR	92.35258353	34.91	14	22	0.640414709	3.8772E-05	***
Q8NF91	SYNE1	92.31227922	4.21	4	38	1		
P05997	COL5A2	92.25800073	21.75	5	28	0.940666246	0.11675213	ns
Q92499	DDX1	92.21397436	35.41	25	25	1		
A0A024RAL1	CSPG2	91.88291097	8.76	1	24	7.03103103	0.00322339	**
Q13740	ALCAM	91.7256602	33.45	4	21	0.878599161	0.34165482	ns
P07942	LAMB1	91.10749769	16.41	31	32	0.605233141	0.00342137	**
Q68CZ2	TNS3	90.98682499	22.56	9	28	0.218466195	3.2306E-06	***
P38159	RBMX	90.72920239	46.29	10	23	0.972675393	0.00029006	***
B7ZLW0	LPP	90.54315674	35.62	20	21	0.722020684	0.00042708	***
Q96T46	HBA2	90.5213629	90.79	1	5	0.750604278	0.18648548	ns
O15523	DDX3Y	90.34439766	42.88	7	26	0.906280951	0.1494872	ns
Q05DA4	P4HA2	90.31031001	38.69	21	21	0.952770231	0.45019318	ns
Q15046	KARS	90.01174033	38.02	19	25	0.949837814	0.37390097	ns
Q7Z6Z7	HUWE1	89.8925755	8.89	34	34	1		
O60701	UGDH	89.82101965	47.77	22	23	1.216758764	0.12519178	ns
O15031	PLXNB2	89.80431116	18.72	30	31	0.41685841	0.00037142	***

Q8NC51	SERBP1	89.68260503	34.8	18	18	0.974010072	0.52244822	ns
Q02952	AKAP12	89.60472488	20.31	34	34	1		
O60565	GREM1	89.48483145	66.3	11	11	1.093498091	0.20867909	ns
E7EQG2	EIF4A2	89.38809741	37.57	3	15	1.04941225	0.40302536	ns
Q96RT1	ERBB2IP	89.12837946	25.28	33	34	0.79504904	0.0488353	*
Q92930	RAB8B	89.06852293	57	4	13	0.679650372	2.1639E-62	***
Q6IB91	PCK2	89.05075336	38.91	1	24	0.876555812	0.03717616	*
O60568	PLOD3	89.01463592	29.81	23	23	0.964337495	0.37390097	ns
P49411	TUFM	88.90843964	47.57	20	20	0.595511736	0.00082411	***
P56730	PRSS12	88.44672012	29.94	28	28	3.116451701	0.03857608	*
Q16531	DDB1	87.85899138	28.51	31	32	0.922333851	0.07801155	ns
P49257	LMAN1	87.27707648	34.12	17	18	0.817947393	0.0572444	ns
P35606	COPB2	86.91517138	34.66	29	29	0.907865223	0.27576085	ns
P02461	COL3A1	86.79572105	20.94	24	25	0.980471318	0.37390097	ns
H0Y827	FKBP10	86.61482263	36.79	1	13	3.893330016	0.00139793	**
P61006	RAB8A	86.56513047	53.62	4	13	1		
P24593	IGFBP5	86.2776891	47.43	13	13	0.14210488	2.0625E-07	***
Q6NTA2	HNRNPL	86.10209298	38.64	17	18	0.963229406	0.37390097	ns
M0QYM7	TUBB4A	85.85119724	32.3	1	4	0.941173685	0.80772835	ns
H0Y5N9	COL12A1	85.5184195	36.77	2	24	0.660226888	0.00294661	**
Q9H4B7	TUBB1	84.99465954	13.75	2	8	1		
Q15063	POSTN	84.41623485	31.58	3	23	2.358312581	0.03619119	*
P26373	RPL13	84.37564003	48.82	14	15	0.89380645	0.25279493	ns
P23142	FBLN1	84.13848925	17.07	6	14	0.671871453	0.00024252	***
A0A087X0K9	TJP1	83.92100108	22.49	1	31	0.288507625	0.00017235	***
Q9H0U4	RAB1B	83.85085106	69.65	5	15	0.607926922	0.00054866	***
Q15366	PCBP2	83.66461349	41.1	4	13	0.863064051	0.01943424	*
H0YAR2	PABPC1	83.61719143	47.54	1	16		0.37390097	ns
P04899	GNAI2	83.44527876	52.39	8	16	0.791796247	0.0129473	*
A9CQZ8	TJP1	83.40687478	21.29	1	31	0.468555845	0.01928762	*
P12081	HARS	83.28454077	46.56	19	27	0.788165505	0.1574194	ns
Q9Y5S2	CDC42BPB	83.16076016	14.9	24	28	1		
Q86UY0	TXNDC5	83.01752412	48.61	17	19	0.95872615	0.44109441	ns
A0A087WUK2	HNRNPDL	83.01145709	34.44	15	17	0.788630327	0.01798671	*
Q7Z2W2	DKFZp686F13142	82.97275841	24.45	23	23	0.513381702	1.0497E-05	***
P09525	ANXA4	82.90509236	64.89	21	22	0.734599641	0.08384147	ns
P37837	TALDO1	82.85037827	45.1	17	17	0.580420937	0.00232871	**
Q9Y4F1	FARP1	82.81395745	23.35	25	25	0.447806601	9.547E-05	***
Q9BR63	FARSB	82.75520492	42.22	25	26	0.784415999	0.04632285	*
P06737	PYGL	82.70175958	35.18	23	28	0.991223941	0.37390097	ns
H0YJ34	FERMT2	82.67003191	31.09	2	20	0.646807297	0.07684835	ns
Q16851	UGP2	82.26187646	42.91	22	22	0.937490208	0.49077356	ns
P63000	RAC1	82.22520256	43.75	4	11	0.580050602	0.00120644	**
P06748	NPM1	82.16358101	43.88	15	15	0.764354626	0.02758225	*
P49748	ACADVL	81.71091866	35.11	22	22	0.381036832	0.00010692	***
P26447	S100A4	81.58446288	45.54	7	7	0.313712447	7.8421E-06	***
P23381	WARS	81.58242118	37.15	18	18	0.65259694	0.0001593	***

P07339	CTSD	81.54867208	41.99	15	15	1		
Q9H2G2	SLK	81.53240502	17.89	26	28	1		
P53675	CLTCL1	81.48850298	10.73	1	21	1		
P21980	TGM2	81.37849486	39.45	24	24	0.260525926	3.9689E-11	***
Q04695	KRT17	81.3106842	44.91	5	24	1.750480225	0.37390097	ns
P18124	RPL7	81.19908905	54.44	20	20	0.888543439	0.39692999	ns
O43242	PSMD3	80.83635092	42.32	1	24	1		
Q5HYL6	DKFZp686E1899	80.83347034	52.56	16	17	0.886655633	0.01455166	*
P17987	TCP1	80.64091802	45.68	24	24	1.008936957	0.85174301	ns
O43854	EDIL3	80.32981241	41.04	20	20	4.429318034	0.00049714	***
Q14157	UBAP2L	80.31015432	25.85	4	21	0.838956935	0.02298445	*
O15144	ARPC2	80.10173786	44.67	18	18	1.007991908	0.37390097	ns
Q9NZB2	FAM120A	79.91535366	22.81	21	22	0.720026615	0.00719579	**
Q16822	PCK2	79.86744857	39.84	2	25	0.313035898	0.00430273	**
A1JUI8	CCT6A	79.72034955	37.09	1	23	1		
A0A087WW66	PSMD1	79.32456446	29.49	26	26	0.748953962	0.03467777	*
Q96D15	RCN3	79.22462451	40.85	11	11	1.08527933	0.37390097	ns
P62277	RPS13	79.21696186	52.98	12	12	0.913607892	0.25524634	ns
H0YDG6	LMO7	79.20644772	58.69	4	17	0.465396883	0.00036798	***
A0A024RDF4	HNRPD	79.03417635	44.77	3	17	0.875013609	0.43135532	ns
Q9NZN3	EHD3	79.01042902	35.33	9	21	1		
Q7RTM4	SYNE1	78.98139596	4.13	1	34		0.37390097	ns
Q99623	PHB2	78.97235096	59.87	19	19	0.857086792	0.33639196	ns
B5BU63	KLC1	78.8706162	38.31	20	24	0.786723861	0.08435921	ns
P54886	ALDH18A1	78.63805079	32.2	24	24	1		
P13010	XRCC5	78.43653989	24.73	20	21	0.833490738	0.12811592	ns
Q08378	GOLGA3	78.28965783	19.89	27	28	1		
Q6IPH7	RPL14	78.12106919	56.82	2	15	0.96515812	0.44861832	ns
Q53SY7	CAD	78.00145459	11.76	25	25	0.950677366	0.11611652	ns
A8MXP9	MATR3	77.97986555	28.83	26	26	0.934031963	0.13859697	ns
P14868	DARS	77.84264374	45.51	22	22	0.986247668	0.37390097	ns
Q5JRA6	MIA3	77.79105484	15.99	27	28	0.809258143	0.11611652	ns
O75095	MEGF6	77.7278918	18.88	21	21	0.48352994	1.1389E-05	***
E9PK01	EEF1D	77.65364206	42.91	11	12	0.983580535	0.37390097	ns
P40925	MDH1	77.57122838	44.01	17	17	0.646064196	0.00040756	***
P09543	CNP	77.49071097	42.76	23	25	0.485419058	0.00079219	***
C9J9K3	RPSA	77.47466826	58.33	10	12	0.919239724	0.00616967	**
P39023	RPL3	77.45591271	41.44	22	22	0.882294847	0.30358051	ns
B4DDB6	HNRPA3	77.42929542	33.71	11	14	0.906726342	0.11963071	ns
Q66K79	CPZ	77.36748588	33.44	19	19	0.147216208	2.4918E-05	***
Q14160	SCRIB	77.29639626	18.47	26	28	0.86621786	0.00044628	***
B9EGA7	CDC42BPA	77.1688813	18.07	26	29	0.520489532	0.00037225	***
B1ALD9	POSTN	77.08961666	29.7	2	22	1.502755106	0.07328439	ns
P60953	CDC42	77.05334044	49.21	9	10	0.680478662	0.01520216	*
P62333	PSMC6	77.0056448	53.21	23	23	0.801019355	0.02629486	*
E9PSG1	CAST	76.77030838	50	1	13	1		
Q13200	PSMD2	76.65857673	31.5	27	27	0.980527557	0.37390097	ns

P25398	RPS12	76.49056327	60.61	8	8	0.853537405	0.02064141	*
P62701	RPS4X	76.16921496	42.97	9	15	0.919164741	0.14765613	ns
Q63ZY3	KANK2	76.16697848	28.79	20	25	0.422893011	0.00302443	**
Q02878	RPL6	76.04871547	39.58	16	16	0.74370658	0.03960985	*
Q6DEN2	DPYSL3	75.82296443	35.53	16	20	0.323677932	5.7899E-05	***
H7BZJ3	PDIA3	75.61649358	57.72	1	7	1		
Q9H2D6	TRIOBP	75.53974903	9.56	21	24	0.543838111	6.5134E-05	***
K7EKE6	LONP1	75.34129238	28.99	23	25	0.84526107	0.03812243	*
Q16527	CSRP2	75.21239614	61.14	11	11	0.683170213	8.8237E-05	***
Q15404	RSU1	75.20766711	46.93	16	16	0.925943968	0.00755262	**
Q14112	NID2	74.75838065	19.71	22	23	0.764852033	0.01830369	*
E9PCT5	CAV1	74.7096051	35.33	1	7	0.424235979	0.04243092	*
Q02790	FKBP4	74.51590455	47.71	20	21	0.999236149	0.37390097	ns
P22102	GART	74.50192559	22.97	24	24	1		
P10316	HLA-A	74.15289962	51.51	0	15		0.37390097	ns
P40222	TXLNA	74.12704945	38.1	20	22	0.941350921	0.37390097	ns
B2RMV2	CYTSA	74.02228665	24.17	26	28	0.939126647	0.37390097	ns
P68431	HIST1H3A	73.97794127	47.79	2	12	1		
P61224	RAP1B	73.87053144	57.07	4	12	0.656015408	0.0058565	**
Q13214	SEMA3B	73.81213999	28.84	18	19	0.860298276	0.00140206	**
Q9BSQ6	RPL13A	73.6729269	51.24	14	14	0.841988391	0.20204743	ns
Q13561	DCTN2	73.5523715	56.36	22	22	0.801898061	0.0005247	***
W6I206	LOXL2	73.52433825	23.59	10	19	1.154708064	0.26722153	ns
D5H3T4	HLA-A	73.46855271	52.33	0	15		0.37390097	ns
H0Y6I0	GOLGA4	73.43535221	13.24	26	29	1		
A0A087WYX9	COL5A2	73.4335233	23.29	1	23	0.612665454	0.12577202	ns
P49589	CARS	73.41204166	35.16	3	25	0.447772203	0.00056037	***
H7BXI1	ESYT2	73.35458028	26.36	20	20	0.339148294	2.2319E-07	***
P62070	RRAS2	73.01520085	54.9	9	11	0.785365378	0.00088271	***
P62191	PSMC1	72.98040426	54.09	21	23	0.866678205	0.0637064	ns
Q9UQ35	SRRM2	72.62336707	12.5	27	27	1		
O15231	ZNF185	72.53855097	40.06	10	26	0.758387103	0.00046511	***
P31939	ATIC	72.47854352	40.71	21	21	0.819853643	0.00051333	***
Q9Y6M1	IGF2BP2	72.26998138	32.05	15	17	0.948585943	0.37390097	ns
P61586	RHOA	72.20305073	41.97	3	8	0.857748508	0.0027597	**
B4DLR8	NQO1	72.14329863	50	13	13	0.340067672	0.00046629	***
P00966	ASS1	72.10724068	32.28	18	18	0.193480969	5.9353E-07	***
A0A087WUA5	EHD4	72.02006745	43.7	17	25	0.586329595	0.0001957	***
D6R9P3	HNRNPAB	71.92216802	35.36	10	12	0.961790907	0.26615254	ns
O60361	NME2P1	71.89366126	52.55	1	7	5.582799263	0.00167699	**
P49023	PXN	71.88088143	33.5	12	17	0.640834642	0.00059146	***
Q32P28	LEPRE1	71.61838961	22.15	15	16	0.619004804	3.2356E-05	***
P08243	ASNS	71.58539736	36.01	2	20	1.408226388	0.00690705	**
P62195	PSMC5	71.5685401	51.48	18	20	0.891855779	0.3203894	ns
P50479	PDLIM4	71.5455097	53.33	16	16	0.611567699	0.00037624	***
P50502	ST13	71.43180037	32.79	15	15	0.9259825	0.11916906	ns
Q1KMD3	HNRNPUL2	71.18356752	26.37	22	22	0.818870848	0.01178588	*

Q13283	G3BP1	71.14020967	34.33	11	12	1		
O75116	ROCK2	71.07349658	17.87	22	27	1		
Q5VZU9	TPP2	71.04133093	23.61	1	27	0.667712739	0.00940548	**
P29144	TPP2	70.98779261	24.58	1	27		0.37390097	ns
P05787	KRT8	70.77582991	21.95	5	13	1		
Q99985	SEMA3C	70.69001579	26.36	22	24	0.247040374	6.3011E-07	***
Q96TA1	FAM129B	70.66360641	27.21	22	22	0.503264948	0.00112683	**
Q04721	NOTCH2	70.46831775	11.45	22	24	0.876730015	0.09833075	ns
P35052	GPC1	70.45983005	41.4	21	21	0.552182279	1.6229E-06	***
P05141	SLC25A5	70.23184228	44.3	6	16	0.761596921	0.00477746	**
P54289	CACNA2D1	70.03432679	24.39	26	26	0.36565156	1.9725E-05	***
P62917	RPL8	69.93753231	46.69	15	16	0.917689495	0.30181605	ns
P05198	EIF2S1	69.47889411	48.89	15	16	0.670484725	0.002763	**
Q15286	RAB35	69.41864502	49.25	7	11	0.609057322	0.00260497	**
O75131	CPNE3	69.3596952	33.71	17	18	0.908563943	0.30425816	ns
O75643	SNRNP200	69.3010844	11.38	24	24	1		
Q06210	GFPT1	69.26823092	32.47	17	21	0.913044577	0.19577993	ns
Q6F3I9	HLA-A	69.0502342	60.81	0	14		0.37390097	ns
P28331	NDUFS1	69.02861035	31.77	23	23	0.620701382	0.00148442	**
O75533	SF3B1	68.92889392	19.63	21	21	0.861668947	0.0993146	ns
Q96N67	DOCK7	68.83096552	13.5	27	28	0.985632595	0.37390097	ns
O00299	CLIC1	68.7690469	74.27	14	15	0.699197016	0.00050773	***
D6R938	CAMK2D	68.72603977	32.73	5	18	0.950051929	0.12345548	ns
R4GN98	S100A6	68.52286184	45.88	6	6	1.06225011	0.5969043	ns
Q9UHB9	SRP68	68.47484922	37.64	23	23	0.846503587	0.00169422	**
P50570	DNM2	68.10611057	24.02	13	23	0.948273165	0.23039944	ns
P60228	EIF3E	68.06295514	39.78	17	17	1		
P18084	ITGB5	67.94779813	31.04	22	22	0.613144245	0.00230251	**
H0Y3P2	EIF4G2	67.84367752	27.5	23	23	0.963135005	0.37390097	ns
Q7Z3Z9	L1CAM	67.32185531	20	23	24	0.578276158		
B4DJV2	CS	67.26569355	28.04	12	13	0.947057949	0.34302382	ns
P55084	HADHB	67.14619243	36.71	18	20	0.995143657	0.37390097	ns
Q9Y266	NUDC	67.14301801	43.81	18	19	0.839554538	0.17338262	ns
Q9UNA0	ADAMTS5	67.03662348	26.02	26	26	0.191816274	1.0783E-05	***
O76094	SRP72	67.00478053	31.15	20	21	0.746165818	0.09078653	ns
Q9H792	PEAK1	66.91825724	16.95	26	26	0.664181018	0.00390143	**
O75396	SEC22B	66.80782104	38.6	8	8	0.91644313	0.16533445	ns
Q9Y696	CLIC4	66.72032475	65.22	14	15	0.73878772	0.0051113	**
P08727	KRT19	66.63347101	44.75	12	20	1.112957343	0.37390097	ns
Q969G5	PRKCDBP	66.60435748	34.87	10	10	0.57089739	0.00091929	***
Q96I99	SUCLG2	66.56942177	40.51	21	21	0.993248715	0.14243384	ns
Q6P2Q9	PRPF8	66.41806674	10.06	26	26	1		
M0R210	RPS16	66.39558995	74.42	15	15	0.977882837	0.23533382	ns
P32455	GBP1	66.29369974	28.89	1	20	1		
Q96AG4	LRRC59	66.24892199	43.97	17	17	0.678814866	0.00232714	**
Q15389	ANGPT1	66.1647141	40.56	18	18	0.269193162	6.2943E-05	***
P15531	NME1	65.88900423	57.89	1	8	1.422756669	0.21867926	ns

Q54A51	hEMMPRIN	65.8220185	43.49	12	12	0.561574529	0.01295495	*
A7XZY7	ITSN1	65.81623733	21.22	23	26	0.790735346	#DIV/0!	#DIV/0!
P28838	LAP3	65.81506443	47.4	20	20	0.681745059	0.0175289	*
Q9Y3I0	RTCB	65.72630847	31.09	15	15	0.866539315	0.19699663	ns
Q99497	PARK7	65.55603647	60.32	13	13	1		
Q12841	FSTL1	65.30360937	37.99	14	14	1		
P07686	HEXB	65.2985369	31.47	17	19	0.431734502	0.00021767	***
B5BUB1	RUVBL1	65.21010828	40.13	16	16	1		
P01023	A2M	65.12464809	4.88	6	9	1.012615354	0.43533182	ns
Q9Y230	RUVBL2	65.03231502	43.2	18	18	0.905006556	0.1979213	ns
E5KLM2	OPA1	64.83521938	24.17	21	21	0.877120568	0.00246189	**
P45880	VDAC2	64.72336519	40.82	11	11	0.977797895	0.37390097	ns
P35232	PHB	64.60958087	47.06	14	14	0.735644746	0.00868107	**
Q13045	FLII	64.43123937	20.8	25	25	0.98231894	0.37390097	ns
Q6UB35	MTHFD1L	64.30128729	20.14	19	20	0.795218335	0.02492876	*
B4DV79	EIF3B	64.11961722	28.46	21	21	0.929064928	0.42534908	ns
Q8WUP2	FBLIM1	64.04281235	40.48	15	15	0.657383061	0.00342502	**
Q5T985	ITIH2	63.9382621	10.16	11	11	1.111033282	0.11724932	ns
P16152	CBR1	63.83604944	58.48	12	16	0.64098785	0.01368647	*
P10301	RRAS	63.81084752	40.83	5	7	0.421548495	0.0005064	***
A0A024R7G6	EPS15L1	63.71085966	26.92	22	22	0.820000905	0.01042991	*
P61088	UBE2N	63.69095266	63.82	10	10	0.861278524	0.02511308	*
Q5JTV8	TOR1AIP1	63.40027344	33.1	2	20	0.330421937	0.00280583	**
P07602	PSAP	63.36603212	23.28	15	15	0.508302033	0.0026181	**
A6NHL2	TUBAL3	63.33344781	15.7	2	7	1		
A0A024R7L5	UPF1	63.17448473	20.13	20	20	0.813231392	0.02467802	*
O43399	TPD52L2	63.15228915	51.94	2	13	0.93899552	0.78011607	ns
Q9Y3F4	STRAP	63.14752293	44.57	15	15	0.937910407	0.40841452	ns
P09874	PARP1	62.93441987	17.16	20	20	0.774504944	0.04959765	*
P61026	RAB10	62.66679537	44	7	12	0.651670371	0.00642928	**
P31943	HNRNPH1	62.60603952	25.84	3	9	0.900944122	0.03705992	*
Q86W92	PPFIBP1	62.56711578	23.44	18	22	0.898955437	0.00914554	**
Q5JXI2	FHL1	62.41635108	56.67	2	14	0.123672159	5.6473E-06	***
A0A024R3F4	PHLDB1	62.33774447	20.92	23	24	0.525677474	6.5003E-06	***
Q13425	SNTB2	62.2586422	33.89	17	20	0.723951252	0.02020509	*
D3DT72	COL11A1	62.20873904	13.97	18	24	0.949761503	0.37390097	ns
Q15293	RCN1	62.16178906	30.82	10	10	0.84175492	0.06894614	ns
Q6NYC8	PPP1R18	61.95135307	36.05	19	19	0.576049929	0.0025835	**
A0A024RDQ0	HSPH1	61.81229413	29.12	17	22	0.949079764	0.12512499	ns
O75955	FLOT1	61.7522763	40.98	18	19	0.68177474	0.00806311	**
Q93008	USP9X	61.6914289	9.03	23	24	1		
P04040	CAT	61.59539318	34.54	18	18	0.52466959	2.2234E-05	***
J3KN66	TOR1AIP1	61.58290303	31.05	1	19	1		
B4DVQ5	EIF3C	61.44728482	21.49	23	23	0.97289073	0.52954041	ns
P62753	RPS6	61.17091453	41.77	15	15	0.884876892	0.31676231	ns
A0A087X2D8	SPAG9	60.98467207	17.76	17	22	1.086305005	0.258016	ns
P17858	PFKL	60.95205975	27.56	14	22	1.129961909	0.27245738	ns

P11387	TOP1	60.92829919	30.85	23	23	0.77630761	0.02622805	*
B5BU83	STMN1	60.89709222	52.35	11	11	0.923242936	0.42526007	ns
H0Y4R1	IMPDH2	60.64984322	37.87	16	17	0.78955077	0.03524461	*
P18085	ARF4	60.61304808	56.11	6	9	1		
O00291	HIP1	60.59991705	19.67	21	24	0.716170235	0.02395862	*
A0A024R201	PSMD13	60.58700371	38.83	1	16	1.06205429	0.78453899	ns
P43034	PAFAH1B1	60.49679661	45.61	17	18	0.958774174	0.37390097	ns
P62244	RPS15A	60.46612036	77.69	4	11	0.846722221	0.12584148	ns
A0A024R4X0	CYB5R3	60.3715564	46.74	3	13	0.965819078	0.82861963	ns
Q13177	PAK2	60.3068856	31.3	8	15	0.838250938	0.23747537	ns
A0A024R0K2	CSDE1	60.29484963	27.38	23	23	1.001430752	0.37390097	ns
P62834	RAP1A	60.09408844	53.26	2	10	0.256965569	8.815E-05	***
P31949	S100A11	59.98114371	61.9	7	7	0.84140123	0.16122117	ns
D3DUG9	USP14	59.97010255	34.4	19	19	1		
A4FU11	RPS4Y1	59.86693263	43.51	7	14	0.848344085	0.13102983	ns
O00231	PSMD11	59.82235885	46.45	19	19	0.896890956	0.05306464	ns
E9PBS1	PAICS	59.81817567	31.48	15	15	1		
Q12884	FAP	59.79344678	19.47	15	15	0.886698062	0.2730828	ns
D9ZGF8	ROCK1	59.62425613	14.55	18	22	1		
P43686	PSMC4	59.62415791	34.69	16	17	1		
Q07955	SRSF1	59.45383036	45.56	13	13	0.985217809	0.35545036	ns
B5BU72	PICALM	59.45357454	26.89	1	18	0.708336422	0.24258527	ns
A7E2Y5	DNAJC13	59.4064436	11.23	24	24	0.801727599	0.00082382	***
Q15599	SLC9A3R2	59.29795432	39.17	16	16	0.720607411	0.000134	***
G8JLD5	DNM1L	59.19023895	30.9	21	21	0.921931933	0.27380158	ns
P13693	TPT1	59.18363214	48.84	10	10	0.714122948	6.6497E-05	***
Q96JY6	PDLIM2	59.11489618	39.77	11	12	0.696792847	0.00222351	**
A0A024R5L7	PICALM	59.10163808	26.89	1	18	0.979895359	0.37390097	ns
P51858	HDGF	59.05915499	43.33	10	11	1		
P62136	PPP1CA	58.96397531	41.52	4	13	0.641054264	0.0081526	**
O94907	DKK1	58.87902141	34.96	8	10	0.742847424	5.3405E-05	***
P52907	CAPZA1	58.8471911	53.15	9	12	0.898693309	0.16791789	ns
A0A087WZZ5	SF3B2	58.83767092	23.88	23	23	0.749462761	0.01881178	*
I3L397	EIF5A	58.72944498	57.82	10	10	0.962873815	0.24472649	ns
I3L4X2	ABCC1	58.6937629	16.46	20	22	1		
Q12904	AIMP1	58.58567071	42.95	12	13	0.685265358	0.0005564	***
Q4L180	FILIP1L	58.56663167	19.12	23	24	0.812796756	0.12031685	ns
P51149	RAB7A	58.5619545	74.88	15	15	0.689711843	0.00405381	**
L7UUZ7	ITGB3	58.50377536	26.78	21	21	0.63560438	0.00046759	***
A0A024R5A3	CAPN1	58.45554948	25.35	20	21	0.899744642	0.33477504	ns
P62826	RAN	58.4547652	40.28	10	10	0.928928593	0.23005839	ns
Q16352	INA	58.39575064	6.81	3	4	1.110564697	0.37390097	ns
P29317	EPHA2	58.38309717	22.03	20	21	0.728252053	0.00046111	***
P13804	ETFA	58.32438374	52.55	15	15	0.540488805	0.0001125	***
P12236	SLC25A6	58.31740558	43.96	1	14	0.729516336	0.17800667	ns
P24752	ACAT1	58.30234838	40.28	17	17	0.537459895	0.00304952	**
Q9NZI8	IGF2BP1	58.26649332	28.08	14	15	1.262344544	0.12595377	ns

X5D2T3	RPL10	58.22658145	52.34	15	15	0.959921727	0.39441679	ns
P46779	RPL28	58.02508044	50.36	10	10	0.897472915	0.05182473	ns
P07954	FH	57.99991751	27.84	15	15	0.387287445	0.00010705	***
Q27J81	INF2	57.95770109	17.37	20	20	0.923670426	0.37390097	ns
P45974	USP5	57.82712984	30.07	22	22	0.763634225	0.02299221	*
Q1ELT0	HLA-A	57.82702792	44.38	0	12		0.37390097	ns
A0A024QZE7	TGFB1I1	57.68644762	42.34	13	13	0.782860105	0.01130507	*
F5GWP8	KRT17	57.65320528	41.26	1	18	1.022716096	0.74492767	ns
Q9H425	C1orf198	57.63413703	40.06	15	15	0.927673375	0.12488478	ns
Q86UE4	MTDH	57.62437546	32.47	18	18	0.864229692	0.00014635	***
P62280	RPS11	57.52647066	52.53	12	12	0.971773877	0.30412568	ns
P35658	NUP214	57.48624706	11.39	19	20	1		
P05387	RPLP2	57.38726497	77.39	5	7	0.989419102	0.37390097	ns
Q14019	COTL1	57.35347295	54.93	13	13	0.986562434	0.73899742	ns
P38606	ATP6V1A	57.09249818	25.93	15	15	0.914168028	0.22414745	ns
A0A024QZ63	hCG_27198	56.9992125	10.69	11	24	0.569563981	0.00015637	***
Q9P2B4	CTTNBP2NL	56.98554575	33.02	18	18	1		
Q9UNM1	EPFP1	56.95705414	78.35	5	10	0.765053527	0.02223362	*
P62263	RPS14	56.72811103	39.07	7	7	1		
K4RH61	MMP14	56.59888959	29.21	15	16	0.994712485	0.82966494	ns
P62750	RPL23A	56.47088742	51.92	15	15	0.978532541	0.37390097	ns
A0A024R5H8	RAB6A	56.45994616	47.12	10	11	0.972932732	0.3596339	ns
Q16777	HIST2H2AC	56.39827549	45.74	1	7	0.731437134	0.0921685	ns
Q9BUZ3	QARS	56.35709143	30.74	18	18	0.902612172	0.17305247	ns
M0R0F0	RPS5	56.31616974	37.5	10	10	0.987672506	0.37390097	ns
A0A024R684	NUMB	56.17478538	24.83	10	16	0.576034597	0.00366492	**
P17301	ITGA2	56.08917999	19.48	5	21	0.885376832	0.17966936	ns
Q5SSJ5	HP1BP3	56.0855484	28.03	19	19	0.552343228	0.00558376	**
P61204	ARF3	56.06589961	50.28	5	9	0.840274726	0.07815589	ns
P60891	PRPS1	55.94533122	38.99	8	13	1.498604167	0.05457185	ns
Q6DD88	ATL3	55.8339932	28.28	15	15	0.783115022	0.04734504	*
P48735	IDH2	55.81786478	38.5	16	17	0.305973009	6.6671E-05	***
O95340	PAPSS2	55.80414021	34.69	20	23	0.514667339	7.6725E-05	***
Q96QK1	VPS35	55.80332279	23.49	17	17	1		
Q6V0I7	FAT4	55.59420955	5.12	22	23	0.686706235	0.00025936	***
A6H8X9	CEP170	55.58303642	17.05	18	25	0.95046073	0.33988271	ns
P08754	GNAI3	55.53127551	27.12	4	12	0.692309257	0.01466038	*
A0A087WZK9	EIF3H	55.49313474	30.37	13	13	0.896219047	0.08676461	ns
P23526	AHCY	55.48897183	40.74	17	18	0.98896732	0.37390097	ns
P63092	GNAS	55.36323988	37.82	14	15	0.555096471	0.00232994	**
E9PLY5	MACF1	55.16595662	14.69	1	20		0.37390097	ns
P25786	PSMA1	55.1415844	51.33	15	15	1.096877371	0.34165988	ns
P00441	SOD1	55.13517833	49.35	11	11	1		
Q01546	KRT76	54.97707975	12.07	1	10	1.253827433	0.37390097	ns
Q9UBI6	GNG12	54.87138534	69.44	5	5	0.66141336	1.2781E-09	***
A0A024R6W0	GOT2	54.6871264	30.93	15	15	0.936504956	0.37390097	ns
P32969	RPL9	54.67424583	51.04	11	11	0.949094259	0.34809735	ns

P24534	EEF1B2	54.64591169	37.78	9	10	0.802457195	0.00019174	***
P62140	PPP1CB	54.62626195	39.76	4	12	0.633112372	0.0014054	**
P05091	ALDH2	54.6209476	33.66	16	18	1.010752469	0.58766879	ns
Q8NE71	ABCF1	54.55142188	23.08	12	18	1		
P49321	NASP	54.50300705	21.07	17	18	1.034289142	0.50904995	ns
Q53EP0	FNDC3B	54.50101805	17.69	18	18	0.840584314	0.05717431	ns
P42766	RPL35	54.44657886	40.65	7	9	0.659464045	0.04537225	*
Q86SQ0	PHLDB2	54.43464601	17.08	21	21	0.699589343	0.01867677	*
A6NKB8	RNPEP	54.38659894	28.81	16	16	0.987150055	0.37644526	ns
Q5JR08	RHOC	54.32960904	36.51	2	7	1		
O94874	UFL1	54.32828367	27.08	20	21	0.741361145	0.00862425	**
P30050	RPL12	54.30472004	71.52	11	11	0.967282203	0.58248587	ns
P17252	PRKCA	54.11555743	23.66	17	17	0.889799978	0.19258112	ns
B2ZRD4	HLA-A	54.09150875	64.47	0	12		0.37390097	ns
A0A087X020	SBDS	53.9237231	42.4	14	14	0.850010327	0.11613106	ns
H0Y360	AMPD2	53.72292137	21.6	19	19	0.999910961	0.37390097	ns
P61106	RAB14	53.70713151	46.05	9	11	0.932016996	0.13526888	ns
Q9H2M9	RAB3GAP2	53.52640343	15.22	18	20	0.913252243	0.29749516	ns
V9HW35	HEL-S-55	53.49629104	73.46	9	9	0.977137415	0.37390097	ns
Q149P0	GBF1	53.44842529	10.89	19	20	1		
P01024	C3	53.40967751	5.53	11	11	1.021162679	0.37390097	ns
P61221	ABCE1	53.32127237	30.88	17	17	0.740378611	0.01273382	*
E9PCX8	TNS3	53.31205976	18.32	2	18	0.528202585	0.000214	***
E7EQV9	RPL15	53.28045535	38.51	7	7	0.909866218	0.31059942	ns
P28300	LOX	53.25587809	33.33	12	13	1.345778614	0.14269178	ns
P63313	TMSB10	53.14172328	47.73	4	7	0.910223165	0.26336129	ns
J3QR09	RPL19	53.0921526	43.01	10	11	0.918111758	0.37907824	ns
P60866	RPS20	53.03583384	36.13	5	5	0.910776223	0.22487846	ns
C9JNW5	RPL24	52.76844049	44	11	11	0.943672599	0.37390097	ns
P09211	GSTP1	52.7200886	51.9	6	8	1.009109684	0.53721847	ns
Q7Z4Y4	AK3	52.71543062	58.15	15	15	0.499991326	0.00083642	***
H0YDQ3	LMO7	52.67328274	48.63	0	13		0.37390097	ns
O00186	STXBP3	52.52977967	25.34	18	18	0.463257106	0.00036113	***
P62328	TMSB4X	52.49831295	45.45	2	5	1.101906251	0.259777	ns
Q9NY33	DPP3	52.48276854	27	18	18	1		
Q02539	HIST1H1A	52.46477926	26.51	2	8	0.493439752	2.0467E-05	***
Q9H3U1	UNC45A	52.43250048	22.25	19	20	1		
Q9NSE4	IARS2	52.40350795	20.95	20	20	0.589934028	0.00291981	**
P62851	RPS25	52.37476993	51.2	9	9	0.981290483	0.37390097	ns
H0Y2W2	ATAD3A	52.36932242	30.42	5	16	0.551491462	0.00846754	**
P22695	UQCRC2	52.20449746	36.64	14	14	0.625844778	0.00097292	***
Q96I24	FUBP3	52.203619	28.5	12	15	0.821607396	0.0009815	***
A0A087WXM6	RPL17	52.17033625	49.7	8	9	0.906386516	0.04429842	*
O15020	SPTBN2	52.13056397	5.9	1	15	0.428586346	0.0345944	*
Q15008	PSMD6	52.07730579	39.85	17	17	0.83592011	0.01129006	*
Q00688	FKBP3	52.05521345	56.25	16	16	0.931068094	0.16737128	ns
P10644	PRKAR1A	52.0089519	34.91	16	16	0.690340848	0.02717431	*

P29590	PML	51.94854689	19.73	20	20	0.68639258	0.00126634	**
P11766	ADH5	51.8630774	41.98	16	16	0.726576124	0.00528083	**
P63096	GNAI1	51.8522656	27.12	4	12	0.270018666	0.00100889	**
C5J3Z8	HLA-B	51.84000421	37.29	0	11		0.37390097	ns
P48047	ATP5O	51.76541245	53.05	11	11	0.439434207	0.00038109	***
Q6UY14	ADAMTSL4	51.76076448	22.63	17	17	1		
P02795	MT2A	51.73393738	83.61	3	5	1.048969882	0.37390097	ns
Q5T123	SH3BGRL3	51.71029365	53.41	6	6	1.011015869	0.37390097	ns
Q15459	SF3A1	51.5820365	24.59	18	19	0.709070837	0.00013575	***
O95336	PGLS	51.55627906	50	11	11	0.902180869	0.0360574	*
A0A024R4A5	TNRC15	51.54666221	14.87	17	17	1		
P08240	SRPR	51.53139424	31.97	20	20	0.972169182	0.37390097	ns
P09486	SPARC	51.496737	37.62	13	14	1.220409573	0.13174141	ns
P60763	RAC3	51.46747923	31.25	1	7	1		
Q59EK6	TRAF1	51.37269521	25.75	18	19	0.854529006	0.14329674	ns
X5D2J9	GTF2I	51.36238682	19.96	22	22	0.966053505	0.21276689	ns
Q9UJU6	DBNL	51.33283067	37.21	2	16	0.893948	0.13212081	ns
O43143	DHX15	51.27046573	22.89	18	19	0.892917603	0.37390097	ns
O75822	EIF3J	51.04224706	37.21	13	13	0.849791685	0.05649969	ns
A0A024QZB7	ATXN2L	50.94420493	19.94	15	18	0.673050183	0.026839	*
Q92878	RAD50	50.94334936	13.57	20	21	1		
Q9NZ56	FMN2	50.91330028	9.29	14	16	0.907556178	0.38365823	ns
P55795	HNRNPH2	50.91277802	21.38	3	8	0.877092984	0.09065494	ns
P0C0S5	H2AFZ	50.89920628	31.25	2	4	0.956170993	0.24874953	ns
P17812	CTPS1	50.8758738	27.58	13	16	0.903487079	0.38829912	ns
A0A024RBE8	SLC25A3	50.86528456	28.25	12	12	0.612472427	0.01716288	*
P60900	PSMA6	50.72527838	55.69	13	13	1.142107115	0.11686258	ns
O95202	LETM1	50.72227442	24.63	18	18	0.787465784	0.00867771	**
F8WDG7	PTK7	50.69403553	67.52	1	9	0.515829508	0.20475373	ns
Q69EZ8	F2	50.66378284	12.88	5	5	1.591765665	0.10202269	ns
P62888	RPL30	50.65268528	80	10	11	0.985917879	0.23663094	ns
P48059	LIMS1	50.64718771	42.77	8	16	0.677094564	0.00418288	**
H0YH87	ATXN2	50.55248117	15.72	1	14	1		
P52926	HMGA2	50.5243094	66.06	7	7	1.038479294	0.25471755	ns
P48163	ME1	50.45949876	28.32	17	18	0.969316904	0.7350765	ns
Q8N1G4	LRRC47	50.33387148	30.53	18	18	0.735996737	0.00620477	**
P09960	LTA4H	50.279814	26.68	17	17	0.942525444	0.21343451	ns
Q70UQ0	IKBIP	50.27283776	41.14	6	16	0.4454613	0.00368744	**
Q12765	SCRN1	50.2549448	28.5	12	13	0.958266598	0.29228111	ns
P30040	ERP29	50.05826211	38.7	10	10	1		
Q7L576	CYFIP1	49.91334033	17.24	21	21	0.892555397	0.14680592	ns
P49189	ALDH9A1	49.82505369	32.39	16	16	0.741784192	0.02625832	*
B7ZLP5	SAFB	49.68134356	19.04	11	18	0.650470868	0.00092558	***
F8WB06	ATXN2	49.67337823	13.14	1	14	1		
K7ELP0	TPM4	49.55998516	56.52	1	5	0.309221722	0.00225854	**
C5IWY4	HLA-A	49.55044746	42.19	1	10	1		
P62879	GNB2	49.53711009	27.65	3	9	1		

F8WAE5	EIF2A	49.38209867	29.83	15	15	0.92125958	0.11611652	ns
Q14258	TRIM25	49.26485705	20.95	12	12	0.831081253	0.0022622	**
Q9BTM1	H2AFJ	49.20391834	45.74	1	7		0.37390097	ns
Q9UPN1	PPP1CC	49.191239	36.73	2	11	1		
P30086	PEBP1	49.18356872	56.15	9	9	0.915134443	0.32651824	ns
H3BN98	H3BN98	49.06933033	30.8	2	9	0.982485564	0.37390097	ns
Q13151	HNRNPA0	48.94784141	39.67	10	12	0.528941327	0.00166506	**
P0C0L4	C4A	48.9421134	5.79	12	12	1.095388728	0.28240709	ns
Q9Y2W1	THRAP3	48.90342772	22.41	20	20	0.566753109	0.00023983	***
O43237	DYNC1LI2	48.85021091	32.72	14	15	0.700655477	0.00666888	**
Q9NVD7	PARVA	48.78780818	32.8	12	13	0.494327732	0.00577176	**
Q12959	DLG1	48.70225763	16.59	18	18	0.287441636	0.00024088	***
Q6PKG0	LARP1	48.65929294	16.61	18	18	1.003149287	0.37390097	ns
Q9HCU0	CD248	48.65883672	17.7	15	15	0.624508774	0.00012986	***
P51148	RAB5C	48.62087655	54.17	6	9	1		
P60903	S100A10	48.61609244	40.21	7	7	0.579095157	0.00826001	**
Q9NTK5	OLA1	48.58594465	34.85	15	15	0.726914594	0.06107745	ns
P62241	RPS8	48.57725084	45.67	10	10	1.003464076	0.82023295	ns
A0AVT1	UBA6	48.56148279	17.11	17	17	0.820456395	0.02098819	*
Q13443	ADAM9	48.49519193	17.22	16	16	0.916275866	0.162589	ns
Q16270	IGFBP7	48.43407822	39.01	10	10	0.806752131	3.7919E-06	***
P30508	HLA-C	48.31305182	40.44	0	11		0.37390097	ns
Q9TP39	HLA-A	48.31213081	55.8	0	10		0.37390097	ns
P13612	ITGA4	48.24296832	14.44	3	15	0.228928286	4.2076E-09	***
P46781	RPS9	48.2374593	46.39	9	10	0.918144129	0.26532745	ns
P14550	AKR1A1	48.2329427	38.77	12	13	0.983805594	0.23915815	ns
Q9BS26	ERP44	48.09795427	36.95	14	16	0.437114354	0.00118654	**
Q96CS3	FAF2	48.08575749	40	14	14	0.974059398	0.23380388	ns
P51153	RAB13	48.08003449	46.31	7	10	0.807558158	0.0678489	ns
Q96PK6	RBM14	47.98778677	26.16	17	17	0.804912448	0.02092911	*
P55060	CSE1L	47.93527699	19.26	20	20	0.95941512	0.60805337	ns
P40123	CAP2	47.86880088	33.54	14	16	0.945740268	0.23068888	ns
Q53T76	GPD2	47.84735334	28.28	21	21	0.840696366	0.13403209	ns
A0A024R9B9	MATN2	47.82757139	20.61	5	17	1		
Q9UNF1	MAGED2	47.76969838	28.38	16	17	1.023739394	0.78355236	ns
G3V1C3	API5	47.73209763	25.88	4	15	0.953563033	0.49239996	ns
O43615	TIMM44	47.67256284	33.85	15	15	0.999024918	0.37390097	ns
P15121	AKR1B1	47.61355615	33.86	11	13	0.566500658	0.00626523	**
A7MD96	SYNPO	47.44941473	22.89	16	16	0.699141779	1.0756E-06	***
O95831	AIFM1	47.35800362	30.02	15	15	0.868404433	0.09333656	ns
Q13162	PRDX4	47.34021091	31.37	5	8	0.982875991	0.63580852	ns
Q6P1N0	CC2D1A	47.29731548	19.98	11	19	1		
Q9Y2A7	NCKAP1	47.24382257	17.02	19	19	0.940268555	0.17462941	ns
Q99988	GDF15	47.20780826	46.43	10	10	1.415212033	8.7181E-05	***
Q13884	SNTB1	47.08775473	25.65	11	14	0.294456206	6.3251E-05	***
P59998	ARPC4	47.07351696	46.43	9	9	0.970171995	0.6361694	ns
Q29941	HLA-B	47.00357294	35.36	0	10		0.37390097	ns

P30084	ECHS1	47.00141549	34.48	12	12	0.870583509	0.13484048	ns
P52565	ARHGDIA	46.94182479	38.73	9	10	1		
P04908	HIST1H2AB	46.72073638	45.38	3	7	0.762170275	0.00836016	**
P07205	PGK2	46.68982649	20.86	3	9	1.308111615	0.12983146	ns
P11177	PDHB	46.6073451	31.48	10	10	1		
Q9NQW7	XPNPEP1	46.55747342	30.66	17	18	0.954661177	0.25275075	ns
A5PLK9	BMP1	46.53188252	15.52	1	16	1.186191406	0.11722647	ns
A0A024R1X8	JUP	46.52573717	23.09	10	15	1.069938587	0.37390097	ns
O43865	AHCYL1	46.46072161	24.72	6	14	0.614107991	4.3981E-05	***
P52597	HNRNPF	46.41823602	26.02	7	9	0.587847371	0.00089195	***
A0A087WT27	PGM3	46.37391996	35.15	15	15	0.880651344	0.21083169	ns
Q16222	UAP1	46.36514473	27.78	15	16	1.652185026	0.06518617	ns
Q9Y570	PPME1	46.31808579	29.02	10	10	0.984982815	0.37390097	ns
P46060	RANGAP1	46.29634714	31.52	16	16	0.975389536	0.14721814	ns
Q32MZ4	LRRFIP1	46.27118349	20.42	9	15	1.15468095	0.50576551	ns
O15143	ARPC1B	46.14720845	35.48	13	13	0.634459459	0.00591369	**
A0A087X142	SEPT8	46.14164221	21.6	5	10	0.910986742	0.17552168	ns
P28074	PSMB5	46.11973429	42.21	11	11	1.021738569	0.37390097	ns
P61254	RPL26	46.10200632	41.38	10	10	0.954737177	0.15947082	ns
Q9BZQ8	FAM129A	46.10091889	14.76	14	15	0.368955807	0.00068762	***
E9PQN2	BCLAF1	46.08865809	20.8	17	17	0.644371452	0.00024955	***
Q9UNZ2	NSFL1C	46.06525254	51.08	14	14	0.688664809	0.00197665	**
A0JP02	PLEKHA5	45.88302374	18.99	15	15	0.830350785	0.00155062	**
P16104	H2AFX	45.73803914	27.97	3	6	1		
O00203	AP3B1	45.73786879	16.54	9	17	0.975135602	0.24634324	ns
Q86VS8	HOOK3	45.70362043	22.84	16	16	0.871732455	0.18171802	ns
Q99536	VAT1	45.70052016	42.24	13	13	0.732371286	4.3627E-05	***
Q9NUQ6	SPATS2L	45.6329608	32.62	9	16	0.861299058	0.01040891	*
Q10471	GALNT2	45.57180119	28.72	16	17	1.295719369	0.26836092	ns
Q14554	PDIA5	45.49527025	25.82	14	14	0.690208932	0.03528473	*
P11233	RALA	45.44930482	39.81	6	9	0.489327262	0.0013934	**
B4DXZ6	FXR1	45.42475653	22.53	6	15	0.970619746	0.73013506	ns
Q6FG43	FLOT2	45.34750116	45.91	20	20	0.654202233	0.02678532	*
P35442	THBS2	45.32183862	15.53	13	14	0.695887722	2.6644E-62	***
Q2VIN3	RBM1	45.23089242	29.43	1	14		0.37390097	ns
Q15393	SF3B3	45.1824857	15.53	17	18	0.817635635	0.09083912	ns
D3DTX6	PPP1R9B	45.15600061	21.79	16	17	0.644558428	0.00113531	**
Q15907	RAB11B	44.96240675	53.67	12	12	0.955838413	0.14052596	ns
P48634	PRRC2A	44.94246209	9.5	16	18	1		
A0A024R895	SET	44.88794661	24.55	7	7	0.745977665	0.00862539	**
A0A024R4S2	PPP1R12C	44.85051787	24.55	16	16	0.95474838	0.11611652	ns
Q2NL95	DDX19B	44.81078255	30.07	1	13		0.37390097	ns
B4DMT5	EIF3F	44.72898602	29.97	9	9	1		
O14776	TCERG1	44.62925851	14.03	15	16	0.920624249	0.43285563	ns
P51610	HCFC1	44.60116959	8.65	16	16	0.876033559	0.01313073	*
P02765	AHSG	44.5839479	8.72	5	5	1.263322754	0.20772953	ns
Q6MZK8	DKFZp686K06110	44.54119802	5.53	1	14	1		

P49419	ALDH7A1	44.52443981	28.94	14	14	0.827764726	0.15239437	ns
B4DY09	ILF2	44.51126218	24.43	9	9	0.810313647	0.01542413	*
Q9UKS6	PACSIN3	44.51007676	36.56	14	14	0.896677336	0.12607459	ns
Q5QPL9	RALY	44.48062801	52.32	13	13	0.83853914	0.15944481	ns
P10319	HLA-B	44.46111727	34.53	0	9		0.37390097	ns
P27487	DPP4	44.428339	16.19	15	15	0.385818016	0.00035165	***
Q0VGA5	SARS	44.39580715	26.42	14	14	0.630492744	0.022755	*
A6H8W6	SIPA1L1	44.33826339	10.32	17	17	1		
A6NNK5	TP53BP1	44.32428718	11.62	17	17	1		
E7EMF1	ITGA2	44.25434208	24.17	1	17	0.885498003	0.12119474	ns
Q15056	EIF4H	44.11675322	38.31	10	10	0.969219566	0.24121388	ns
Q5T9W8	HSP90AB1	44.08511484	38.69	1	8	1		
E7EV99	ADD1	44.0591805	26.58	15	15	0.494344044	0.00025027	***
P17096	HMGA1	44.00474858	33.64	4	4	1.085447869	0.22342511	ns
Q9HDC9	APMAP	43.98139071	23.32	12	12	0.801389211	0.09546914	ns
O75368	SH3BGRL	43.97217572	51.75	8	8	0.869083214	0.09196913	ns
P29536	LMOD1	43.93568313	21.83	16	16	0.969877824	0.37390097	ns
Q29940	HLA-B	43.93099082	29.83	0	8		0.37390097	ns
Q63HN8	RNF213	43.9303956	3.4	17	17	1		
O94855	SEC24D	43.90003228	19.77	19	19	0.976707321	0.67920702	ns
Q96CV9	OPTN	43.89511907	24.61	14	14	0.872958381	0.03364671	*
C3VMY8	CRYAB	43.87130475	42.86	9	9	13.61069539	0.00690306	**
A0A087WSV8	DCAF5	43.85815263	32.38	14	14	0.870079517	0.1191283	ns
A0A024RB48	TENC1	43.78991103	15.64	14	17	0.958258431	0.04227135	*
P84085	ARF5	43.72943306	48.33	4	8	0.735519527	0.02893688	*
Q9NZW5	MPP6	43.71386576	30.19	13	15	0.507896671	3.1273E-05	***
P14735	IDE	43.69811916	15.11	15	15	0.985650805	0.24180094	ns
Q92804	TAF15	43.54660571	30.74	8	12	0.647670815	0.00390974	**
A6NLN1	PTBP1	43.50396001	24.86	10	14	0.434748939	0.00023863	***
P31930	UQCRC1	43.50361276	28.96	11	12	0.913636236	0.11611652	ns
Q9BR76	CORO1B	43.50304484	31.9	16	16	0.769926582	0.04321456	*
P31153	MAT2A	43.40812063	29.87	13	14	0.969687115	0.14790899	ns
P48637	GSS	43.37692845	29.96	14	14	0.897919274	0.38378011	ns
A0A075B730	EPPK1	43.33674729	7.54	1	9	0.696074947	0.41764485	ns
A0A024R3J7	hCG_2032701	43.24754381	17.64	12	14	0.619120105	0.0201486	*
H0Y5B0	EPB41L2	43.18641162	30.53	2	12	0.848480789	0.10664628	ns
P13073	COX4I1	43.14111805	41.42	9	9	0.617905548	0.00047485	***
K7EIV0	CAPNS1	43.09474874	35.2	8	8	0.773187848	0.01807536	*
Q13442	PDAP1	43.07516909	49.17	11	11	0.723725532	0.00873176	**
P36957	DLST	43.03335464	24.5	11	11	0.746633554	0.00546615	**
A7E2F7	CLIP2	42.98899627	14.34	10	14	1		
Q15155	NOMO1	42.8519845	11.54	13	13	0.574568789	0.00020632	***
Q14344	GNA13	42.82661653	31.03	9	11	0.773994837	0.00046464	***
Q2M2I8	AAK1	42.76971245	15.82	12	12	0.922310586	0.26853535	ns
Q06124	PTPN11	42.76725888	26.97	16	17	1		
E7EQT4	ACIN1	42.76008403	12.99	6	16	0.833631188	0.31471765	ns
Q13724	MOGS	42.69714975	21.39	16	16	0.966930325	0.1360964	ns

O95373	IPO7	42.66823649	14.16	11	12	0.90697424	0.14663342	ns
G3XAJ6	RFTN1	42.62381887	25.83	1	15	0.507179489	0.03191806	*
P21964	COMT	42.48347259	34.32	10	10	0.923319621	0.04886261	*
Q9HD26	GOPC	42.47546029	25.32	13	13	0.769439537	0.00170875	**
P10155	TROVE2	42.44148886	24.54	14	14	1.14308157	0.28143729	ns
Q7L1Q6	BZW1	42.43539357	26.01	13	13	0.974053785	0.47021122	ns
Q9BQS8	FYCO1	42.42522144	11.64	15	17	1		
E5RHW4	ERLIN2	42.42228079	41.12	10	15	1		
Q9UNF0	PACSIN2	42.42099833	27.78	16	16	0.922679033	0.06134363	ns
A6H591	HLA-A	42.4200424	47.99	0	10		0.37390097	ns
Q8TD55	PLEKHO2	42.39681935	23.27	14	14	0.389612885	0.00081104	***
P51572	BCAP31	42.28150034	32.11	12	13	0.484865653	0.00021317	***
O43633	CHMP2A	42.271065	38.74	10	11	0.979040941	0.14114463	ns
P13798	APEH	42.22582221	19.67	14	14	0.969897354	0.49091344	ns
D3DUJ0	AFG3L2	42.09403348	17.26	15	16	0.678634032	0.00982639	**
P30493	HLA-B	42.08456528	29.56	0	8		0.37390097	ns
P09496	CLTA	42.04541266	29.03	10	11	0.84136751	0.07485487	ns
P62081	RPS7	42.03246546	34.54	10	10	0.972911717	0.37390097	ns
P28066	PSMA5	41.91897345	39	8	8	0.817141103	0.31227676	ns
E9PNW4	CD59	41.91281176	29.63	4	4	0.967318693	0.37390097	ns
P17174	GOT1	41.76369405	27.12	12	12	0.906131187	0.44274271	ns
Q9ULT8	HECTD1	41.72650981	6.63	15	16	1		
Q9NR45	NANS	41.67264307	39	10	14	1		
Q9UM54	MYO6	41.66956961	10.12	13	13	1		
Q14677	CLINT1	41.50658059	20.48	12	12	1		
Q05DH1	PSMA7	41.46153164	42.86	10	10	1		
Q8TD16	BICD2	41.39714658	16.14	14	14	1		
P12259	F5	41.3907187	5.49	13	13	1		
A0A087WXK9	TRIP11	41.38892031	8.8	17	19	1		
Q15121	PEA15	41.31657529	47.69	6	6	0.984518684	0.7009085	ns
Q9BWM7	SFXN3	41.28382051	38.15	10	11	0.746003189	0.10636577	ns
Q7Z478	DHX29	41.27651775	14.54	17	19	0.850588178	0.18990992	ns
Q9Y6G9	DYNC1LI1	41.25989652	33.27	13	14	0.911253699	0.2398422	ns
P21266	GSTM3	41.16396642	53.78	11	13	0.501260328	0.00488581	**
G3V0I5	NDUFV1	41.15685606	26.04	14	14	0.6044763	0.00090704	***
Q99584	S100A13	41.12758946	48.98	6	6	0.915978937	0.34389058	ns
P30479	HLA-B	41.09264648	27.07	0	8		0.37390097	ns
Q9NQR4	NIT2	41.00511265	53.99	14	14	0.72784967	0.0075592	**
Q9H7C4	SYNC	40.94234562	25.31	13	13	1.009549403	0.96030129	ns
Q15113	PCOLCE	40.91448069	36.3	13	13	0.614468659	0.00172301	**
P15153	RAC2	40.82555056	37.5	4	8	0.865814265	0.16156682	ns
P46937	YAP1	40.80094123	34.33	12	12	1		
O95865	DDAH2	40.79659462	47.72	12	13	0.838618334	0.06389446	ns
Q9UKY7	CDV3	40.79029465	61.24	9	9	0.801619865	0.10666968	ns
O14980	XPO1	40.75293708	11.11	12	12	0.963075224	0.57239174	ns
Q08209	PPP3CA	40.70726514	22.26	5	11	0.783025666	0.07446716	ns
P29373	CRABP2	40.70422423	64.49	11	11	0.223437339	3.1206E-05	***

Q68J68	HLA-B	40.64322758	32.64	0	9		0.37390097	ns
Q68D38	DKFZp686O15119	40.63025892	28.97	5	9	0.840338268	0.11037556	ns
P84095	RHOG	40.56979227	35.6	8	9	0.620320895	0.00116401	**
A0A024R7S3	CLTB	40.56480575	37.44	11	11	0.514759721	0.00631006	**
A0A024R2W4	DAG1	40.54068494	14.64	12	12	0.492040249	8.0214E-05	***
Q96HI4	NMT1	40.53281403	25.91	10	14	0.819079036	0.00705189	**
J3QL06	HYOU1	40.51090455	53.55	1	11	1		
H0UI49	LAMA4	40.50789905	8.7	16	16	0.811504553	#DIV/0!	#DIV/0!
P61020	RAB5B	40.50458288	47.91	5	8	0.960493791	0.11611652	ns
Q14978	NOLC1	40.48645091	16.74	14	14	0.759981145	5.941E-07	***
Q9H6S3	EPS8L2	40.47226071	20.42	14	14	0.818840822	3.2935E-06	***
Q9UJ70	NAGK	40.46573639	38.66	13	13	0.985325227	0.37390097	ns
Q9ULH1	ASAP1	40.43743002	14.44	15	16	0.887584176	0.12595486	ns
A0A024R172	LTB4DH	40.42788911	30.09	12	12	0.662470134	0.00531329	**
O15173	PGRMC2	40.37809491	33.63	8	10	1		
P49207	RPL34	40.37689829	46.15	8	8	1		
P49773	HINT1	40.35333216	64.29	7	7	0.679405166	0.00069076	***
A0A024RAI6	BIN1	40.29622483	28.36	11	13	0.668478256	0.00047291	***
E4W6B6	RPL27	40.2693069	57.14	8	9	0.978289057	0.82174207	ns
Q04760	GLO1	40.2578696	39.13	11	11	0.864255384	0.00845697	**
P21281	ATP6V1B2	40.23532283	27.59	14	14	0.703633661	0.06945356	ns
P19022	CDH2	40.2272321	18.21	13	13	0.893717719	0.1273368	ns
M0R3D6	RPL18A	40.16166425	46.81	7	7	1.031205363	0.37390097	ns
Q15654	TRIP6	40.15808272	36.13	13	14	0.872584163	0.00027939	***
Q6IBS0	TWF2	40.13458419	43.84	10	14	0.893674505	0.08901051	ns
P46087	NOP2	40.12695456	16.87	11	15	0.701590796	0.00477721	**
F8W1A4	AK2	40.08463514	43.53	10	10	1		
Q9UKK3	PARP4	40.03951192	8.24	14	15	1		
O75094	SLIT3	39.97249687	8.6	13	13	0.766565621	2.3504E-06	***
P62316	SNRPD2	39.9497689	66.95	9	9	1.010830119	0.30759376	ns
P23193	TCEA1	39.89303684	44.52	13	13	1		
F5GYN4	OTUB1	39.89160371	46.89	11	11	0.995571491	0.37390097	ns
P09429	HMGB1	39.84018826	46.98	8	11	0.643712782	0.00075937	***
C9JFR7	CYCS	39.69723105	41.58	6	6	0.748649721		
Q7L014	DDX46	39.69667959	13.77	16	16	0.684166959	0.00104065	**
A6NGP5	HN1L	39.69634461	73.03	11	11	0.862320484	0.04290513	*
P48426	PIP4K2A	39.68686366	27.59	5	11	0.567786011	0.01069362	*
O15400	STX7	39.63655674	34.87	8	9	0.666208471	0.00678911	**
G3V3M6	APEX1	39.6107893	35.74	11	11	0.77916485	0.03150574	*
Q13011	ECH1	39.54004049	34.15	11	11	0.943579636	0.1150547	ns
Q9Y5M8	SRPRB	39.52865422	47.97	13	13	0.94790741	0.26737304	ns
Q13347	EIF3I	39.48833692	32.31	11	11	1		
Q5T9B9	ENG	39.45841646	21.92	7	12	0.676624957	0.00078892	***
O75347	TBCA	39.38171625	73.15	12	12	0.99941741	0.9645169	ns
Q9Y680	FKBP7	39.32089436	42.08	11	11	0.617794735	0.00012452	***
Q15262	PTPRK	39.31468773	12.65	14	14	1		
Q92888	ARHGEF1	39.31168079	17.11	14	14	0.624733196	0.03305859	*

Q01650	SLC7A5	39.30803335	8.09	4	4	0.892966974	0.16777125	ns
Q00169	PITPNA	39.26889062	41.11	10	13	1		
B7Z7P8	ETF1	39.24925613	30.5	13	13	0.99980057	0.9990605	ns
O95292	VAPB	39.23873591	37.45	8	9	0.482090166	0.00202431	**
B5BU01	EIF2S2	39.17231631	36.34	11	11	0.919462695	0.18991243	ns
Q13136	PPFIA1	39.12281847	17.14	17	18	0.725334908	0.00120514	**
Q16543	CDC37	39.08455348	38.89	17	17	0.85636781	0.14297658	ns
G0KXI4	HLA-A	39.08005857	47.51	0	9		0.37390097	ns
O94813	SLIT2	39.07223237	10.6	14	14	0.937779019	0.11611652	ns
Q13838	DDX39B	39.03401434	26.4	5	14	0.66346105	0.02472171	*
M4QFU4	HLA-B	38.94090307	28.45	0	8		0.37390097	ns
P10768	ESD	38.94006443	27.66	9	9	0.898928367	0.34661759	ns
P28161	GSTM2	38.92908716	60.55	7	14	1		
A5YKK6	CNOT1	38.91231656	5.93	14	14	1		
F8VU51	YLPM1	38.85337913	9.79	2	14	1		
H3BR35	GSPT1	38.81044698	25.68	8	16	0.590282269	0.00283545	**
P56159	GFRA1	38.78332829	22.15	13	13	0.264565692	0.00019757	***
O95479	H6PD	38.75012958	20.48	15	15	0.990619882	0.11611652	ns
Q96J84	KIRREL	38.72193217	21.14	11	11	0.995251085	#DIV/0!	#DIV/0!
B4DQF6	EIF3L	38.68029928	20.53	12	12	0.740801945	0.08745421	ns
P16989	YBX3	38.64552367	25.27	2	8	1		
O75937	DNAJC8	38.53723001	38.74	10	10	0.926590212	0.10195842	ns
P18463	HLA-B	38.51033103	29.83	0	8		0.37390097	ns
Q9NX63	CHCHD3	38.48989534	43.17	13	13	0.675223065	0.00118134	**
Q8IWE2	FAM114A1	38.44893217	24.87	13	13	0.733125838	0.01547153	*
F1T0I1	SEC16A	38.36507297	7.28	14	14	0.71221153	0.00476385	**
Q99733	NAP1L4	38.35773933	23.73	10	11	0.781285838	0.00820579	**
Q7YQB3	HLA-Cw	38.32414222	31.69	0	10		0.37390097	ns
P50148	GNAQ	38.31048357	37.05	8	14	0.638957976	0.0067195	**
P21399	ACO1	38.28525376	16.42	16	16	0.732523919	0.00970213	**
Q5JWQ6	NRP1	38.27474332	20.95	13	13	1		
H0Y9J2	CAMK2D	38.26421142	46.7	1	10	0.740811431	0.02341707	*
Q99714	HSD17B10	38.21370554	61.69	11	11	1		
B8YBG3	HLA-Cw	38.20128965	30.6	0	10		0.37390097	ns
Q9NRV9	HEBP1	38.18284059	61.9	10	10	0.438676145	1.7998E-05	***
Q16630	CPSF6	38.17254019	23.41	12	12	0.998199568	0.37390097	ns
B4E1L0	ADSS	38.14500391	24.6	12	12	0.974215666	0.3236772	ns
P49750	YLPM1	38.12407196	8.15	2	14	0.500387595	0.06866765	ns
Q07960	ARHGAP1	38.0465281	25.97	11	11	0.85892186	0.16693356	ns
A0A024RDA1	EXOC1	38.00639331	17.18	16	16	0.702336147	0.02387646	*
Q9Y263	PLAA	37.97602439	21.76	14	14	0.849554763	0.26521282	ns
O75976	CPD	37.96614945	11.81	16	16	0.929556106	0.11611652	ns
Q16698	DECR1	37.93008065	33.43	10	10	0.657683534	0.00421513	**
Q96C19	EFHD2	37.86658776	44.17	9	11	0.875656551	0.31671098	ns
P18754	RCC1	37.82595682	26.84	7	8	0.90314291	0.00037887	***
P62857	RPS28	37.80447829	52.17	4	4	0.893308247	0.26612473	ns
P30492	HLA-B	37.79426706	27.9	0	7		0.37390097	ns

Q4LE74	MYO9B	37.72695553	8.58	16	17	1		
Q9BPW0	PPP5C	37.70646691	24.59	13	13	1		
P61201	COPS2	37.70282662	27.54	13	13	0.820329408	0.00359953	**
Q9HC35	EML4	37.69406378	15.8	14	14	0.870418338	0.05004916	ns
P26440	IVD	37.6847229	26.48	11	11	0.392530781	3.6894E-05	***
Q3B7X1	TMX3	37.67374766	28.37	11	12	0.723571788	0.06371385	ns
Q01970	PLCB3	37.622365	12.97	14	14	0.829319778	0.00102905	**
O75367	H2AFY	37.54600334	31.18	9	9	0.730032012	0.00242527	**
O75828	CBR3	37.53661132	44.4	8	12	0.94341426	0.52541927	ns
P46063	RECQL	37.44352973	17.87	12	12	0.984564919	0.28647107	ns
Q7Z417	NUFIP2	37.40804482	21.01	11	11	1		
P55809	OXCT1	37.2924211	32.69	15	15	0.88738257	0.37142684	ns
E9PHK0	CLEC3B	37.2220782	27.5	3	3	1.013309244	0.60391156	ns
O75935	DCTN3	37.21798253	40.32	11	11	0.858245527	0.11092837	ns
Q6FH24	VBP1	37.06200898	61.25	11	12	1		
Q9Y639	NPTN	37.02808011	21.11	9	9	0.685950453	0.00184236	**
B2RNR6	ZFR	37.01314867	14.62	17	17	0.67609775	0.04742109	*
P08237	PFKM	37.00428987	18.21	12	16	1.008633029	0.37390097	ns
P20339	RAB5A	36.9792254	53.95	6	9	0.901467413	0.11023312	ns
D6RD46	LIMCH1	36.91343713	16.12	14	14	0.629240657	5.6502E-06	***
Q53FA7	TP53I3	36.88733029	34.04	12	12	0.848037451	0.2422022	ns
Q9UDY4	DNAJB4	36.87416172	35.91	9	11	1.06418037	0.37390097	ns
P27361	MAPK3	36.8468678	28.76	7	11	0.828842286	0.15296846	ns
Q9UQN3	CHMP2B	36.83947742	34.27	9	9	0.640200316	2.2115E-05	***
P50402	EMD	36.82394528	39.37	9	9	0.827954945	0.00268476	**
O76021	RSL1D1	36.79170775	21.84	12	12	0.717829768	0.01437377	*
O15230	LAMA5	36.72321939	5.3	14	14	1		
B7ZKY2	CASK	36.71524763	14.94	13	14	0.522711357	0.00016068	***
Q3B7K3	IKIP	36.65045285	35.96	1	11	3.045974528	0.12130282	ns
Q8NBJ5	COLGALT1	36.59585333	23.15	17	17	0.877969869	0.25559745	ns
A0A087WYK8	NRD1	36.58415294	10.54	11	11	0.944746712	0.54094269	ns
O95747	OXSR1	36.58006597	28.27	12	12	1		
P30519	HMOX2	36.55791831	35.13	11	11	0.977521865	0.37390097	ns
Q8IX12	CCAR1	36.4938395	9.83	13	13	0.81250569	0.01219521	*
P00813	ADA	36.46246672	31.68	11	11	0.927270428	0.37390097	ns
P46778	RPL21	36.4509064	40	8	9	0.900450976	0.26298646	ns
H7C597	SND1	36.43320131	46.75	1	10		0.37390097	ns
Q9BXP5	SRRT	36.40180945	15.41	14	14	1		
Q15843	NEDD8	36.36421156	40.74	5	5	0.89627649	0.38273167	ns
A0A024RAD5	DDOST	36.33711243	22.81	11	11	1		
Q8IWJ2	GCC2	36.32789564	5.82	10	13	0.958728634	0.23438059	ns
J3KQ45	TGOLN2	36.29591405	31.5	15	15	0.454972844	0.00053909	***
Q02218	OGDH	36.29217255	12.61	13	13	1		
P22061	PCMT1	36.28618109	44.93	10	10	0.709472765	0.01351101	*
O76031	CLPX	36.26699138	18.8	11	11	1		
P54709	ATP1B3	36.2521255	32.97	12	12	0.553628532	5.7532E-07	***
Q8IVL6	LEPREL2	36.23539531	16.58	6	12	1.010171071	0.37390097	ns

Q9H0B6	KLC2	36.23285437	21.06	9	12	1		
S4R3N1	HSPE1-MOB4	36.20700622	23.75	3	8	1		
O00487	PSMD14	36.19867301	26.13	9	9	0.980911542	0.37390097	ns
P30487	HLA-B	36.16809535	28.18	0	8		0.37390097	ns
P62269	RPS18	36.08852911	53.29	11	11	0.944078943	0.41243668	ns
Q14669	TRIP12	36.01521266	8.48	14	15	0.972802279	4.4169E-06	***
P61764	STXBP1	35.94871616	25.93	16	16	0.950121291	0.28946605	ns
P61019	RAB2A	35.93903661	41.98	3	9	0.995379034	0.86906191	ns
O94804	STK10	35.92545891	15.19	15	16	0.68111504	0.00016834	***
P35625	TIMP3	35.89544201	41.71	10	10	0.281881727	0.00042501	***
D6RAN1	PDLIM7	35.89337945	45.56	1	5	0.818877161	0.47762021	ns
Q9Y277	VDAC3	35.83217454	21.91	6	7	1		
A1X283	SH3PXD2B	35.71404493	13.5	11	12	1.506136953	0.1545606	ns
P20674	COX5A	35.68738317	30.67	7	8	0.488815133	0.00014846	***
P25788	PSMA3	35.68648136	34.9	10	10	1.282467621	0.09300899	ns
P36543	ATP6V1E1	35.65825045	34.96	10	11	1		
Q9BRK5	SDF4	35.648579	28.45	10	10	0.689414863	0.00692578	**
P51116	FXR2	35.59006166	20.36	9	12	1.019364904	0.37390097	ns
Q14151	SAFB2	35.58292007	17.21	7	14	0.466738053	0.00025661	***
Q99961	SH3GL1	35.49360704	30.43	12	12	0.947833342	0.18739332	ns
B3LEU8	TMEM214	35.41569865	15.9	12	12	0.94985529	0.25140792	ns
A0A087WXM8	BCAM	35.38511276	24.66	12	12	1		
O75962	TRIO	35.38291037	5.33	13	14	1.063160074	0.13420159	ns
O15511	ARPC5	35.3617177	56.95	8	9	0.791404021	0.065982	ns
H0YN26	ANP32A	35.34737539	51.98	5	11	0.919013135	0.37838107	ns
P52948	NUP98	35.34142947	8.04	15	15	0.930039837	0.31059151	ns
Q9UHX1	PUF60	35.31169331	17.89	6	12	0.826571936	0.00439774	**
Q08397	LOXL1	35.26627958	21.08	11	12	1.0091834	0.87130113	ns
Q71UH4	TOP2B	35.26564455	13.27	16	20	1		
P55010	EIF5	35.24485135	27.15	11	11	0.593452066	0.00176889	**
R4GMR5	PSMD8	35.22147179	39.37	11	11	0.922593856	0.30663315	ns
P55036	PSMD4	35.21575117	27.06	9	9	0.803136432	0.04611662	*
Q6LEU0	STX12	35.16597772	31.6	8	8	1		
Q5JSH3	WDR44	35.1481694	13.91	12	12	1.288244344	0.2000105	ns
C1ICA6	HLA-B15	35.14748669	49.45	0	8		0.37390097	ns
F8W020	NAP1L1	35.10179806	40.1	6	7	1		
Q8IUE6	HIST2H2AB	35.08166587	24.62	1	4	0.758505667	0.02028686	*
Q96AQ6	PBXIP1	34.95911849	18.19	1	12	0.820673095	0.39762042	ns
Q96BS4	FBL	34.95245385	34.23	10	10	0.623181733	0.01887451	*
Q9NQC3	RTN4	34.9193399	11.83	9	9	0.913768699	0.16520517	ns
Q96CT7	CCDC124	34.90507567	47.09	14	14	0.831718559	0.14841177	ns
P83111	LACTB	34.89280462	19.93	9	13	0.55470373	0.01676217	*
A0A087WTA5	EIF2B4	34.88427234	25.19	12	12	0.890435357	0.21140957	ns
P23368	ME2	34.86597073	22.09	11	12	0.987986383	0.37390097	ns
Q9H0A0	NAT10	34.82051051	11.32	11	11	1		
P18031	PTPN1	34.81796718	31.03	13	13	1		
A0A075B7B1	SYNM	34.796018	11.33	15	15	1		

Q13619	CUL4A	34.71892738	14.89	3	14	0.704483525	0.05152424	ns
Q15717	ELAVL1	34.6656363	38.65	11	11	0.902851825	0.13002695	ns
P12429	ANXA3	34.65826714	35.6	12	12	0.458495623	6.146E-05	***
O78052	HLA-B	34.62335372	45.05	0	8		0.37390097	ns
Q8N766	EMC1	34.61989522	16.01	14	14	0.859103692	0.30435446	ns
A0A024R588	SF1	34.60271907	17.88	8	10	1		
O00161	SNAP23	34.597561	47.87	12	12	0.642858297	0.00023869	***
O43252	PAPSS1	34.55141354	21.63	10	13	0.702164402	0.003711	**
Q9UHN6	TMEM2	34.54940152	9.62	12	13	1		
B5BU25	U2AF2	34.46636939	17.62	9	9	1		
O78107	HLA-B	34.43732238	45.86	0	8		0.37390097	ns
P23743	DGKA	34.34795976	21.22	13	14	0.987361571	0.37390097	ns
P20618	PSMB1	34.34557581	45.64	9	9	1.241540747	0.10980009	ns
P19784	CSNK2A2	34.33360767	33.14	8	10	1		
Q15435	PPP1R7	34.29205441	39.72	13	13	0.858775977	0.226592	ns
Q9UBU2	DKK2	34.27613211	32.05	6	8	0.329176768	0.00050342	***
O43765	SGTA	34.24206018	33.87	10	10	0.992477365	0.77131373	ns
Q9H845	ACAD9	34.23251629	18.2	12	12	0.785916437	0.01222538	*
Q9HA77	CARS2	34.21666133	22.34	12	12	0.575974009	0.01047478	*
Q9BXF6	RAB11FIP5	34.20077395	22.36	11	11	0.848807367	0.05303019	ns
P01111	NRAS	34.18649459	46.03	4	8	0.424594712	0.02406746	*
Q8N3D4	EHBP1L1	34.15987122	8.86	10	11	0.901516643	0.11611652	ns
Q8TCS8	PNPT1	34.15618944	16.22	13	13	0.85559594	0.00819027	**
P63167	DYNLL1	34.04350185	51.69	4	5	0.954551845	0.10288631	ns
P62266	RPS23	34.04060912	38.46	7	8	0.99822825	0.57812985	ns
O75964	ATP5L	34.03338981	51.46	6	7	0.702598148	0.04004333	*
I2G9F9	HLA-C	34.01034117	30.38	0	9		0.37390097	ns
A0A024RAV4	CSDA	33.9701587	30.69	1	7	0.917772567	0.37390097	ns
Q9NRX4	PHPT1	33.95712972	58.4	8	8	0.882704001	0.11856589	ns
Q9Y2X3	NOP58	33.92920351	21.17	10	10	0.663828224	0.02488897	*
Q9Y371	SH3GLB1	33.87978542	26.58	8	11	0.599517043	0.00866765	**
I6L9E8	FAM98A	33.86326241	17.57	6	9	0.986342472	0.37390097	ns
Q15185	PTGES3	33.85357583	40	8	8	0.77380957	0.0094423	**
P31937	HIBADH	33.83994567	33.04	9	9	1		
Q08379	GOLGA2	33.82613301	13.87	7	13	1.012653685	0.11611652	ns
A0A075B6E5	ENAH	33.75945938	35.21	1	8	0.921213942	0.37390097	ns
E9PKG1	PRMT1	33.73755598	28	10	10	1.120757662	0.27655049	ns
E7EU96	CSNK2A1	33.73114073	29.09	9	11	0.882577327	0.03191678	*
P00568	AK1	33.7161243	56.19	10	11	0.81585049	0.11543259	ns
A0A024R1M8	APOL2	33.69489741	32.05	11	11	0.542382236	0.00282095	**
O15439	ABCC4	33.6687274	8.08	10	12	0.673245366	6.1359E-07	***
P14543	NID1	33.6431427	13.87	13	14	0.981016628	0.11611652	ns
Q02252	ALDH6A1	33.58657932	25.98	13	14	0.884371608	0.00010801	***
Q52LJ0	FAM98B	33.55148315	28.48	6	9	1		
Q9UG63	ABCF2	33.54568052	18.62	12	12	0.910169018	0.01105055	*
Q15042	RAB3GAP1	33.5342412	13.25	11	11	0.978958076	0.48796064	ns
Q9BQG0	MYBBP1A	33.5319289	10.02	13	13	0.863012665	0.10479325	ns

Q14161	GIT2	33.52923203	15.15	8	11	0.640873942	0.00218871	**
P31040	SDHA	33.46666574	17.62	11	11	0.608207423	0.00012624	***
Q8N1N4	KRT78	33.41636229	13.46	5	8	1		
B4E2V5	STOM	33.35067201	42.62	9	9	1		
O94776	MTA2	33.2452327	19.61	13	14	0.966295692	0.37390097	ns
Q9Y608	LRRFIP2	33.11669898	15.81	9	11	0.696364813	0.00018567	***
Q16666	IFI16	33.10602188	14.27	7	10	0.905688783	0.08736719	ns
Q9UIW2	PLXNA1	33.09642684	7.07	11	15	0.776945264	3.6227E-06	***
A0A087WUQ6	GPX1	33.09416986	42.57	8	8	0.479754961	0.00078733	***
Q9Y3P9	RABGAP1	33.08035707	12.16	9	12	1.063585126	0.43249543	ns
I3L0A0	TMEM189-UBE2V1	33.07650757	27.3	8	12	0.930052091	0.35813776	ns
A0A024R326	RPL29	33.06718278	30.57	7	7	0.75256729	0.00025042	***
Q8N556	AFAP1	33.06712031	13.84	11	12	0.970047345	0.63465884	ns
D3DVW9	PTPNS1	33.06115675	28.37	12	12	1.48767128	0.04372223	*
E9PHV5	SSFA2	33.05424154	11.48	14	14	1		
O75475	PSIP1	32.97928357	18.87	11	12	1		
Q5VYK3	ECM29	32.97018158	8.78	14	14	0.94456831	0.13147887	ns
P30038	ALDH4A1	32.92073572	24.33	13	13	0.689143127	0.00041975	***
J3KN29	PSMD9	32.90214324	40.09	9	9	0.987012691	0.37390097	ns
O95433	AHSA1	32.88024354	33.73	12	12	0.938113323	0.28208584	ns
P10599	TXN	32.80686855	51.43	7	7	0.327078214	0.00088185	***
Q9BRK3	MXRA8	32.79612005	29.64	12	12	0.882169065	0.20535872	ns
Q6UVY6	MOXD1	32.75838935	17.62	12	12	0.236258518	5.7282E-05	***
P61587	RND3	32.7560823	27.87	7	7	0.347930678	5.1559E-05	***
Q53S54	CUL3	32.71317005	14.08	11	12	1		
A0A087WUM2	LDHAL6A	32.71101344	10.3	1	3	1.090635128	0.67896062	ns
D6RB85	CANX	32.67939365	51.39	1	9	0.746649124	0.341356	ns
Q08J23	NSUN2	32.65332437	18.38	13	13	1		
C5IWY9	HLA-A	32.64860404	33.7	0	9		0.37390097	ns
Q8N3C0	ASCC3	32.63950157	4.59	3	12	0.719155563	0.09376316	ns
F2Z2V0	CPNE1	32.62105513	16.89	10	10	0.716085566	0.06299599	ns
Q13185	CBX3	32.55944419	47.54	9	11	0.664523165	0.02731657	*
Q9NP72	RAB18	32.54373157	47.57	9	10	0.829421068	0.17956002	ns
H0YBJ4	MATN2	32.52951717	18.19	1	13	0.590911263	0.02381204	*
O14737	PDCD5	32.52274561	45.6	8	8	1		
Q14444	CAPRIN1	32.48652244	10.58	9	9	0.566600567	0.01967668	*
Q08AF3	SLFN5	32.48587561	15.6	13	14	1		
Q15057	ACAP2	32.46284294	14.4	12	12	0.706852538	0.14660452	ns
O43747	AP1G1	32.43104136	12.04	12	13	0.890374755	0.24969801	ns
Q9P2R3	ANKFY1	32.38950658	11.46	11	13	0.983484783	0.37390097	ns
Q6EMK4	VASN	32.38617253	17.38	11	11	0.284373272	0.00015849	***
Q9BVJ8	HEXA	32.36448812	29.34	11	12	0.611123095	0.00758881	**
Q9UN86	G3BP2	32.34110737	21.99	10	11	0.945303758	0.37390097	ns
P38919	EIF4A3	32.32304907	21.17	7	10	1		
P09661	SNRPA1	32.30079579	41.18	11	11	0.595967079	0.00015933	***
P04424	ASL	32.2383374	27.59	12	12	1.103055587	0.08310969	ns
Q96T51	RUFY1	32.22537482	17.51	11	13	0.962644124	0.37390097	ns

Q8N4P8	GTPBP4	32.17783678	17.88	11	12	0.983422256	0.16224364	ns
P40763	STAT3	32.16469884	14.16	10	11	0.518918045	0.00099637	***
O75947	ATP5H	32.14869833	45.96	8	9	0.59773669	0.00046264	***
Q96RP9	GFM1	32.10989952	16.25	1	13		0.37390097	ns
Q9UPT5	EXOC7	32.08785796	16.19	11	11	1		
Q06323	PSME1	32.07900715	48.59	13	13	0.81801183	0.03519762	*
P67775	PPP2CA	32.01972425	41.42	1	10	1		
Q6NX51	EXOC4	32.01710808	14.07	13	13	0.777129198	0.02944828	*
A5PLK7	RCC2	31.96793592	23.85	10	10	0.906362651	0.3105979	ns
P50452	SERPINB8	31.94906545	30.48	11	13	0.686308374	2.8921E-05	***
P25789	PSMA4	31.91953611	34.87	11	11	1.020849141	0.88982121	ns
P54687	BCAT1	31.90304291	17.62	8	8	1.836965354	0.1888629	ns
O00232	PSMD12	31.90297437	26.32	10	12	0.994128869	0.82624084	ns
C1KJK7	HLA-A	31.89236689	38.67	0	7		0.37390097	ns
A0A024R529	DAK	31.78817916	20.7	10	10	1		
Q9UJZ1	STOML2	31.78512049	34.27	11	11	0.546917212	0.00359409	**
P30566	ADSL	31.74935651	23.35	11	11	1		
Q3B874	STRN	31.70114851	17.09	9	12	1		
E9PFR3	PPP2R5D	31.69478858	21.55	9	12	1.008804838	0.37390097	ns
E5KND7	GFM1	31.68201017	16.25	1	13	1		
P0CW22	RPS17L	31.67376351	45.93	8	9	0.87073838	0.31329641	ns
B8ZZU8	TCEB2	31.65570021	54.87	6	6	1.048598153	0.25654008	ns
Q9H6X2	ANTXR1	31.64629638	18.97	9	10	0.320884321	0.00030388	***
Q9BTV4	TMEM43	31.64007545	23.25	9	10	0.588373342	1.4089E-06	***
G8JLG1	SMC1A	31.63903069	11.73	15	15	0.940391471	0.37134761	ns
P12004	PCNA	31.62953305	42.15	11	11	0.855922985	0.29803026	ns
O75400	PRPF40A	31.6008513	8.67	10	10	0.500427247	4.112E-05	***
C9J712	PFN2	31.59997463	74.73	4	8	1.071654226	0.14102116	ns
P68036	UBE2L3	31.58882689	42.86	3	8	1.029588763	0.91176802	ns
E9PPJ5	MDK	31.51809144	61.07	9	9	3.645394328	0.07022279	ns
Q96A33	CCDC47	31.42645574	26.5	12	12	0.905886748	0.11867909	ns
Q9H3P7	ACBD3	31.40539253	21.21	9	9	0.992485252	0.37390097	ns
A0PJ92	NOP56	31.39938641	25.5	12	12	0.735338909	0.06730888	ns
Q5QNZ2	ATP5F1	31.2984935	29.23	7	7	0.57086081	0.00014173	***
Q8N0Y7	PGAM4	31.28821492	26.77	1	6	1.010581787	0.37390097	ns
B7ZKK7	EIF2AK2	31.28203344	18.68	10	10	0.942308157	0.01803925	*
P63173	RPL38	31.23867154	42.86	4	5	0.556591766	0.01613117	*
P17948	FLT1	31.17425239	8.97	12	13	0.707527203	1.1982E-05	***
B4E043	KHDRBS1	31.14391983	17.87	6	9	1		
Q92609	TBC1D5	31.08004093	14.97	10	10	1		
Q8TAT6	NPLOC4	31.02178097	17.76	12	12	1.007465948	0.83900693	ns
P61970	NUTF2	30.99466133	34.65	3	4	0.863676552	0.16803894	ns
Q0PHV0	HLA-B	30.99440742	42.54	0	7		0.37390097	ns
P12931	SRC	30.98775291	22.39	5	11	0.931961611	0.25649597	ns
Q13242	SRSF9	30.98380744	42.99	10	10	0.990438761	0.37390097	ns
P30048	PRDX3	30.97947741	31.64	8	8	0.762153448	0.00087419	***
Q9UNE7	STUB1	30.97360682	35.97	11	12	0.998975499	0.37390097	ns

P43490	NAMPT	30.95937359	25.87	12	12	0.699095054	0.00218264	**
P16333	NCK1	30.75835848	27.85	8	10	0.986462459	0.37390097	ns
P48739	PITPNB	30.74430537	35.79	6	10	0.855614945	0.31680819	ns
B2RMN7	SPTB	30.69524097	3.7	1	11		0.37390097	ns
Q96G03	PGM2	30.68490744	14.38	7	9	0.635243818	0.00271298	**
Q31612	HLA-B	30.64455676	32.51	0	8		0.37390097	ns
O00148	DDX39A	30.56325734	20.14	1	10	1		
Q4KMQ2	ANO6	30.52022672	12.64	13	13	0.353809126	4.0222E-06	***
P04181	OAT	30.51305664	17.77	10	10	0.556210257	0.01108233	*
C9J0K6	SRI	30.48727942	63.87	9	9	0.663583043	0.00358318	**
Q9NTZ6	RBM12	30.47421467	10.52	9	10	1		
B0QYK0	EWSR1	30.46820116	19.09	10	10	1		
P02458	COL2A1	30.4675144	5.31	1	6	0.316241918	2.0283E-05	***
P25685	DNAJB1	30.46667361	32.35	10	11	0.585040106	0.00019591	***
K7ERI7	RPL22	30.42252755	44.21	5	5	0.628442597	0.00889998	**
Q15181	PPA1	30.41729331	33.56	7	8	1.010624857	0.85402126	ns
A0A024QZJ7	CCDC6	30.40591192	20.04	10	10	0.93316726	0.22477404	ns
O75821	EIF3G	30.40334725	32.19	10	10	0.972958865	0.66676592	ns
G3V203	RPL18	30.40209138	43.9	8	8	0.935450187	0.37390097	ns
P61619	SEC61A1	30.35184717	17.23	10	10	0.879855494	0.3803541	ns
Q07812	BAX	30.34377635	35.94	5	5	1		
Q9ULC3	RAB23	30.3030014	40.51	8	8	1		
O43290	SART1	30.29833996	15.13	9	11	0.966522626	0.37390097	ns
Q13217	DNAJC3	30.27003872	22.42	11	12	0.743191788	0.1251071	ns
A5PKX5	MAN2A1	30.26864111	10.06	11	11	1.121132772	0.37390097	ns
Q5FYB0	ARSJ	30.26619935	14.86	11	11	3.914305943	0.00802979	**
D3YTB1	RPL32	30.26444745	45.86	8	8	0.910737398	0.49078598	ns
Q14573	ITPR3	30.20138359	3.93	10	11	0.756752679	0.00823942	**
Q9H3N1	TMX1	30.19079351	19.64	7	7	0.494131417	0.00046737	***
A0A024R258	UBQLN1	30.17786384	16.58	2	7	0.912851989	0.37390097	ns
A4D0Y7	LOC392781	30.14054871	24.48	1	5	1		
P49841	GSK3B	30.12739182	29.76	5	9	0.860022487	0.17375697	ns
P16435	POR	30.11532617	17.28	12	12	0.930352353	0.28693065	ns
O15187	TIAL1	30.08958149	24.15	4	9	0.431147667	0.00111274	**
Q9UBE0	SAE1	30.08075833	21.1	9	9	0.805903103	0.17828923	ns

Supplementary Table 3:
Adhesion fraction proteins also reproducibly detected in adhesions by Kuo et al

AAK1	ATP5B	CS	ENO1	HIP1	MDH2	PCK2	RAB5C	RPS3A	TJP1
ABCC1	ATP5F1	CSDA	EPB41L2	HMGA1	MEGF6	PDAP1	RAB7A	RPS4X	TLN1
ABCC4	ATP5H	CSPG4	EPHA2	HSD17B10	MME	PDGFRB	RAB8A	RPS5	TLN2
ABCF2	ATP5L	CSRP2	EPRS	HSP90AA1	MMP14	PDHB	RAC1	RPS7	TMEM2
ACAT1	ATP5O	CTNNA1	ERP29	HSPA5	MOXD1	PDIA3	RAC2	RPS8	TMEM43
ACTA2	BASP1	CTNND1	FAM129B	HSPA8	MPRIP	PDIA6	RAI14	RPS9	TNC
ACTBL2	C1ORF198	CTSD	FAM62A	HSPB1	MRC2	PDLIM1	RALA	RRAS	TNKS1BP1
ACTN1	CACNA2D1	CTTN	FAM98A	HSPD1	MSN	PDLIM4	RAN	RRAS2	TNS1
ACTN4	CALD1	CTTNBP2NL	FAP	HSPG2	MVP	PDLIM5	RAP1B	RSU1	TNS3
ACTR2	CALU	CYB5R3	FARP1	HYOU1	MXRA5	PDLIM7	RDX	RTN4	TPD52L2
ACTR3	CANX	CYCS	FBLIM1	ICAM1	MXRA8	PEBP1	RFTN1	S100A10	TPM1
ADAM9	CAPN1	CYFIP1	FERMT2	IDH2	MYH10	PFN1	RHOA	S100A11	TPM2
ADAMTSL4	CAPRIN1	DAG1	FHL1	ILK	MYH9	PGK1	RHOG	S100A13	TPM3
ADD1	CAPZA1	DBN1	FHL2	INF2	MYL6B	PGRMC2	RND3	S100A4	TPM4
AFAP1	CAPZB	DDAH2	FLNA	IQGAP1	MYL9	PHB	RPL10A	S100A6	TRIOBP
AGRN	CASK	DDX1	FLNB	ITGA2	MYLK	PHB2	RPL12	SCRIB	TRIP6
AHNAK	CAT	DDX3X	FLNC	ITGA4	MYO1B	PHLDB1	RPL13A	SCUBE3	TUBB
AKAP12	CAV1	DDX3Y	FLOT1	ITGAV	MYO1C	PICALM	RPL18	SERBP1	UACA
ALCAM	CC2D1A	DECR1	FLOT2	ITGB1	NCKAP1	PKM2	RPL19	SF1	UBAP2L
ALDH7A1	CCDC124	DLG1	FLT1	ITGB3	NDUFV1	PLS3	RPL22	SFPQ	UGDH
ALDOA	CD109	DNAJC3	FMN2	ITGB5	NES	PLXNA1	RPL27	SIPA1L1	UQCRC1
ANO6	CD248	DNAJC8	FXR2	JUP	NEXN	PLXNB2	RPL3	SLC25A3	UQCRC2
ANPEP	CD44	DNM2	G3BP1	KANK2	NME1	PPFIBP1	RPL30	SLC25A5	UTRN
ANXA1	CD59	DOCK7	G3BP2	KIRREL	NOTCH2	PPP1CB	RPL38	SLC7A5	VAPB
ANXA2	CDC42	DPP4	GANAB	KLC1	NPM1	PPP1CC	RPL4	SLC9A3R2	VASN
ANXA5	CDC42BPB	DST	GAPDH	L1CAM	NPTN	PPP1R12C	RPL5	SNAP23	VASP
ANXA6	CDH2	DSTN	GARS	LACTB	NQO1	PRDX1	RPL6	SNTB1	VCL
AP2A1	CFL1	DYNC1LI2	GDI2	LAP3	NRP1	PRDX3	RPL7	SNTB2	VDAC1
AP2A2	CKAP4	DYNLL1	GIT2	LASP1	NUFIP2	PRDX4	RPL7A	SPTAN1	VDAC2
AP2B1	CLIC1	ECHS1	GNA13	LDHA	NUMB	PRDX6	RPL8	SPTBN1	VDAC3
AP2M1	CLIC4	EEF1A1	GNAI2	LIMCH1	OGDH	PRKCDBP	RPL9	STOML2	VIM
ARHGEF2	CLTC	EEF2	GNAQ	LIMS1	OLA1	PTK7	RPLP2	STX12	WARS
ARPC1B	CNN1	EHD1	GNAS	LMNA	P4HA1	PTRF	RPN1	STXBP1	WDR1
ARPC2	CNN2	EHD2	GNB2	LMO7	P4HA2	PXDN	RPS10	SYNPO	YWHAB
ARPC5	CNN3	EHD3	GNG12	LPP	P4HB	PXN	RPS11	SYNPO2	YWHAE
ASPH	CNP	EHD4	GOT2	LRP1	PABPC1	RAB10	RPS13	TAGLN	YWHAG
ATL3	COMT	EIF3B	GPC1	LRPPRC	PACSIN2	RAB11FIP5	RPS14	TAGLN2	YWHAQ
ATP1A1	CORO1B	EIF3E	GSTP1	LRRC59	PACSIN3	RAB14	RPS16	TCEB2	YWHAZ
ATP1B3	COTL1	EIF4H	HADHB	LUZP1	PALLD	RAB18	RPS18	TENC1	ZYX
ATP2B1	COX5A	ELAVL1	HDLBP	MACF1	PARK7	RAB1B	RPS19	TFRC	
ATP2B4	CPNE1	ENAH	HEXB	MAP4	PARVA	RAB23	RPS2	TGFB1I1	
ATP5A1	CPNE3	ENG	HIBADH	MARCKS	PCBP2	RAB35	RPS3	TGM2	

Supplementary Table 4: Proteins matching Naba et al's matrisome

Proteins detected matching those predicted as core matrisome proteins by Naba *et al*	Of which, detected with reduced abundance in *TMEM67*	Detected ECM glycoproteins	Detected collagens	ECM glycoproteins with reduced abundance in *TMEM67*	Collagens with reduced abundance in *TMEM67*	Detected proteins matching lung ECM (Naba *et al*)
AGRN	COL12A1	AGRN	COL11A1	EMILIN2	COL12A1	ADAMTSL1
COL11A1	COL1A1	CYR61	COL12A1	FBLN1	COL1A1	AGRN
COL12A1	COL2A1	EDIL3	COL1A1	FBN1	COL2A1	ANXA1
COL1A1	COL6A1	EFEMP2	COL1A2	FBN2	COL6A1	ANXA2
COL1A2	COL6A2	EMILIN1	COL2A1	FN1	COL6A2	ANXA5
COL2A1	COL6A3	EMILIN2	COL3A1	IGFBP5	COL6A3	ANXA6
COL3A1	EMILIN2	FBLN1	COL5A1	IGFBP7		COL12A1
COL5A1	FBLN1	FBLN2	COL5A2	LAMA2		COL1A1
COL5A2	FBN1	FBN1	COL6A1	LAMB1		COL1A2
COL6A1	FBN2	FBN2	COL6A2	LAMB2		COL3A1
COL6A2	FN1	FN1	COL6A3	LAMC1		COL5A1
COL6A3	HSPG2	IGFBP3		LTBP1		COL5A2
CYR61	IGFBP5	IGFBP5		MATN2		COL6A1
EDIL3	IGFBP7	IGFBP7		MXRA5		COL6A2
EFEMP2	LAMA2	LAMA2		NID2		COL6A3
EMILIN1	LAMB1	LAMA4		PCOLCE		CSPG4
EMILIN2	LAMB2	LAMA5		SLIT3		EFEMP2
FBLN1	LAMC1	LAMB1		THBS1		EMILIN1
FBLN2	LTBP1	LAMB2		THBS2		EMILIN2
FBN1	MATN2	LAMC1				FBLN1
FBN2	MXRA5	LTBP1				FBLN2
FN1	NID2	LTBP2				FBN1
HSPG2	PCOLCE	LTBP4				FN1
IGFBP3	SLIT3	MATN2				HSPG2
IGFBP5	THBS1	MXRA5				HTRA1
IGFBP7	THBS2	NID1				IGFBP7
LAMA2		NID2				ITIH2
LAMA4		PCOLCE				LAMA2
LAMA5		POSTN				LAMA4
LAMB1		PXDN				LAMA5
LAMB2		SLIT2				LAMB2
LAMC1		SLIT3				LAMC1
LTBP1		SPARC				LOX
LTBP2		TGFBI				LOXL1
LTBP4		THBS1				LTBP1
MATN2		THBS2				LTBP2
MXRA5		THSD4				LTBP4
NID1		TNC				NID1
NID2						PLOD3
PCOLCE						PLXNB2
POSTN						POSTN
PXDN						PXDN
SLIT2						S100A11
SLIT3						S100A13
SPARC						SEMA3C
TGFBI						SERPINH1
THBS1						TGFBI
THBS2						TGM2
THSD4						THBS1
TNC						VCAN
VCAN						

Detected proteins matching colon ECM (Naba *et al*)	Proteins matching colon ECM (Naba *et al*) with reduced abundance in *TMEM67*	Proteins matching colon ECM (Naba *et al*) with reduced abundance in *TMEM67*
ADAMTSL1	ANXA1	ANXA1
AGRN	COL12A1	COL12A1
ANXA1	COL1A1	COL1A1
ANXA2	COL6A1	COL6A1
ANXA6	COL6A2	COL6A2
COL12A1	COL6A3	COL6A3
COL1A1	CSPG4	CSPG4
COL1A2	EMILIN2	EMILIN2
COL5A1	FBLN1	FBN1
COL5A2	FBN1	FN1
COL6A1	FN1	HCFC1
COL6A2	HSPG2	HSPG2
COL6A3	HTRA1	IGFBP7
CSPG4	IGFBP7	LAMA2
EMILIN1	LAMA2	LAMB2
EMILIN2	LAMB2	LAMC1
FBLN2	LAMC1	LTBP1
FBN1	LTBP1	MATN2
FN1	PLXNB2	PLXNB2
HSPG2	SEMA3C	TGM2
IGFBP7	TGM2	
ITIH2	THBS1	
LAMA2		
LAMA4		
LAMA5		
LAMB2		
LAMC1		
LOXL1		
LTBP1		
LTBP4		
NID1		
PLXNB2		
POSTN		
PXDN		
S100A11		
SERPINH1		
TGFBI		
TGM2		
VCAN		

Appendix 2

Book chapter: Analysis of high-throughput datasets

Analysis of high-throughput datasets

Summary

The era of high-throughput "-omics" approaches to data acquisition has created an environment in which many biologists find themselves "data-rich but knowledge-poor" due to the difficulty of extracting meaningful information from vast datasets. This is especially true in the case of centriole biology, where there has been a surge in publication of high-throughput studies. Here, we describe two approaches for analysis of high-throughput datasets: functional annotation clustering, which can be used to analyse lists of genes in the context of gene annotation databases; and pathway mapping, which can be used to visualise expression changes in the context of interactome databases. We approach these from the context of differential gene expression, but both are applicable to proteomic or other analyses that produce similar datasets.

Introduction

Centrioles have been studied since the early era of cell biology in the 19th century due to their central role in cell division[1]. The fundamental research questions – how do centrioles function in mitosis? What is their molecular structure? How do they replicate? – have remained relevant[2], but the tools used to study them have changed profoundly. Since the advent of genomics, proteomics and other high-throughput approaches, many studies have applied these tools to the centrioles[3–9] and generated rich datasets. Analysis of these datasets in the context of ever-increasing information about all cellular and biological processes requires new approaches. A researcher may be tempted to "eyeball" the data, manually searching it for interesting alterations. This can be a productive approach if the dataset is small or if only a few transcripts exhibit large changes in expression, but as datasets grow to

the hundreds or thousands of transcripts, manual analysis becomes increasingly prone to confirmation bias (where the researcher takes note only of changes that are consistent with their working hypothesis), and may miss important changes in less obvious molecular pathways. Furthermore, when trying to map expression changes onto signalling pathways, the complexity of the pathways themselves often precludes manual analysis.

Fortunately, tools to assist and automate these analyses have been developed. To illustrate the use of these analytical tools, we present basic tutorials for functional annotation clustering using the online DAVID resource and pathway mapping using the free, open source software package Cytoscape.

Gene set enrichment analysis and functional annotation clustering

Set enrichment analysis (or category over-representation analysis) is a statistical technique designed to identify categorical bias within lists. Gene set enrichment analysis takes as an input a list of genes, relates them to annotations in an annotation database (e.g. gene ontology), and identifies within the gene list annotations that are overrepresented in comparison to what would be expected in a randomly chosen list of genes from the same background (see Note 1).

Functional annotation clustering analysis is a refinement of this technique that identifies similar annotations within and across annotation databases and clusters them together, then reports an enrichment score for the entire cluster, rather than for each annotation individually (see Note 2). This improves human readability of the data and helps reveal underlying biology by eliminating the problem of overrepresentation of redundant annotations; for example, where a simpler analysis might show enrichment separately for the GO terms "centrosome cycle", "centrosome organization", and "microtubule organizing center organization", a functional annotation cluster combines all three as essentially equivalent and reports an overall enrichment score (Fig. 1).

Annotation Cluster 59	Enrichment Score: 1.18			Count	P_Value	Benjamini
GOTERM_BP_FAT	centrosome cycle	RT		5	2.0E-2	4.1E-1
GOTERM_BP_FAT	centrosome organization	RT		5	1.1E-1	7.6E-1
GOTERM_BP_FAT	microtubule organizing center organization	RT		5	1.3E-1	8.1E-1

Annotation Cluster 183	Enrichment Score: 0.37			Count	P_Value	Benjamini
SP_PIR_KEYWORDS	kinetochore	RT		6	2.1E-1	7.1E-1
GOTERM_CC_FAT	chromosome, centromeric region	RT		9	3.5E-1	8.7E-1
GOTERM_CC_FAT	kinetochore	RT		6	4.0E-1	9.0E-1
GOTERM_CC_FAT	condensed chromosome, centromeric region	RT		5	4.8E-1	9.2E-1
GOTERM_CC_FAT	condensed chromosome kinetochore	RT		4	6.1E-1	9.6E-1
GOTERM_CC_FAT	condensed chromosome	RT		7	7.0E-1	9.7E-1

Figure 1: Example functional annoatation clusters

This approach is ideal for examining large differential gene expression datasets that are difficult to interpret manually. It is possible to quickly identify the overall patterns within the data, such as particular molecular pathways that may be altered, and to find the genes of most interest. However, basic set enrichment analysis has a number of limitations that result from its simplified input: since it takes only a list of genes and no further attributes, the analysis cannot take into account information such as whether a particular gene was up- or downregulated, or the degree of altered expression (i.e. fold change). Care must therefore be taken to consider the biological question being asked when choosing the list of genes to submit for set enrichment analysis. It may be appropriate to separately submit lists of up- and downregulated genes from a dataset to identify which processes are activated and which are suppressed under the experimental conditions; conversely, if you suspect, for example, dysregulation of a particular signalling pathway where some of the pathway-associated transcripts are upregulated and others are downregulated, submitting the entire list of differentially expressed genes may increase the chance of identifying the pathway (see Note 3).

Gene set enrichment analysis makes the assumption that, under the null hypothesis, all genes are equally likely to be selected by chance as significantly altered in expression. This is a safe assumption for datasets such as those from microarray experiments, but due to the technical

details of RNA-seq differential expression analysis it is not a safe assumption for these datasets, which are more likely to report significant differences in high-abundance transcripts and long transcripts. This bias should be corrected for with an additional data processing step; for example, the GOseq method[10].

DAVID (the Database for Annotation, Visualisation and Integrated Discovery; david.ncifcrf.gov) is an online tool for automated gene set enrichment and functional annotation clustering analysis. The following is a step-by-step guide to basic analysis of a gene list using this tool (written for DAVID version 6.7; be aware that later versions may introduce changes in the interface). Much more comprehensive documentation is available within the DAVID website's Help and Tool Manual section, and in Huang *et al*[11].

Materials

A computer with at least 1 GHz CPU and 1 GB of memory, running at least Windows 2000/XP or Mac OS 10.

A web browser. DAVID recommends Internet Explorer 6.0 or higher, Firefox 1.5 or higher, Netscape 8.0 or higher, or Safari. Google Chrome is not officially recommended but appears to work without issue (version 49.0).

An internet connection (broadband recommended).

A list of gene identifiers in an appropriate format (eg Affymetrix ID, Ensembl gene ID).

Method

Submitting a gene list to DAVID

1. On the DAVID homepage (david.ncifcrf.gov), select "Start Analysis" from the top menu.

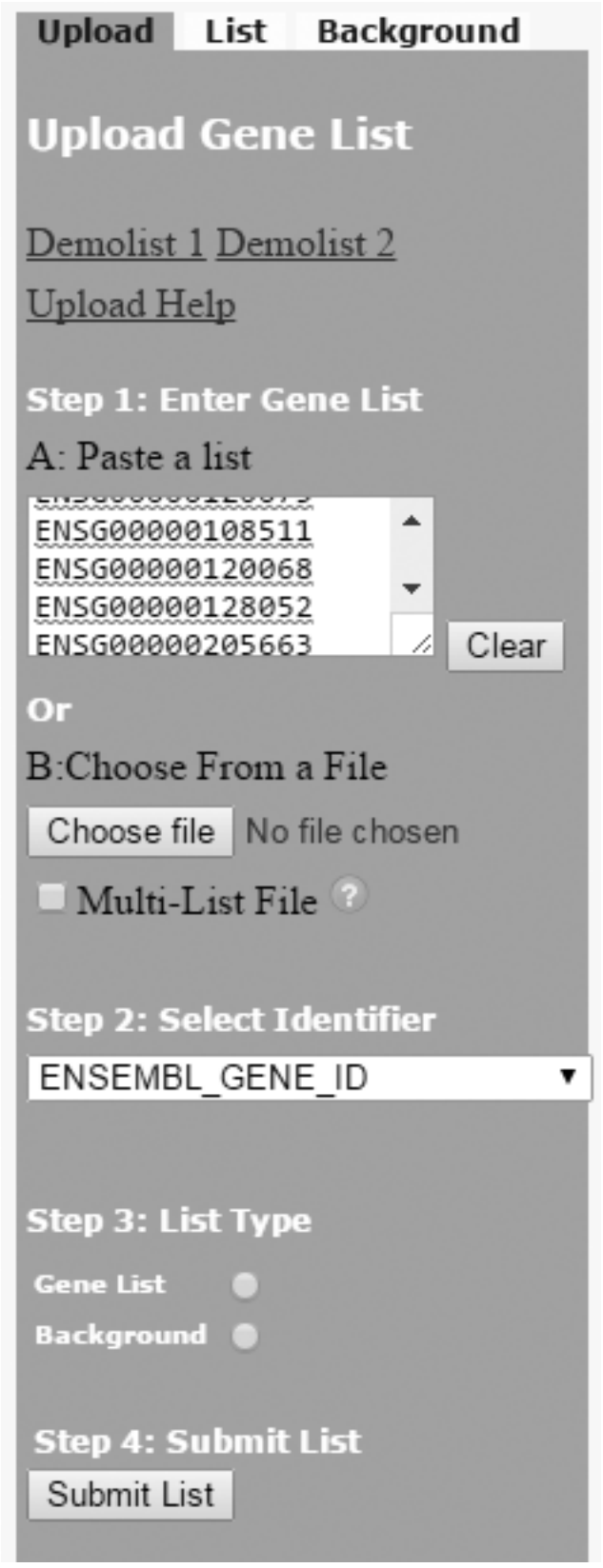

Figure 2: Upload a gene list

2. Under “Step 1: Enter Gene List” on the left panel (. 2), either paste your gene list into box A, or upload a file using the “Choose file” button.

3. Under “Step 2: Select Identifier” on the left panel, select the correct identifier for your gene list from the drop-down menu. In the example image (Fig. 2), a gene list has been entered using Ensembl IDs, and therefore “Ensembl gene ID” has been selected as the identifier. A variety of other identifiers can be used with DAVID including Affymetrix and Entrez IDs (see Note 4).

4. Under “Step 3: List Type”, Select “gene list”.

5. Click the “Submit List” button under “Step 4: Submit List”. Uploading the list may take a few seconds depending on connection speed. Once the upload is complete, the Gene List Manager will open (. 3, left). In the Gene List Manager, select a species to limit your analysis to, or opt to use all species, by selecting the option in the list and pressing the “Select Species” button.

6. In most cases, DAVID will automatically select an appropriate background. If this is not already shown, click “Start Analysis” on the top menu, which will display the Analysis Wizard and the current background. (Once a gene list has been uploaded, the “Start Analysis” button will take you to the Analysis Wizard instead of the upload panel). In the example image (Fig. 3), a gene list has been successfully submitted and the background correctly recognised as *Homo sapiens*. If you wish to manually select the background, this can be done via the “Background” tab above the Gene List Manager (see Note 5).

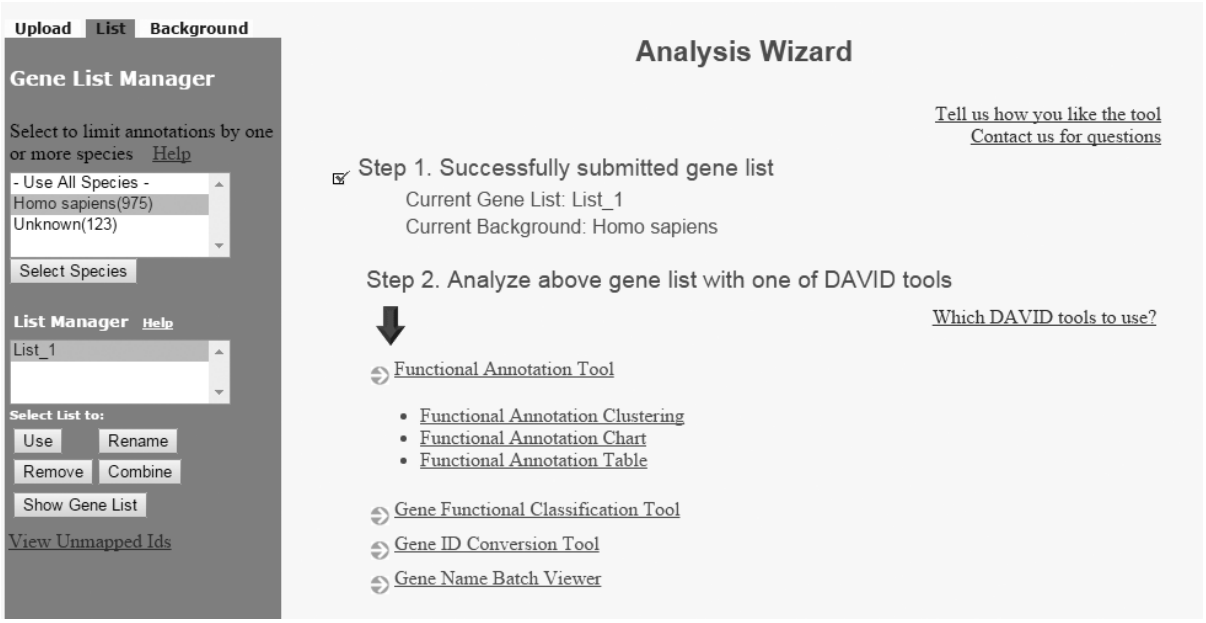

Figure 3: Gene List Manager and Analysis Wizard

Analysing the sequencing-derived gene list

1. To begin analysing your gene list, select “Functional Annotation Tool” in the Analysis Wizard (Fig. 3, right). This will take you to the Annotation Summary Results page (Fig. 4). This page contains many options; click the “Help and Tool Manual” link at the right for an explanation of what the various options and numbers mean. A similar link is available on most of the analysis pages.

2. Each line in this list represents a set of annotation categories. To expand one of the sets and see the individual categories, click the small grey plus symbol next to it.

Figure 4: Annotation Summary Results

3. Within an expanded set, click the "Chart" button next to a category to see the detailed report, which will open in a new window. This displays the annotation categories that are enriched in your gene list for this particular annotation category. This data can be downloaded (as a tab-delimited text file) for further analysis by clicking "Download File" at the top right of the chart. By default, the chart is sorted by P-value; click the column header to sort by another column.

Functional annotation clustering

1. So far we have looked only at results within one annotation category. To combine information from multiple annotation categories, they must be selected on the Annotation Summary Results page (Fig. 4). This is done by clicking the box to the

left of the category name so that a tick appears. DAVID has a default set of categories which are selected initially; these can be deselected if desired.

2. To see the functional annotation clustering report on the selected categories, click the Functional Annotation Clustering button toward the bottom of the Annotation Summary Results page (Fig. 4). It may take a few seconds for the report to display. Each cluster represents multiple related annotations, potentially from different annotation categories (Fig. 1). The Enrichment Score for each cluster indicates how highly the set of proteins matching the cluster annotations are enriched; higher is more enriched (see Note 6). The list of proteins associated with a cluster can be viewed by clicking on the red "G". As before, these data can be downloaded in their entirety via the link at the top-right of the table for analysis in an external application (see Note 7).

Pathway mapping in Cytoscape

Cytoscape (www.cytoscape.org) is a free and open source software platform for visualisation of networks. Cytoscape has a number of features built-in to allow rapid import and visualisation of biological interaction networks, and it is possible to visually overlay differential expression data onto these networks. This is a powerful way to put gene expression changes in the context of wider biological systems. The quality and completeness of information in public interaction databases is variable, however, so interpretation can be challenging, especially when investigating less well-studied parts of the interactome.

The following is a guide to quickly set up Cytoscape to visualise differential expression (see Note 8). Cytoscape is a complex program with much more functionality than is described here; a complete manual is available at the official Cytoscape wiki (wiki.cytoscape.org).

Materials

A PC or Mac running Windows, Linux, or Mac OS X. Cytoscape will run on most computers, but its resource demands scale with the data analysed; even high-performance machines may struggle with the memory and processing requirements of very large or highly interconnected interaction networks.

A broadband internet connection

Cytoscape (free to download from www.cytoscape.org).

A gene expression dataset, properly formatted for import into Cytoscape (see wiki.cytoscape.org/Cytoscape_User_Manual/Expression_Data).

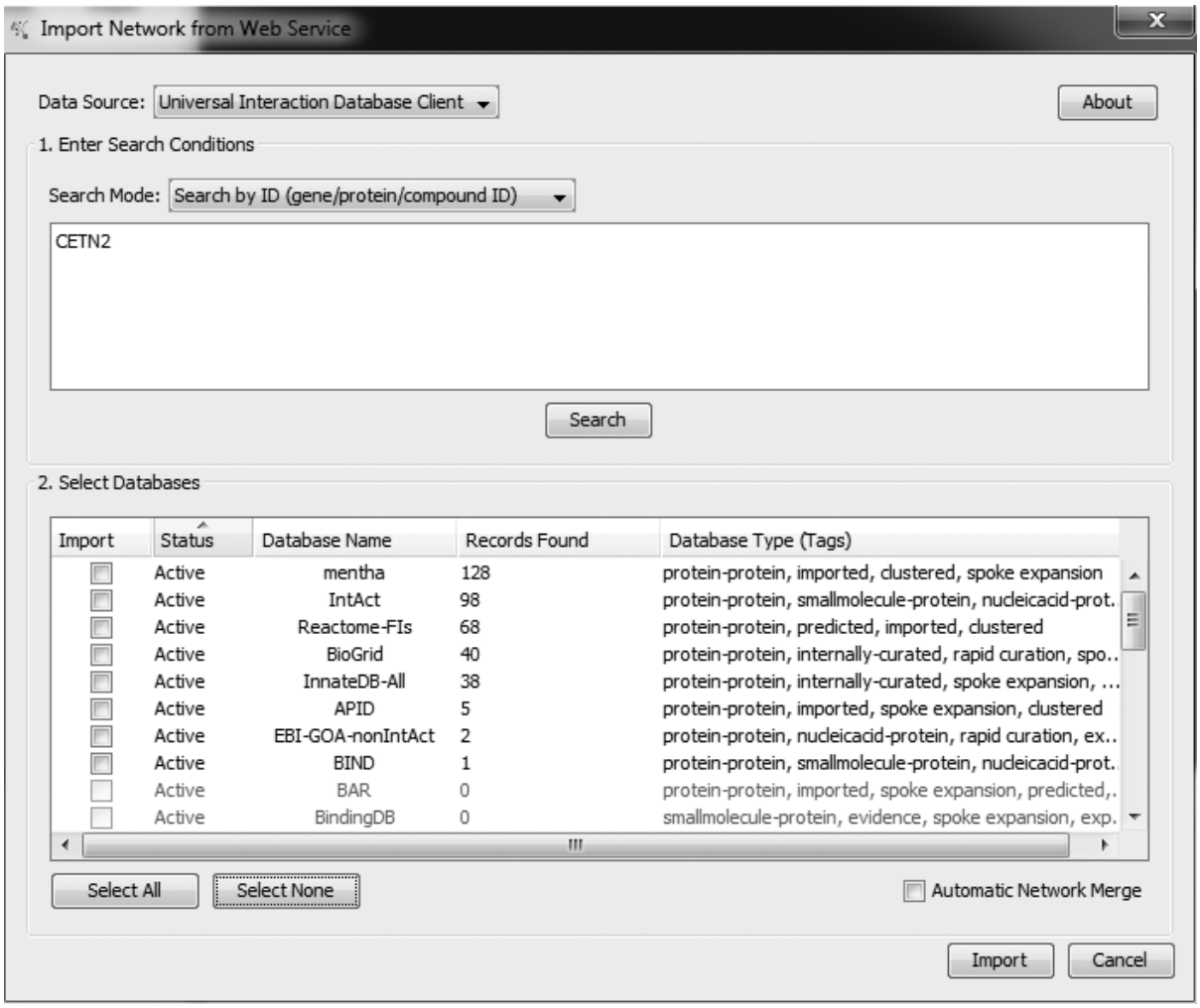

Figure 5: Import Network from Web Service

Method

Loading an interaction network into Cytoscape

1. Start Cytoscape and select File > Import > Network > Public Databases…
2. This invokes the "Import Network from Web Service" window (. 5). Type a protein name (or official gene symbol; e.g. "centrin 2" or "CETN2") into the search box and click the "Search" button. This will poll a set of online databases; it may take some time for all the databases to respond, depending on competing requests and your connection speed.
3. A list of databases containing interactions involving your protein of interest will appear. In the example image (Fig. 5), interaction records have been found in eight databases, with the most in the "mentha" interactome database.
4. Select the databases you wish to retrieve interaction networks from by clicking the checkboxes in the "Import" column, or press the "Select All" button beneath. Databases with no results for your search query will be automatically excluded. You may wish to exclude databases that do not contain information relevant to your research question even if there were matches for your protein of interest.
5. If you have selected multiple databases, Cytoscape can automatically merge the interaction networks together (see Note 9). Click the checkbox next to "Automatic Network Merge" at the bottom of the Import window to toggle this function.
6. Click "Import". Cytoscape will retrieve the interactions and build the network, then confirm by displaying an "Import Finished" dialog box. Click "close" to dismiss this box.
7. The network will now appear visualised in the largest panel of the Cytoscape interface (. 6). Proteins and other entities (such as complexes and functional RNAs) are represented by default as rectangles; Cytoscape terms these "nodes". Interactions

between nodes are represented by lines; Cytoscape terms these “edges” (following the terminology used in graph theory).

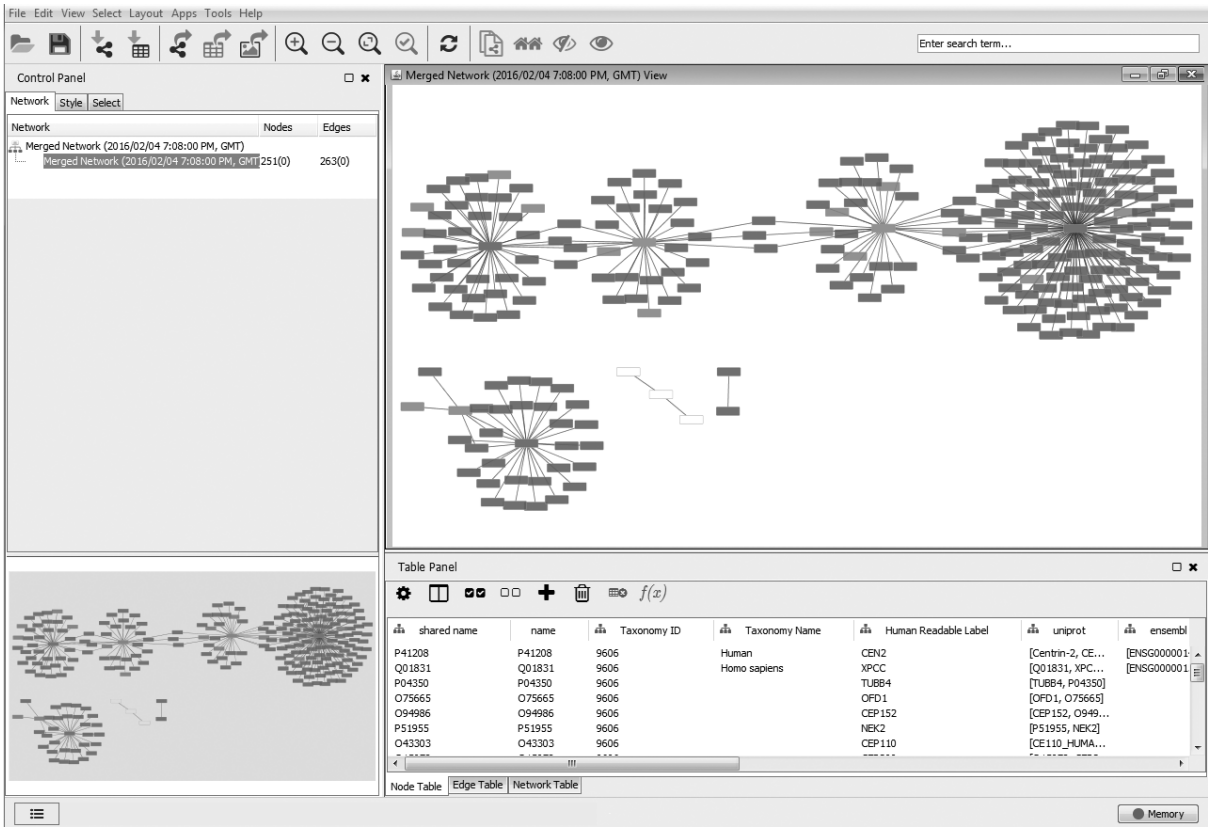

Figure 6: CETN2 network visualised in Cytoscape

8. Information about nodes and edges can be seen in the Table Panel to the bottom of the Cytoscape interface (. 6). Click and drag over the network visualisation to bandbox-select multiple nodes and edges. Attributes of only the selected nodes will appear in the Table Panel. Switch to the “Edge Table” tab at the bottom of the Table Panel to see the attributes of the selected edges instead (see Note 10).

Importing gene expression data into an interaction network

1. Load an interaction network that contains at least some of the genes in your expression dataset (see Note 11).
2. Prepare a text file with your expression data according to the Cytoscape expression data file format (see wiki.cytoscape.org/Cytoscape_User_Manual/Expression_Data).

The simplest way to input this data is as a list of genes, each with a single associated fold change figure; the rest of these instructions will assume this.

3. In Cytoscape, select File > Import > Table > File…
4. In the dialog box, select your expression data file.

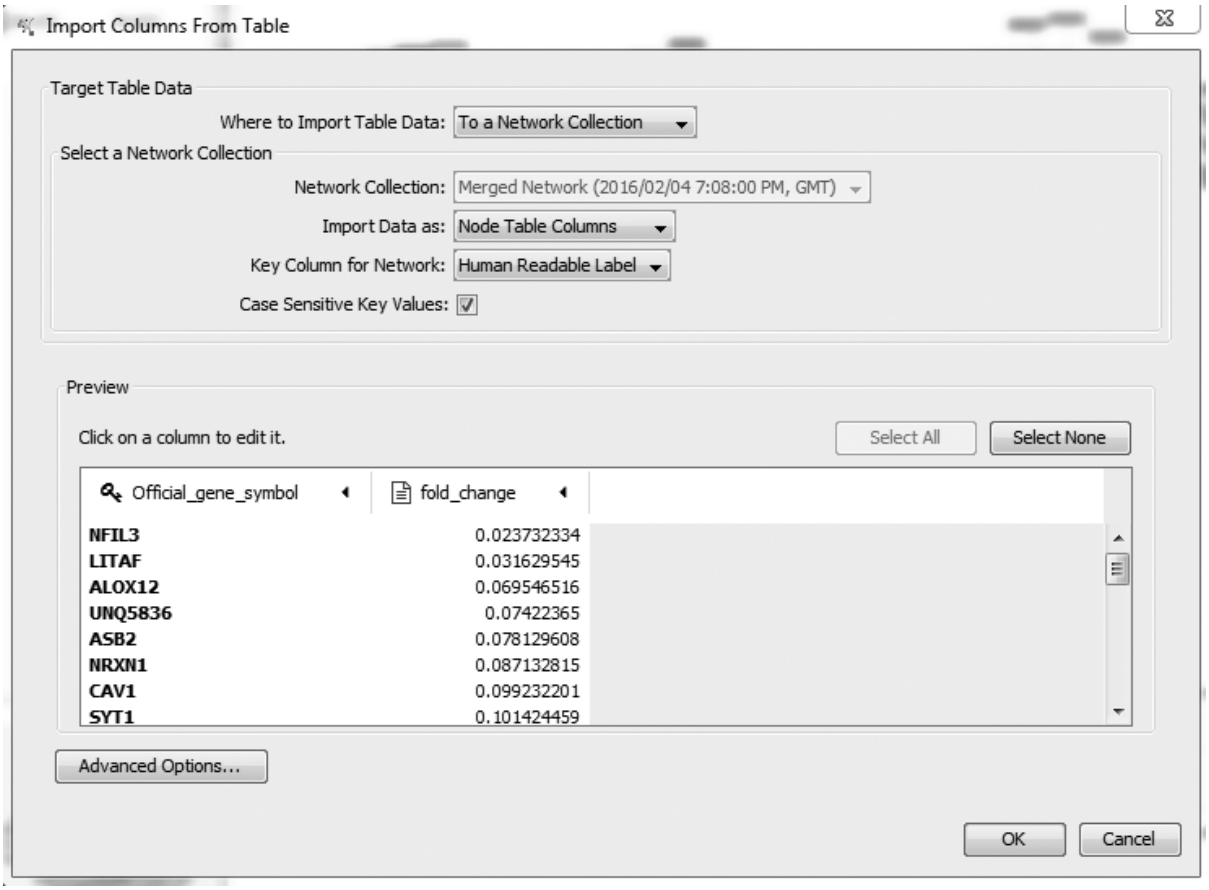

Figure 7: Import Columns From Table

5. The “Import Columns From Table” dialog box should appear (. 7). Under “Key Column for Network”, ensure that the correct key is selected. In this case, gene symbols have been used as identifiers; the corresponding option in Cytoscape is “Human Readable Label”.
6. Click “OK” (see Note 12).
7. Verify that the expression data has been imported correctly by selecting a node in the interaction network representing one of the differentially expressed genes. A new column in the Node Table should have appeared showing the transcript’s expression

value. If this does not appear, click the gear icon at the top right of the Table Panel and select “show all” to make sure all columns are displayed.

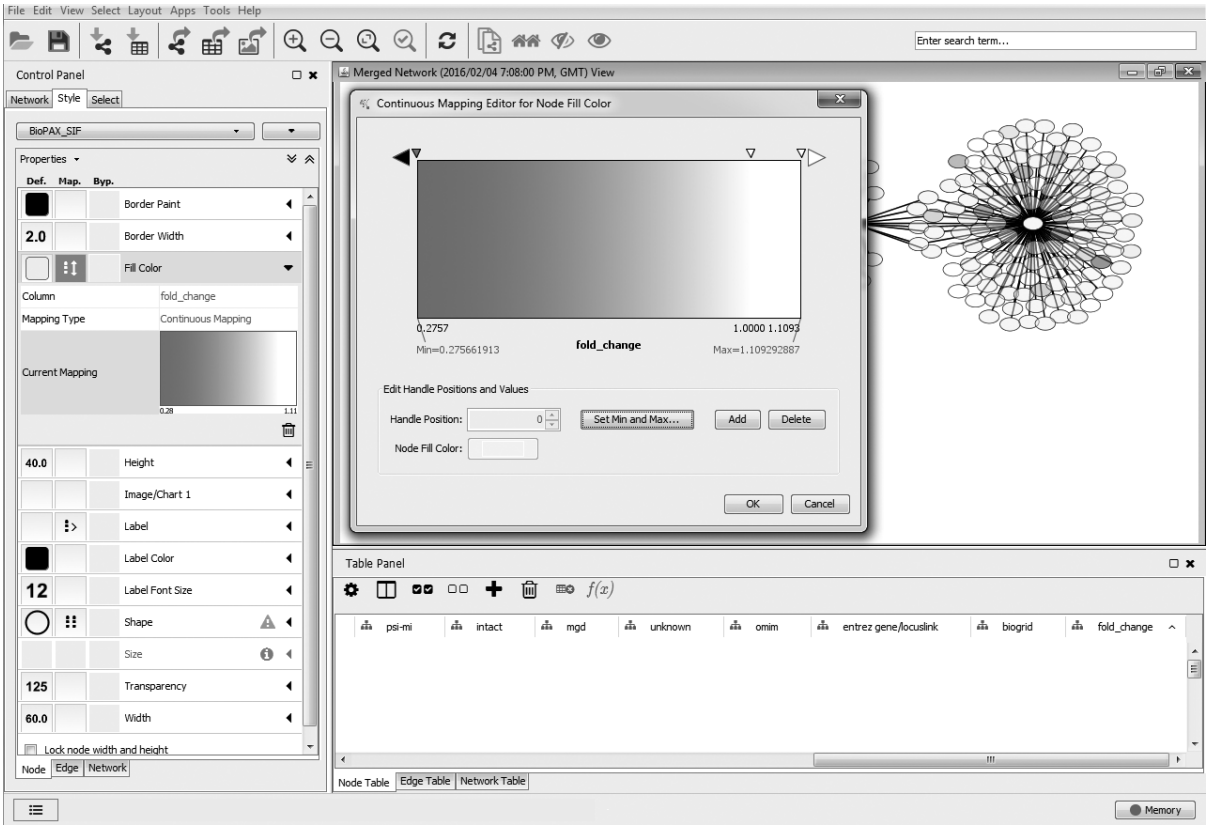

Figure 8: Continuous Mapping Editor

Visualising gene expression changes in an interaction network

1. With an interaction network loaded and a set of expression data imported, right click on the network’s entry in the “Network” tab of the “Control Panel” toward the left of the Cytoscape window.
2. Select “Apply Style…” and choose one of the options. Try selecting several different options. Observe how the network’s appearance changes – these are “Visual Styles” that control the graphical representation of the network without affecting its underlying data or its arrangement. To visualise your fold change data, you can edit the Visual Style settings so that node colour is controlled by the value of the fold change attribute.
3. Select the “Style” tab at the top of the Control Panel (Fig. 8).

4. Either select an existing visual style to modify with the drop-down menu or create a new style by clicking the arrow button to the right of the drop-down menu.
5. In the Style tab, select “Fill Color”
6. If not already expanded, expand “Fill Color” by clicking the arrow.
7. Set the default colour to white by clicking the rightmost box next to “Fill Color” and choosing white.
8. To the right of “Column”, select your expression attribute.
9. To the right of “Mapping Type”, select “Continuous Mapping”. This will apply a colour to the nodes that depends on the value of their associated expression attribute. By default the colour varies from black (low numbers) to white (high numbers).
10. Click on the gradient image to the right of “Current Mapping” to open the Continuous Mapping Editor (Fig. 8), which allows you to alter the colours used and the way the gradient varies with the expression values.
11. Double-click the arrows at the top of the gradient display to modify their colour. Try changing the gradient from black/white to red/green so that upregulated genes and downregulated genes are clearly distinguished. You may also want to modify the gradient so that “no change” has a neutral colour; new arrows can be placed with the “Add” button to create a series of gradients.
12. To view the expression changes overlaid on a network, go to the Network tab and switch the network’s Visual Style to your modified Visual Style. Nodes with no associated expression will remain white, while nodes with altered expression will become appropriately coloured.
13. The network can now be analysed visually: for example, if a series of connected nodes are all coloured to indicate expression changes, this may suggest disruption of a pathway that merits further analysis. To check the actual expression value of an

individual node, select the node and find the expression column in the Node Table tab of the Data Panel below the main view.

14. Now that the custom Visual Style is set and the expression data is loaded, any new interaction networks you load can have your expression data overlaid onto them by setting the Visual Style. This can be used to rapidly examine candidate pathways for patterns of altered expression (see Note 13).

Notes

Note 1: The background is a list of all the potential genes that could have appeared in the list under analysis; for example, the entire human genome, or a list of the genes that were detectable in principle in a particular experiment; for example, if your experiment was a microarray, it would be appropriate to use as a background the list of all transcripts probed for on the array, whereas if it was a whole-transcriptome mRNA-seq experiment, the entire genome would be the background.

Note 2: A functional annotation cluster is therefore a cluster of annotations, not a cluster of genes; a cluster may have many associated differentially expressed genes or only one, and the annotations may have genes in common – in the extreme case, you may have a cluster with many annotations, each of which is associated with a few genes shared between all of them. Whether any cluster is biologically meaningful is dependent upon many factors including the quality of the underlying data and annotation databases; therefore interpretation may be required.

Note 3: Keep in mind that “enrichment” is not equivalent to upregulation. If analysing a list of downregulated genes, the “most enriched” annotations are likely ones for which many genes are downregulated. If analysing a list of up- and downregulated genes, the most enriched annotations may represent any pattern of alteration to the associated genes; for example, half may be upregulated and half downregulated.

Note 4: While it is possible to use official gene symbols with DAVID, this is not recommended because they require conversion and are sometimes ambiguous. If another form of IDs are available for your gene list, those should be used in preference.

Note 5: As described above (Note 1), the background is a list of all the potential genes that could have appeared in the list under analysis, and will depend on the nature of your dataset.

Note 6: DAVID calculates enrichment scores as the geometric mean of the p-values of all members of the cluster, expressed in –log scale, so in technical terms, higher enrichment scores indicate lower probability that the observed overrepresentation of genes associated with the cluster would occur purely by chance.

Note 7: Various options are available to fine-tune the results of DAVID's functional annotation clustering. The most prominent is the "Classification Stringency" (controlled by a drop-down list found at the top of the Functional Annotation Clustering results list). Higher stringency groups annotations into smaller, more closely-related clusters, whereas lower stringency will result in clusters with more, less closely-related annotations. Either may be appropriate depending on your dataset; if, for example, you find that DAVID is forming functional annotation clusters out of groups of annotations that should, for the purposes of your analysis, be considered separately, increasing stringency may help. More advanced options to fine-tune clustering are available within "Options" next to the Classification Stringency drop-down list.

Note 8: These instructions were written for Cytoscape version 3.3.0. If you are using a future version, or an earlier version for legacy or compatibility reasons, the details of some dialog boxes and options may differ.

Note 9: merging networks is useful as it reduces redundancy in the resulting network and may indicate the presence of pathways by showing chains of connections not apparent in the individual databases. However, due to incompatibilities between different databases,

automatic merging is not always completely successful. It may be necessary to manually fix errors in a combined network, such as multiple nodes for a single protein.

Note 10: Understanding what a particular edge represents can be especially important when trying to interpret an interaction network, as several very different kinds of relationship are represented this way: for example, an "in_same_component" relationship may indicate two proteins are part of a complex, whereas a "reacts_with" relationship indicates chemical interaction.

Note 11: In previous versions of Cytoscape, it was necessary to load a network prior to importing expression data, because any expression data that did not relate to a node currently loaded in Cytoscape would not be imported, resulting in missing values when loading further interaction networks. This behaviour was corrected in Cytoscape version 3.1, so expression data and interaction networks can now be imported in any order.

Note 12: Errors at this stage are often due to the delimiter setting, which defines which character separates entries in the data file (often tab or space characters, which can be easily confused as they are both rendered as whitespace). If your file fails to import, check the "Advanced Options…" dialog and ensure that the set delimiter matches the delimiter used in your expression data file.

Note 13: to improve readability of cluttered networks, it may be desirable to delete nodes that appear irrelevant; for example, nodes representing non-proteins, or proteins that have no expression data in your dataset. This may, however, obscure connections between relevant nodes that were linked via the deleted nodes, so should be done with caution.

Figure legends

Figure 1 – **Examples of functional annotation clusters generated by DAVID.** The first cluster combines three different Biological Process GO annotations pertaining to the centrosome into a single centrosome-related annotation cluster. In the second cluster, five

Cellular Component GO annotations and one Protein Information Resource annotation have been clustered as they all indicate a similar kinetochore association. The enrichment score for each cluster is shown above the list of annotations.

Figure 2 – **DAVID's "Upload Gene List" interface.** A list of Ensembl gene IDs has been entered (A: Paste a list) and Ensembl gene ID has been selected as the identifier (Step 2: Select Identifier).

Figure 3 – **DAVID's Gene List Manager and Analysis Wizard.** The Gene List Manager (left pane) allows selection of species to limit annotation searches; the Analysis Wizard (right pane) shows the assigned background and options to begin analysis.

Figure 4 – **DAVID's Annotation Summary Results page.** This page contains multiple categories of analysis, only some of which are selected by default (as shown).

Figure 5 – **Cytoscape's "Import Network from Web Service" window,** showing search results for centrin 2 (CETN2) from multiple online databases.

Figure 6 – **Cytoscape's network visualisation.** The merged CETN2 interaction network has been loaded into Cytoscape and is visualised in the large top-right panel. Proteins are represented as rectangles (nodes), and interactions as lines (edges). In the Table Panel (bottom-right), node details are displayed.

Figure 7 – **Cytoscape's "Import Columns From Table" window.** A list of gene symbols with associated fold change values have been selected for import from an external text file and are previewed.

Figure 8 – **Cytoscape's Style panel (left) and Continuous Mapping Editor (centre).** This interface allows you to place node colour under the control of your expression attribute. In this example, as expression (fold change) reduces, nodes are coloured darker grey; in the network visible to the right, white nodes indicate little or no reduction in expression, and darker nodes have greatly reduced expression in this dataset.

References

1. Chapman, M. J. One hundred years of centrioles: the Henneguy–Lenhossék theory. *Int Microbiol* **1,** 233–236 (1998).
2. Ishikawa, H. & Marshall, W. F. Ciliogenesis: building the cell's antenna. *Nat. Rev. Mol. cell Biol.* **12,** 222–234 (2011).
3. Keller, L. C., Romijn, E. P., Zamora, I., Yates, J. R. & Marshall, W. F. Proteomic analysis of isolated chlamydomonas centrioles reveals orthologs of ciliary-disease genes. *Curr. Biol.* **15,** 1090–1098 (2005).
4. Li, J. B. *et al.* Comparative genomics identifies a flagellar and basal body proteome that includes the BBS5 human disease gene. *Cell* **117,** 541–552 (2004).
5. Kilburn, C. L. *et al.* New Tetrahymena basal body protein components identify basal body domain structure. *J. Cell Biol.* **178,** 905–912 (2007).
6. Keller, L. C. *et al.* Molecular architecture of the centriole proteome: the conserved WD40 domain protein POC1 is required for centriole duplication and length control. *Mol. Biol. Cell* **20,** 1150–1166 (2009).
7. Jakobsen, L. *et al.* Novel asymmetrically localizing components of human centrosomes identified by complementary proteomics methods. *EMBO J.* **30,** 1520–1535 (2011).
8. Hoh, R. A., Stowe, T. R., Turk, E. & Stearns, T. Transcriptional program of ciliated epithelial cells reveals new cilium and centrosome components and links to human

disease. *PLoS One* **7,** e52166 (2012).

9. Bauer, M., Cubizolles, F., Schmidt, A. & Nigg, E. A. Quantitative analysis of human centrosome architecture by targeted proteomics and fluorescence imaging. *EMBO J.* e201694462 (2016).

10. Young, M. D., Wakefield, M. J., Smyth, G. K. & Oshlack, A. Gene ontology analysis for RNA-seq: accounting for selection bias. *Genome Biol.* **11,** 1 (2010).

11. Huang, D. W., Sherman, B. T. & Lempicki, R. A. Systematic and integrative analysis of large gene lists using DAVID bioinformatics resources. *Nat. Protoc.* **4,** 44–57 (2008).